DECEMBER 1986
ENVIRONMENTAL SCIENCE & TECHNOLOGY

ES&T

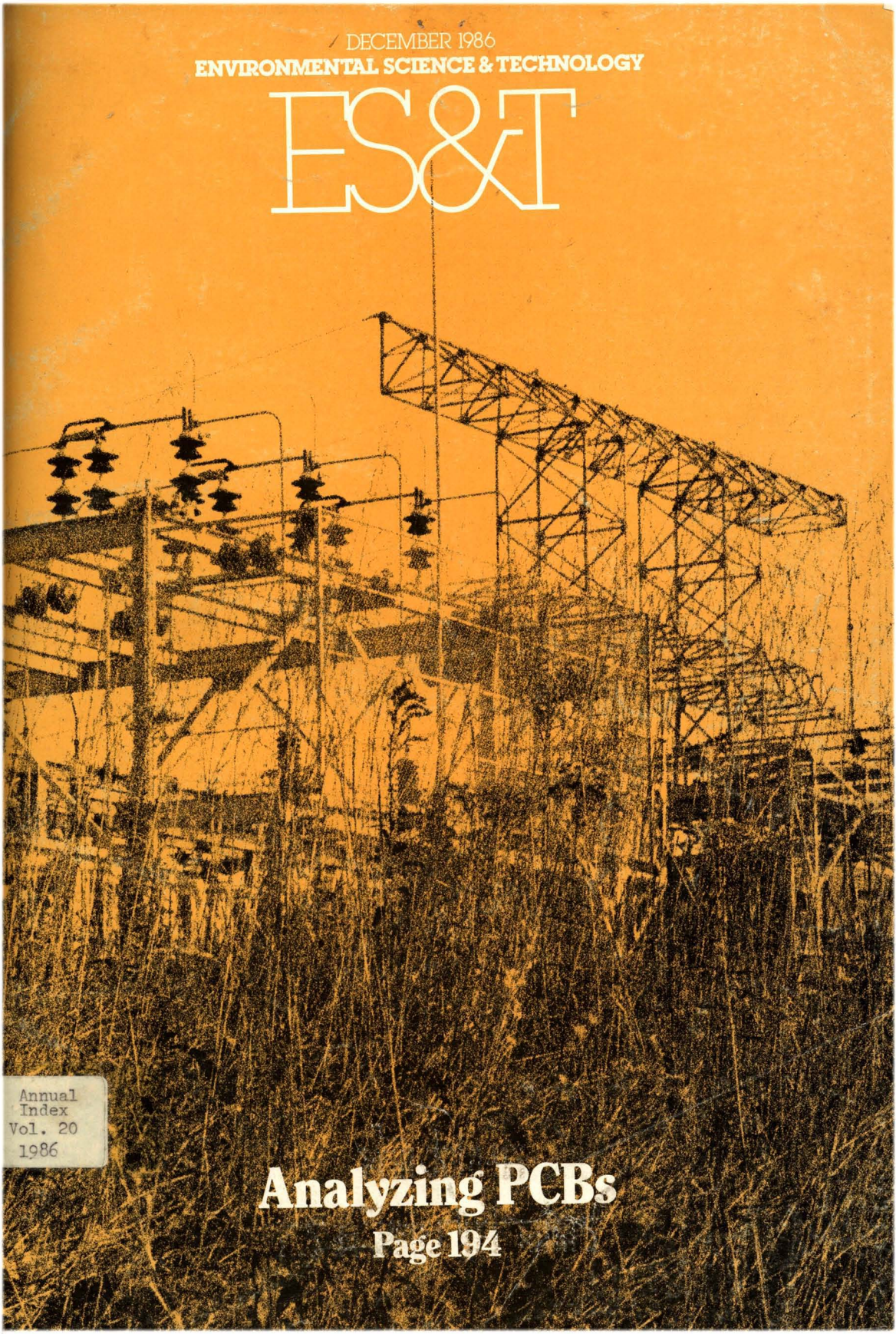

Analyzing PCBs

Page 194

CURRENT TITLES IN ENVIRONMENTAL SCIENCE

Air Pollution
Volumes VI, VII, and VIII

Edited by *Arthur C. Stern*
University of North Carolina, Chapel Hill

Published as a supplement to the first five volumes of the second edition, these three volumes cover many new topics such as asbestos, carbon dioxide, lead, nuclear accidents, nonionizing radiation, stratospheric ozone, and visibility. This state-of-the-art compilation will facilitate the work of air pollution control agency personnel, research scientists, consultants, law firms involved in air pollution litigation, and manufacturers of air pollution equipment and instrumentation.

Volume VI: Supplement to Air Pollutants, Their Transformation, Transport, and Effects

Contents: The Pollutants. The Transformation Pollutants. The Transport of Pollutants. Air Pollution Effects on Physical and Economic Systems. Effects on Vegetation, Native Crops, Forests. Effects on Acidic Deposition on Aquatic Ecosystems. Effects on Human Health.

1986, 496 pages, $70.00,
ISBN: 0-12-666606-7

Volume VII: Supplement to Measurements, Monitoring, Surveillance, and Engineering Control

Contents: Air Pollution Information Resources. Sampling and Analysis. Ambient Air Surveillance. Source Surveillance. Control Concepts. Control Devices-Centrifugal Force and Gravity; Filtration; and Dry Flue Gas Scrubbing. Control Devices—Electrostatic Precipitation, Scrubbing, Mist Elimination, Adsorption, and Combustion of Toxic and Hazardous Wastes. Process Emissions and Their Control-Parts I and II.

1986, 544 pages, $69.50,
ISBN: 0-12-666607-5

Volume VIII: Supplement to Management of Air Quality

Contents: Air Quality Management in the United States. United States Clean Air Act Litigation. Air Pollution Control Programs—Worldwide. Air Pollution Personnel and Their Development. Air Pollution Standards. Cumulative Index.

1986, 197 pages, $43.50,
ISBN: 0-12-666608-3
Set Price for all three volumes: $155.50

Environmental Radioactivity
From Natural, Industrial, and Military Sources
Third Edition

Merril Eisenbud
New York University Medical Center

An important reference for health workers, nuclear engineers, environmental students, researchers, managers, administrators, and operators of power plants.

Contents: Introduction. The Biological Basis of Radiation Protection. Radiation Protection Standards. Some General Considerations Concerning Environmental Radioactivity, Including the Use of Models. Transport Mechanisms in the Environment. Terrestrial and Aquatic Pathways. Natural Radioactivity. Production and Processing of Nuclear Fuels. Power Reactors. Various Other Sources of Exposure. Radioactive Waste Management. Fallout from Nuclear Explosions: I. Short-Term Effects. Fallout from Nuclear Explosions: II. Worldwide Effects. Accidents that Resulted in Contamination of the Environment. Radiation Exposure and Risk: Some Contemporary Social Aspects. Appendix: The Properties of Certain Radionuclides. References. Index.

1986, 444 pages, $55.00,
ISBN: 0-12-235153-3

Geology and Radwaste

A.G. Milnes
Swiss Federal Institute of Technology, Zurich

This book gives background material on the sources, types, and amounts of radwaste and an overview of the various disposal practices and concepts. The book concentrates on the contribution of the earth sciences to an understanding of the long-term performance of any radwaste isolation system and the selection of repository sites.

Contents: **Background:** Radioactive Wastes. Radwaste Disposal. **Earth Science Perspectives:** The Earth's Crust. Geological Time. Surface Processes: Biogeochemical Aspects. Surface Processes: Denudation and Deposition. Sedimentary Rocks: Formation and Properties. Volcanic Processes and Products. Natural and Synthetic Crystalline Rocks. Physical Processes in the Upper Crust. Fluid–Rock Interactions. Ocean Processes. Climatic Change and Continental Glaciation. **Application:** Predictive Geoscience. Repository Site Selection. Index.

1985, 344 pages
In Paperback: $39.95, ISBN: 0-12-498071-6
Casebound: $60.00, ISBN: 0-12-498070-8

Atmospheric Chemical Compounds
Sources, Occurrences, and Bioassay

Edited by *T.E. Graedel*
and *Donald T. Hawkins*
AT&T Bell Laboratories, Murray Hill, NJ
Larry D. Claxton
U.S. EPA, Research Triangle Park, NC

This practical reference examines the structure and properties of the atmosphere, including listings of compounds in clouds, fog, rain, snow and ice; a listing of compounds detected in the stratosphere; and a compendium of compounds in indoor air. Readers will find the extensive cross-referencing especially useful—compounds can be located by chemical type, name, CAS registry number, or source.

Contents: Introduction. Inorganic Compounds. Hydrocarbons. Ethers. Alcohols. Ketones. Aldehydes. Organic Acid Derivatives. Organic Acids. Heterocyclic Oxygen Compounds. Nitrogen-Containing Organic Compounds. Sulfur-Containing Organic Compounds. Halogen-Containing Organic Compounds. Organometallic Compounds. Synthesis and Summary. References. Indexes.

1986, 816 pages, $55.00,
ISBN: 0-12-294485-2

Order from your local bookseller or directly from

ACADEMIC PRESS
Harcourt Brace Jovanovich, Publishers
Orlando, FL 32887-0510, U.S.A.

Call Toll Free
1-800-321-5068

Orlando San Diego New York Austin
Boston London Sydney Tokyo Toronto
Prices subject to change without notice. GP/BE—16126

Environmental Science & Technology

Please send *research* manuscripts to Manuscript Reviewing, *feature* manuscripts to Managing Editor. For editorial policy and author's guide, see the January 1986 issue, page 30, or write Janice L. Fleming, Manuscript Reviewing Office, *ES&T*. A sample copyright transfer form, which may be copied, appears on the inside back cover of the February 1986 issue.

Environmental Science & Technology, ES&T (ISSN 0013-936X), is published monthly by the American Chemical Society at 1155 16th Street, N.W., Washington, D.C. 20036. Second-class postage paid at Washington, D.C., and at additional mailing offices. POSTMASTER: Send address changes to *Environmental Science & Technology*, Membership & Subscription Services, P.O. Box 3337, Columbus, Ohio 43210.

SUBSCRIPTION PRICES 1986: Members, $28 per year; nonmembers (for personal use), $42 per year; institutions, $164 per year. Foreign postage, $8 additional for Canada and Mexico, $16 additional for Europe including air service, and $23 additional for all other countries including air service. Single issues, $15 for current year; $17 for prior years. Back volumes, $198 each. For foreign rates add $2 for single issues and $8 for back volumes. Rates above do not apply to nonmember subscribers in Japan, who must enter subscription orders with Maruzen Company Ltd., 3-10 Nihon bashi 2 chome, Chuo-ku, Tokyo 103, Japan. Tel: (03) 272-7211.

SUBSCRIPTION SERVICE: Orders for new subscriptions, single issues, back volumes, and microform editions should be sent with payment to Office of the Treasurer, Financial Operations, ACS, 1155 16th St., N.W., Washington, D.C. 20036. Phone orders may be placed, using Visa, Master Card, or American Express, by calling toll free (800) 424-6747 from anywhere in the continental U.S. Changes of address, subscription renewals, claims for missing issues, and inquiries concerning records and accounts should be directed to Manager, Membership and Subscription Services, ACS, P.O. Box 3337, Columbus, Ohio 43210. Changes of address should allow six weeks and be accompanied by old and new addresses and a recent mailing label. Claims for missing issues will not be allowed if loss was due to insufficient notice of change of address, if claim is dated more than 90 days after the issue date for North American subscribers or more than one year for foreign subscribers, or if the reason given is "missing from files."

ES&T CONTENTS

Volume 20, Number 12, December 1986

FEATURES

1144
Analyzing PCBs. Basic information is presented about how polychlorinated biphenyls are identified and measured. Ann L. Alford-Stevens, EPA, Cincinnati

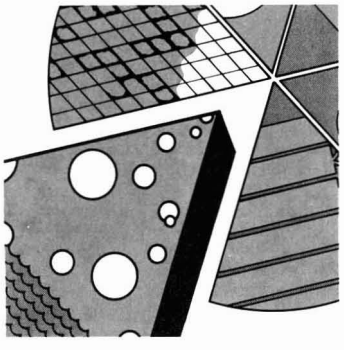

1200
Water treatment processes. Anaerobic wastewater treatment is the subject of the fourth article in a six-part series on water treatment. Perry L. McCarty and Daniel P. Smith, Stanford University, Stanford, Calif.

REGULATORY FOCUS

1207
Superfund. Richard Dowd discusses ramifications of the reauthorized law.

VIEWS

1208
Atmospheric warm-up. Action must be taken to slow emissions of carbon dioxide and other substances that accelerate changes in climate. Sandra L. Postel, Worldwatch Institute, Washington, D.C.

DEPARTMENTS

1189 Editorial
1191 Currents
1210 Consulting services
1211 Classified

1986 INDEX

1277 Author index
1282 Front section subject index
1283 Keyword index

UPCOMING

Aquatic chemistry of acid deposition
More on anaerobic water treatment processes

ESTHAG 20(12) 1187–1288 (1986)
ISSN 0013 936X

Cover: Alan Kahan
Credits: p. 1194, Alan Kahan

RESEARCH

1213
Gas-partitioning approach for laboratory and field studies of mirex fugacity in water. Chengqing Yin and John P. Hassett*

Dynamic headspace gas-partitioning methods measure fugacity and free dissolved concentration of mirex in water.

1218
Chlorination of ω-cyanoalkanoic acids in aqueous medium. Ed W. B. de Leer,* Theo Baggerman, Petra van Schaik, Coby W. S. Zuydeweg, and Leo de Galan

The production of **ω-cyanoalkanoic acids from precursor amino acids and further chlorination reactions at different pH values are studied.**

1224
Heterocoagulation vs. surface precipitation in a quartz–$Mg(OH)_2$ system. Santhana V. Krishnan* and Iwao Iwasaki

The attachment of $Mg(OH)_2$ precipitates on surfaces of quartz by heterocoagulation and by surface precipitation is compared and related to the stability of quartz suspensions.

1229
Degradation of tributyltin in San Diego Bay, California, waters. Peter F. Seligman,* Aldis O. Valkirs, and Richard F. Lee

Radiolabeled or unlabeled TBT, at concentrations near those found in harbor areas, is added to water from San Diego Bay.

1235
Contribution of fine particle sulfates to light scattering in St. Louis summer aerosol. Teri L. Vossler and Edward S. Macias*

Light scattering by $(NH_4)_2SO_4$ is calculated from measured sulfur size distributions and estimates of water.

1243
Molecular beam mass spectroscopic study of trichloroethylene flames. Wen-Donq Chang, Sankaram B. Karra, and Selim M. Senkan*

The detailed chemical structures of C_2HCl_3 flames are investigated, and the identity and mole fractions of combustion intermediates are determined.

1249
On the nature of the atmospheric oxidation process of SO_2 to sulfate and of NO_2 to nitrate on the basis of diurnal variations of sulfate, nitrate, and other pollutants in an urban area. Satoshi Kadowaki

Results indicate that droplet-phase reactions are important for the oxidation of SO_2 to sulfate, whereas gas-phase reactions are predominant in the oxidation of NO_2 to nitrate.

1254
Determination of organofluorine in air. Erik Kissa

Organofluorine air contaminants at sub parts per million or higher levels are collected on a solid adsorbent or in water and then burned in an oxyhydrogen torch.

NOTES

1257
Radioactivity size distributions of ambient aerosols in Helsinki, Finland, during May 1986 after the Chernobyl accident: Preliminary report. Esko I. Kauppinen,* Risto E. Hillamo, S. Hannele Aaltonen, and Kari T. S. Sinkko

This study reports preliminary results of ambient radioactive aerosol size distribution measurements made at Helsinki last May.

1260
Field audit results with organic gas standards on volatile organic ambient air samplers equipped with Tenax GC. Howard L. Crist* and William J. Mitchell

These audits assess the accuracy and precision of an EPA-operated ambient air sampler that collects VOCs.

1263
Influence of the nature of soil organics on the sorption of toluene and trichloroethylene. Doug R. Garbarini and Leonard W. Lion*

The capacity of selected soil components to sorb toluene and trichloroethylene, two nonionic volatile organic pollutants found in contaminated groundwater, is examined.

1269
Calibration of peroxyacetyl nitrate measurements with an NO_x analyzer. L. Fortunat Joos,* Werner F. Landolt, and Heinz Leuenberger

This new calibration method for PAN measurement uses an NO_x analyzer in the field.

1273
A passive sampler for formaldehyde in air using 2,4-dinitrophenylhydrazine-coated glass fiber filters. Jan-Olof Levin,* Roger Lindahl, and Kurt Andersson

A method of diffusive sampling of formaldehyde in air is developed and evaluated in the field.

* To whom correspondence should be addressed.

This issue contains no papers for which there is supplementary material in microform.

ES&T
GUEST EDITORIAL

Waste reduction: The time has come

Ten years ago this month a United Nations conference in Paris formally introduced a new concept in resource management and environmental control—the front-end approach to minimizing resource input and effluent output through revamping and redesigning industrial processes and products.

The first U.N. Economic Commission for Europe Seminar on Non-Waste Technology called on member countries to adopt comprehensive approaches to shrinking the sources of hazards and wastes. In that pre-Love Canal–Bhopal era, this call was met with indifference to what many deemed an impractical and idealistic agenda.

Yet a decade later, nonwaste technology—or what is now called waste reduction or waste minimization—is looked upon as our best hope for reversing the flood of toxic substances and hazardous wastes into the environment. The congressional Office of Technology Assessment terms waste reduction "critical to the prevention of future hazardous waste problems." Industries from the Fortune 500 companies on down have begun to minimize waste production. States, and even local governments, have set up waste minimization assistance activities. And in Washington there is growing sentiment in favor of a sizable increase in federal involvement, including direct regulation, to stimulate reduction.

What has happened? Industry and government alike have begun to see that the toxics-as-usual approach to hazardous-waste management is not working. Building better landfills and tighter drums is not the way to reduce the nation's hazardous-waste burden. Totally secure containment is impossible; and the rapidly inflating costs of liability for toxic mishaps, and for handling and disposal of hazardous substances, are becoming intolerable.

Fortunately, there are emerging approaches to toxics management that can reduce costs as well as effluents. 3M discovered years ago that "pollution prevention pays." Its 3P waste minimization effort saved that company $200 million and cut wastewater emissions by 1.4 billion gal annually in the first eight years of operation. Other industries have only recently started to look to front-end approaches to eliminate hazardous wastes.

There is clear forward movement in waste reduction. Its net effect, though, has been small. Despite estimates that waste reduction could cut our hazardous-waste stream by one-half or more, that stream is in fact still growing. The long-sought light, in the form of waste reduction systems, may be at the end of the hazardous-waste tunnel—but that tunnel must be straightened out to let the light through.

For this to occur, industry and government must step up efforts to develop cooperative approaches to meet priority waste reduction needs. Lack of adequate information in the private sector has proven a significant barrier to waste reduction. The federal government, with its superior resources, can take a cue from fledgling state programs to formulate strong programs for information development and dissemination. Research and development grant programs, mandated yearly waste reduction targets, and regulatory concessions to encourage waste reduction in place of end-of-pipe treatment have been suggested as needed federal actions. It is not clear what mix of government and private-sector programs will best serve waste minimization. What is clear, however, is that it is very much in the federal government's interest to invest time, leadership, and money in waste reduction.

The success of waste minimization in the United States will have important international implications. As a recent conference of European hazardous-waste facility operators documented, developing countries are eyeing the industrialized world's progress in hazardous-waste management as they formulate their own programs. The more success in waste reduction here, the greater will be the benefit to the global community.

Arthur H. Purcell *is founding director of the Resource Policy Institute (Washington, D.C.) and heads its Waste Reduction Services program. He was a member of the U.S. delegation to the first U.N. Seminar on Non-Waste Technology. He is the author of* The Waste Watchers *(Doubleday/Anchor Press). He is a graduate of Cornell University and holds a Ph.D. and an M.S. in materials science and engineering from Northwestern.*

0013-936X/86/0920-1189$01.50/0

Northwestern Costa Rica will be the site of the world's first project to restore a tropical dry forest. The creation of the 1114-km^2 Guanacaste National Park is being led by Daniel Janzen of the University of Pennsylvania and has several U.S. and Costa Rican sponsors. Janzen's team will reintroduce trees, other plants, and animals during a period of several years and, by constant experimentation, determine the correct mix of species. Dry forests receive an average of about 1 m of precipitation during the rainy season; most rain forests receive 7–8 m each year.

President Ronald Reagan has signed the Superfund reauthorization. The new law calls for $9 billion to be spent on toxic waste cleanup over the next five years. The Superfund law that expired Sept. 30, 1985, had provided $1.6 billion since 1980. An estimated $2.5 billion will be raised by levying a tax of $25 for every $10,000 of a company's earnings in excess of $2 million/yr. Other sources of funding include excise taxes on petroleum products and chemicals, interest on the Hazardous Substance Response Trust Fund, recovery of cleanup costs from responsible parties, and about $1 billion from general revenues.

Vaun Newill was confirmed in October by the Senate as EPA's assistant administrator for research and development. Before his appointment to EPA, Newill was regional medical director for Esso Europe (London). He has a master's degree in hygiene (epidemiology) from Harvard and an M.D. from the University of Pittsburgh. During his confirmation hearings, Newill told members of the Senate Environment and Public Works Committee that a great deal of additional information on the causes and effects of acid deposition is needed before appropriate measures can be chosen. He also told the committee he plans to place more emphasis on basic, long-term research. Newill replaces Bernard Goldstein, who has returned to an academic post at the University of Medicine and Dentistry of New Jersey.

EPA has issued a final guidance document for monitoring groundwater at hazardous waste sites as required by the Resource Conservation and Recovery Act. The document is oriented toward site-specific variables. For example, site characteristics rather than arbitrary distances between monitoring wells are to govern spacing. The document requires that well materials be appropriate for the anticipated lifetime of monitoring programs and that they be chosen for their durability. It also sets forth factors to be considered in determining the number of wells necessary to assess the extent of groundwater contamination.

EPA has proposed regulations aimed at reducing wood stove emissions by as much as 70% (*Fed. Regist.* **1986,** *51,* 34672). Final regulations are to be issued Jan. 1, 1987, under a court order issued May 9 (*New York v. Thomas*). Initially, particulate emissions will be limited to 5.5 g/h for stoves fitted with catalytic converters and 8.5 g/h for other stoves. Typical catalytic converters consist of honeycombed chambers that contain a material such as platinum. They add $100–$250 to the cost of a wood stove. These standards will apply to stoves manufactured after July 1, 1988, and to those sold after July 1, 1990. For stoves made after July 1, 1990, and sold after July 1, 1992, the standards are lowered to 4.1 g/h and 7.5 g/h, respectively. The objective is to reduce emissions of carbon monoxide and hydrocarbons, especially polynuclear aromatics, some of which are suspected carcinogens. The regulations are modeled after those now in effect in Oregon. Open fireplaces, boilers, and furnaces are not covered under the new rules.

A report by the congressional Office of Technology Assessment warns that the federal government does not have enough scientific information to frame the laws and regulations necessary to protect the public from exposure to mutagens. The methods being developed to detect new mutations in human DNA and proteins have not yet reached the level of sophistication that will support their general use. However, the report forecasts that methods could be available for wide-scale use within the next decade if enough scientific and financial support for their development is provided. One of these new methods involves detecting altered DNA sequences that indicate mutation. Current techniques can detect sporadic genetic disease, chromosome aberrations, and variant blood proteins.

EPA steps up wetlands protection

EPA administrator Lee Thomas has announced the creation of a new Office of Wetlands Protection. The director of the office will report to the assistant administrator for water. The office will coordinate federal wetlands research and promote understanding of the scientific and economic values and uses of wetlands. It also will work toward the identification, protection, and restoration of wetlands and protect them as required by Section 404 of the Clean Water Act. The creation of the new office places EPA wetlands protection functions under one roof.

Management of EPA's Chesapeake Bay Program is poor, according to a report by the agency's Office of the Inspector General. One complaint charges that of 90 items of work required in 23 grants and contracts the office reviewed, only 44 were received. Another complaint faulted work planning and contract and grant monitoring by EPA Region 3 and the Chesapeake Bay Liaison Office, the

0013-936X/86/0920-1191$01.50/0

program's managers. The report cited lost records and lax attention by the program managers. A spokesman for Region 3 (Philadelphia, Pa.) acknowledged that better controls on contracts and grants are needed but denied that planning is poor. Region 3 officials agree that contract and grant files must be safeguarded, completed grants and contracts must be closed out immediately, grantees need to be monitored to ensure compliance with grant conditions, and complete work programs must be submitted with each grant or contract proposal. The study covered 1978–1984, during which more than $25 million in grants and contracts was awarded.

Idaho's government and industries are having difficulty reaching a consensus on methods of abating nonpoint source water pollution. In September, a governor's task force announced a plan that would involve the application of best management practices by the timber industry and other users of streams. The streams would be monitored by the Idaho Department of Health and Welfare's Division of Environment, which would require changes in water management practices if clean-water criteria are not met. The snag is the issue of sedimentation. Al Murrey, chief of the division's Water Quality Bureau, says that neither EPA nor state authorities currently have numerical criteria for assessing sedimentation in streams, although EPA is developing a standard that may eventually be used. Without at least a best management practices provision to address sedimentation, those in the timber industry fear that lawsuits will lead to the issue being decided in federal court.

The California Air Resources Board (CARB) has set aside $2.4 million to study dry acid deposition. CARB will establish a network of 10 monitoring sites in urban and coastal areas, where the problem is said to originate, and in national parks and the Sierra Nevada Mountains, where the material is deposited. CARB officials say there is evidence that the deposited dry material reacts with moisture to form acids that damage vegetation, degrade building materials, and leach through soils. They believe that because of its unusual geology, the Sierra Nevada may be particularly vulnerable to damage. CARB scientists also will determine what role lake and stream bed sediments play in neutralizing acidity.

The state government of North Carolina should not assume responsibility for the administration of Section 404 of the Clean Water Act, according to recommendations in a study by North Carolina State University's Center for Environmental Studies. Section 404 regulates the discharge of dredge-and-fill material into U.S. waters. After reviewing the study, officials of the state's Department of Natural Resources and Community Development have concluded that legal authority would be weakened under state administration. They also cite a lack of reliable data on which to base projections for administrative costs. Moreover, for the state to assume Section 404 primacy, action by the state legislature would be needed. The study was paid for by an EPA grant.

SCIENCE

The stratospheric ozone hole over Antarctica still has scientists in a quandary. There is not enough chlorine from chlorofluorocarbons to explain the phenomenon. Natural processes, such as excess solar radiation from sunspots cannot explain the ozone loss, because there is insufficient nitrogen dioxide in the hole; neither are there declines in ozone concentrations at higher altitudes. Strong winter updrafts fail as an explanation because identifiable particles that would be carried aloft are absent. Susan Solomon of the National Oceanic and Atmospheric Administration suggests that the cause may be a combination of the effects of chemical pollution and natural events such as the seasonal evaporation of stratospheric clouds over the polar region.

Tracing the migration of chemicals from nonpoint sources to groundwater is the objective of a study by Clifford Fedler of Texas Tech University (Lubbock, Tex.). One approach he is using is to inject a salt solution at a rate of 7.57 L/min for 24 h into a test well on the Texas Tech campus. The next step is to draw two samples a day from nine other wells in a grid extending 7.6–61 m away from the injection well. After the first week, sampling frequency is reduced to one sample a day for two more weeks. Sampling will continue for a year. Fedler says it is becoming apparent that agricultural chemicals are not reaching groundwater by saturation. Rather, erosion by wind and water deposits the chemicals into points of concentration from which they migrate to groundwater. Fedler's study is funded by a grant from the Texas Water Development Board.

Soils in the Southeast are retaining large quantities of sulfur deposited by acid rain, according to a study by the U.S. Geological Survey (USGS). USGS scientists say that slow accumulations of sulfur in the soil may temporarily mask long-term damage to streams in the region. After the soils are saturated with sulfur, however, their buffering ability could be overcome to allow a rapid rise in the streams' acidity. In a study reported in the Aug. 21, 1986, issue of *Nature,* Richard Smith and Richard Alexander of USGS estimate that 59% of the sulfur emitted by fossil-fuel-burning plants is retained in southeastern soils. They say 35% is retained by northeastern soils. They also note that about 25% of emitted sulfur is transported by air out of the southeast; 41% is transported out of the Northeast.

TECHNOLOGY

Principal organic hazardous components (POHCs) are destroyed by intense heat, not by flames, according to results of a study done for EPA by Barry Dellinger and his colleagues at the University of Dayton Research Institute (Ohio). The researchers also found that improperly controlled pyrolytic conditions (high temperatures without air) in an incinerator are responsible for most emissions and for the formation of products of incomplete combustion (PICs), some of which also may be hazardous. With funding from EPA (Cincinnati), Dellinger studied PIC formation under pyrolytic and starved-air conditions to assess pyrolytic techniques for thermal decomposition. His group concludes that laboratory testing of actual or simulated wastes under pyrolytic conditions is effective for predicting POHC stabilities and PIC emissions.

***Pseudomonas putida* may be able to decompose low-molecular-weight hydrocarbons** (LMWHs). Vincent Vilker of the University of California at Los Angeles found that *P. putida* grown on camphor generates the same enzymes as those made by the human liver. He says the enzymes "chewed right through" trichloroethylene, a widely used solvent that frequently contaminates groundwater. Vilker developed his program from observations that liver enzymes detoxify such LMWHs as chloroform, which is used as an anesthetic. He

Analyzing effluent products

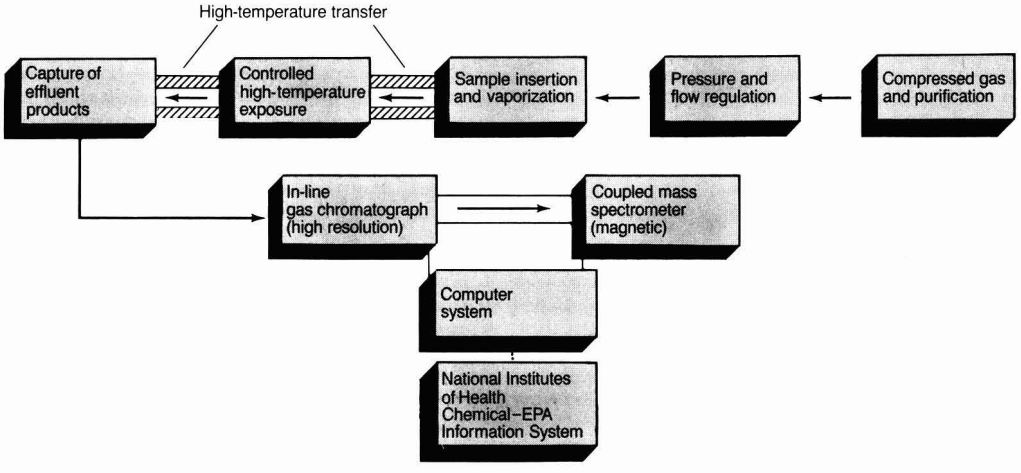

Source: EPA (Cincinnati)

expects the use of microbial methods to gain wide acceptance.

Four standard reference materials (SRMs) for analyzing airborne toxic organic compounds are now available from the National Bureau of Standards. The SRMs contain certified concentrations of benzene, bromobenzene, chlorobenzene, and toluene in nitrogen gas. One contains the compounds at the 250-ppb level, and the other contains the same compounds at the 10-ppm level. Each SRM is provided in a compressed-gas cylinder. The four compounds come from sources such as industrial emissions, hazardous-waste incineration, and automobile exhaust.

The world's largest reverse-osmosis (RO) desalting plant will provide water for irrigation near Yuma, Ariz., beginning in 1989. The facility will produce 72.4 million gal/day of desalted water; its capacity is expandable to about 96 million gal/day. The feed water to the plant, which contains about 3000 mg/L of salt, will be treated by chlorination and grit sedimentation. Next, the water will be softened, and substances harmful to the RO units will be removed. During that step, the water will be mixed, flocculated, and clarified. Chlorine will be injected to disinfect the clarified water, which will be filtered. The filtered water will pass through the RO units, where its salinity will be reduced to 285 mg/L. That water will be combined with untreated water to achieve a salinity of 700 mg/L and then discharged to the lower Colorado River. The softening and preparation reactors are furnished by Graver Company (Union, N.J.). The facility is to be administered by the U.S. Bureau of Reclamation.

BUSINESS

Du Pont company officials are advocating worldwide limits on production of chlorofluorocarbons (CFCs). In a policy statement sent to customers, they express their belief that CFCs pose no immediate threat to the stratospheric ozone layer. Nevertheless, they say that there is no knowledge of what a safe emissions growth rate for CFCs is. Du Pont officials recommended that EPA form an advisory group consisting of CFC users, CFC manufacturers, and environmental groups to deal with the question. Du Pont first introduced CFCs, also known as Freons, during the 1930s. The company produces 20–25% of the world's 1.09 billion kg/yr of CFCs.

Hazardous-waste-management permit processes should be made more flexible for companies not involved in landfilling, says Richard Fortuna, executive director of the Hazardous Waste Treatment Council (Washington, D.C.). The current system requires a draft permit and a 45-day comment period. Fortuna says that permit procedures take too long in cases involving waste generators' plans to use on-site mobile incinerators to destroy wastes. He calls for a process that accounts for new technology and the speed with which it can be put to work at a site. He also suggests statewide permits for mobile units. The current requirement is for a permit at each site.

Fortuna: Permit flexibility needed

ICF (Washington, D.C.) has won the first major contract awarded by EPA's newly created Office of Underground Storage Tanks. The terms of the contract call for ICF to assist in reducing health and environmental risks posed by leaking underground tanks. ICF's chief executive officer James Edwards says his company will provide analytical and economic support for evaluating the more than 1 million tanks used in the United States to store chemicals and petroleum products. ICF also will assess environmental risks posed by leaking tanks and develop, analyze, and implement approaches to manage these risks. EPA is authorized to award more than $9 million in contracts in this area during the next three years.

ES&T FEATURES

Analyzing PCBs

Basic information about PCBs and how they are identified and measured

Ann L. Alford-Stevens
Environmental Protection Agency
Cincinnati, Ohio 45268

Polychlorinated biphenyls (PCBs) were first reported in environmental samples in 1966 (*1*) and by 1974 were the most discussed of the organic pollutants (*2*). Although they may no longer have that distinction, PCBs are still a serious environmental problem, and many articles have been published about them. A recent review of the analytical chemistry of PCBs contained a bibliography of more than 1200 references (*3*). Most writers on the subject assume basic knowledge that is not readily available to many professionals, including lawyers, engineers, and journalists, whose work involves PCBs.

Probably the most important factor in selecting appropriate procedures for determining PCBs and in understanding analytical data is communication between knowledgeable analysts and data users. The basic information provided in this article should facilitate such discussions.

What is a PCB?

A PCB is any one of 209 compounds of the general formula $C_{12}H_xCl_y$, where $x = 0$–9 and $y = 10$–x. PCBs are produced by chlorinating the biphenyl compound, which has 10 positions (labeled 2–6 and 2′–6′ in Figure 1) available for chlorine atoms. Different structural arrangements make possible 209 compounds distributed among the 10 levels of chlorination (Table 1). Although 46 PCBs contain 5 chlorines (Cl_5 PCBs), only one contains 10.

The term congener is applied to any of the 209 possible PCBs. Isomers are PCBs that have the same number of chlorine atoms but differing arrangements of the chlorines on the biphenyl rings. For example, all 46 possible Cl_5 PCBs are isomers that make up an isomer group. Because chemical names include all the numbers of the chlorine positions on the two phenyl rings, such cumbersome nomenclature as 2,2′,3,3′,4,5,5′,6,6′-nonachlorobiphenyl (Cl_9 PCB) results. Ballschmiter and Zell devised a system that assigns each compound a number from 1 to 209 (*4*). This system has been adopted by the International Union of Pure and Applied Chemists; the numbers are also called IUPAC numbers.

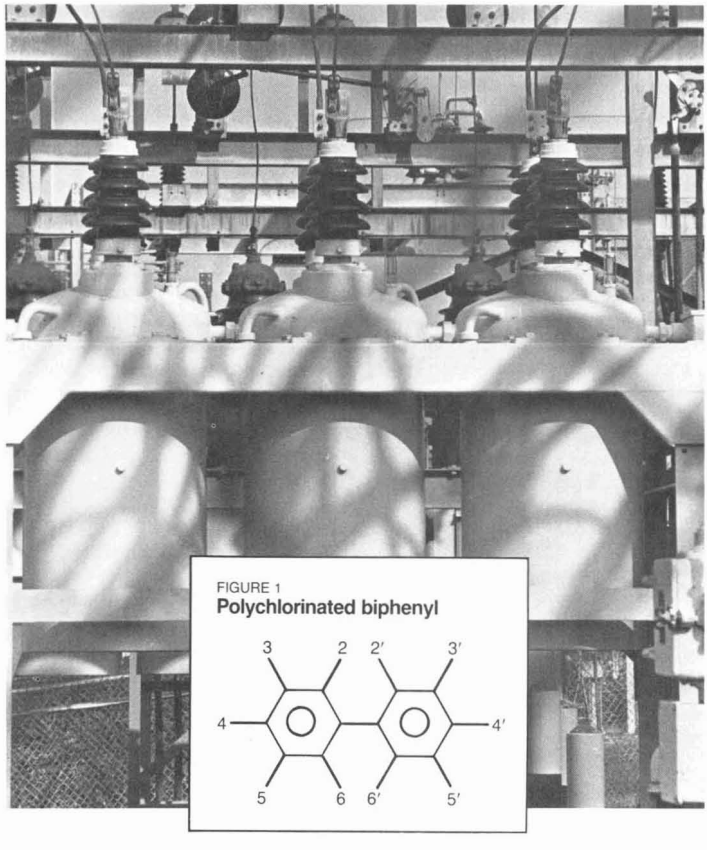

FIGURE 1
Polychlorinated biphenyl

Commercial formulations

Commercial PCBs were produced by collecting boiling-point fractions (Table 2) during distillation of chlorinated bi-

phenyl mixtures. In the United States, the only large producer of PCBs was Monsanto Chemical Company, which sold them from 1929 to 1975 under the Aroclor trademark. Not all PCBs are Aroclors, but most Aroclors are mixtures of PCBs. The name Aroclor is frequently used interchangeably with "PCB." In fact, a few Aroclor formulations were chlorinated terphenyls or mixtures of chlorinated terphenyls and chlorinated biphenyls (*2*). Non-PCB Aroclors have not attracted widespread concern; virtually all attention has focused on PCB Aroclors. The term Aroclor is used in this article to refer to commercial PCB formulations.

Each Aroclor is assigned a four-digit number (Table 2). For most PCB Aroclors (such as 1242), the first two numbers indicate the 12 carbons in the biphenyl ring, and the last two numbers indicate the weight percent of chlorine. Aroclor 1016, which is similar to 1242, was not named according to the standard designation.

Not all PCBs are present in Aroclors, because some biphenyl positions are more susceptible than others to chlorination. Although 125 PCBs have been found in Aroclors (*5*), the number of reported components of each Aroclor varies (Table 2), depending on the type of analysis performed and the quantity analyzed.

Properties of PCBs and Aroclors

The number of chlorine atoms contained in major Aroclor components increases with increasing percentage of chlorine. For example, Aroclor 1221 is composed principally of Cl_1 PCBs, but Aroclor 1260 contains mostly Cl_5, Cl_6, and Cl_7 PCBs. Most PCB congeners are solids at room temperature, but Aroclor formulations are viscous fluids that are resistant to acids, bases, and heat. PCBs have low water solubility, which decreases with increasing level

Analytical problems

Appropriate analytical procedures for PCB determinations must be selected to obtain needed information, depending on the particular situation. The range of potential PCB environmental problems is illustrated by two quite different situations.

- A transformer fluid that contains Aroclor 1254, along with chlorinated (Cl_3 and Cl_4) benzenes, has been spilled, and PCB-contaminated soil must be removed and disposed of appropriately.

Here the issue is not the identification of the PCBs but the measurement of Aroclor concentrations to determine whether PCB contamination exceeds the concentration of 50 μg/g. Conventional gas chromatography–electron capture (GC–EC) determinations of PCBs as Aroclors will provide the needed information. The Cl_3 and Cl_4 benzenes will produce EC detector responses that can be distinguished from the target Aroclors by retention times.

Furthermore, calibration of detector response over a wide concentration range is not necessary. The analyst should be given this information rather than being presented with a form requesting "PCB determinations."

- After a transformer fire, an area is contaminated, and the level of contamination must be determined before cleanup begins.

Here the problem is not only with PCBs but also with combustion products, which frequently include chlorinated dibenzo-*p*-dioxins and dibenzofurans. The information produced by a mass spectrometric detector is essential, because these three classes of compounds and other potential sample components have similar GC retention times and EC detector responses. In addition, samples would not be expected to contain intact Aroclors. Furthermore, the broad range of concentrations of concern and the variety of samples (wipe samples, ash, and soot) will require extensive consultation among data requesters, samplers, analysts, and data users.

TABLE 1
Distribution of PCBs by level of chlorination

Isomer group	Molecular formula	No. of compounds
Monochlorobiphenyls	$C_{12}H_9Cl$	3
Dichlorobiphenyls	$C_{12}H_8Cl_2$	12
Trichlorobiphenyls	$C_{12}H_7Cl_3$	24
Tetrachlorobiphenyls	$C_{12}H_6Cl_4$	42
Pentachlorobiphenyls	$C_{12}H_5Cl_5$	46
Hexachlorobiphenyls	$C_{12}H_4Cl_6$	42
Heptachlorobiphenyls	$C_{12}H_3Cl_7$	24
Octachlorobiphenyls	$C_{12}H_2Cl_8$	12
Nonachlorobiphenyls	$C_{12}HCl_9$	3
Decachlorobiphenyl	$C_{12}Cl_{10}$	1
Total number of congeners		**209**

TABLE 2
Properties of Aroclors

Property	Aroclor 1221	1232	1016	1242	1248	1254	1260	1262	1268
Density (lb/gal, 25 °C)	9.85	10.6	11.4	11.5	12.0	12.8	13.5	—	—
Distillation range (°C)	275–320	290–325	323–356	325–366	340–375	365–390	385–420	390–425	435–450
Viscosity (100 °F)	38–41	44–51	71–81	82–92	185–240	1400–2500	—	—	—
Vapor pressure (20 °C, mm Hg)	—	—	—	9.0×10^{-4}	8.3×10^{-4}	1.8×10^{-4}	0.9×10^{-4}	—	—
Vaporization rate[a] (mg/cm²/h)	1.7	0.87	—	0.34	0.15	0.053	0.009	0.013	—
Principal components	Cl_1	Cl_1–Cl_3	Cl_2–Cl_4	Cl_2–Cl_4	Cl_3–Cl_5	Cl_4–Cl_6	Cl_5–Cl_7	Cl_6–Cl_8	Cl_8–Cl_{10}
Reported number of components	10–25	16–34	27–49	27–74	43–63	27–116	35–124	—	—

[a]Exposure at 100 °C for 12 h; surface area 12.3 cm².
Sources: References 1, 3, and 6.

of chlorination. For example, the water solubility of one of the Cl_1 PCBs is 5.9 mg/L but that of Cl_{10} PCB is only 0.015 mg/L (*6*).

Vapor pressure (volatility) and degradability also decrease with increasing chlorine content. In addition, susceptibility to degradation depends on the structural arrangement of chlorine atoms among isomers. Some PCBs are preferentially accumulated in biota, whereas others are excreted. PCBs are strongly sorbed onto sediment, clay, and soil and are transported, for example, by runoff, erosion, precipitation, and wind.

The more soluble and volatile congeners are transported preferentially, and PCBs are now found in remote areas where Aroclors have never been used. These variable characteristics indicate why environmental samples frequently contain PCBs that are quite different from Aroclor formulations.

PCBs in the environment

During the 45 years that PCBs were in production and use, they were disseminated throughout the world. The very characteristics that made Aroclors desirable commercial products cause the persistent problems with PCBs. Originally, they were used as coolants and dielectric fluids in transformers and capacitors, as heat transfer fluids, and as coatings to reduce the flammability of wood products. Later, PCBs were incorporated into paints, inks, dust control agents, carbonless paper, and pesticides.

In 1976, Congress banned the manufacture, processing, distribution, and use of PCBs except in totally enclosed systems (electrical transformers, capacitors, and electromagnets). Since then, various regulations have attempted to control further distribution of PCBs, including those that are incidentally generated along with some desired product.

By 1978, U.S. landfills had accumulated 140×10^6 kg, and an additional 8.25×10^7 kg of PCBs and Aroclors had been introduced into the environment in forms available for transport, transformation, or accumulation (*6*). PCBs are still being used in 2.8 million capacitors and some 150,000 transformers. Some of these fail each year and release additional quantities into the environment (*7*).

Analytical procedures

Understanding results of PCB and Aroclor determinations requires some basic knowledge of the analytical procedures used to acquire the data. The basic elements of all PCB and Aroclor determinations are as follows:

- removal (extraction) of the compounds of interest from the sample matrix into one that can be analyzed,
- enrichment of the concentration relative to that of other sample components,
- separation of extracted components, and
- identification and measurement of the compounds of concern.

The first two items, which depend on the nature of the sample (for example, soil vs. biota), were reviewed recently (*3*); they are beyond the scope of this article. The third and fourth areas, separation and identification and measurement, are its focus.

Separation. Sample components are separated by gas chromatography (GC). The separation device is a GC column, which is a glass tube installed in an oven. After injection of a few microliters of a sample extract into the GC column, vaporized components move through the column with the carrier gas.

Components are separated because they travel at different rates depending on their affinities for the stationary liquid phase and the mobile gas phase. As sample components exit the GC column, they are observed as peaks on a graph (called a chromatogram) of relative abundance vs. time.

Gas chromatography columns are either low resolution (packed) or high resolution (capillary). A packed column is a glass tube (2–3 m × 0.7 cm i.d.) filled with an inert material that is coated with a liquid stationary phase. A capillary column is a glass tube (25–60 m × 0.25–0.5 mm i.d.) coated with a thin film of a liquid stationary phase. Capillary columns are widely used because they provide better separation of

FIGURE 2
GC separation of Aroclor 1260

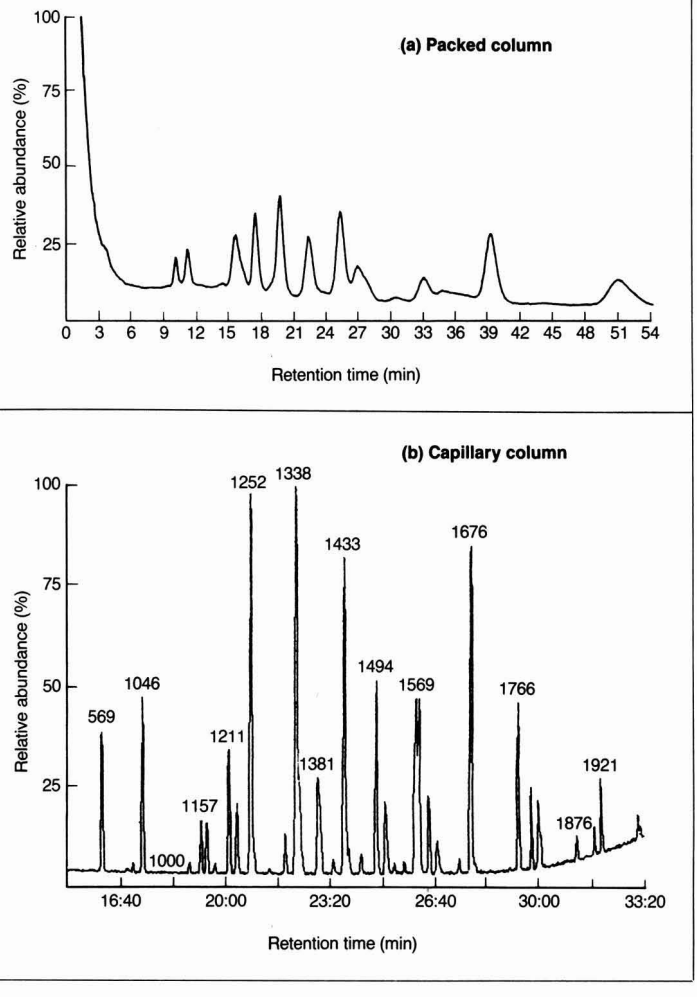

sample components than packed columns do.

The difference between separations obtained in packed and capillary columns can be demonstrated by chromatograms of Aroclor 1260 (Figure 2). The time required for a PCB to travel through a GC column (retention time) can be correlated with the level of chlorination, because retention times tend to increase with increasing chlorine content. This correlation is only approximate, however, because PCB retention times also vary with the structural arrangement of their chlorine atoms. For example, 3,3′,4,4′-Cl_4 PCB may be retained longer than any other Cl_4 PCB and even longer than some Cl_6 PCBs (*8*).

Identification and measurement. Sample components must be detected and measured as they elute from the GC column. Detectors can provide information about chemical structure or may give only general information about some chemical characteristic of the sample. Most PCB determinations are performed either by mass spectrometry (MS) or with an electron capture (EC) detector.

EC detectors. During the past two decades, most PCB determinations have involved the use of EC detectors to identify and measure PCBs in terms of Aroclors. The EC detector responds to any chlorinated or brominated compound, but it does not provide additional information about compound structure. It cannot distinguish between chlorinated or brominated compounds, and it does not provide information about the number of chlorine or bromine atoms present.

As sample components pass through the EC detector, electronegative compounds absorb (capture) electrons to produce a proportional decrease in base line electrical current, which is recorded continuously. The analyst must rely on appearance of a detector signal (peak) at the appropriate retention time to identify a sample component. The retention time must be determined by analyzing a standard of the compound of interest under the same conditions used to analyze the sample.

Unfortunately, another sample component to which the EC detector responds might have the same retention time as a PCB. Although all 209 PCBs have been synthesized (*8*), only about 90 are available commercially for use in laboratories that perform PCB determinations. Therefore, Aroclors have been used to determine when PCBs should appear in a sample chromatogram. Although Aroclors vary somewhat in composition from one batch to another and the samples frequently do not contain intact Aroclors, no alternative standards are available.

FIGURE 3
Comparison of Aroclor 1221 with an unknown

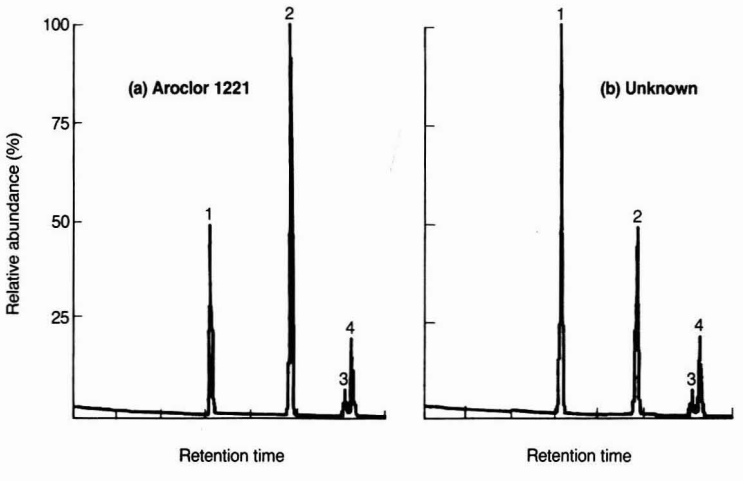

In using EC detectors to identify Aroclors, analysts rely on comparison of a chromatogram of a standard with that produced by a sample. In each case, analysts must judge whether the samples and Aroclor chromatograms are sufficiently similar, because acceptable differences have not been defined. This problem of pattern recognition is illustrated by comparison of chromatograms for Aroclor 1221 and an unknown (Figure 3). If all four peaks appear in the sample chromatogram (Figure 3b) at the same retention times and relative abundances as in the Aroclor 1221 chromatogram (Figure 3a), the pattern is easily recognized. If, however, their relative abundances are not equivalent, one identification criterion is not met. The absence of one of the peaks would make the identification of the sample component as Aroclor 1221 questionable. Most samples that contain PCBs produce far more complex patterns than the ones shown in Figure 3.

After identification of the Aroclor, concentrations of the components must be measured. In general, EC detector response to PCBs increases with increasing level of chlorination, but it also varies among isomers. Measured GC areas (or heights) of peaks produced by sample components must be related to those produced by Aroclor standards.

The most widely used Aroclor measurement procedure was developed in 1973 by Webb and McCall (*9*). They determined the weight percent of the major components of each GC peak observed from packed-column separation of Aroclors. This calibration procedure cannot be used with capillary columns. The Webb–McCall procedure involves measuring every sample component peak corresponding to an Aroclor peak, but analysts frequently select only a few GC peaks and relate measured peak heights or areas in samples to those in Aroclor standards.

The choice of the particular peaks measured can be a significant source of data variability. For example, if the height of peak 1 in Figure 3b is compared with Aroclor 1221 (Figure 3a), the reported sample concentration is twice that of the standard. If the height of peak 2 is selected, however, the reported concentration is half that of the standard.

The data user must understand the phrase "reported as Aroclor *x*." It means that the analyst thought the sample chromatogram more closely resembled Aroclor *x* than any other Aroclor, and the reported concentration was based on an Aroclor *x* standard.

When a sample contains a degraded Aroclor or a mixture of Aroclors, opportunities for qualitative and quantitative error increase substantially. Although some analysts can identify an Aroclor or mixture of Aroclors by a brief examination of a sample chromatogram, many cannot.

MS determination. In addition to all of the information obtained with an EC detector, a mass spectrometer provides the molecular weight and the number of chlorine atoms in a PCB. This information significantly increases the likelihood that the component has been correctly identified.

A brief discussion of how electron

FIGURE 4
Mass spectrum of a tetrachlorobiphenyl

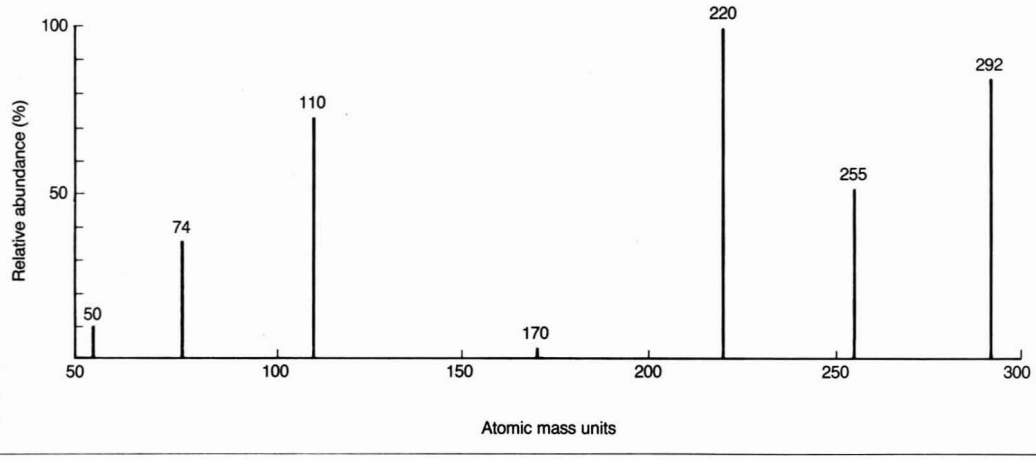

impact (EI) mass spectra are produced should facilitate an understanding of the data obtained. When sample components exit a GC column and enter a mass spectrometer, they are bombarded with electrons and lose electrons and atoms to form positive ions. When one electron is lost, the resulting ion (the molecular ion) has essentially the same mass as the original molecule. When the molecule loses an atom or groups of atoms, fragment ions are formed. With PCBs, molecular and fragment ions alike are formed.

In MS, the ions are subjected to conditions that cause them to travel through the mass analyzer at different rates, depending on the mass-to-charge ratio (m/z). A mass spectrum is produced by detecting and measuring the relative abundance of each m/z as a function of time. The characteristic features of a mass spectrum, such as that for a Cl_4 PCB (Figure 4), are among the data used to identify a PCB.

As sample components exit a gas chromatograph and enter a mass spectrometer, the molecules that are fragmented continually change. Therefore, rapid, frequent measurement of mass spectra is necessary, and a computer is needed to control the instrument and to receive and store data. With PCBs, the mass range of interest is usually about 45–520 atomic mass units (amu).

The computer is programmed to control MS operation to scan the mass range (about 475 amu) in 1 s or less. Therefore, only about 2 ms is spent acquiring data for each mass unit. Mass spectra are acquired repetitively and numbered sequentially from the beginning of data acquisition to its end. Information about the mass and relative abundance of each detected ion in each spectrum is stored, and all information acquired for a particular sample composes a data file.

A plot of the sum of the abundances of all ions in all spectra vs. spectrum number for each spectrum in a data file shows a total ion current profile (TICP). A TICP is similar to a chromatogram and is sometimes called a mass chromatogram or a reconstructed gas chromatogram. (The chromatogram in Figure 2b is a TICP).

Each sample component mass spectrum can be displayed by selecting an appropriate spectrum number and plotting mass vs. relative intensity. The data can be manipulated to enhance a spectrum when sample components are not completely separated or to eliminate ions produced from column coating materials and residual air. Using the TICP, the analyst can select an appropriate background spectrum and instruct the computer to subtract it from the spectrum of a sample component.

These actions can be illustrated with the GC peak labeled 1433 (which is actually a mass spectrum number) in Figure 2b. When this peak was expanded with computer software (Figure 5), two peaks (apex at 1433 and 1440) could be seen. Each dot shows where a scan (acquisition of a mass spectrum) ended, ion abundances were summed to produce a point on the TICP plot, and another scan began (at m/z 45). When that scan ends at m/z 520, measured ion abundances are added to produce the next point, and the points are connected to produce the TICP.

In this example, the mass spectrometer scanned from m/z 45 to m/z 520 18 times (spectra 1427–1444) while the two peaks were eluting. Spectrum 1433 could be selected to indicate the characteristics of the components producing one peak, and 1440 could show the other. Spectra 1437 and 1438 probably contain ions characteristic of both components. Therefore, spectrum 1437 or spectrum 1438 could be subtracted from 1433 to obtain one that does not contain ions produced only by the sample components represented by the peak that has its apex at 1440.

Because chlorine isotopes of mass 35 and mass 37 exist in known relative abundance in nature, the measured abundance of ions that contain chlorine in molecular ion isotope clusters indicates the level of chlorination of each detected PCB. PCBs that contain the same number of chlorine atoms produce very similar mass spectra. For example, all Cl_4 PCBs produce ions of known relative abundance in a cluster from m/z 290 to m/z 298, with major ions spaced 2 amu apart (Figure 4). Therefore, although mass spectra cannot be used to distinguish isomers, this spectral similarity allows identification of PCBs by level of chlorination.

Even with identification of PCBs by level of chlorination, measurement of PCB concentrations in samples that contain a variety of these compounds is a problem. A relatively recent approach to the problem of MS detector calibration is to use one PCB at each level of chlorination to represent all members of that isomer group (*3, 10*). Because the response varies from one isomer to the next, this approach produces results with an inherent error. This error is minimized by using a compound that produces a response near the mean response for all available members of the isomer group. A concentration for each isomer group is calculated, and a total PCB concentration is obtained by sum-

FIGURE 5
Repetitive acquisition of mass spectra produces a total ion profile

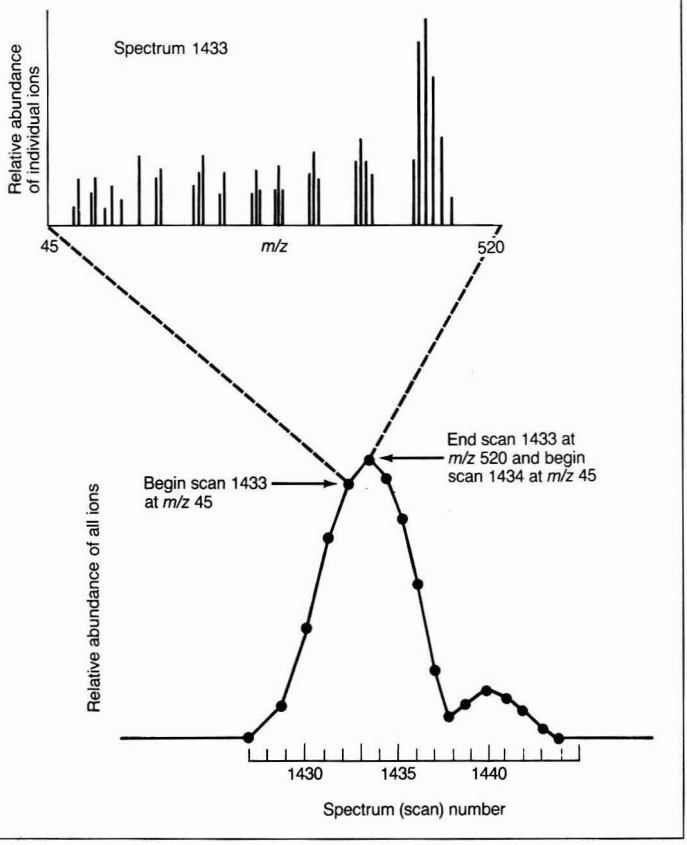

ming up the isomer group concentrations. One major advantage of this approach is that it is applicable to all samples that contain PCBs, whether they are intact Aroclors, degraded Aroclors, preferentially bioaccumulated congeners, or PCBs produced incidentally during some manufacturing or treatment process.

Although specific compounds are not identified with this approach, information about individual sample components is not lost. The number of PCBs identified in each sample can be reported, and a concentration can be estimated for each, if desired. In addition, measured retention times of identified PCBs can provide information about the probable presence or absence of specific PCBs because retention times for all 209 congeners have been published (*8*). The data user must remember, however, that retention times do not provide absolute identification.

Identification and measurement

Specific PCBs can be identified and measured by use of capillary column GC and standards for all 209 congeners. Although no one GC column has been found to separate all 209 PCBs well enough to produce discrete peaks, a single capillary column has been used to separate 187 congeners (*8*). To achieve maximum GC resolution, analysis times of 140–200 min are used.

Tentative identification based on relative retention time can be confirmed or refuted by introducing a pure standard of each candidate compound along with the sample extract aliquot. This approach is useful for seeking one or a few individual compounds but is not practical for routine monitoring for all possible PCBs.

Automated interpretation

Many analytical instruments incorporate computers to control operations and process data, and efforts to take advantage of their data-handling, interpretation, and computational abilities are continually expanding. Chemometrics, the application of computerized multivariate statistical methods to pattern recognition, is a rapidly expanding field that eliminates reliance on an individual's recognition of GC peak profiles to identify PCB sample components as specific Aroclors (*5*).

Other specialized software provides automated interpretation of mass spectra to identify and measure PCBs by level of chlorination (*11*). It evaluates sample component spectra by emulating human data interpretation and computational logic. A concentration is automatically calculated for each isomer group, and a total PCB concentration is calculated by summing isomer group concentrations. Undoubtedly, automated data interpretation will be applied increasingly in the future as new software becomes widely available and as analysts become more familiar with its operation.

Acknowledgment

This article has not been subjected to review by EPA. Therefore, it does not necessarily reflect the views of the agency, and no official endorsement should be inferred.

This article has been reviewed for suitability as an *ES&T* feature by Lawrence Keith, Radian Corporation, Austin, Tex. 78766.

References

(1) Jensen, S. *New Sci.* **1966,** *32,* 612.
(2) Hutzinger, O.; Safe, S.; Zitko, V. *The Chemistry of PCBs;* CRC Press: Boca Raton, Fla., 1980.
(3) Erickson, M. D. *Analytical Chemistry of PCBs;* Butterworth: Stoneham, Mass., 1986.
(4) Ballschmiter, K.; Zell, M. *Fresenius Z. Anal. Chem.* **1980,** *302,* 20.
(5) Dunn, W. J. III et al. *Anal. Chem.* **1984,** *56,* 1308.
(6) National Research Council Committee on the Assessment of Polychlorinated Biphenyls in the Environment. *Polychlorinated Biphenyls;* National Academy of Sciences: Washington, D.C., 1979.
(7) Miller, S. *Environ. Sci. Technol.* **1982,** *16,* 98A.
(8) Mullin, M. D. et al. *Environ. Sci. Technol.* **1984,** *18,* 468.
(9) Webb, R. W.; McCall, A. C. *J. Chromatogr. Sci.* **1973,** *11,* 366.
(10) Gebhart, J. E. et al. *Anal. Chem.* **1985,** *57,* 2458.
(11) Slivon, L. E. et al. *Anal. Chem.* **1985,** *57,* 2464.

Ann L. Alford-Stevens *is a research chemist in the Physical and Chemical Methods Branch of EPA's Environmental Monitoring and Support Laboratory. She manages research projects to develop and demonstrate analytical methods for the identification and measurement of organic chemical pollutants.*

Anaerobic wastewater treatment

Fourth of a six-part series on wastewater treatment processes

Perry L. McCarty
Daniel P. Smith
Stanford University
Stanford, Calif. 94305

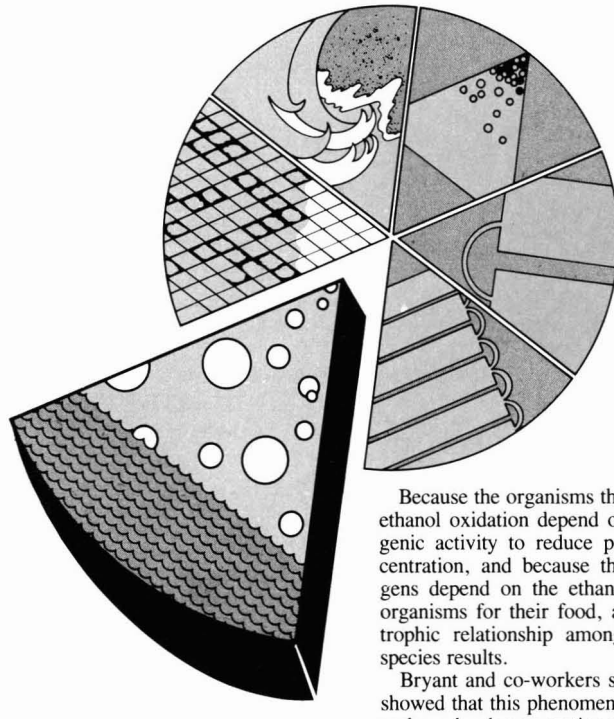

Anaerobic processes have been used for the treatment of concentrated municipal and industrial wastewaters for well over a century (*1*). These processes convert organic materials into methane, a fuel that can yield a net energy gain from process operations. Because of recent advances in treatment technology and knowledge of process microbiology, applications are now extensive for treatment of dilute industrial wastewaters as well. Europe has been the leader in applying the new technology, with far more installations than in the United States. The advantages of anaerobic treatment over aerobic treatment, current understanding of microbiology, and the newer processes have been described in detail by Speece (*2*).

It is apparent that biofilm processes offer greater stability than dispersed-growth processes do for treating dilute wastewaters. The reasons for this are not entirely obvious, and are probably multiple. One factor that makes biofilm processes more favorable is related to the role of diatomic hydrogen (H_2) in the control of process dynamics.

Interspecies hydrogen transport

Among the significant recent advances in the understanding of the ecology of the anaerobic process was that prompted by the discovery of Bryant et al. (*3*) that the conversion of ethanol to methane requires the combined activity of three separate species of bacteria, each carrying out one of the reactions listed in Table 1. The first species oxidizes ethanol, and in the process produces acetate and H_2. The second species is a methanogen that combines the hydrogen with carbon dioxide to form methane. The third species is also a methanogen, but one that splits acetic acid into carbon dioxide and methane.

The value $\Delta G^{o\prime}$ represents the standard Gibbs free energy available from the reactions when reactants and products are at unit activity and pH is 7. As indicated by the net equation in Table 1, $\Delta G^{o\prime}$ is negative; therefore, the overall reaction under such conditions is favorable thermodynamically. However, $\Delta G^{o\prime}$ for the conversion of ethanol is positive, and thus under standard conditions is not favorable. For this reaction to proceed, it is necessary for the concentrations of the reaction products (acetate and H_2) to be reduced sufficiently by the methanogens to yield a negative value for the actual free-energy ($\Delta G^{o\prime}$) change as given by

$$\Delta G' = \Delta G^{o\prime} + RT \sum_{i=1}^{m_k} \nu_{ik} \ln a_i \quad (1)$$

where ν_{ik} is the stoichiometric coefficient for component i in reaction k with m_k components, a_i is the activity of component i, R is the universal gas constant, and T is absolute temperature (*5*).

Because the organisms that carry out ethanol oxidation depend on methanogenic activity to reduce product concentration, and because the methanogens depend on the ethanol-oxidizing organisms for their food, a close syntrophic relationship among the three species results.

Bryant and co-workers subsequently showed that this phenomenon is a general one by demonstrating that the conversion of butyrate (*6*) and propionate (*7*), which are important intermediates in the process, also requires three species for conversion to methane gas, as indicated in Table 2. There is now general agreement that methane formation of complex organic materials is a three-stage process as illustrated in Figure 1 (*1, 9, 10*).

Complex organic materials are first hydrolyzed and fermented by facultative (those that live either in the presence or in the absence of oxygen) and anaerobic microorganisms into fatty acids. The fatty acids are then oxidized by β-oxidation to produce H_2 and acetate, processes termed dehydrogenation and acetogenesis, respectively. The last stage is methanogenesis. Although there are other ways in which methane can be formed, the pathways shown in Figure 1 tend to be most significant in anaerobic treatment of wastewaters.

The importance of H_2 in process control is illustrated perhaps better with propionate than it is with ethanol. This compound is formed through hydrolysis and fermentation of proteins and

0013-936X/86/0920-1200$01.50/0

carbohydrates and through oxidation of longer chained fatty acids. In treatment of complex mixtures, such as sewage sludge, as much as 30% of the electrons associated with the methane product will flow through propionic acid, as illustrated in Figure 1 (*8*). Thus, H_2 is an important intermediate, and the bacteria responsible for its conversion must be present in sufficient numbers for the process to operate efficiently. The amount of energy required to convert propionate to hydrogen and acetate is even less than that needed for ethanol conversion. This is illustrated by the relatively high positive $\Delta G^{o\prime}$ for its oxidation (Table 2).

The concentration of either acetate or hydrogen, or both together, could be reduced sufficiently to provide a favorable free-energy change for propionate oxidation. In fact, it is H_2 that tends to be most important in the control of the process. During anaerobic treatment, its concentration is reduced to a much lower level than that of acetate. The acetate concentration in an anaerobic treatment process tends to range between 10^{-4} M and 10^{-1} M; H_2 ranges between 10^{-8} M and 10^{-5} M, or about four orders of magnitude less. In addition, the H_2 partial pressure can change rapidly, perhaps varying by an order of magnitude or more within a few minutes. This is related to its rapid turnover rate, which is discussed later.

Figure 2 illustrates the relationship between H_2 partial pressure and $\Delta G'$ for the three steps in conversion of ethanol or propionate to methane, as calculated in Equation 1. The relationship between H_2 partial pressure (P_{H_2}) and H_2 molar concentration is given by Henry's law, which at 35 °C is as follows:

$$\frac{([H_2](g)\ (atm))}{([H_2](aq)\ (mol/L))} = 1330\ atm \cdot L/mol \qquad (2)$$

The concentrations of acetate and ethanol, the partial pressures of carbon dioxide and methane, and the pH values assumed for the calculations are typical of those in an efficiently operating anaerobic process. Figure 1 illustrates that for the three organisms responsible for conversion of ethanol to methane, the H_2 partial pressure must lie between 10^{-1} atm and 10^{-6} atm. This is a fairly large range. The energy available to the acetate-using methanogens is independent of H_2 partial pressure, whereas that of the hydrogen-producing and hydrogen-consuming species is very dependent on it. Higher H_2 partial pressures tend to supply more energy to the hydrogen-consuming species, whereas lower partial pressures result in a greater portion of the

TABLE 1
Conversion of ethanol to methane[a]

	$\Delta G^{o\prime}$ kJ
Ethanol	
$CH_3CH_2OH(aq) + H_2O(l) = CH_3COO^-(aq) + H^+(aq) + 2H_2(g)$	9.65
Hydrogen	
$2H_2(g) + {}^1/_2CO_2(g) = {}^1/_2CH_4(g) + H_2O(l)$	−65.37
Acetate	
$CH_3COO^-(aq) + H^+(aq) = CH_4(g) + CO_2(g)$	−35.83
Net	
$CH_3CH_2OH(aq) = {}^3/_2CH_4(g) + {}^1/_2CH_2(g)$	−91.55

[a]Thermodynamic values from Reference 4.

TABLE 2
Conversion of propionate and butyrate to methane[a]

	$\Delta G^{o\prime}$ kJ
Propionate	
$CH_3CH_2COO^-(aq) + 2H_2O(l) = CH_3COO^-(aq) + 3H_2(g) + CO_2(g)$	71.67
Hydrogen	
$3H_2(g) + {}^3/_4CO_2(g) = {}^3/_4CH_4(g) + {}^3/_2H_2O(l)$	−98.06
Acetate	
$CH_3COO^-(aq) + H^+(aq) = CH_4(g) + CO_2(g)$	−35.83
Net	
$CH_3CH_2COO^-(aq) + H^+(aq) + {}^1/_2H_2O(l) = {}^7/_4CH_4(g)\ {}^5/_4CO_2(g)$	−62.22
Butyrate	
$CH_3CH_2CH_2COO^-(aq) + 2H_2O(l) = 2CH_3COO^-(aq) + 2H_2(g) + H^+(aq)$	48.30
Hydrogen	
$2H_2(g) + {}^1/_2CO_2(g) = {}^1/_2CH_4(g) + H_2O(l)$	−65.37
Acetate	
$2CH_3COO^-(aq) + H^+(aq) = 2CH_4(g) + 2\ CO_2(g)$	−71.66
Net	
$CH_3CH_2CH_2COO^-(aq) + H_2O(l) + H^+(aq) = {}^5/_2CH_4(g) + {}^3/_2CO_2(g)$	−88.73

[a]Thermodynamic values from Reference 4.

FIGURE 1
Three stages of methanogenesis[a]

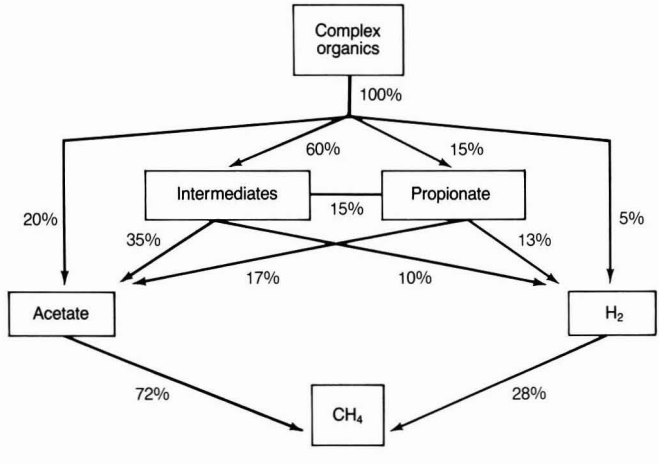

[a]Electron flow and the significance of propionate in the conversion of complex substrates are illustrated.
Source: Reference 8. Adapted with permission from *Biotechnological Advances in Processing Municipal Wastes for Fuels and Chemicals*, Argonne National Laboratory, 1984.

energy going to the hydrogen-producing bacteria.

With propionate use, the H_2 partial pressure must lie in a relatively narrow range, between 10^{-4} atm and 10^{-6} atm, assuming that the concentrations of other reactants and products do not change greatly. Because propionate is a major intermediate in the anaerobic treatment of most complex mixtures, H_2 partial pressures must remain within this range for such treatment systems to operate efficiently. This has significant implications for the way in which anaerobic treatment systems respond to perturbations, such as the sudden introduction of waste in a relatively high concentration. This will be addressed later.

The low concentration of H_2 within the digester also has implications for the rate of H_2 turnover within the system. Loading rates to anaerobic treatment systems are frequently reported as chemical oxygen demand (COD), with typical values of 1–30 kg COD/m^3·day. Theoretically, 0.064 kg COD can be converted into 1 mol CH_4 (*11*). With most complex wastes, about one-third of the methane results from H_2 consumption; the other two-thirds comes from acetate use (Figure 1).

Because 1 mol CH_4 requires 4 mol H_2, in a moderately loaded system that converts 10 kg COD/day per m^3 of reactor volume, H_2 generation would be 0.33(4)(10)/0.064 or 206 mol H_2/m^3·day. For H_2 partial pressure of 4×10^{-5} atm, the corresponding H_2 solution concentration would be 3×10^{-5} mol/m^3. This calculation is derived from Equation 2.

For this example, the turnover rate of the H_2 pool would then have to be 206/3.0×10^{-5}, which corresponds to 6.8×10^6/day or ~80/s. H_2 is therefore transferred rapidly from the H_2-consuming bacteria. How can this be accomplished? The producing and consuming species must be close together within the treatment reactor.

For processes on this microscale, diffusion is the main mechanism for H_2 transport between species. This is illustrated in Figure 3. As a simple example, consider one-dimensional flow of H_2 between species separated by a distance of Δz:

$$\text{Flux} = J = R_t M_d = R_t A \Delta z \left(\frac{C_1 + C_2}{2}\right) \quad (3)$$

where J is the flux of H_2 between the organisms (mol·sec^{-1}); R_t is the H_2 turnover rate (sec^{-1}), M_d is the H_2 mass in solution (mol); Δz is the distance between species (cm); C_1 and C_2 are the H_2 concentrations at the surface of the H_2-producing and H_2-consuming species, respectively (mol·cm^{-3}); and A is the cross-sectional area across which diffusion occurs (cm^2).

Because the flux results from diffusion

$$J = -DA \frac{(C_2 - C_1)}{\Delta z} \quad (4)$$

where D is the molecular diffusivity of H_2 in water (cm^2 sec^{-1}).

Making Equations 3 and 4 equal to one another (as for steady-state operation) and rearranging them gives Equation 5:

$$\Delta z = \left[-\frac{2D}{R_t} \cdot \frac{C_2 - C_1}{C_1 + C_2}\right]^{1/2} \quad (5)$$

Consider the case in which $D = 5.85 \times 10^{-5}$ cm^2 sec^{-1}, $R_t = 320$ sec^{-1}, $C_2 = 5 \times 10^{-11}$ mol cm^{-3} (log $P_{H_2} = -4.2$), and $C_1 = 5 \times 10^{-12}$ mol cm^{-3} (log $P_{H_2} = -5.2$). Here, the calculated Δz is 11 μm. This distance is equal to about 10 bacterial widths. With higher reported COD loadings of 40 kg COD/m^3·day, Δz would be about 5 μm. The bacteria must indeed be close together. This simple analysis suggests that process designs that encourage different species to live in proximity to one another are more favorable for high rates of conversion per unit volume of reactor.

The case for biofilm

In an ideal completely mixed or continuous-stirred-tank reactor (CSTR) as illustrated in Figure 4, the individual bacterial species are dispersed uniformly throughout the system, and the composition of reactants, intermediates, products of biotransformation, and bacterial species is homogeneous throughout the reactor. In such a system, the composition of the effluent stream is identical to that within the reactor itself. Given a model for the relationship among reactant, product concentration, and reaction rate, the rate

FIGURE 2
Effect of H_2 partial pressure on free energy[a]

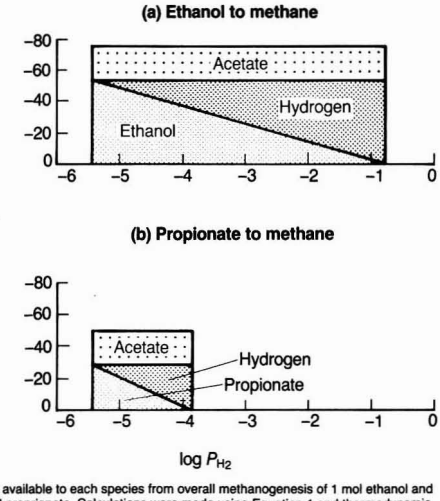

[a]$\Delta G'$ available to each species from overall methanogenesis of 1 mol ethanol and 1 mol propionate. Calculations were made using Equation 1 and thermodynamic values from Tables 1 and 2, assuming that [ethanol] = [propionate] = [acetate] = 0.0001; [methane] = 0.7 atm; [carbon dioxide] = 0.3 atm, pH = 7.0; [water] = 1.0, pH = 7.0, and T = 308 K.

FIGURE 3
Transport of H_2 from hydrogen-producing to hydrogen-consuming species[a]

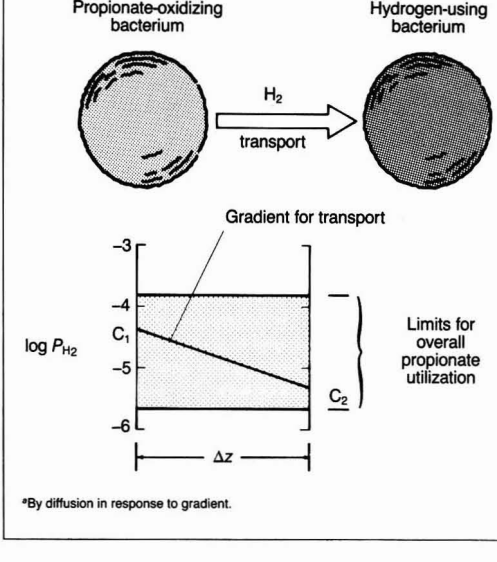

[a]By diffusion in response to gradient.

can be estimated from an analysis of effluent characteristics alone. This is not the case with biofilm reactors.

A biofilm is often thought of as a dense layering of microorganisms attached to an inert surface, but it also can be a dense aggregation of microorganisms held together by electrostatic forces or synthetic or natural polymers. As such, a CSTR can contain biofilms in suspension in addition to dispersed microorganisms. Thus, the distinction between dispersed-growth and biofilm reactors may not always be obvious. It may be necessary to examine the microorganism distribution within a given reactor to know how to characterize it.

The important distinction relates to whether the kinetics of the biological reactions that occur can best be described by equations appropriate for dispersed growth or biofilms. With dispersed growth, the microorganisms at any given location respond to the substrate concentration, which is the same as that in the bulk liquid phase surrounding it; in a biofilm, the substrate concentration can be different from that in the bulk liquid.

A cross section of a hypothetical biofilm growing on a support medium in a reactor is illustrated in Figure 5 for the case in which both ethanol and propionate are substrates fed to the reactor. The two substrates move from the bulk liquid within the reactor to the biofilm surface by mass transport at a rate governed by reactor hydrodynamics. They then diffuse into the biofilm, where they are transformed by ethanol- and propionate-using bacteria into acetate and hydrogen.

These products are then converted by the two physiological groups of methanogens. In response to gradients, some of the hydrogen and acetate diffuses or is otherwise transported back to the bulk liquid. The activities of the four bacterial species within the biofilm cannot be deduced readily from the bulk liquid composition. This is in contrast to dispersed growth. Indeed, the activity of the various species can vary markedly throughout the biofilm.

In the hypothetical example shown in Figure 5, the H_2 partial pressure is higher just inside the biofilm than it is in the bulk liquid itself. However, within the depths of the biofilm, partial pressure can be much lower. Reactant and product concentrations vary throughout the biofilm. Ethanol conversion is favored thermodynamically at much higher acetate and hydrogen concentrations than is propionate conversion. Therefore, ethanol conversion would be likely to occur near the face of the biofilm. At some depth within the biofilm, the concentrations of acetate and H_2 are lowered enough that propionate use is favorable.

FIGURE 4
Reactor configurations

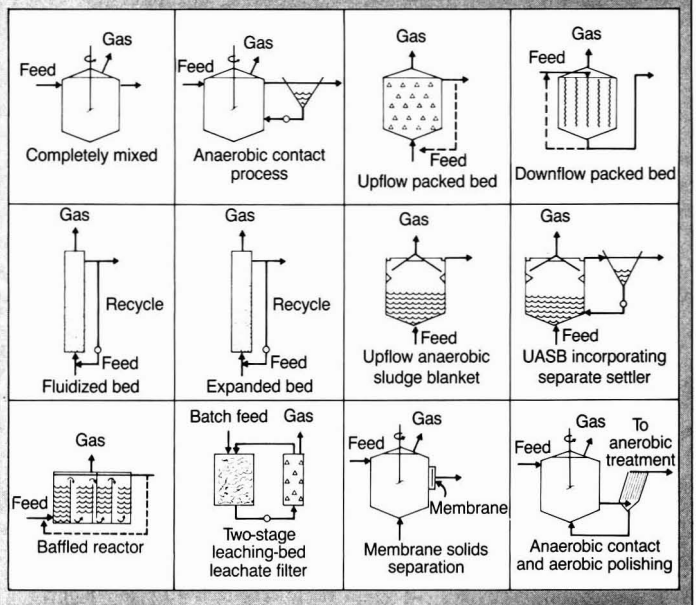

Source: Reference 2. Adapted with permission from *Environmental Science & Technology*
© 1983, American Chemical Society.

This could be true even if the bulk liquid composition was such that propionate could not occur at the biofilm surface. A significant advantage of biofilms is that reactions can take place within their depths, even though the bulk liquid composition may not be favorable for this. In addition, bacterial mass is generally much denser in a biofilm. This narrows the distances between species, allowing higher conversion rates. These factors may help to explain why biofilm systems seem to offer a distinct advantage over dispersed-growth systems.

Other reactor systems have been suggested to separate the different phases in the overall methane fermentation process, thus offering an opportunity to optimize each phase separately (*12*). Such separation is obviously not possible where different species must be close together, as is the case for propionate use. However, the first stage of fermentation and hydrolysis (Figure 1) could be separated from the last two.

The use of tubular reactors or two or more CSTRs connected in series are similar approaches. Fermentations that might result in high H_2 concentrations can take place at the head end of a tubular reactor or in the first stage of a staged reactor. For example, carbohydrate hydrolysis and fermentation might be encouraged in the first stage. In making such a separation, the potential danger posed by high H_2 concentrations, which could prevent propionate or butyrate oxidation, can be minimized. Short-chain fatty acid conversion could then take place within the middle sections, at the end of tubular reactors, or in the later stages of series reactors.

Indeed, tubular and staged reactors for anaerobic treatment are in common use. Many biofilm reactors tend to operate as tubular reactors as well, thus further increasing their reliability. One danger, however, is that organic acid production tends to be higher near the entrance to such systems, where fermentation occurs. This can increase the risk of unfavorably low pH, perhaps offsetting some of the advantages discussed here. Recycling can help overcome this potential problem by lowering influent concentrations.

Reactor configurations

Figure 4 illustrates various reactor configurations used in anaerobic treatment as described in greater detail by Speece (*2*). The completely mixed (CSTR) and anaerobic contact processes are systems that have been in operation for years. They are generally considered dispersed-growth systems. However, when they contain flocculated particles, they may feature some characteristics of biofilm systems. Upflow and downflow packed beds have been gaining popularity since 1970.

They tend to respond as biofilm reactors.

Of particular interest here are the upflow anaerobic sludge blanket (UASB), fluidized, expanded-bed, and baffled reactors that have been introduced within the past decade. All are capable of exceptionally high volumetric rates of treatment (6–20 kg COD/m^3·day) for relatively dilute industrial wastewaters ($\leq$ 1000 mg/L COD). All offer the possibility of maintaining a large bacterial mass within the reactor system as required for high decomposition rates per unit volume. In addition, they tend to act more like biofilm than like dispersed-growth systems.

The success of the UASB reactor is the result of the development of a granular sludge of nearly spherical particles 1–5 mm in diameter (*13*). These particles consist of a dense packing of the mixture of microorganisms responsible for anaerobic treatment. As such, this system acts like a biofilm in that there is substrate diffusion into the particles of microorganisms and product diffusion out. It thus offers the same advantages as biofilms do for anaerobic wastewater treatment.

In fluidized-bed and expanded-bed systems, an active biofilm develops on small, dense, inert substrate material. Granular particles also develop within the baffled reactor. Thus, most of the newer anaerobic reactors that offer stable and reliable treatment of industrial wastewaters can be modeled mathematically and conceptually as biofilm systems. The presence of the biofilms appears to be one of several reasons for their operating stability.

Studies of H_2 control

To verify that anaerobic treatment operates in accordance with free-energy considerations, a series of anaerobic treatment systems was operated in the Stanford University Water Quality Control Research Laboratory. Several CSTRs were included, as were an anaerobic filter and a baffled reactor (Figure 4). Ethanol and propionate were used as the feed for some of these systems, one CSTR received combined primary and secondary municipal wastewater sludge, and the anaerobic filter received pulp evaporator condensate wastewater and a synthetic organic mixture of acetone and isopropanol. Appropriate pH buffers and inorganic nutrients required for microbial growth were included.

All but one of the reactors were operated as continuous-flow systems (the sludge CSTR was operated semi-continuously), and H_2 partial pressure in the gas phase was determined under steady-state conditions of operation using a reduction gas detector. This instrument permits the quantification of H_2 to less than 10^{-7} atm in the gas phase. Hydrogen was passed through a heated mercuric oxide bed to release mercury vapor, which was measured by ultraviolet photometry. With steady-state operation, it was assumed that H_2 in the bulk liquid and H_2 in the gas were in equilibrium. This assumption can be used only with caution.

FIGURE 5
Substrate and product diffusion[a]

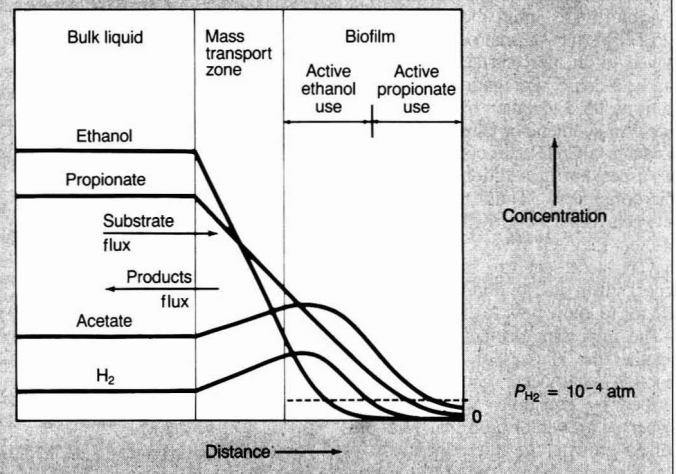

[a]Into and out of biofilm to show the effect of resulting H_2 partial pressure for ethanol- and propionate-using bacteria.

Table 3 is a summary of typical H_2 partial pressures measured during steady-state operation of the various systems. Estimated H_2 turnover rates (R_t) also are included. In all cases P_{H_2} was in the range of 1–20 × 10^{-5} atm. This is the range within which propionate use is thermodynamically favored. In general, reactors that received ethanol operated near the higher end of the range; those with other substrates operated near the lower end.

Thus, under normal conditions of operation, and even with an energetic substrate such as ethanol in the feed, hydrogen-using bacteria do reduce H_2 concentrations to a range that allows use of less energetic propionate and longer chained fatty acids. In addition, reactors that fostered biofilms (the baffled reactor and the anaerobic filter) produced lower P_{H_2} values for a given H_2 turnover rate than did reactors that favored dispersed growth (CSTRs). This is to be expected in light of the closer packing of microorganisms in biofilms.

The reactions proceeded at practical rates even though reactants and products were very near to equilibrium concentrations. Microbial enzymes are indeed amazing chemical converters.

Now, let us examine the effect of a sudden overload of a substrate such as ethanol. Figure 6 shows how the concentrations of propionate, acetate, and H_2 were affected by the sudden introduction of 0.023 M ethanol to a CSTR operated at steady state with a 15-day hydraulic residence time and a continuous feed of 0.05 M ethanol and 0.05 M propionate. Because the reactor in this case contained an active population of ethanol-oxidizing bacteria, ethanol concentration dropped rapidly. As a result, both the acetate concentration and the H_2 concentration increased. The H_2 concentration rose rapidly by an order of magnitude, but nevertheless stayed within a range that was compatible with ethanol use, as it must.

This elevated H_2 concentration resulted in a positive $\Delta G'$ for propionate oxidation, and propionate use stopped. This is evidenced by the fact that propionate concentration increased at a rate consistent with the rates of its introduction and withdrawal from the reactor (Figure 6). After the ethanol was consumed and the P_{H_2} dropped to near its former steady-state concentration, propionate use resumed. These results are consistent with expectations of dispersed-growth reactor performance based on free-energy considerations. They can help explain why propionate concentrations can increase in a heavily loaded reactor.

A similar experiment was conducted using a baffled reactor. Here, the feed concentrations were 0.1 M propionate and 0.1 M ethanol, and the detention time was 48 h. A high recycle rate (100:1) of effluent to influent was used

to obtain near-uniform substrate concentrations throughout the reactor. The response, illustrated in Figure 7, was somewhat more dramatic than that of the CSTR because the loading per unit volume was much higher.

Again, there was an increase in propionate. However, because the propionate concentrations did not follow the tracer line, some biological removal is assumed, even though the measured H_2 partial pressure in the gas phase reached nearly 10^{-3} atm. This gas-phase partial pressure would result in a positive $\Delta G'$ such that the observed biological removal of propionate would not be expected. However, a possible explanation is provided if one considers the two factors discussed previously. First, the baffled reactor does function similarly to a staged reactor. A high rate of ethanol use in the first stage could result in high H_2 production so that even when mixed with lower H_2 concentration gases from subsequent stages, the resulting gaseous H_2 concentration would be high.

In addition, the biofilm resulting from the granular sludge in this reactor would allow propionate use to occur within its depths, where H_2 concentration would be low. The relative importance of these possibilities is not known at this point. However, this example illustrates the potential advantages of staged and biofilm processes.

Caveats for use

Anaerobic treatment processes require the presence of a diverse and closely dependent group of bacteria to

FIGURE 6
Response of a completely mixed reactor

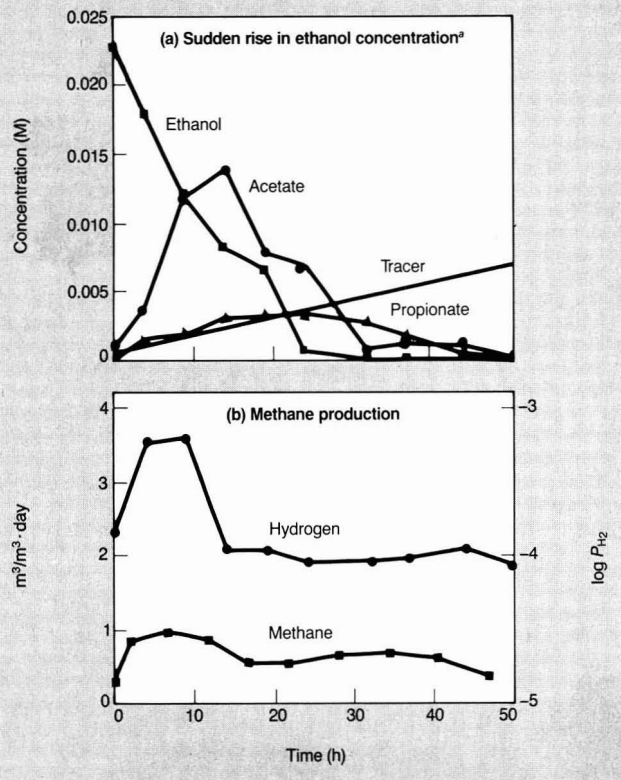

[a]Concentration raised by 0.023 M at time zero. Tracer line shows hypothetical change in propionate concentration without use. The reactor was fed 0.05 M ethanol and 0.05 M propionate continuously at a 15-day hydraulic detention time.

TABLE 3
H_2 Partial pressures measured under steady-state conditions

Reactor configuration	Feed substrate	Hydraulic detention time (days)	COD loading (kg COD/m³·day)	COD conversion to CH_4 (%)	P_{H_2} (10^{-5} atm)	Estimated H_2 turnover rate (R_t, sec^{-1})[a]
CSTR	0.05M Ethanol	15	0.3	>90	19	0.5
CSTR	0.10M Ethanol	9.1	1.0	>90	20	1.7
CSTR	0.10M Ethanol	5.0	1.8	30	7	9
CSTR	0.05M Ethanol 0.05M Propionate	15	0.7	>90	12	2
CSTR	0.10M Ethanol 0.10M Propionate	10	2.0	>90	15	5
CSTR	0.10M Propionate	9.1	1.2	>90	6	8
CSTR	0.10M Propionate	10	1.1	>90	5	9
CSTR[b]	Sludge 0.10M Ethanol	10	3.0	>70	7	11
CSTR[b]	Sludge	30	0.7	>60	1	15
Baffled reactor	0.10M Propionate	2	5.6	>50	2	86
Baffled reactor	0.10M Ethanol 0.10M Propionate	2	10	>70	12	26
Baffled reactor	No feed	Infinite	—	90	1	0
Anaerobic filter	0.0017M Acetone 0.0017M Isopropanol	6	0.08	>90	0.7	4
Anaerobic filter	Pulp evaporator condensate	1	15	>80	2	32

[a]Based on Tables 1 and 2, otherwise assuming 33% of CH_4 results from H_2 use.
[b]Operated semicontinuously.

FIGURE 7
Response of a baffled reactor

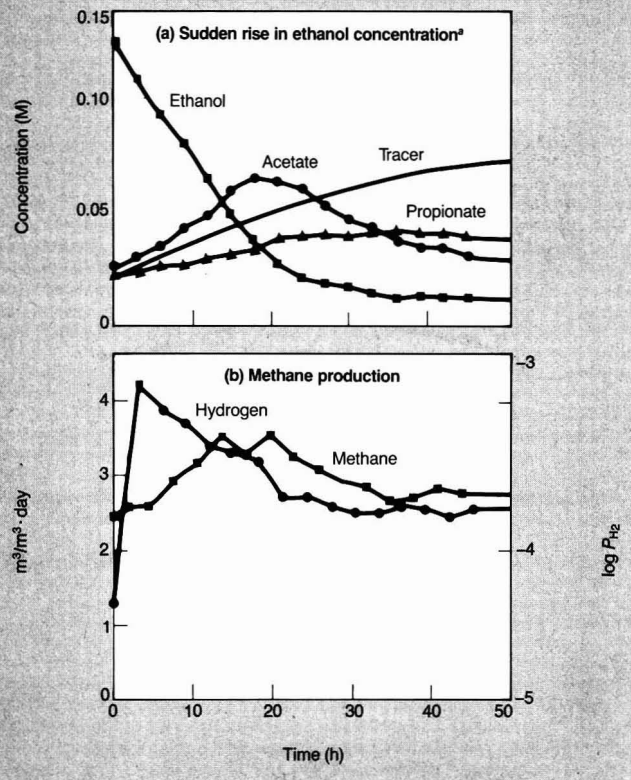

[a]Concentration raised by 0.12 M at time zero. Tracer line represents hypothetical change in propionate concentration

bring about the complete conversion of complex mixtures of substrates to methane gas. It is puzzling that single species of bacteria have not evolved to convert at least simple substrates such as carbohydrates, amino acids, or fatty acids all the way to methane.

In any event, the fact that multiple species are required should be recognized by engineers because it affects the choice of treatment system. H_2, which is produced by substrate oxidation, must be consumed rapidly and efficiently by methanogenic bacteria for the oxidation of many substrates and intermediates to occur. This requires the hydrogen-producing and hydrogen-consuming species to remain in proximity to one another, a requirement met by processes in which biofilms develop. Biofilms also permit a diversity of environments to develop in proximity to one another so that suitable conditions for the oxidation of each substrate and intermediate product can exist somewhere within the biofilm.

Most of the newer anaerobic treatment systems, including the UASB, fluidized-bed, and baffled reactors, tend to act as biofilm reactors. As such, they permit development of the dense packing of microbial species required for high rates of substrate use. These reactors offer efficient and reliable conversion of relatively dilute industrial wastewaters into methane gas at high loading rates. Although experience with these systems is still rather limited in the United States, there are many successful installations in Europe. There is a need to learn more so that the most appropriate applications can be determined.

With the ability to monitor H_2 partial pressure at levels of significance to anaerobic treatment, more attention might be given to use of this as a tool in the control of the process and in the diagnosis of process problems. The recent recognition of the broad spectrum of wastewaters, including phenolic wastewaters, that can be treated by this process suggests that much is to be gained from research directed toward understanding this important and interesting wastewater treatment process.

Acknowledgement

This research has been supported in part by National Science Foundation Grant CEE-8215436.

This article has been reviewed for suitability as an *ES&T* feature by Richard Speece, Drexel University, Philadelphia, Pa. 19104.

References

(1) McCarty, P. L. In *Anaerobic Digestion 1981;* Hughes, D. E. et al., Eds.; Elsevier: Amsterdam, Netherlands, 1981, pp. 3–22.
(2) Speece, R. E. *Environ. Sci. Technol.* **1983,** *17,* 416–27.
(3) Bryant, M. P. et al. *Arch. Mikrobiol.* **1967,** *59,* 20–31.
(4) Thauer, R. K.; Jungerman, K.; Decker, K. *Bacteriol. Rev.* **1977,** *41,* 100–180.
(5) McCarty, P. L. *Anaerobic Biological Treatment Process;* Pohland, F., Ed.; Advances in Chemistry 105; American Chemical Society: Washington, D.C., 1971; pp. 91–107.
(6) McInerney, M. J.; Bryant, M. P.; Pfennig, N. *Arch. Microbiol.* **1979,** *122,* 129–35.
(7) Boone, D. R.; Bryant, M. P., *Appl. Environ. Microbiol.* **1980,** *40,* 626–32.
(8) McCarty, P. L.; Smith, D. In *Biotechnological Advances in Processing Municipal Wastes for Fuels and Chemicals,* AML/CNSV-TM-167; Antonopoulos, A. A., Ed.; Argonne National Laboratory: Argonne, Ill., 1984; pp. 53–66.
(9) Zehnder, A. J. E. *Water Pollution Microbiology;* Wiley: New York, 1978; Vol. 2, pp. 349–76.
(10) McInerney, M. J.; Bryant, M. P. *Anaerobic Digestion;* Stafford, D. A.; Wheatley, B. I.; Hughes, D. E., Eds.; Applied Science: London: 1980; pp. 91–98.
(11) McCarty, P. L. *Public Works* **1964,** *95,* 107–12.
(12) Ghosh, S.; Conrad, J. R.; Klass, D. L. *J. Water Pollut. Control Fed.* 1975, *47,* 30–45.
(13) Hulshoff Pol, L. W. et al. In *Preprints of Papers Presented at the International Association of Water Pollution Research Specialized Seminar on Anaerobic Treatment of Wastewater in Fixed Film Reactors*; Henze, M.; Harremoës, P., Eds.; Department of Sanitary Engineering, Technical University of Denmark: Lyngby, Denmark, 1982; pp. 305–18.

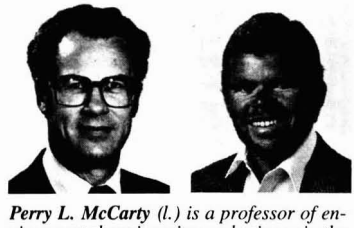

Perry L. McCarty *(l.) is a professor of environmental engineering and science in the civil engineering department of Stanford University. He holds a B.S. in civil engineering from Wayne State University and an M.S. and an Sc.D. in sanitary engineering from the Massachusetts Institute of Technology.*

Daniel P. Smith *(r.) is a doctoral candidate in environmental engineering and science at Stanford University. His research is on hydrogenotrophic control in methanogenic processes. He previously served as water quality chief for the New Orleans District Corps of Engineers. He has a B.S. in civil engineering from the State University of New York at Buffalo and an M.S. in sanitary engineering from Tulane University.*

Finally . . . Superfund

Richard M. Dowd

After nearly two years of conflict and debate, Congress has passed and President Ronald Reagan has signed the Superfund Amendments and Reauthorization Act of 1986. The statute contains four titles. Titles 1 and 2 rewrite the original Superfund law, the Comprehensive Environmental Response, Compensation and Liability Act of 1980.

The financing portions of the bill will, over its five-year lifetime, raise $8.5 billion from a general manufacturing tax, specific levies on chemical and petroleum products, and a tap on general treasury funds. These monies will be used to pay for cleaning up abandoned hazardous waste sites for which the responsible parties cannot be found and assessed for the costs. In addition, the bill finances a new Leaking Underground Storage Tank Trust Fund by levying a new tax of 0.1¢/gal on all types of motor fuels.

The new Title 3 contains emergency planning and community right-to-know provisions that require communities to gather and publish information on hazardous substances that can affect them either through accidental releases or through routine emissions of hazardous materials. EPA must publish an acute-hazards list naming 400 of these substances within 30 days.

The agency must also begin drawing up rules establishing a threshold planning quantity (TPQ) for each substance on the acute-hazards list. If EPA does not establish TPQs, the new law will automatically set the quantity at 2 lb for each substance. If a TPQ for a hazardous substance exists at a facility, the facility is subject to Superfund's emergency planning requirements.

Finally, Title 4 establishes a radon gas and indoor air quality research program.

Other highlights

Superfund requires a total reevaluation of the existing Hazardous Ranking System (HRS) that determines whether a site is to be placed on the National Priority List (NPL) of facilities that require cleanup.

Tight timetables are set for EPA to begin remedial investigation feasibility studies for some 650 sites within five years, and EPA is directed to clean sites at a pace much more rapid than the previous rate of fewer than a dozen over the past five years. The bill also authorizes EPA to provide technical assistance grants of up to $50,000 per site to assist participation by the general public in decisions involving cleanups.

The new law authorizes potentially responsible parties (PRPs)—entities that are liable, as contributors of wastes to specific abandoned sites—to carry out their own remedial investigation and feasibility studies and to take action to clean up sites. In these cases, the government would supervise qualified contractors paid by the PRPs.

Superfund explicitly authorizes EPA to negotiate settlements with those responsible for a hazardous-waste site, and the bill establishes procedures to encourage settlements instead of lengthy, costly law suits.

The new law gives special relief from non-negligent liability to contractors who carry out cleanup activities. The inability of many firms to obtain liability insurance in the market has hindered recent cleanup projects.

Addressing the "how clean is clean?" issue, the law specifies criteria for EPA to use in determining appropriate cleanup levels. These standards are to take effect 30 days after enactment and require, as a minimum, that cleanups meet any legally applicable federal, state, or local standard, criterion or limitation. In many cases, the most stringent standards would be the Safe Drinking Water Act's maximum contaminant level goals, which are set at zero for carcinogens. All cleanups are required to be done as cost-effectively as possible.

An initial $50 million is provided for the agency to fund the Toxic Substance and Disease Registry (ATSDR)—an independent arm of the Department of Health and Human Services, which will conduct health research at sites as deemed necessary by the ATSDR administrator. By mid-April 1987, ATSDR and EPA are to prepare a list of the 100 substances most commonly found at Superfund sites; an additional 100 substances are to be added within 24 months. Each listing must be accompanied by a summary of the substance's characteristics, toxicity, and known health effects.

Superfund explicitly establishes programs for research, development, demonstration, and training to encourage alternative and innovative treatment technologies and to improve detection and assessment of effects and risks regarding human health.

The law requires that each state certify, within three years, that it has sufficient disposal capacity to handle all hazardous wastes generated within its borders for the next 20 years. Without that assurance, Superfund monies will be withheld from any noncomplying state except in certain emergency cases.

Superfund will drive EPA's work agenda for some time to come. These highlights are only a sample of the bill's major provisions; others will be discussed in future columns.

Richard M. Dowd, Ph.D., is a Washington, D.C., consultant to Environmental Research & Technology, Inc.

0013-936X/86/0920-1207$01.50/0

ES&T VIEWS

Atmospheric warm-up

By Sandra L. Postel

Sandra L. Postel

Scientists now expect that over the next several decades the atmospheric buildup of carbon dioxide and other "greenhouse" gases will raise the Earth's temperature to levels unprecedented in human history. The costs of adapting to higher temperatures, shifts in rainfall patterns, and a rise in ocean levels will severely strain the economies of industrial and developing countries alike. Maintaining food security, for example, could require worldwide investments of nearly $200 billion to adjust irrigation patterns alone. According to some estimates, the annual cost of climate change could approach 3% of the world's gross economic output, perhaps negating the benefits of economic growth.

Many uncertainties about the warming trend remain, and more research is urgently needed. Yet waiting for a definitive picture of how climate change will unfold invites costly consequences and potential disaster. By the time researchers document a marked shift in climate, it will be irrevocable, and its consequences unavoidable. This irreversibility, combined with unacceptably high costs of adaptation, justifies immediate action.

Because of our dependence on fossil fuels, some change in the world's climate is already inevitable. And because CO_2 is the key variable in the climate equation, the ultimate magnitude of climatic change—and the pace at which it unfolds—will depend greatly on the future use of coal, oil, and natural gas.

If worldwide CO_2 emissions from fossil fuels return to their pre-1973 rate of growth—more than 4% annually—atmospheric concentrations will double their preindustrial levels in about 40 years. Because of the rising concentrations of other greenhouse gases, the equivalent of a CO_2 doubling would occur perhaps a decade or so earlier. On the other hand, holding that growth to just 1% annually would delay a CO_2 doubling for more than a century.

A goal of limiting the annual growth of CO_2 emissions to 1% may have seemed utterly unrealistic 10 years ago. Now, however, it appears entirely feasible. For the decade following 1973, worldwide carbon emissions grew at an encouragingly low average rate of 1.1% per year. Carbon emissions actually fell between 1980 and 1983. But with the recent drop in oil prices, an upward trend could easily resume. Moreover, maintaining a 1% rate of growth worldwide will require that industrial countries at least cap their emissions to allow for needed energy growth in the Third World.

The energy connection

Achieving such a target will require investments in energy efficiency and alternative energy sources beyond those the market alone would induce. By reducing fossil fuel combustion, these investments would simultaneously curb air pollution and acid rain. Strategies that focus only on pollution control technologies—such as scrubbers for power plants—ignore cost-effective opportunities to limit acid-forming pollutants and the CO_2 buildup.

The rise in energy costs during the 1970s triggered some impressive efficiency gains. Yet there is still vast potential for cutting energy use in industries, automobiles, and homes. In Sweden, for example, houses with heating requirements that are one-seventh those of average Swedish homes are now on the market. Legislation there calls for 30% energy savings in buildings over 10 years, which, if achieved, will cut the nation's total energy consumption by 15%.

State and federal governments in West Germany also have taken some impressive steps. Between 1978 and 1982, they invested nearly $2 billion to promote conservation of heating energy. Projections indicate a 30% drop in the amount of energy needed for space heating by 2000. Because of these and other efforts to boost efficiency, West German analysts now expect no increase in the nation's total primary energy needs through the end of this century. That means West Germany will cap its carbon emissions and indeed may reduce them.

Standards and strategies

Setting standards for residential appliances, which in the United States account for about one-third of all electricity needs, could cut energy use substantially. In the absence of federal initiatives, several states have taken the lead. California's standards call for a 50% increase in the efficiency of refrigerators and freezers by 1992, which would eliminate the need for one large power plant. Prospects now look promising for the establishment of federal standards. The National Appliance Energy Conservation Act of 1986, expected to receive congressional approval in 1987, sets standards for most major electrical appliances. Its enactment will defer the need for 20–25 large electric power plants nationwide.

Shifting energy sources away from those that emit large quantities of carbon also would be part of an effective strategy. Selected use of natural gas in place of coal and oil could reduce emissions fairly quickly and economically and would provide a practical bridge to an energy economy less dependent on all fossil fuels. Natural-gas burning emits 30% less CO_2 than oil and 42%

0013-936X/86/0920-1101$01.50/0

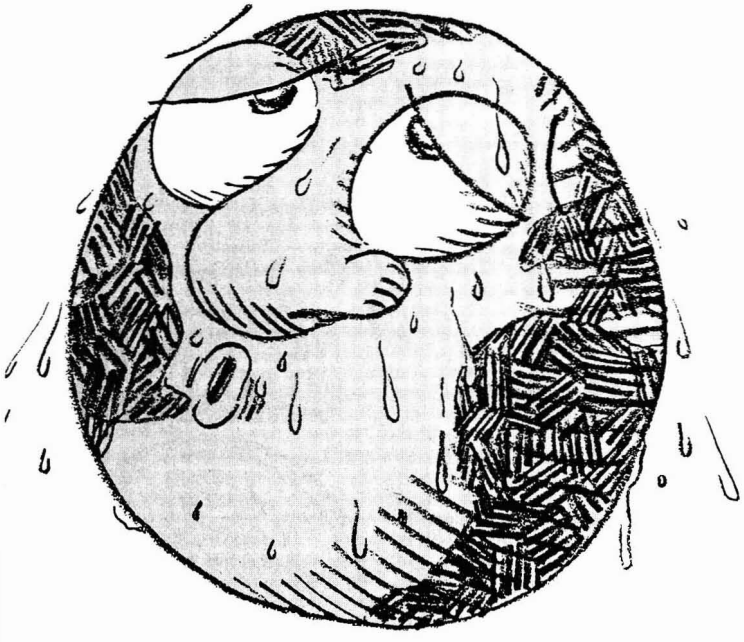

less than coal per unit of useful energy output. On the other hand, use of synthetic fuels, which some see as an eventual replacement for dwindling oil supplies, results in a substantial increase in CO_2 emissions compared with any of the natural fossil fuels.

A few nations have begun to shift away from fossil fuels. In West Germany, alternative sources are expected to produce 17% of primary energy by the beginning of the next century, up from 4% in 1960. Nuclear power dominates this non-fossil-fuel contribution. Yet where concerns about radioactive-waste disposal, high costs, or safety lead energy planners to shy away from the nuclear option, other sources—including solar, wind, and hydropower—could in many cases greatly expand the share of energy generated without fossil fuels.

In the United States, for example, nearly 1300 small-scale power projects using a mix of alternative sources have been planned since 1980. Their combined capacity will equal that of 25 large coal or nuclear plants. Sweden's long-term energy policy includes reducing its dependence on oil, while phasing out nuclear power. Along with increasing energy efficiency, Sweden plans to meet a greater share of its needs from wind, water, and solar power.

Along with reducing CO_2, controlling releases of the synthetic chlorofluorocarbons (CFCs) can help slow the pace of climatic change. Because they act as greenhouse gases, these chemicals contribute significantly to the warming trend, while also threatening to deplete the protective layer of ozone in the upper atmosphere. The United States and several Scandinavian countries have already banned or restricted nonessential uses of CFCs in aerosols. This action actually proved beneficial to the U.S. economy, with available substitutes saving consumers an estimated $165 million in 1983 alone.

A worldwide ban on nonessential aerosol uses thus appears a cost-effective first step toward reducing the threats CFCs pose. Under the auspices of the United Nations Environment Programme, international negotiations regarding CFCs are in progress but so far have resulted only in a framework for adopting control measures if they are deemed necessary.

Forest preservation, essential for a host of reasons, plays a dual role in minimizing risks of climate change. The clearing and burning of tropical forests contribute substantially to the annual release of CO_2 to the atmosphere. Aside from this, of course, is the fact that trees remove CO_2 from the air during photosynthesis. Currently, 10 trees are cleared in the tropics for every one planted. Working with tropical countries to plant trees and to protect natural forests could thus do much to lessen the damage.

In mid-1985, a promising development emerged with the unveiling of an ambitious tropical forest protection plan. Designed by an international task force coordinated by the World Resources Institute and supported by leading aid agencies, it calls for investments totaling $8 billion over five years in tree-planting projects and efforts to arrest deforestation. If adequately funded and implemented, the plan may help begin a much-needed reversal of deforestation trends.

International challenge

No nation acting alone can avert the costly consequences of altering the Earth's climate. CO_2 emissions anywhere contribute to climate change everywhere. Yet translating shared risks into cooperation aimed at minimizing them is no easy task. A decision to place a hefty tax on fossil fuel combustion, for example, would have serious political and economic repercussions. Few nations would view it in their interests to adopt such a preventive measure without guarantees that others will do the same.

A host of institutions can help build the cooperation needed among governments. The United Nations Environment Programme, the U.N. Economic Commission for Europe, the European Economic Community, the World Meteorological Organization, and others have in various ways been instrumental in achieving progress toward global environmental management. But only with leadership from individual nations will concrete measures result.

Action by only a few countries can lead to action by many, as shown by progress in controlling acid rain. Ten nations initially made the commitment in March 1984 to reduce their sulfur dioxide emissions by 30% within a decade. Twenty-one nations now have made similar commitments. Meaningful reductions in worldwide CO_2 emissions would begin with concerted measures by just three nations—China, the Soviet Union, and the United States, the world's three largest users of coal.

Fossil fuels have figured prominently in our quest for economic growth and higher standards of living. But a changing climate brought about by their use threatens to undermine a substantial share of the gains won. Prudence and responsibility dictate that industrial societies act now to limit alterations of the Earth's climate.

Sandra L. Postel is a senior researcher with Worldwatch Institute in Washington, D.C. She is author of the institute's report, "Altering the Earth's Chemistry: Assessing the Risks," from which this article is largely drawn.

professional consulting services directory

CLASSIFIED SECTION

DEPARTMENT HEAD
DEPARTMENT OF CIVIL AND ENVIRONMENTAL ENGINEERING
UNIVERSITY OF CINCINNATI

The College of Engineering invites applications and nominations for the position of Head of the Department of Civil and Environmental Engineering. The department offers comprehensive educational and research programs in the major specialties of civil and environmental engineering and environmental science. The department currently has 20 full-time faculty positions, 134 graduate students, 298 undergraduate students and offers the B.S., M.S., and Ph.D. degrees. All undergraduate students participate in cooperative education. The department currently has in excess of 2.1 Million dollars in research contracts.

The Department Head is the chief administrative and academic officer in the department and is responsible for budget, evaluation and initiation of recommendations for promotions, and for creating a stimulating environment for teaching, research, and faculty development. The Head is directly responsible to the Dean of the College of Engineering and holds the rank of professor with tenure.

The search committee is looking for a distinguished educator and engineer, with excellent credentials in teaching and research, who has the ability to interface successfully with students, colleagues, and the community. The salary is commensurate with qualifications and experience. All applications received by January 15, 1987 will be considered. Applicants should send resume and references to: **Dr. Andrew Bodocsi, Civil and Environmental Engineering, Search Committee Chairman, Mail Location #71, University of Cincinnati, Cincinnati, Ohio 45221. Phone: (513) 475-5618.** The University of Cincinnati is an Affirmative Action/Equal Opportunity Employer.

GC/MS OPERATOR

POLLUTION CONTROL SYSTEMS, INC., an environmental consulting firm, located in the Fort Wayne, IN area is seeking an experienced GC/MS operator to assist in the establishment of a GC/MS and GC section of existing laboratory. Position requires a minimum of a BS in Chemistry and 2 to 3 years experience performing GC/MS analyses on environmental sample matrices, with a working knowledge of USEPA regulations and procedures. Must possess ability to evaluate GC/MS data. Send resume, references, transcripts, and salary history to:

Sandra L. Mort
Pollution Control Systems, Inc.
State Road 3 at County Road 550 S.
Laotto, IN 46763

Environmental analyst to head up atomic absorption unit in laboratory which performs chemical analyses of water and soil samples with aid of automated chemistry instruments. Must be able to operate atomic absorption system with computer interface to test for ions, metals, minerals, nutrients and other contaminants; evaluate quality control data; process data to produce required statistical data. Req: one year experience and B.S. in biology, chemistry or environmental sciences. Mon-Fri, 7 a.m.-4 p.m., $1,909/mo. Job site and interview in Sacramento. Send this ad and resume or letter stating qualifications to job # 8816, P.O. Box 9560, Sacramento, CA 95823-0560 by January 5, 1987.

HAZARDOUS MATERIALS LABORATORY MANAGER Experienced scientist or engineer with demonstrated analytical laboratory and staff management skills. Contract research and/or industrial experience preferred. Will be responsible for planning and operation of a major $9 million, 43,000 sq. ft. Hazardous Materials Laboratory. Salary $40,000 $50,000 per annum. Closing date January 1, 1987. Submit resume and three letters of reference to Dr. David L. Thomas, Hazardous Waste Research and Information Center, 1808 Woodfield Drive, Savoy, IL 61874. Equal Opportunity/Affirmative Action Employer.

POSTDOCTORAL

Tropospheric Chemistry

The Isotope Geochemistry Group of the Los Alamos National Laboratory is seeking candidates for a postdoctoral appointment in tropospheric chemistry.

This opportunity will include participation in a study of the atmospheric chemistry of organic oxidants in remote areas (J. Phys. Chem., 90, 152, (1986)). This project will involve development of analytical methods for field monitoring and theoretical modeling of peracids, peroxides, and both peroxyacyl- and peroxyalkyl-nitrates.

The Laboratory, one of the nation's foremost scientific research organizations, is operated by the University of California for the United States Department of Energy. Our location in the mountains of northern New Mexico offers an uncrowded lifestyle with ample recreational activities.

Our postdoctoral appointments are for one year, renewable for a second year with a starting salary of $31,260 to $32,940 per annum. We provide a comprehensive employee benefits package, including incoming travel and moving expenses. Candidates no more than three years past their Ph.D. are invited to apply.

To formally apply, please send resume, employment application, three letters of reference, and graduate and undergraduate transcripts to: Carol M. Rich, Human Resources Development Division POSTDOC-AA, Los Alamos National Laboratory, Los Alamos, New Mexico 87545.

Affirmative Action/Equal Opportunity Employer
U.S. Citizenship Required

University of California
LOS ALAMOS

Environmental

Superintendent — Water Quality

Wisconsin Electric Power Company has an industry-wide reputation for innovation and leadership in the energy field. Our careful attention to business has made us one of the most financially sound utility companies in the U.S.

The Position

You will direct the Water Quality and Solid & Hazardous Waste Program areas functioning as liaison between the company and various regulatory agencies, monitoring compliance, interfacing with operating departments, and providing technical support. This involves supervision over a small professional staff.

The Qualifications

A minimum of a bachelor's degree in Civil Engineering, Environmental Science or a related discipline is required in addition to a minimum of five years of significant project management experience in surface and groundwater quality, and/or solid and hazardous waste. Experience dealing with utility environmental issues is an asset. Supervisory experience is preferred.

The Rewards

You'll have the prestige of working for a leader in the field of energy and environmental issues. Our leadership allows us to offer a competitive salary, excellent benefits and the opportunity for professional growth. Send resume to:

Patricia J. Butler
Wisconsin Electric Power Company
333 W. Everett Street, Room A125
Box 2046
Milwaukee, WI 53201
An Equal Opportunity Employer M/F/V/H

CLASSIFIED SECTION

Environmental Chemists. Junior and senior levels, organic and inorganic chemists with chemistry degree. Experience dealing with EPA, GC/MS, AA and ICP instrumental methods for water and waste and knowledge of EPA QA procedures desirable for advanced positions. Positions to involve combination management, field work and data evaluation. Send resume immediately to:

ecology and environment, inc.
4105 E. Florida Ave., STE 350
Denver, CO 80222

Attn: Karl Ford. Offices in Buffalo, Tallahassee, Chicago, Kansas City, Denver, Dallas, Los Angeles, San Francisco and Seattle. State first preference.

GRADUATE STUDY IN ENVIRONMENTAL SCIENCE AND ENGINEERING at the Oregon Graduate Center. High quality, strongly motivated students sought for aggressive research programs in groundwater and surface water contamination, toxic organic pollutants, analytical environmental chemistry, atmospheric chemistry. Intensive research experience, state-of-the-art instrumentation, maximal student–faculty interaction. Research assistantships with tuition remission available to qualified Ph.D. applicants. Write: **Carl D. Palmer, Assistant Professor, Department of Environmental Science and Engineering, Oregon Graduate Center, 19600 N.W. Von Neumann Dr., Beaverton, OR 97006.** AAEO Employer.

USE THE CLASSIFIED SECTION

CLASSIFIED ADVERTISING RATES

Rate based on number of insertions used within 12 months from date of first insertion and not on the number of inches used. Space in classified advertising cannot be combined for frequency with ROP advertising. Classified advertising accepted in inch multiples only.

Unit	1-T	3-T	6-T	12-T	24-T
1 inch	$100	$95	$90	$895	$80

(Check Classified Advertising Department for rates if advertisement is larger than 10″.)
SHIPPING INSTRUCTIONS: Send all material to

Environmental Science & Technology
Classified Advertising Department
500 Post Road East
Westport, CT 06881
(203) 226-7131

INDEX TO THE ADVERTISERS IN THIS ISSUE

ADVERTISERS	PAGE NO.
Academic Press ..... Academic Advertising	**IFC**
Cambridge Analytical Associates ... Graphic Inc.	**1190**
Environmental Protection Agency ..	**1190**

Advertising Management for the American Chemical Society Publications

CENTCOM, LTD.

President
Thomas N. J. Koerwer

Executive Vice President **James A. Byrne**
Senior Vice President **Benjamin W. Jones**
Alfred L. Gregory, *Vice President*
Clay S. Holden, *Vice President*
Robert L. Voepel, *Vice President*
Joseph P. Stenza, *Production Director*

500 Post Road East
P.O. Box 231
Westport, Connecticut 06881
(Area Code 203) 226-7131
Telex No. 643310

ADVERTISING SALES MANAGER
James A. Byrne, *VP*

ADVERTISING PRODUCTION MANAGER
Jay S. Francis

SALES REPRESENTATIVES

Philadelphia, Pa. . . . Patricia O'Donnell, CENTCOM, LTD., GSB Building, Suite 725, 1 Belmont Ave., Bala Cynwyd, Pa 19004 (Area Code 215) 667-9666

New York, N.Y. . . . Dean A. Baldwin, CENTCOM, LTD., 60 E. 42nd Street, New York 10165 (Area Code 212) 972-9660

Westport, Ct. . . . Edward M. Black, CENTCOM, LTD., 500 Post Road East, P.O. Box 231, Westport, Ct 06881 (Area Code 203) 226-7131

Cleveland, Oh. . . . Bruce Poorman, CENTCOM, LTD., 325 Front St., Berea, OH 44017 (Area Code 216) 234-1333

Chicago, Ill. . . . Michael J. Pak, CENTCOM, LTD., 540 Frontage Rd., Northfield, Ill 60093 (Area Code 312) 441-6383

Houston, Tx. . . . Michael J. Pak, CENTCOM, LTD., (Area Code 312) 441-6383

San Francisco, Ca. . . . Paul M. Butts, CENTCOM, LTD., Suite 1070, 2672 Bayshore Frontage Road, Mountainview, CA 94043. (Area Code 415) 969-4604

Los Angeles, Ca. . . . Clay S. Holden, CENTCOM, LTD., 3142 Pacific Coast Highway, Suite 200, Torrance, CA 90505 (Area Code 213) 325-1903

Boston, Ma. . . . Edward M. Black, CENTCOM, LTD., (Area Code 203) 226-7131

Atlanta, Ga. . . Edward M. Black, CENTCOM, LTD., (Area Code 203) 226-7131

Denver, Co. . . . Paul M. Butts, CENTCOM, LTD., (Area Code 415) 969-4604

United Kingdom:
Reading, England—Technomedia, Ltd. . . . Wood Cottage, Shurlock Row, Reading RG10 OQE, Berkshire, England 0734-343302 Telex No. 848800 TECHNOG

Lancashire, England—Technomedia, Ltd. . . . c/o Meconomics Ltd., Meconomics House, 31 Old Street, Ashton Under Lyne, Lancashire, England 061-308-3025

Continental Europe . . . International Communications Inc., Rue Mallar 1, 4800 Verviers, Belgium. Telephone (087) 22-53-85. Telex No. 49263

Tokyo, Japan . . . Shuji Tanaka, International Media Representatives Ltd., 2-29, Toranomon 1-Chrome, Minatoku, Tokyo 105 Japan. Telephone: 502-0656

ES&T RESEARCH

Gas-Partitioning Approach for Laboratory and Field Studies of Mirex Fugacity in Water

Chengqing Yin[‡] and John P. Hassett*

Department of Chemistry, College of Environmental Science and Forestry, State University of New York, Syracuse, New York 13210

■ Dynamic headspace gas-partitioning methods were developed to measure fugacity and free dissolved concentration of mirex in water. Results obtained with gas chromatography (GC) were comparable to those obtained with ^{14}C liquid scintillation spectroscopy. Henry's law constant for mirex in distilled water is 5.16×10^{-4} ($\sigma = 0.82 \times 10^{-4}$) atm M^3 mol^{-1} at 22 °C. The effect of temperature on Henry's law constant can be expressed by $\log H = 12.709 - 4711/T$. The binding of mirex to Aldrich humic acid substantially reduces the volatility and apparent Henry's law constant of mirex. K_{DOC} is 2.8×10^6 at 1.1 mg/L DOC but decreases with increasing DOC. The dynamic headspace technique can be used to measure dissolved vs. bound mirex much like previously reported techniques such as solubility enhancement, dialysis, and reverse-phase sorption. However, with a GC detection limit of 1 pg/L for free mirex under ideal conditions, the dynamic headspace technique can make these measurements in unaltered natural water samples using mirex native to the sample.

Hydrophobic organic compounds can bind to natural dissolved organic matter (DOM) in water, and this significantly changes their behavior in aquatic systems (*1*, *2*). This binding increases the apparent solubility of these compounds (*3–5*), lowers their recovery by solvent extraction, decreases their sorption onto particulates (*6*), and reduces toxicity to organisms (*7*). It also changes the rate of volatilization and bioaccumulation (*8–10*). These phenomena can be explained as a decrease in the activity or fugacity (*11*, *12*) of these compounds due to binding. Therefore, a method for direct determination of fugacity or activity of these compounds in the presence of DOM is needed in order to understand their chemical behavior in aquatic systems.

Several laboratory methods have been developed to quantitatively distinguish between bound and free hydrophobic organic compounds. These include solubility methods (*2*), equilibrium dialysis (*13*), reverse-phase separation techniques (*14*), and gas-phase partitioning (*8*). Solubility methods are inherently unsuitable for analysis of natural samples. Dialysis is not promising as a field technique because of potential biodegradation of cellulose membranes and because the membranes strongly adsorb some hydrophobic compounds (*14*, *15*). Reverse-phase partitioning might be suitable for field studies but would require pretreatment of samples by filtration or centrifugation to remove particles that otherwise would be trapped in the extraction column. We have chosen gas-phase partitioning as the most promising method for field studies because it offers direct measurement of fugacity of a hydrophobic compound in the presence of particles and dissolved organic matter with no pretreatment.

Hassett and Milicic (*8*) have demonstrated the use of gas purging for measurement of binding of a PCB congener by dissolved humic acid. We have adapted this approach for determination of the insecticide mirex ($C_{10}Cl_{12}$) in water. If gas bubbles are allowed sufficient time to equilibrate with the analyte in the water phase, then

$$C_g = K_h C_{aq} \tag{1}$$

where C_g is the concentration of the analyte in the gas phase, C_{aq} is the concentration in true solution in the aqueous phase, and K_h is the nondimensional Henry's law constant. Assuming ideal behavior in the gas phase, C_g can be related to the fugacity of the analyte in the aqueous phase by the ideal gas law.

During gas purging, the solution concentration will decline (*8*) as described by

$$dC_{aq}/dt = -(F/V)C_g \tag{2}$$

Assuming that the gas and aqueous phases equilibrate and that all analyte in the aqueous phase is in true solution, C_g can be eliminated by combining eq 1 and 2. Integration of the resulting equation yields

$$\ln C_{aq} = -(F/V)K_h t + \ln C^0_{aq} \tag{3}$$

where F is the purge gas flow rate, V is the water sample volume, t is duration of purging, and C^0_{aq} is the initial concentration of the analyte in water. Note that if an experiment is carried out with sufficiently small F or t or sufficiently large V, C_{aq} essentially equals C^0_{aq}. Under these conditions, determination of C_g will yield C^0_{aq} from eq 1 if K_h is known and will yield fugacity even if K_h is not known. This approach is advantageous if particles or dissolved organic matter are present in the sample since equilibria with these phases are not perturbed and, therefore, do not have to be considered. This approach is similar to static headspace methods in that the gas and water phases equilibrate, but it makes practical the use of large gas volumes. We therefore term our approach the

[‡] Present address: Institute of Environmental Chemistry, Bijing, People's Republic of China.

0013-936X/86/0920-1213$01.50/0

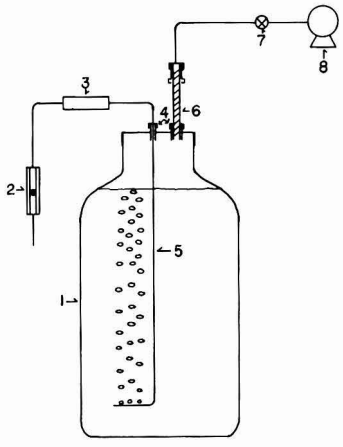

Figure 1. Purging apparatus: (1) 20-L glass carboy with metal screw cap; (2) rotameter; (3) activated carbon trap; (4) bored-through Swaglok bulkhead fittings; (5) $^1/_8$-in. (o.d.) stainless steel purge tube; (6) Tenax trap; (7) needle valve; (8) vacuum pump.

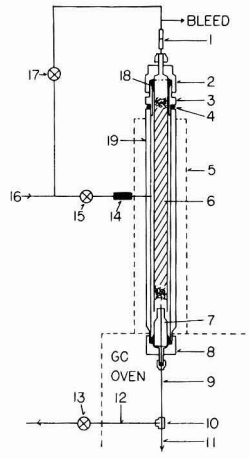

Figure 2. Tracor MT-220 packed column injector modified for Tenax trap thermodesorption–capillary column gas chromatography: (1) Swaglok quick connect; (2) $^1/_4$-in. female/$^1/_8$-in. male Swaglok union; (3) bored out $^1/_4$-in. Swaglok union; (4) Teflon O-ring; (5) injector heated zone; (6) $^1/_4$-in. (o.d.) glass Tenax trap; (7) $^1/_4$-$^1/_8$-in. (o.d.) brass tube; (8) $^1/_4$-in. female/$^1/_{16}$-in. male Swaglok union; (9) 1-m fused silica capillary column; (10) zero dead volume tee; (11) 25-m fused silica capillary column; (12) $^1/_{16}$-in. (o.d.) stainless steel tubing; (13) needle valve; (14) stainless steel frit filter in standard injector carrier gas inlet fitting; (15) shutoff valve; (16) helium carrier/desorb gas at 32 psig; (17) shutoff valve; (18) 15% graphite/85% vespel ferrule on Tenax trap; (19) standard injector body.

"dynamic headspace" technique. For operational purposes in this study, C_{aq} is considered essentially equal to C^0_{aq} if $C_{aq}/C^0_{aq} > 0.9$.

Experimental Section

Apparatus. The gas-purging system is shown in Figure 1. The sample bottle, a 20-L glass carboy with a 13-cm (o.d.) metal screw cap, contains 19 L of water sample. The purging tubing is 3.2 mm o.d. stainless steel with six 0.7-mm holes. The analytical traps are 115.0 mm long by 6.4 mm o.d. (3.8 mm i.d.) borosilicate glass tubes with 0.15 g of Tenax-GC (25% 60–80 mesh, 75% 35–60 mesh). The downstream end of the trap is plugged with Pyrex glass wool and heated in a flame to bond it before packing with Tenax-GC. The upstream end is plugged with glass wool but not heated. This end is fitted with a 15% graphite-/85% vespel ferrule (Figure 2). Prior to use, the traps are extracted with 50 mL of acetone and then with 150 mL of hexane at about 3.5 mL/min. The traps are conditioned for 60 min at 300 °C in a heating block with a 200 mL/min flow of high-purity charcoal-filtered nitrogen. The conditioned traps are stored in clean glass test tubes with aluminum foil lined screw caps.

The gas chromatograph used was a Tracor MT 220 on which the standard packed column injector was modified (Figure 2) as follows. A $^1/_4$-in. (6.4-mm) stainless steel Swaglok union was bored out to 6.5 mm i.d., fitted with a Teflon O-ring, and screwed into the top of the injector after removing the septum support and septum retaining nuts (the interior threads of the standard injector are compatible with Swaglok fittings). The trap was inserted through this fitting and sealed with a custom-made $^1/_4$-in. (6.4-mm) female to $^1/_8$-in. (3.2-mm) male brass Swaglok union. At the bottom of the injector, a 6.4 mm o.d. × 2.5 cm brass tube, tapered to 3.2 mm o.d. at the end so it protruded into the trap, was retained by a custom-made $^1/_4$-in. (6.4-mm) female to $^1/_{16}$-in. (1.6-mm) male brass Swaglok union. A 1-m fused silica capillary column (Supelco, Inc. SPB-5, 0.25 mm i.d., 0.25 μm film) was connected at one end to the bottom of the injector so that it protruded into the trap and at the other end to a zero dead volume tee. A 25-m fused silica capillary column (SE-30, 0.2 mm i.d.) was attached to the tee, with its end butting against the other piece of capillary column, and to a ^{63}Ni electron capture detector via a makeup gas fitting. A $^1/_{16}$-in. stainless steel tube connected to the tee was led outside the column oven and attached to a needle valve. Desorption/carrier gas (He) was supplied at 32 psig. Desorption gas passed through a shutoff valve and a Swaglok quick connect fitting to the analytical trap. A small flow (2–5 mL/min) of desorption gas was allowed to bleed from the line at all times. Carrier gas passed through a shutoff valve to the normal injector carrier gas fitting. Detector purge gas (not shown) was 95% argon/5% methane.

Reagents. Two lots of [^{14}C]mirex were obtained from Pathfinder Lab, Inc., with purity of 98+%, and with specific activities of 6.13 and 37.5 mCi/mmol, respectively. Unlabeled mirex standard was obtained from the U.S. Environmental Protection Agency with purity of 99.9%. Purity information was supplied by the mirex sources. All mirex was used without further purification. All solvents for ^{14}C experiments were ACS grade. All solvents for unlabeled mirex experiments were pesticide grade. Standard solutions of mirex were prepared in acetone. The water used in experiments was distilled, deionized, and passed through a Barnstead "Organic Removal" cartridge. Humic acid was purchased from Aldrich Chemical Co. It was dissolved in 0.1 N NaOH, filtered, reprecipitated by adding HCl to pH 2, and centrifuged. Humic acid was redissolved in water by adjusting the pH to 6.7 with 0.1 N NaOH and then filtered through an Amicon XM300 Diaflo ultrafilter (M_r 300 000 cutoff). The stock solution was kept at 4 °C.

Procedures. A total of 100–300 μL of mirex standard acetone solution was spiked into 19 L of water, which was then sealed and kept stirring in a constant temperature room. After at least 14 h the water sample bottle was put in a water bath of the same temperature and connected to the nitrogen gas and the analytical trap. The flow rate was kept at 560 mL min^{-1}. For most studies, the purging

time was 120 min per experiment.

For [^{14}C]mirex experiments, traps were eluted with 40 mL of hexane, the volume of which was then reduced to about 3 mL by evaporation with a stream of carbon-filtered air. Before and after purging, 500-mL aliquots of water were removed and extracted twice with 60 mL of hexane by shaking for 10 min. The extract volume was also reduced to about 3 mL. Mineral oil (1–2 drops) was added before vaporization to minimize loss of mirex. The radioactivity of mirex was determined by liquid scintillation counting. The concentration of mirex in the water sample was calculated as the average of the aliquots collected before and after purging.

Unlabeled mirex was analyzed by thermodesorption/gas chromatography. Mirex was loaded on an analytical trap either by adsorption from the gas phase or by direct injection of hexane solutions (2–150 μL). In both cases, the trap was placed in a heating block at 65 °C and purged with N_2 at 200 mL/min for 10 min to remove air, water, and solvent. A desorption/chromatography sequence was then initiated to thermally desorb mirex from the Tenax trap, cold trap it on the 1-m capillary column, transfer it through a zero dead volume tee to the 25-m column, and analyze for it by gas chromatography with electron capture detection. The procedure was as follows. Valves 15 and 17 (Figure 2) were closed, the quick connect fitting uncoupled, the trap in the injector port removed, and valve 13 opened. The trap to be analyzed was inserted into the hot (265 °C) injector port, sealed with fitting 2, and connected to the system with the quick connect fitting. Valves 15 and 17 were then opened. A sintered metal filter in the carrier gas inlet acted as a flow restrictor so that the helium flowed mainly through the trap to transfer the analyte to the first 1 m of capillary column. The purge gas flowed out valve 13 via the zero dead volume tee at a flow rate of 80 mL/min. The desorption period lasted 8 min. During this period the oven was kept open, and part of the 1-m capillary column was immersed in an ice–water bath at 0 °C so that the compound of interest was condensed in a narrow band.

At the end of the desorption period, valves 17 and 13 were closed, the column was taken out of the ice–water bath, and the oven door was closed. Column oven temperature stabilization required 30 s after the oven door was closed. The temperature programmer (65–265 °C at 7.5 °C/min) and chart recorder were started simultaneously, and the analytes trapped initially on the SPB-5 column started to separate chromatographically. Mirex was quantified by peak height on the chart recorder. Injector and detector temperatures were 265 and 315 °C, respectively.

The concentration of mirex in water solution was determined by extracting hexane, reducing the hexane volume with a stream of carbon-filtered nitrogen (*16*) to 100 μL, injecting aliquots of 10–80 μL onto the analytical trap, and analyzing with the same procedure as above. Mirex was quantified by peak height against a standard mirex hexane solution injected onto the trap and analyzed with the same method.

Results and Discussion

Tenax is a very effective adsorbent for mirex. In a trap that was sectioned into quarters before extraction, over 95% of the mirex was retained by the glass wool and the first 25% of the Tenax. The trap flow resistance and hydrostatic backpressure caused the pressure in the headspace to be 27.5 mmHg less than ambient atmospheric pressure. This would contribute a 3.6% positive error in Henry's law determination. Because this effect was small and because the method was identical for all experiments, no correction was made.

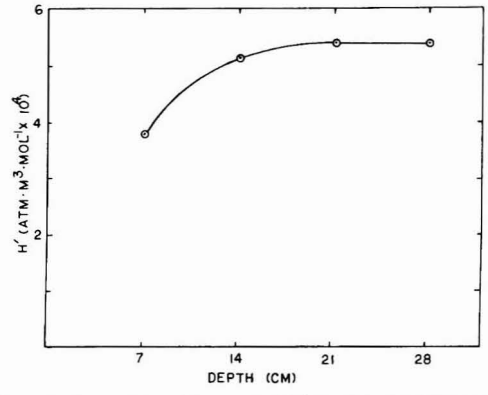

Figure 3. Apparent Henry's law constant (H') for mirex in distilled water vs. depth of bubble inlet tube.

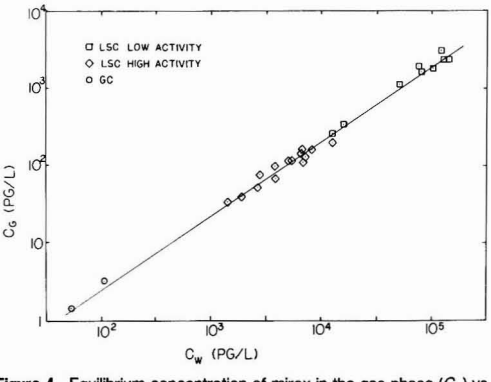

Figure 4. Equilibrium concentration of mirex in the gas phase (C_g) vs. concentration in distilled water.

The dynamic headspace method is based on the assumption of equilibrium between the gas and water phases. To test this assumption, apparent Henry's law constants were obtained by purging at different depths (Figure 3). At depths greater than 14 cm, the measured Henry's law value was constant, indicating that purging from 28-cm depth allowed the bubbles sufficient time to approach equilibrium with the water. Mackay et al. (*17*) reported that for benzene each 10-cm increase in purging depth would yield an 80% approach to equilibrium, which is similar to the results shown in Figure 3.

Mirex concentration in purging gas is proportional to that in distilled water solution over a range of at least 3 orders of magnitude (Figure 4). The slope of the line in Figure 4 is 0.966. The regression coefficient of the non-log-transformed data is 0.976. At 22 °C, 23 experiments were done, and Henry's law constant was determined as 5.16×10^{-4} ($\sigma = 0.82 \times 10^{-4}$) atm M^3 mol^{-1} ($K_H = 2.13 \times 10^{-2}$). Substituting this value into eq 3 along with a flow rate of 0.56 L/min, sample volume of 19 L and purge time of 120 min yield $C_{aq}/C^0_{aq} = 0.93$. This satisfies the operational condition that C_{aq}/C^0_{aq} be greater than 0.90.

Temperature strongly affected Henry's law constant (Figure 5). The temperature effect can be expressed by an equation analogous to the Clausius–Clapeyron equation (*18*):

$$d(\ln H)/dT = L_i/(RT^2) \quad (4)$$

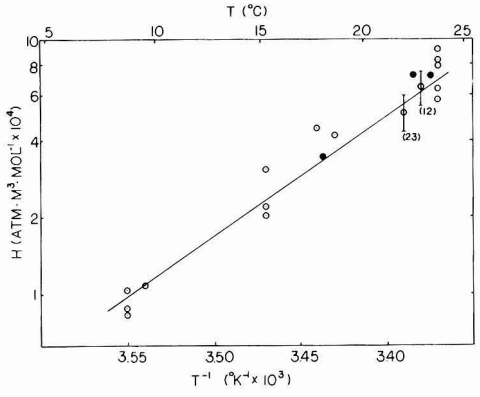

Figure 5. Effect of temperature (T) on Henry's law constant (H) of mirex in distilled water.

where L_i is the partial molar vaporization enthalpy of the solute. From the experimental data, L_i for mirex in dilute aqueous solutions is 21.6 kcal mol^{-1}, and the relationship of Henry's law constant to absolute temperature is

$$\log H = 12.709 - 4711/T \quad (5)$$

over the tested temperature range (8–24 °C). The strong temperature dependence of H demonstrates the importance of temperature control in these experiments. We found it absolutely necessary to stir spiked water samples in a constant temperature environment for at least 14 h before purging and to purge samples at the same temperature.

Ejection of droplets enriched in mirex during bubbling (*19*) and deposition of these droplets in the trap might introduce errors in results obtained by the dynamic headspace technique. To test this, static headspace experiments were done for comparison. The apparatus was the same, but in the 20-L bottle there was only 5 L of distilled water so that the purging tube was above the water surface, and no water droplets could be formed. After equilibration, the concentration of mirex in the headspace gas was measured along with the concentration in the water. The determined Henry's Law constants (single experiments) were 9.8×10^{-4} atm M^3 mol^{-1} at 26 °C and 7.4×10^{-4} at 23 °C. These agree well with respective values of 8.9×10^{-4} and 6.5×10^{-4} atm M^3 mol^{-1} determined by the dynamic headspace method. This indicates that droplet contribution onto the trap was not a significant interference.

In Aldrich humic acid solution, the apparent Henry's law constant of mirex was significantly lower than that in distilled water (Figure 6), because one portion of mirex was bound to dissolved humic acid and, therefore, was not volatile (*8*). The partition coefficient (K_{DOC}) of mirex between humic acid and water can be calculated from these results. K_{DOC} is defined as

$$K_{DOC} = C_b/[C_{aq}(DOC)] \quad (6)$$

and the apparent Henry's law constant (K_h') in humic acid solutions is

$$K_h' = C_g/(C_{aq} + C_b) \quad (7)$$

where C_b is the aqueous concentration of bound mirex, (DOC) is the dissolved organic carbon concentration expressed as a weight fraction, C_g is the equilibrium concentration of mirex in the gas phase, and C_{aq} is the free

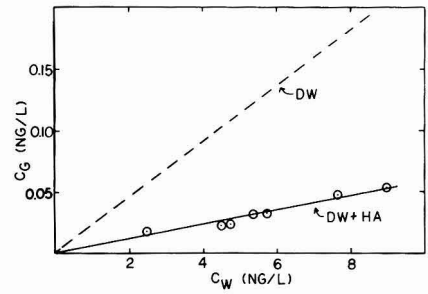

Figure 6. Concentration of mirex in the gas phase (C_g) vs. concentration in distilled water (DW) and in distilled water + 1.1 mg/L humic acid DOC (DW + HA).

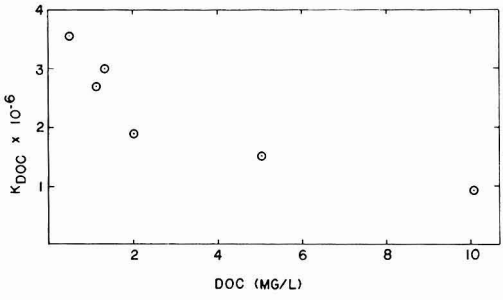

Figure 7. Dimensionless constant for binding of mirex by dissolved humic acid (K_{DOC}) vs. humic acid dissolved organic carbon (DOC) concentration.

dissolved mirex concentration. Equations 6 and 7 can be combined with eq 1 to give the expression

$$K_{DOC} = [(K_h/K_h') - 1][1/(DOC)] \quad (8)$$

Since K_h, K_h', and (DOC) can all be measured, K_{DOC} can be calculated.

When a solution contains 1.1 mg of humic acid carbon/L (Figure 6), the calculated K_{DOC} is 2.8×10^6. This is higher than values observed for binding of 2,2′,5,5′-tetrachlorobiphenyl (*8*, *14*), benzo[*a*]pyrene, DDT, anthracene, and biphenyl (*14*) by dissolved Aldrich humic acid. However, this observation is predicted by work of Carter and Suffet (*2*), who demonstrated that K_{DOC} increases with the octanol–water partition coefficient (K_{OW}). log K_{OW} for mirex is 6.89 (*20*) and is higher than that for the other compounds.

The fraction of free mirex to total mirex can also be calculated as the ratio of apparent Henry's law constant over Henry's law constant in distilled water. In this solution, 76% of the aqueous mirex is bound by dissolved humic acid. Figure 6 demonstrates that K_{DOC} is independent of mirex concentration over the range studied.

With increased humic acid concentration, the fraction of bound mirex increased, but K_{DOC} showed a declining trend (Figure 7). This result agrees with results for several other compounds using equilibrium dialysis (*13*) and reverse-phase separation techniques (*14*). However, K_{DOC} for 2,2′5,5′-tetrachlorobiphenyl, as determined by two separate groups of investigators (*8*, *14*), is apparently independent of DOC concentration. The dependence of K_{DOC} concentration for some (but not all) compounds indicates that binding may involve more complicated mechanisms than simple phase partitioning.

All of the results reported above were obtained with [^{14}C]mirex. One of the most important advantages of the

dynamic headspace method, however, is that it can be linked to gas chromatography to study unlabeled samples. Henry's law constants obtained at 22 °C were 5.04×10^{-4} atm M^3 mol^{-1} ($\sigma = 0.75 \times 10^{-4}$; $n = 9$) for the low specific activity batch of [^{14}C]mirex, 5.21×10^{-4} ($\sigma = 0.90 \times 10^{-4}$; $n = 14$) for the high activity batch, and 6.57×10^{-4} ($\sigma = 0.48 \times 10^{-4}$; $n = 2$) for unlabeled mirex as determined by GC. The hypothesis that the means are equal (null hypothesis) cannot be rejected at the 50% confidence level when the results from the two batches of [^{14}C]mirex are compared by a t test. The null hypothesis cannot be rejected at the 90% confidence level when the GC results for unlabeled mirex are compared to results for either batch of [^{14}C]mirex. At 18 °C, H for labeled mirex was 3.28×10^{-4} ($\sigma = 0.95 \times 10^{-4}$; $n = 3$), and for unlabeled mirex, it was 3.46×10^{-4} ($n = 1$). The close agreement of results obtained with three batches of mirex analyzed by two different techniques indicates that no errors were introduced by radiochemical impurities or by systematic errors in one of the analytical techniques. This is operationally convenient since Henry's law data obtained with the radiochemical technique can be directly applied to fugacity determination with the more complicated GC technique.

Compared with other methods to determine binding and fugacity, the dynamic headspace method has an important advantage, i.e., it can be applied to the study of natural waters. Because only volatile and semivolatile compounds are purged and trapped, the gas chromatogram is relatively simple, and often cleanup procedures are not necessary. Because water samples can be purged directly from the sampling bottle, and the traps can be analyzed right after purging, this direct determination much simplifies the analytical procedure and reduces the chance of contamination. Under the conditions used here (purge at 560 mL/min for 120 min; $K_H = 2.13 \times 10^{-2}$) mirex in the equivalent of 1.4 L of water is deposited in the trap and transferred to the GC. This makes it possible to directly determine the fugacity and free dissolved concentration of organic compounds in the natural water samples even at very low concentration. Total mirex recovered by solvent extraction from water can also be analyzed at high sensitivity by using trap thermodesorption–GC because a large fraction of the extract can be injected onto the trap. GC response for 23 pg of mirex is constant for injected solvent volumes from 6 μL to at least 150 μL. Relative standard deviation is 0.12 ($n = 8$) for replicate injections into different traps. Detection limit for total (extractable) mirex in a 1.5-L water sample is 1 pg/L under ideal (low background) conditions. The detection limit for free mirex in water is approximately 1 pg/L. We collected water from Lake Ontario and the Oswego River, NY, several times and found the free dissolved mirex fraction and particulate-adsorbed fraction in those samples were both small and a large fraction (80%) of mirex was bound to dissolved organic matter (*21*).

Conclusions

Dynamic headspace technique is a direct method to determine the fugacity and free dissolved concentration of organic compounds in aqueous solution at very low concentrations. The apparent Henry's law constant of mirex from humic acid solution was much lower than that from distilled water, because part of the mirex was bound to dissolved humic acid and became inactive in gas–liquid exchange. By comparison of the apparent Henry's law constant with that determined in distilled water as a reference, the free dissolved and bound fraction can be determined. This method can be applied to determine the fugacity and free dissolved concentration of organic compounds in natural aquatic systems with simplicity and accuracy.

Acknowledgments

We thank Mark S. Driscoll for his assistance in this research.

Registry No. H_2O, 7732-18-5; mirex, 2385-85-5.

Literature Cited

(1) Hassett, J. P.; Anderson, M. A. *Environ. Sci. Technol.* **1979**, *13*, 1526–1529.
(2) Carter, C. W.; Suffet, I. H. In *Fate of Chemicals in the Environment: Compartmental and Multimedia Models for Predictions*; Swann, R. L.; Eschenroeder, A., Eds.; American Chemical Society: Washington, DC, 1983; ACS Symp. Ser. No. 225, pp 216–229.
(3) Wershaw, R. L.; Burcar, P. J.; Goldberg, M. C. *Environ. Sci. Technol.* **1969**, *3*, 271–273.
(4) Matsuda, K.; Schnitzer, M. *Bull. Environ. Contam. Toxicol.* **1973**, *6*, 200–204.
(5) Boehm, P. D.; Quinn, J. G. *Geochim. Cosmochim. Acta* **1973**, *37*, 2459–2477.
(6) Hassett, J. P.; Anderson, M. A. *Water Res.* **1982**, *16*, 681–686.
(7) Dell'Agnola, G. M.; Ferrari, G.; Nordi, S. *Pestic. Biochem. Physiol.* **1981**, *15*, 110–114.
(8) Hassett, J. P.; Milicic, E. *Environ. Sci. Technol.* **1985**, *19*, 638–643.
(9) Leversee, G. J.; Landrum, P. F.; Giesy, J. P.; Fannin, T. *Can. J. Fish. Aquat. Sci.* **1983**, *40*(Suppl. 2), 63–69.
(10) Boehm, P. D.; Quinn, J. G. *Estaurine Coastal Mar. Sci.* **1976**, *4*, 93–105.
(11) Mackay, D. *Environ. Sci. Technol.* **1979**, *13*, 1218–1223.
(12) Mackay, D.; Paterson, S.; Joy, M. In *Fate of Chemicals in the Environment: Compartmental and Multimedia Models for Predictions*; Swann, R. L.; Eschenroeder, A., Eds.; American Chemical Society: Washington, DC, 1983; ACS Symp. Ser. No. 225, pp 175–196.
(13) Carter, C. W.; Suffet, I. H. *Environ. Sci. Technol.* **1982**, *16*, 735–740.
(14) Landrum, P. F.; Nihart, S. R.; Eadie, B. J.; Gardner, W. S. *Environ. Sci. Technol.* **1984**, *18*, 187–192.
(15) Klein, E.; Eichelberger, J.; Eyer, C.; Smith, J. *Water Res.* **1975**, *9*, 807–811.
(16) Erickson, M. D.; Giguere, M. T.; Whitaker, D. A. *Anal. Lett.* **1981**, *14*, 841–857.
(17) Mackay, D.; Shiu, W. Y.; Sutherland, R. P. *Environ. Sci. Technol.* **1979**, *13*, 333–337.
(18) Nicholson, B. C.; Maguire, B. P.; Bursill, D. B. *Environ. Sci. Technol.* **1984**, *18*, 518–521.
(19) Gershey, R. M. *Limnol. Oceanogr.* **1983**, *28*, 395–400.
(20) Mackay, D. *Environ. Sci. Technol.* **1982**, *16*, 274–278.
(21) Yin, C.-Q., Ph.D. Dissertation, College of Environmental Science and Forestry, State University of New York, Syracuse, NY, 1985.

Received for review October 11, 1985. Revised manuscript received April 14, 1986. Accepted June 9, 1986. This work is the result of research sponsored by NOAA Office of Sea Grant, Department of Commerce, under Grant NA85AADSG021.

Environ. Sci. Technol. 1986, 20, 1218-1223

Chlorination of ω-Cyanoalkanoic Acids in Aqueous Medium

Ed W. B. de Leer,* Theo Baggerman, Petra van Schaik, Coby W. S. Zuydeweg, and Leo de Galan

Laboratory for Analytical Chemistry, Delft University of Technology, De Vries van Heystplantsoen 2, 2628 RZ Delft, The Netherlands

■ The production of 3-cyanopropanoic acid (CPA) and 4-cyanobutanoic acid (CBA) in the chlorination of humic acid (HA) was confirmed by comparison with synthetic standard compounds. The probable precursor structure is a protein material, because glutamic acid and lysine produce CPA and CBA in high yield on chlorination at pH 7. The further chlorination reactions of CPA, CBA, and cyanoethanoic acid (CEA) were studied in aqueous medium at different pH values. CBA and CPA were quite unreactive at pH 4 and 7, while at pH 10 partial hydrolysis of the cyano group and partial disubstitution of the alkyl chain occurred. CEA reacted rapidly with chlorine at all pH values, producing mixtures of dichloroacetic acid and dichloropropanedioic acid. Dichloroacetonitrile was detected as the only intermediate at pH 4, while at pH 10 the reaction proceeded through hydroxamoyl chlorides as the major intermediates. These hydroxamoyl chlorides [R—(Cl)C=N—OH] represent a new class of chlorination products, previously not detected after aqueous chlorination reactions.

Introduction

The production of cyano compounds on chlorination of amino acids was discovered early in this century (*1–3*). Recently, Burleson et al. (*4*) confirmed the structure of a number of these compounds with gas chromatography–mass spectrometry (GC/MS). Alanine, valine, leucine, phenylalanine, and tyrosine all produced cyano compounds on chlorination in aqueous medium by decarboxylation and conversion of the α-amino group into a cyano group.

The presence of chlorinated cyano compounds in drinking water as a result of chlorination processes was reported by Trehy and Bieber (*5, 6*). They identified dihaloacetonitriles (DHAN's) and demonstrated that dichloroacetonitrile was produced in the chlorination of aspartic acid in aqueous medium. Later Keith et al. (*7*) developed a gas chromatographic method for the analysis of DHAN's and also identified trichloroacetonitrile (TCAN) for the first time. Coleman et al. (*8*) confirmed the production of DHAN's and TCAN in the chlorination of Ohio River and Fluka humic acid and detected di- and trichloropropenenitrile as new chlorinated cyano compounds.

Oliver (*9*) showed that DHAN's were quite ubiquitous and were present in 10 chlorinated drinking waters from Ontario in a range of 0.3–8.1 μg/L. They were produced in a molar concentration of 10% of the average molar trihalomethane concentration. He also indicated that certain aquatic algae and aquatic fulvic acid yielded DHAN's under conditions similar to those used for water treatment.

Recently, de Leer et al. (*10*) identified 3-cyanopropanoic acid (CPA) and 4-cyanobutanoic acid (CBA) after chlorination of terrestrial humic acid. Cyanoethanoic acid (CEA) was not detected in this study, possibly as the result of a rapid conversion to dichloroacetonitrile (DCAN) and dichloroacetic acid (DCA).

Because the relation between ω-cyanoalkanoic acids and chlorinated cyano compounds such as the DHAN's and other organochlorine compounds is not known, we report here on a study of the chemical identity of their precursors, their reactions with chlorine at different pH values, and the identification of the final reaction products and several intermediates.

Experimental Section

Chlorination Procedure. The chlorination of the cyano acids was carried out at pH 4.5, 7.2, and 10.0. For pH 4.5 and 7.2, 0.3 M phosphate buffers were used, and for pH 10.0, a 0.3 M carbonate buffer was used.

For the identification studies, a solution (160 mL) of the cyano acid (6.25 mM) and sodium hypochlorite (62.5 mM) was allowed to react in the dark without head space. After a selected reaction time, the excess of chlorine was destroyed by addition of solid sodium arsenite, 50 g of sodium chloride was added, and the solution was acidified to pH 0.5 with concentrated sulfuric acid. The chlorination products were extracted with 3 portions of 25 mL of freshly distilled ethyl acetate. The extracts were dried with sodium sulfate, concentrated in a Kuderna Danish apparatus to about 5 mL, methylated by passing a stream of diazomethane gas through the solution, and finally concentrated to about 1 mL with a gentle stream of nitrogen.

The chlorination of the amino acids was carried out at pH 7.2 in a 0.3 M phosphate buffer. The extraction of the reaction products was carried out with diethyl ether after acidification to pH 2. The concentration and methylation procedures were as described above.

Chlorine Consumption. Chlorine concentrations before and after chlorination were measured iodometrically (*11*).

Chlorate Formation. To correct the chlorine demand at pH 7.2 for the disproportionation reaction of chlorine to chlorate and chloride, the chlorate concentrations were measured iodometrically according to Gordon and Ikeda (*12*). The sum of chlorine and chlorate was determined by adding 1 mL of the reaction mixture to a solution of 2 g of potassium iodide in 15 mL of water and 20 mL of 12.5 M HCl. Air was carefully excluded by performing the whole procedure under nitrogen. After 30 min, the solution was partially neutralized with a 10 mL of 12.5 M NaOH, and the iodine was titrated immediately with a standard sodium thiosulfate solution. The concentration of the chlorate was found by difference from the sum of chlorine and chlorate and of chlorine.

Nitrate Formation. Nitrate was determined according to a proposed standard of the Deutsche Einheitsverfahren (*13*). In this method, nitrate ions react with 2,6-dimethylphenol in a concentrated solution of sulfuric acid and phosphoric acid to form 4-nitro-2,6-dimethylphenol, which is measured spectrophotometrically.

Quantitation of Dichloroacetic Acid and the Cyano Acids. To 160 mL of reaction mixture were added some solid sodium arsenite, to destroy any excess of chlorine, and 50 g of sodium chloride. After acidification to pH 0.5 with concentrated sulfuric acid, the solution was extracted 3 times with 25 mL of freshly distilled ethyl acetate. The volume was adjusted to 100 mL. A total of 1 mL of the solution was methylated with diazomethane. The final solution was analyzed by gas chromatography with a fused

 0013-936X/86/0920-1218$01.50/0

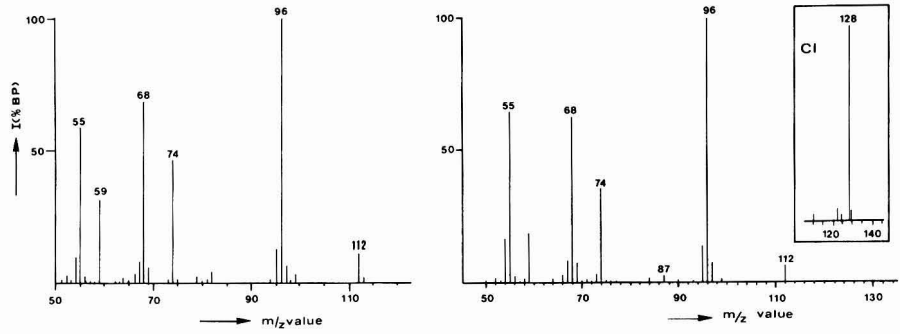

Figure 1. Comparison of EI mass spectra of CBA methyl ester isolated after chlorination of terrestric HA (right) and a synthetic standard (left). An explanation for the major fragments is given in ref 8.

silica capillary column (0.22 mm × 25 m), CP-SIL-5 (Chrompack, Middelburg): injector 290 °C; column 35 °C (5 min) programmed to 300 °C (15 min), program rate 6 °C/min; detector FID 290 °C; carrier gas N_2; flow rate 0.8 mL/min. The quantitation was carried out with nonane as internal standard.

Apparatus. The gas chromatograph was a Varian 3700, equipped with a flame ionization detector. The GC/MS combination was a Varian MAT 44 capillary GC–quadrupole MS with a computerized data system of our own design. The fused silica capillary column (CP-SIL-5) was connected to the mass spectrometer by an open atmospheric split. GC conditions used were as above, except that helium was used as the carrier gas. Electron impact spectra were obtained at 80 eV and chemical ionization spectra at 160 eV with isobutane as the reagent gas. Ionization current was 700 and 200 μA, respectively. Cyclic scanning from m/z 50 up to 500 was used with a cycle time of 2 s.

Results and Discussion

Confirmation of Structures of CPA and CBA. The structural assignment of CPA and CBA produced on chlorination of terrestrial HA was based on the electron impact (EI) and chemical ionization GC/MS spectra of their methyl esters. In the case of CPA, an EI spectrum was available in the literature (*14*), which was in close agreement with the experimental spectrum.

The assignments of CPA and CBA were fully confirmed after synthesizing their methyl esters according to literature procedures starting with glutamic acid (*15*) and γ-butyrolactone (*16*), respectively. The final comparison was based on the criteria given by Christman (*17–19*) and included the comparison of the retention indices on two columns with stationary phases of different polarity and the comparison of the EI mass spectra. The EI mass spectra for the methyl ester of CBA produced on chlorination of HA and of the standard are given in Figure 1.

CPA and CBA Precursors. Cyano compounds are produced on chlorination of α-amino acids (*4*). The α-amino group is converted into a cyano group through chloroamine formation and concurrent decarboxylation, according to a reaction scheme proposed by Le Cloirec and Martin (*20*). If a similar reaction mechanism is active in the production of ω-cyano carboxylic acids, the precursor is an α-amino dicarboxylic acid. Glutamic acid and glutamine are then logical precursors for CPA. Because the HA used in the chlorination studies contained 1.5% nitrogen, it is possible that a protein material supplies the precursor structure. By analogy, the precursor amino acid for CBA would then be α-aminoadipic acid, which, however, is not a natural amino acid.

We therefore envisaged a reaction scheme for the conversion of the natural amino acid lysine into CBA (eq 1).

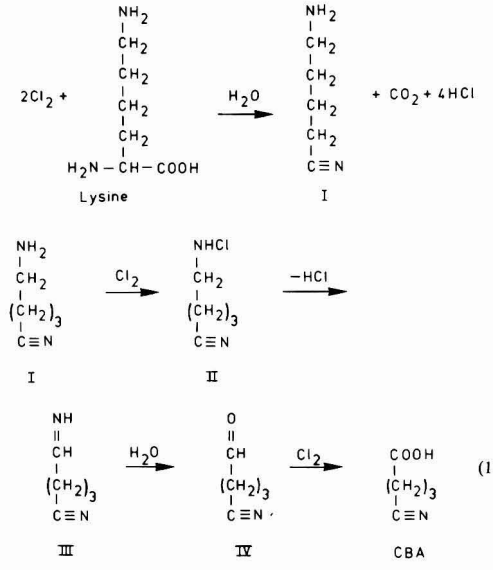

Reaction of lysine with chlorine would produce 1-cyano-4-aminobutane (I) as a hypothetical intermediate. Reaction of the ω-amino-group with chlorine produces a chloroamine (II) that is converted into an imine (III) by a dehydrochlorination. The imine is not stable in aqueous medium and produces an aldehyde (IV), which can be oxidized to CBA as the final product.

The production of CPA and CBA from respectively glutamic acid and lysine was confirmed by chlorination of these amino acids at pH 7.2. The reaction products were isolated by extraction at pH 2 with diethyl ether, converted into their methyl esters with diazomethane, and analyzed with GC/MS with electron impact and chemical ionization.

Chlorination of glutamic acid produced CPA as the major product, completely in accordance with the scheme of the Le Cloirec and Martin. Some traces of butanedioic acid were detected, resulting from hydrolysis of the cyano group.

The chromatogram of the chlorination products of lysine is given in Figure 2. The two major products (peak numbers 4 and 8) were identified as the methyl esters of CBA and 4-cyano-2,2-dichlorobutanoic acid (V), respec-

Table I. Chlorination Products of Lysine at pH 7.2[a]

major products	minor products	
(4) $NCCH_2CH_2CH_2COOH$	(1) CCl_3COOH	(6) $HOOCCH_2CH_2CH_2COOH$
(8) $NCCH_2CH_2CCl_2COOH$	(2) $NCCH_2CH_2COOH$	(7) $HOOCCCl_2CH_2COOH$
	(3) $HOOCCH_2CH_2COOH$	(9) $C_6H_7ONCl_2$
	(5) $NCCH_2CH_2CCl_2CHO$	(10) $HOOCCCl_2CH_2CH_2COOH$

[a] The compound numbers refer to the peak numbers in Figure 2. The compounds were identified as their methyl esters with EI and CI GC/MS.

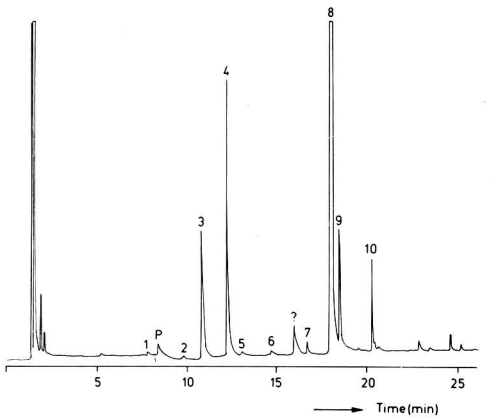

Figure 2. Gas chromatogram of methylated products isolated after chlorination of lysine at pH 7.2. The major chlorination products, 4 and 8, were also identified after chlorination of HA. The structure of the products is given in Table I.

tively. Apart from CBA and V, small amounts of other compounds were detected, which are given in Table I.

The production of V was unexpected, but a reexamination of the GC/MS runs produced during our earlier chlorination studies of HA (*10*) revealed that V was then present also but remained unidentified, although both the CI and EI spectra were recorded. The structural assignment of V as the 2,2-dichloro isomer was based partially on a possible mechanism for its production (eq 2). The

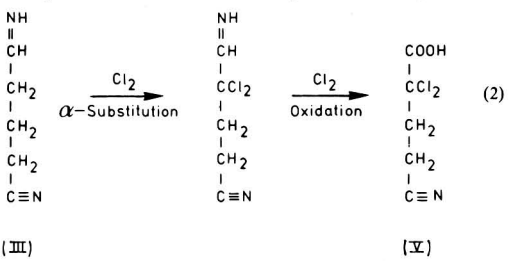

intermediate imide (III) or aldehyde (IV) may be chlorinated at the carbon atom next to the imide or aldehyde group by a base-catalyzed carbanion mechanism, followed by an oxidation that will produce V. Production of the 4,4-dichloro isomer is not very likely, because it would involve chlorination next to the cyano group and should be expected to occur also in the chlorination of other amino acids. However, chlorination of glutamic acid produced only traces of chlorinated products.

Chlorination Reactions of Cyanoalkanoic Acids. CPA and CBA were identified after the chlorination of HA (*10*) when a large excess of chlorine was used. We may therefore expect that CPA and CBA show some stability under these conditions. However, cyanoethanoic acid

Table II. Chlorine Demand of Cyanoalkanoic Acids (CAA)[a]

	chlorine demand, mol of Cl_2/mol of CAA		
pH	CEA	CPA	CBA
4.5	3.38		
7.2	4.85	0.02	0.12
10.0	3.56	0.20	0.63

[a] Contact time = 24 h. Initial excess = 10 equiv of Cl_2.

(CEA), which is the expected chlorination product of aspartic acid or asparagine, was never detected in these experiments. We speculated (*10*) that CEA reacts very rapidly with chlorine to produce dichloroacetic acid (DCA) as the final product. To complete the studies on the chlorination behavior of cyanoalkanoic acids, CEA was included with CPA and CBA.

The chlorine demand of CEA, CPA, and CBA was determined at pH 4.5, 7.2, and 10 with varying contact times of 5 min to 48 h and an initial excess of 10 equiv of chlorine. At pH 7.2, the determination was hampered by the disproportionation reaction of chlorine to chloride and chlorate, which shows a maximum rate at pH 6.9 (*21*). Therefore, both residual chlorine (*11*) and chlorate (*12*) were determined iodometrically, and the chlorine demand was corrected both for the blank demand and for the disproportionation reaction. The results are given in Table II.

4-Cyanobutanoic Acid. CBA showed no significant chlorine demand at pH 4 and 7, while at pH 10 a small amount of chlorine was consumed. GC/MS analysis of the reaction products at pH 10 showed residual CBA (62%) and pentanedioic acid as the only products. Hydrolysis of the cyano group to a carboxylic group and ammonia, followed by a break-point chlorination (*22*) of the ammonia (eq 3) may explain both the chlorine demand and the

$$HOOC(CH_2)_3CN + 1.5Cl_2 + 2H_2O \rightarrow HOOC(CH_2)_3COOH + 0.5N_2 + 3HCl \quad (3)$$

products formed. The conversion of 38% of CBA in pentanedioic acid and nitrogen requires 0.57 mol of Cl_2/mol of CBA, in good accordance with the experimental figure.

3-Cyanopropanoic Acid. CPA showed a chlorine demand behavior comparable to that of CBA at all pH values. The products at pH 10, however, were identified as residual CPA and some 2,2-dichlorobutanedioic acid (DCBDA), which demonstrates that the chlorine demand was caused not only by partial hydrolysis of the cyano group and break-point chlorination of the ammonia produced but also by a substitution reaction producing DCBDA as the end product.

Christman et al. (*23*) identified DCBDA as one of the major chlorination products of humic acid at pH 7. However, the conversion of CPA into DCBDA cannot explain its production, because at pH 7 and the chlorine dose used CPA was not converted into DCBDA.

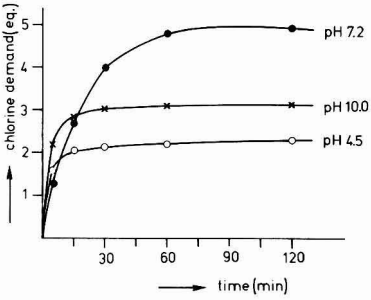

Figure 3. Chlorine consumption of cyanoethanoic acid as a function of time at different pH values. A consumption of 2 equiv corresponds with the production of DCAN and 3.5 equiv with a complete oxidation to DCA or DCPDA and nitrogen.

Cyanoethanoic Acid. CEA showed a large chlorine demand, and the reaction proceeded quite rapidly at all pH values as indicated in Figure 3.

pH 4.5. The final chlorine demand at pH 4.5 was in accordance with the overall reaction as proposed by de Leer et al. (*10*) producing DCA as the major end product of the chlorination reaction (eq 4a). It also indicates that

$$NCCH_2COOH + 3.5Cl_2 + 2H_2O \rightarrow CHCl_2COOH + CO_2 + 0.5N_2 + 5HCl \quad (4a)$$

$$NCCH_2COOH + 3.5Cl_2 + 2H_2O \rightarrow HOOCCCl_2COOH + 0.5N_2 + 5HCl \quad (4b)$$

humic protein material containing aspartic acid may contribute in the production of DCA, one of the major chlorination products of HA. GC/MS analysis after a reaction time of 48 h showed that apart from DCA only traces of dichloropropanedioic acid (DCPDA) and trichloroacetic acid (TCA) were produced. The conversion of CEA into either DCA or DCPDA requires 3.5 equiv of chlorine (eq 4).

Reaction 4a may proceed by chlorination of the methylene group, followed by a decarboxylation to produce DCAN (eq 5). The production of DCAN was apparently

$$NCCH_2COOH + 2Cl_2 \rightarrow CHCl_2CN + CO_2 + 2HCl \quad (5)$$

complete in 15 min after consumption of 2 mol of Cl_2 (Figure 3), which was confirmed by GC/MS.

The conversion of DCAN into DCA proceeded slowly but was complete in 24 h. This hydrolysis reaction was studied by Oliver (*9*), who demonstrated that DCAN was quite stable in water at pH 6 for 10 days. Although the reaction was not studied at pH 4, Oliver found a decreasing hydrolysis rate with decreasing pH. At low pH values we may expect that the hydrolysis rate will become acid catalyzed, which will give an increase in the reaction rate. The involvement of chlorine as a catalyst in this conversion was never studied, but the increased reaction rate may indicate a crucial role in the mechanism.

The GC and GC/MS analyses of extracts containing both DCAN and DCA gave several peaks after methylation with diazomethane, which appeared to be produced by a 1,3-dipolar cycloaddition reaction of diazomethane to the activated cyano group of DCAN (*24*, *25*). One of the products was identified as a methylated 4-(dichloromethyl)-2*H*-1,2,3-triazine (VI), while the others were identified as subsequent methylene insertion products (eq 6). The mass spectrum of VI is given in Figure 4.

$$CHCl_2CN + CH_2N_2 \rightarrow C_3H_4N_3CHCl_2\ (VI) + C_4H_5N_3CHCl_2 + C_5H_8N_3CHCl_2 \quad (6)$$

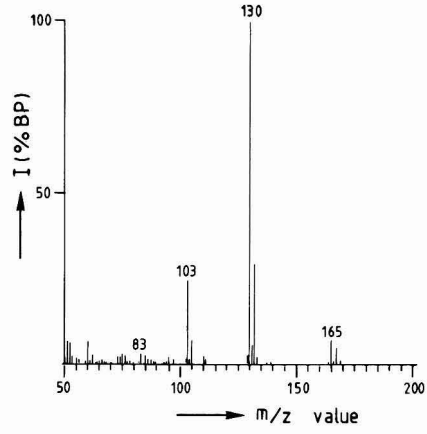

Figure 4. EI mass spectrum of a methylated (dichloromethyl)-1,2,3-triazine ($C_3H_4N_3CHCl_2$) obtained from the reaction between diazomethane and DCAN. *m/z* 165, 167, and 169 (M); *m/z* 130 and 132 (M – Cl); *m/z* 103 and 105 (M – Cl – HCN).

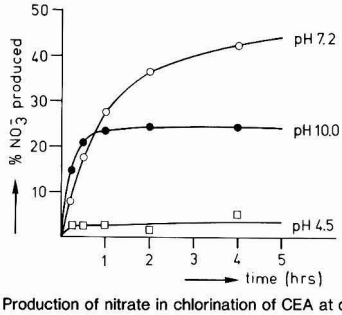

Figure 5. Production of nitrate in chlorination of CEA at different pH values.

pH 7.2. At pH 7.2 the chlorine demand of 4.85 equiv after 24 h exceeded by far the 3.5 equiv necessary for the complete conversion of CEA into DCA or DCPDA and nitrogen. GC/MS showed DCA (80%) and DCPDA as the only products, while DCAN and dichloroacetamide were detected as intermediates, although only in small amounts. The explanation was found in the partial oxidation of the cyanide nitrogen to nitrate instead of molecular nitrogen. The nitrate production in the first 4 h of the reaction is given in Figure 5. After 24 h at pH 7.2, 53% of the cyanide nitrogen was converted into nitrate.

The complete conversion of CEA into DCA or DCPDA and nitrate will require 6 equiv of chlorine (eq 7). The

$$NCCH_2COOH + 6Cl_2 + 5H_2O \rightarrow CHCl_2COOH + CO_2 + HNO_3 + 10HCl \quad (7)$$

experimental chlorine consumption of 4.85 equiv is in excellent agreement with the theoretical value of 4.83 equiv for the conversion of CEA in DCA, DCPDA, and a mixture of NO_3 and N_2 in a mole ratio of 0.53:0.27.

pH 10. At pH 10, the total chlorine consumption of 3.56 equiv seems in agreement with the conversion of CEA into DCA (50%) and DCPDA according to eq 4. GC/MS demonstrated that they were produced as the major products together with small amounts of TCA. However, measurement of the nitrate production demonstrated that 24% of the cyanide nitrogen was converted into nitrate according to eq 7, which gives a theoretical Cl_2 demand of 4.1 equiv.

Scheme I

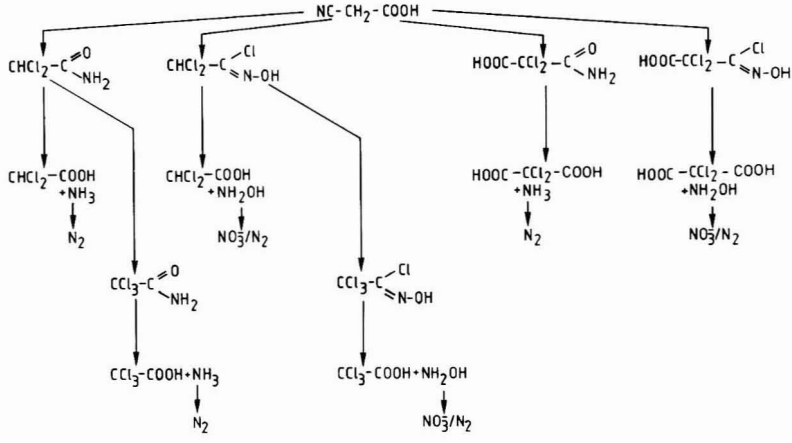

Table III. Chlorination Products of CEA at pH 10 and 1-h Reaction Time[a]

number	product or intermediate
1	$CHCl_2COOH$
2	$CHCl_2CONH_2$
3	CCl_3COOH
4	CCl_3CONH_2
5/7	$CHCl_2CCl{=}NOH$ (two isomers)
6	$HOOCCCl_2CONH_2$
8	$HOOCCCl_2COOH$
9	$CCl_3CCl{=}NOH$
10/11	$HOOCCCl_2CCl{=}NOH$ (two isomers)

[a] All compounds were identified as their methylated product. The compound numbers refer to the peak numbers given in Figure 6.

GC/MS analysis after 1-h reaction time showed an initially confusing number of products (Figure 6, Table III). DCA, TCA, and DCPDA were detected together with their amides, demonstrating that a base-catalyzed hydrolysis of the cyano group occured. However CEA reacted not only through substitution and hydrolysis reactions but also by addition of HOCl to the cyano group producing hydroxamoyl chloride intermediates, a new class of chlorination products that may occur in drinking water (eq 8). The

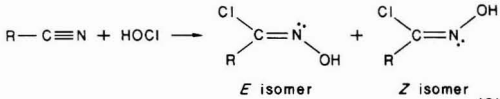

(8)

hydroxamoyl chlorides were identified as their methylated products, which showed mass spectra with a very characteristic fragment ($H_3C{-}O{-}N{=}C{-}Cl+$) at m/z 92/94 (Figure 7).

The amide intermediates will produce ammonia, which will be converted to nitrogen by the break-point chlorination. The hydroxamoyl chlorides will produce hydroxylamine, which will be converted to a mixture of nitrate and nitrogen as summarized in Scheme I.

Oxidation of hydroxylamine with bromine in acidic solution (*26*) gave a complete oxidation to nitrate, while in alkaline solution about 55% was oxidized to nitrogen. In our hands, oxidation of hydroxylamine with chlorine gave a conversion into nitrate of only 20–40% depending on the pH, in better accordance with the total amount of nitrate produced on chlorination of CEA.

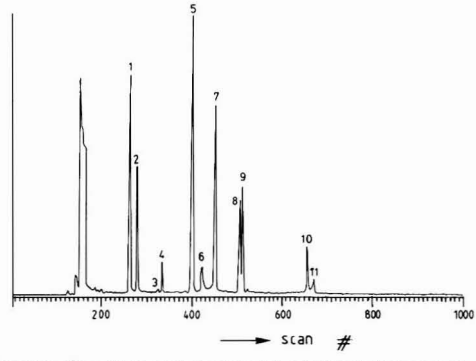

Figure 6. Gas chromatogram of methylated chlorination products of CEA after a reaction time of 1 h at pH 10. The structure of the products is given in Table III.

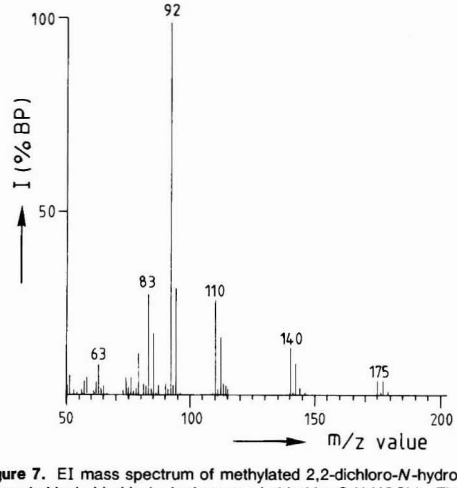

Figure 7. EI mass spectrum of methylated 2,2-dichloro-*N*-hydroxyethaneimidoyl chloride (=hydroxamoyl chloride, $C_3H_4NOCl_3$). The *Z* and *E* isomers (compounds 4 and 5 in Figure 6) showed identical mass spectra: m/z 175, 177, and 179 (M); m/z 140, 142, and 144 (M – Cl); m/z 110, 112, and 114 (M – Cl – CH_2O); m/z 92 and 94 (M – $CHCl_2$); m/z 83, 85, and 87 ($CHCl_2$).

Finally, aspartic acid was chlorinated. The chlorine demand and the chlorination products were in complete

agreement with the production of CEA as a reactive intermediate. The products DCA and DCPDA were produced in the same ratio as on the chlorination of CEA.

Conclusions

The production of CPA and CBA in the chlorination of HA was standard confirmed by an independent synthesis and a comparison of the products on the basis of their GC and GC/MS behavior. It was demonstrated that glutamic acid and lysine can be their precursor structures in HA. CPA and CBA were shown to be quite stable under chlorination conditions at different pH values, which explains why they could be isolated. CEA, which is the expected chlorination product of aspartic acid, was shown to be very reactive under chlorination conditions. CEA was converted into DCA and DCPDA. The reaction mechanism was dependent on the pH. At pH 4.5, DCAN was the intermediate, while at pH 10 hydroxamoyl chlorides were detected as the intermediate products. These hydroxamoyl chlorides represent a new class of chlorination products that may need further study of their biological effects.

Registry No. CPA, 16051-87-9; CBA, 39201-33-7; CEA, 372-09-8; DCA, 79-43-6; DCPDA, 56857-23-9; TCA, 76-03-9; DCBDA, 15519-38-7; $HOOCCH_2CH_2COOH$, 110-15-6; $NCCH_2CH_2CCl_2CHO$, 104156-84-5; $HOOCCH_2CH_2CH_2COOH$, 110-94-1; $HOOCCCl_2CH_2COOH$, 15519-38-7; $HOOCCCl_2CH_2CH_2COOH$, 50901-13-8; glutamic acid, 56-86-0; lysine, 56-87-1.

Literature Cited

(1) Langheld, K. *Chem. Ber.* **1909**, *42*, 2360–2374.
(2) Dakin, H. D. *Biochem. J.* **1916**, *10*, 319–323.
(3) Dakin, H. D. *Biochem. J.* **1917**, *11*, 79–95.
(4) Burleson, J. L.; Peyton, G. R.; Glaze, W. H. *Environ. Sci. Technol.* **1980**, *14*, 1354–1359.
(5) Trehy, M. L.; Bieber, T. I. In *Advances in the Identification and Analysis of Organic Pollutants in Water*; Keith, L. H., Ed; Ann Arbor Science: Ann Arbor, MI, 1981, pp 941–975.
(6) Bieber, T. I.; Trehy, M. L. In *Water Chlorination: Environmental Impact and Health Effects*; Jolley, R. L.; et al., Eds.; Ann Arbor Science: Ann Arbor, MI, 1983; Vol. 4, pp 85–96.
(7) Keith, L. H.; Hall, R. C.; Hanish, R. C.; Landolt, R. G.; Henderson, J. E. *Water Sci. Technol.* **1982**, *14*(II), 59–71.
(8) Coleman, W. E.; Munch, J. W.; Kaylor, W. H.; Streicher, R. P.; Ringhand, H. P.; Meier, J. R. *Environ. Sci. Technol.* **1984**, *18*, 674–681.
(9) Oliver, B. G. *Environ. Sci. Technol.* **1983**, *17*, 80–83.
(10) de Leer, E. W. B.; Sinninghe Damstė, J. S.; Erkelens, C.; De Galan, L. *Environ. Sci. Technol.* **1985**, *19*, 512–522.
(11) American Public Health Association *Standard Methods for Examination of Water and Wastewater*; APHA: Chicago, 1980; p 408A.
(12) Gordon, G.; Ikeda, Y. *J.—Am. Water Works Assoc.* **1984**, *76*, 98–101.
(13) Vorabdruck Deutsche Einheitsverfahren *Vom Wasser* **1974**, *43*, 529–531.
(14) Del'Nik, V. B.; Kagna, S. Sh.; Katsnel'son, M. G.; Rabinovich, A. S.; Skop, S. L. *J. Gen. Chem. USSR (Engl. Transl.)* **1982**, *51*, 1623–1626.
(15) Cohen, P. *Biochem. J.* **1939**, *33*, 551–558.
(16) Reppe, W. *Liebigs Ann. Chem.* **1955**, *596*, 198.
(17) Christman, R. F. *Environ. Sci. Technol.* **1982**, *16*, 143A.
(18) Christman, R. F. *Environ. Sci. Technol.* **1982**, *16*, 594A.
(19) Christman, R. F. *Environ. Sci. Technol.* **1984**, *18*, 203A.
(20) Le Cloirec, C.; Martin, G. In *Water Chlorination: Environmental Impact and Health Effects*; Jolley, R. L.; et al., Eds.; Lewis Publishers: Chelsea, MI, 1985; Vol. 5, pp 821–834.
(21) Chapin, R. M. *J. Am. Chem. Soc.* **1934**, *56*, 2211–2215.
(22) White, G. C. *Handbook of Chlorination*; Van Nostrand-Reinhold: New York, 1972.
(23) Christman, R. F.; Norwood, D. L.; Millington, D. S.; Johnson, J. D.; Stevens, A. A. *Environ. Sci. Technol.* **1983**, *17*, 625–628.
(24) Huisgen, R. *Angew. Chem.* **1963**, *75*, 604–637.
(25) Martin, D.; Weise, A. *Chem. Ber.* **1966**, *99*, 317–327.
(26) Rupp, E.; Mäder, H. *Arch. Pharm. (Weinheim, Ger.)* **1913**, *251*, 295–300.

Received for review February 25, 1986. Accepted June 18, 1986.

Environ. Sci. Technol. 1986, 20, 1224–1229

Heterocoagulation vs. Surface Precipitation in a Quartz–$Mg(OH)_2$ System

Santhana V. Krishnan* and Iwao Iwasaki

Mineral Resources Research Center, University of Minnesota, Minneapolis, Minnesota 55455

■ The stability of fine quartz suspensions in process water is of concern in several mineral processing and water clarification applications. In alkaline solutions, the presence of magnesium ions, arising from such sources as hardness of water and dissolution of impurity minerals, leads to the precipitation of $Mg(OH)_2$, which coats the surfaces of quartz. The conditions under which heterocoagulation or surface precipitation of $Mg(OH)_2$ on quartz occurs and the manner in which they influence the settling behavior of ground quartz were studied by means of settling tests, coating density determinations, ζ potential measurements, and electron microscope observations. Coating density was greater when $Mg(OH)_2$ nucleated on the surface of quartz than when the precipitates heterocoagulated on the quartz surface. The settling curves of quartz suspensions as a function of pH showed maxima at different concentrations of $MgCl_2$, and the highest settling rate was observed at 10^{-3} M $MgCl_2$ and pH 11. Interactions between quartz and $Mg(OH)_2$ and flocculation–dispersion characteristics of quartz suspensions in this system are discussed.

Introduction

The stability of fine quartz suspensions in aqueous media is of considerable interest in mineral processing and water clarification applications. Stability of these suspensions is primarily controlled by the surface chemistry of quartz, which in turn is influenced by the quality of water.

The influence of water quality on stability of quartz has been documented (*1, 2*). Magnesium ion is one of the most common soluble species in process water. These ions may arise from such sources as magnesium-containing minerals like dolomite and clays and hardness of water. At alkaline pH values, magnesium ions precipitate as $Mg(OH)_2$. The interdependence of the quantity of Mg^{2+} and $Mg(OH)_2$ present and suspension pH with the surface of quartz may determine the stability behavior of quartz suspensions.

In this article the attachment of $Mg(OH)_2$ precipitates on surfaces of quartz by heterocoagulation and surface precipitation is compared and related to stability of quartz suspensions.

Experimental Section

Materials. The quartz sample was prepared from high-purity Brazilian rock crystal. The crystals were crushed in a roll crusher, and the size fraction 65/100 mesh was screened out. The screened sample was scrubbed and deslimed with distilled water, leached with hot, concentrated hydrochloric acid, and washed repeatedly with distilled water until free of chloride ions. The sample was then dried at about 100 °C and ground in 600-g batches in an Abbé pebble mill for 120 min to give a size modulus of 60 μm, determined by the Andreasen pipet technique. This sample was used in all tests.

Magnesium chloride used was of analytical grade. Sodium hydroxide and hydrochloric acid were used to adjust pH. All tests were performed in distilled water.

*Address correspondence to this author at Battelle Columbus Division, Columbus, OH 43201.

Methods and Apparatus. Flocculation tests were performed by weighing out 25 g of quartz in a 500-mL graduated cylinder. For heterocoagulation tests, the following procedure was adopted: about 50 mL of distilled water at the desired pH was added to the quartz sample. In a separate beaker, about 450 mL of a $MgCl_2$ solution of a chosen concentration was placed, and the pH was adjusted to a desired value to induce precipitation. The contents of the beaker were well stirred with a magnetic stirrer during the addition of NaOH. The precipitate suspension was transferred to the cylinder containing the quartz suspension, and the final volume was adjusted to 500 mL. Any precipitate of $Mg(OH)_2$ formed was thus allowed to heterocoagulate onto the surface of quartz. The cylinder was inverted 5 times while being shaken manually and set on a flat surface, and its settling rate was determined by noting the time taken for the mudline to descend a fixed distance. When no mud line was seen even after 3 min, an arbitrary value of zero was assigned to the settling rate.

For surface precipitation tests, about 500 mL of distilled water was added to 25 g of quartz in a 500-mL graduated cylinder. Appropriate amounts of $MgCl_2$ were added, and the contents of the jar were then well agitated manually by repeated inversions. NaOH was added to adjust the pH to the desired value to induce precipitation. The final volume then was made up to 500 mL. Under these conditions, much of the $Mg(OH)_2$ precipitate nucleated on the surface of quartz, but bulk precipitation also occurred, particularly at high concentrations of $MgCl_2$. The settling rate was determined as described earlier.

After the determination of settling rate, the cylinder was inverted 3 times and set on a flat surface. After 3 min, 200 mL of the suspension from the top of the cylinder was collected by placing a siphon at the 300-mL level. The collected sample was well agitated, 50 mL of it was pipetted into a breaker, dried, and weighed, and the suspended solids concentration was determined. The amount of suspended solids was obtained by correcting for dissolved salt concentration by evaporating centrifuged solution to dryness. Another 50 mL of the collected sample was centrifuged in an International Equipment Co. Model HT centrifuge at 12000 rpm for 30 min. The clear solution was analyzed for residual concentration of Mg^{2+} by atomic absorption.

The final pH of the flocculated suspension was checked after siphoning off 200 mL, and the suspension was filtered through a 270-mesh screen. The +270-mesh fraction was washed thoroughly with denatured alcohol, dried at 80 °C, weighed, and leached with concentrated hydrochloric acid. The leachate was diluted and analyzed for Mg concentration by atomic absorption spectroscopy. The abstraction density was then calculated. The −270-mesh fraction was collected in a breaker, and the ζ potential of the particles was determined by means of a flat-cell, electrophoresis apparatus. A description of the setup has been reported previously (*2*).

Samples for electron microscope observations were set aside from abstraction and flocculation tests at the stage preceding the leaching of the mineral with hydrochloric acid. The samples were sprinkled evenly on copper holders and coated with gold in a vacuum chamber. The samples

 0013-936X/86/0920-1224$01.50/0

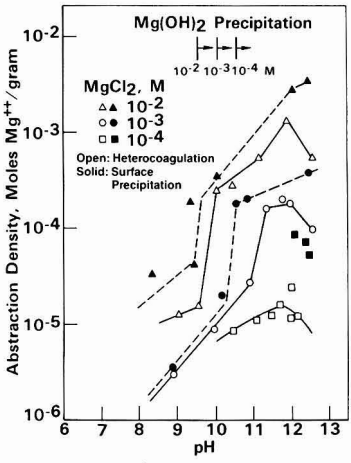

Figure 1. Abstraction of Mg^{2+} and $Mg(OH)_2$ by quartz in the presence of 10^{-4}, 10^{-3}, and 10^{-2} M magnesium chloride as a function of pH.

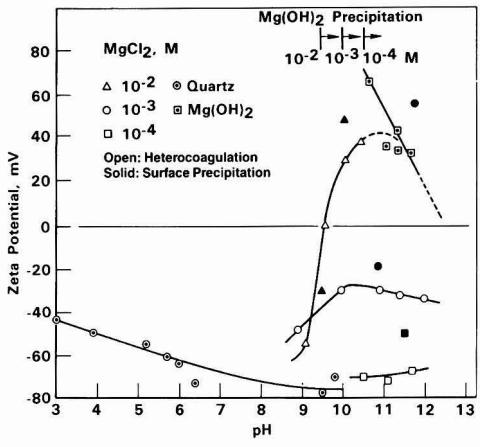

Figure 2. ζ potentials of $Mg(OH)_2$ precipitates and of quartz in the absence and presence of 10^{-4}, 10^{-3}, and 10^{-2} M magnesium chloride as a function of pH under heterocoagulation and surface precipitation conditions.

were then observed in the scanning mode in a JEOL Model 100 CX scanning and transmission electron microscope.

Results

Differences in occurrence and behavior of heterocoagulation and surface precipitation in quartz–$MgCl_2$ were examined by abstraction tests, ζ potential determinations, scanning and transmission electron microscope observations, and flocculation tests. The results are given below.

Abstraction Tests. Abstraction of Mg^{2+} as ions or precipitates onto quartz is indicated in Figure 1 as a function of pH for different $MgCl_2$ concentrations. It is observed in general that the abstraction increased sharply with pH, indicating a strong interaction between a Mg^{2+} and a quartz surface. The steep rise in abstraction at or above the pH of bulk precipitation of $Mg(OH)_2$ denotes the affinity between the precipitates and quartz. The points-of-zero-charge (pzc) of quartz and $Mg(OH)_2$ are between pH 1 and pH 3 and pH 12 and pH 13, respectively (*3*). Hence, electrostatic attraction between the negatively charged quartz and the positively charged $Mg(OH)_2$ below pH 12 is evident.

It is seen that surface precipitation of $Mg(OH)_2$ onto quartz surface led to a higher abstraction density than in the case of heterocoagulation. Abstraction by heterocoagulation depends on the electrostatic affinity between $Mg(OH)_2$ and quartz surfaces. The electrostatic nature of the interaction between these surfaces is brought out clearly in the curves where it is observed that abstraction increased steadily with pH until pH 12. Above pH 12, where $Mg(OH)_2$ is uncharged or is mildly negative, the abstraction curves showed a decrease due to repulsion between the precipitate and mineral surfaces.

ζ Potential Measurements. ζ potentials of $Mg(OH)_2$ precipitates and of quartz in the absence and presence of $MgCl_2$ are shown as a function of pH in Figure 2. Quartz showed a high negative charge in the alkaline pH range, with a ζ potential of about −80 mV at pH 11. Precipitates of $Mg(OH)_2$ showed positive ζ potentials below pH 12.5, and a value of 55 mV at pH 11. Therefore, when ground quartz was mixed with $MgCl_2$ solutions at pH values below 12.5, where $Mg(OH)_2$ was precipitated, heterocoagulation of positively charged $Mg(OH)_2$ onto the negative surfaces of quartz took place readily, as noted in the abstraction tests.

The figure also shows ζ potentials of fine particles from flocculation tests. Since the flocs formed in these tests were large and settled quickly in the microelectrophoresis cell, the ζ potentials reported in this figure are those of individual particles of quartz. In the presence of 10^{-2} M $MgCl_2$ solutions, the ζ potentials of quartz particles, at pH values well below that of bulk precipitation, increased sharply from −70 mV to about 40 mV at pH values well above that of bulk precipitation. The results show the change of the surface of the mineral from quartz-like to $Mg(OH)_2$-like as the surface became coated with the precipitate. This trend was much less pronounced at 10^{-3} M $MgCl_2$, where the negative values of ζ potentials indicated inadequate precipitate coating on the mineral surfaces. At 10^{-4} M $MgCl_2$, the quartz particles showed little effect by the presence of the precipitates. A similar picture has also been reported of silica in $Co(NO_3)_2$ solutions in the pH range where precipitation of $Co(OH)_2$ occurred (*5*).

It was noted also that quartz particles obtained from flocculation tests by surface precipitation showed more positive ζ potentials than those obtained from tests by heterocoagulation. This was obviously due to the higher coating of $Mg(OH)_2$ on the quartz surface as was seen in abstraction test results.

STEM Observations. Scanning and transmission electron micrographs of surfaces pertaining to the quartz–$MgCl_2$ system are shown in Figure 3A–H. The clean surface of quartz at pH 11, conditioned in distilled water, is shown in Figure 3A. Morphology of $Mg(OH)_2$ precipitates at pH 11 is shown in Figure 3B. Figure 3C–F shows increasing amounts of $Mg(OH)_2$ precipitates dotting quartz surfaces under heterocoagulation conditions in the presence of 10^{-3} M $MgCl_2$ and at pH values of 8.9, 11.0, 12.0, and 12.6, respectively.

The differences occurring in surface topography between heterocoagulation and surface precipitation are shown in Figure 3G,H. Quartz conditioned with 10^{-3} M $MgCl_2$ at pH 11 by surface precipitation (Figure 3H) showed a denser coating than that conditioned by heterocoagulation.

Flocculation Tests. Flocculation behavior of ground quartz in $MgCl_2$ solution was examined as a function of pH by standardized jar tests from which the settling rate (cm/min), suspended solids concentration (ppm), and residual concentration of Mg^{2+} were determined. Figures

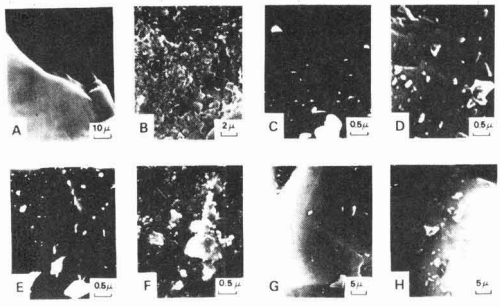

Figure 3. Scanning and transmission electron micrographs of quartz surfaces at various pH values under heterocoagulation conditions in 10^{-3} M $MgCl_2$. (A) Surface of Brazilian quartz, pH 11; (B) magnesium hydroxide precipitate, pH 11 (TEM); (C) surface of quartz with 10^{-3} M $MgCl_2$, pH 8.9; (D) surface of quartz with 10^{-3} M $MgCl_2$, pH 11.0; (E) surface of quartz with 10^{-3} M $MgCl_2$, pH 12.0; (F) surface of quartz with 10^{-3} M $MgCl_2$, pH 12.6; (G) quartz with 10^{-3} M $MgCl_2$ at pH 11, heterocoagulation conditions; (H) quartz with 10^{-3} M $MgCl_2$ at pH 11, surface precipitation conditions.

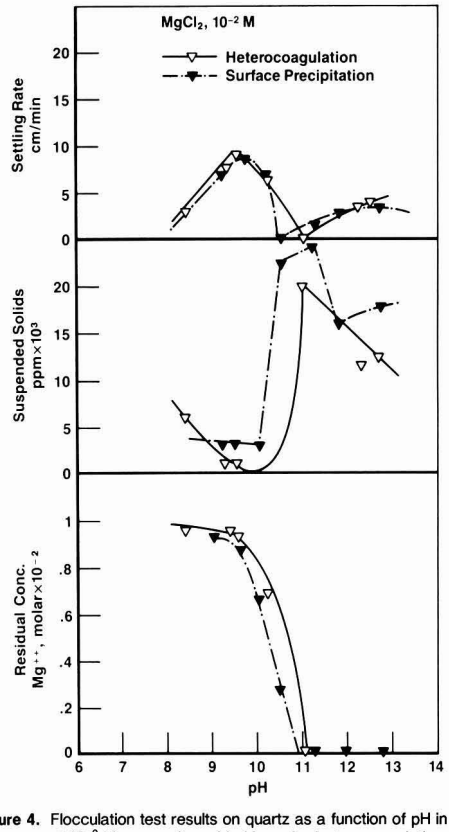

Figure 4. Flocculation test results on quartz as a function of pH in the presence of 10^{-2} M magnesium chloride under heterocoagulation and surface precipitation conditions.

4–6 show flocculation test results on quartz as a function of pH in the presence of 10^{-2}, 10^{-3}, and 10^{-4} M $MgCl_2$, respectively, under heterocoagulation and surface precipitation conditions.

At 10^{-2} M $MgCl_2$ (Figure 4), it was observed that the settling rates under heterocoagulation and surface precipitation were similar. Under free-settling conditions, settling rates were indicative of the floc size, the larger flocs resulting in higher settling rates. The largest flocs at 10^{-2} M $MgCl_2$ were formed at a pH of about 9.6. The settling rate curve shows two regions of flocculation reaching a maximum settling rate of 9.5 cm/min at pH 9.6 and dispersing fully near pH 11.0. As the pH was further increased, a second flocculation region was observed where precipitates of $Mg(OH)_2$ themselves started settling on their own, weighed down by the quartz particles. Flocculation of $Mg(OH)_2$ precipitates by themselves in a separate test showed that the precipitates settled as a thick gelatinous mass with a sharp mud line and a clear supernatant, reaching a settling rate of about 0.7 cm/min at pH 12.5. The nature of the pulp in the second flocculation region at 10^{-2} M $MgCl_2$ in Figure 4 was observed to be similar to that of $Mg(OH)_2$ precipitates.

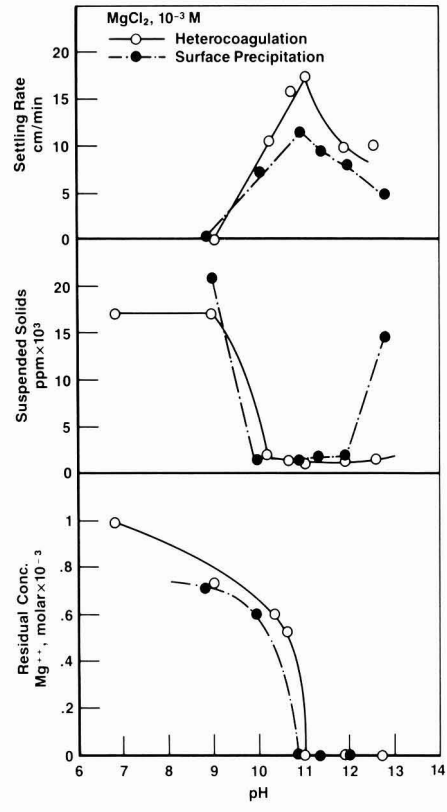

Figure 5. Flocculation test results on quartz as a function of pH in the presence of 10^{-3} M magnesium chloride under heterocoagulation and surface precipitation conditions.

In the absence of any foreign ions in the pulp, ground quartz gave suspended solids concentrations of 17 000–20 000 ppm. In Figure 4, the suspended solids concentration of quartz in the presence of 10^{-2} M $MgCl_2$ was below 2000 ppm between pH 9 and pH 10 but reached as high as 20 000 ppm near pH 11. Residual concentrations of Mg^{2+} in the supernatant indicated gradual initial removal of Mg^{2+} from solution due to adsorption onto the quartz surface and sharp reduction of Mg^{2+} on account of precipitation as $Mg(OH)_2$. Very little Mg^{2+} remained in solution at pH above 11 for all concentrations of $MgCl_2$ employed in these tests.

(800) 424-6747 (U.S. only)

NO POSTAGE
NECESSARY
IF MAILED
IN THE
UNITED STATES

BUSINESS REPLY MAIL

FIRST CLASS PERMIT NO. 10094 WASHINGTON, D.C.

POSTAGE WILL BE PAID BY ADDRESSEE

American Chemical Society
Marketing Communications Department
1155 Sixteenth Street, N.W.
Washington, D.C. 20036-9976

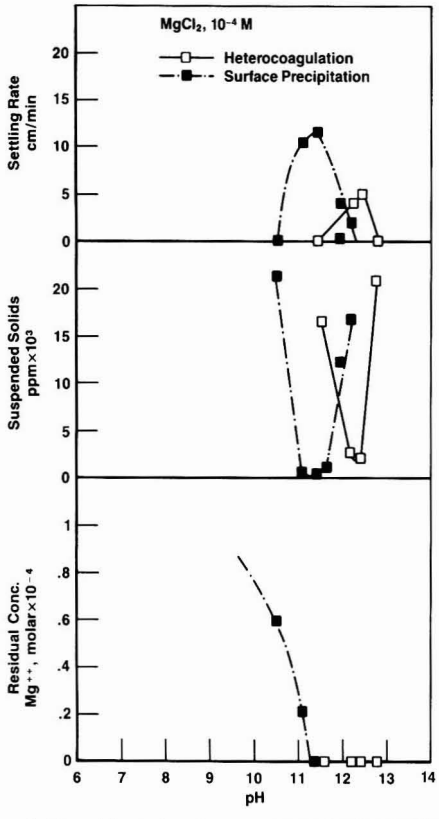

Figure 6. Flocculation test results on quartz as a function of pH in the presence of 10^{-4} M magnesium chloride under heterocoagulation and surface precipitation conditions.

The settling rate curve at 10^{-3} M $MgCl_2$ (Figure 5) had a wider spread, showing appreciable flocculation of quartz between pH 9.5 and pH 12.5. A significant observation in this figure is that the settling rate under heterocoagulation conditions was higher than that for surface precipitation. Under both conditions, the settling rates peaked at pH 11. The peak settling rates under both conditions were the highest of the three $MgCl_2$ concentrations tested. The suspended solids content was at low levels (2000 ppm or less) for a wider range of pH (10–12), corresponding to the settling rate curves.

At 10^{-4} M $MgCl_2$, the settling behaviors of quartz under heterocoagulation and surface precipitation conditions were different. The peaks under these conditions occurred at pH of 11.4 and 12.3 with settling rates of about 11 and 5 cm/min, respectively. Values of the suspended solids concentrations reflected the settling rates obtained, with clarification of the pulp occurring in a narrow range at about pH 12.2 and pH 11 for heterocoagulation and surface precipitation conditions, respectively.

Comparing the flocculation curves at 10^{-2}, 10^{-3}, and 10^{-4} M $MgCl_2$ (Figures 4–6), it was noted that at all concentrations of $MgCl_2$ quartz flocculated appreciably in certain pH ranges. Flocculation in all the three cases commenced at a pH below that of bulk precipitation of $Mg(OH)_2$, increased steadily to peak at unique pH values, and gradually decreased at higher pH. This behavior corresponded with increasing abstraction of Mg^{2+} and $Mg(OH)_2$ on quartz as shown in Figure 1.

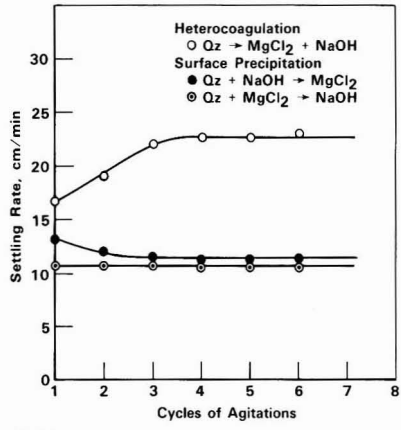

Figure 7. Effect of agitation on settling of quartz in the presence of 10^{-3} M magnesium chloride at pH 11 under heterocoagulation and surface precipitation conditions.

Also, comparison of the flocculation curves at three concentrations of $MgCl_2$ shows that at 10^{-2} M there was an excess of $Mg(OH)_2$ precipitates formed. There was no distinct difference between heterocoagulation and surface precipitation systems. The surfaces of quartz would be expected to be heavily coated with $Mg(OH)_2$ under both conditions. Heavy coating by $Mg(OH)_2$ of quartz surfaces was observed by means of an electron microscope. At 10^{-3} M, where bulk precipitation of $Mg(OH)_2$ does not begin to occur at pH below 10.4, the difference between the two systems was most distinct. At 10^{-4} M, bulk precipitation of $Mg(OH)_2$ did not occur until a pH of 10.9 was reached. In this system, where a lesser quantity of $Mg(OH)_2$ precipitates formed, nucleation on the surface and precipitation in situ appeared to be predominant over heterocoagulation. This was evident from the fact that surface precipitation occurred at a lower pH than heterocoagulation in Figure 6. The three systems (Figures 4–6) differ in the quantities of $Mg(OH)_2$ precipitated and illustrate the difference between surface precipitation and heterocoagulation under these conditions.

Since the sequence of addition of reagents in the flocculation tests led to differences in settling behavior, it was of interest to study the nature of the flocs formed in each case. Figure 7 shows settling rates as a function of the number of cycles (three each) of jar inversions of flocculation tests performed at pH 11 by heterocoagulation and surface precipitation methods in the presence of 10^{-3} M $MgCl_2$. Two sequences of reagent additions characterized surface precipitation, as indicated in the figure. The plot shows that continued agitation led to a substantial difference in settling rates between heterocoagulation and surface precipitation, the settling rate in the case of the former increasing to a higher value of 23 cm/min compared to a value of about 11.5 cm/min in the case of the latter. Both sequences of reagent addition employed to bring about surface precipitation gave similar results.

It should be noted that the heterocoagulation and surface precipitation results reported earlier in Figures 4–6 were obtained with only one cycle of agitation. The increase in settling rates with agitation for heterocoagulation suspensions might be due to additional abstraction of $Mg(OH)_2$ onto the quartz surface and the consequent promotion of a more favorable reorientation of quartz particles leading to larger flocs. This did not occur in quartz suspensions with surface precipitated $Mg(OH)_2$

because nearly all the precipitates nucleated on the surface with almost no rearrangement of $Mg(OH)_2$ precipitate occurring on the quartz surface.

Discussion

Heterocoagulation, or mutual coagulation, involves the coagulation of dissimilar particles of either the same or the opposite charge. Although the principal factors governing heterocoagulation and coagulation of identical particles are fundamentally the same, they differ in some important aspects. Electrostatic interaction between two dissimilar particles is always attractive when the particles are oppositely charged or when one of them has a zero charge. When the charges of the particles are of like sign but of different magnitude, the interaction is at first repulsive, tending toward a maximum repulsive energy (energy barrier), and thereafter attractive as the particles approach each other. The location of the energy barrier depends on the ratio of surface potentials of the particles, while the magnitude of the energy barrier depends entirely on the lower surface potential. Heterocoagulation is favored by a large difference in surface potentials and a relatively low value of the lower potentials (*6*).

The pronounced affinity between $Mg(OH)_2$ precipitates and quartz surfaces was evident from the abstraction and ζ potential data. Results of other investigations also support these findings (*4*, *7*). Under conditions where quartz and $Mg(OH)_2$ were oppositely charged, their ζ potentials showed a large difference, with that of $Mg(OH)_2$ being relatively low. These favorable conditions for heterocoagulation, therefore, form a basis for their strong affinity. The overall picture of charge interaction between quartz surfaces and $Mg(OH)_2$ precipitates shows good correspondence to the model presented by James and Healy (*5*) for an oxide–precipitate system in which three charge reversals occur as a function of pH: at the pzc of the substrate [quartz]; at the pzc of the precipitates [$Mg(OH)_2$]; at a pH value between the two depending upon the surface coverage of the metal hydroxide species.

The manner in which the precipitates were deposited on quartz surfaces markedly influenced the extent of abstraction and overall surface charge of the particles. Nucleation and growth of the precipitates on the surface appeared to result in a more abundant and adherent coating than in the case when the precipitates were allowed to heterocoagulate onto the surfaces of quartz. The denser coating produced by surface precipitation in turn exhibited more positive surface charge of the coated quartz particles. Also, in the surface precipitation method, the nucleation of the precipitate occurred at pH values below those for bulk precipitation. This might be due to the strong electric field at the interface resulting in a lower dielectric constant of the medium, which in turn results in a lowering of the solubility product of the precipitates (*5*). Hence, precipitation at the surface might have preceded bulk precipitation. Precipitates that heterocoagulate onto the surface must do so predominantly by means of Coulombic forces. The difference was indicated by the increase in abstraction of surface-precipitated $Mg(OH)_2$ even above pH 12, under which conditions heterocoagulated precipitates showed lower abstraction.

A simple model is presented in Figure 8 to show the formation of a quartz floc in the presence of $Mg(OH)_2$ precipitates. It was noted with electron microscopy that $Mg(OH)_2$ particles formed a spotty coating on the surface of quartz. This type of coating is analogous to the "electrostatic patches" of polymer adsorption described by Kasper (*8*) and Gregory (*9*). A mosaic charge pattern made up of spots of positive charge covering an area of negative

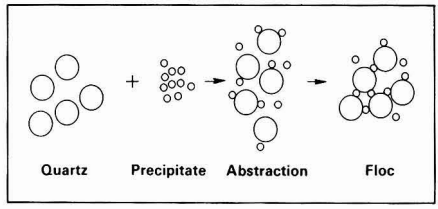

Figure 8. Schematic representation of formation of a floc of quartz particles in the presence of $Mg(OH)_2$ precipitates.

charge results in charge neutralization of the particles. Repulsion forces between particles are greatly reduced when the ζ potentials are in the critical range of about 30 mV (*10*). One such quartz particle on collision with a similar particle can effectively attach itself to the second particle by means of "electrostatic bridges" between $Mg(OH)_2$ spots on one particle and the uncovered quartz surface of the other. Several such particles may thus come together to form a floc. The number of particles joining together to form a floc increases until the overall charge of the floc is zero. If a large portion of the quartz surface is covered by $Mg(OH)_2$, less free surface is available for attachment by other particles, leading to fewer particle attachments and hence smaller flocs. Conversely, a sparse coating of $Mg(OH)_2$ provides less anchor points for other particles, resulting again in smaller flocs. The dependence of settling rates on $MgCl_2$ concentration and pH can, therefore, be directly correlated to this model.

Sedimentation potential tests on this system showed that the charge on the floc was zero at conditions where maximum settling rates of quartz suspensions were obtained (*11*). Coverage of more or less than a critical level increases the positive or negative charge on the floc. Under these conditions, repulsion forces between like charges prevent close approach of the particles, leading to dispersion of the pulp. This was readily seen with 10^{-2} M $MgCl_2$ solutions, where at pH values above 10 a dense coating of $Mg(OH)_2$ on the mineral surface raised the ζ potential to highly positive values resulting in slow-settling pulps. At a pH below 9.6, below bulk precipitation of $Mg(OH)_2$, the charge was still negative, and the suspension exhibited lower settling rates. In addition, the existence of a critical surface coverage is supported by the fact that the peaks of the settling rates at different $MgCl_2$ concentrations occurred at approximately the same abstraction density of Mg^{2+} on quartz. Smellie and LaMer (*12*) suggested that optimum flocculation by polymers is obtained when about half the available adsorption sites on the mineral are occupied by the polymer. A similar picture may be visualized in the present system, with $Mg(OH)_2$ occupying about half the adsorption sites on a quartz particle and forming "electrostatic bridges" with the adsorption sites of the uncovered surface of another particle.

The difference in settling behaviors between surface precipitation and heterocoagulation systems might be related in a complex way to the difference in the formation and extent of coating of the precipitates and the subsequent formation of flocs. Surface precipitation of $Mg(OH)_2$ on quartz resulted in a higher coating density than did heterocoagulation. The nucleated $Mg(OH)_2$ precipitates are rigidly held with no subsequent rearrangement on the surface. The flocs formed undergo less reorientation of disintegration with agitation. On the other hand, in heterocoagulation systems, coating of $Mg(OH)_2$ depends entirely on the frequency of collision among particles and electrostatic forces between the precipitates and the quartz surfaces. The lesser coating density that resulted led to

the formation of smaller flocs due to fewer "electrostatic bridges" between particles. Precipitates not abstracted by quartz remained suspended in the bulk solution. On vigorous and repeated agitation of the suspension, increased collision resulted in more of the free precipitates becoming attached to the surfaces of quartz particles and rearranging to a more favorable configuration for the formation of larger flocs.

Registry No. $Mg(OH)_2$, 1309-42-8; quartz, 14808-60-7.

Literature Cited

(1) Iwasaki, I.; Smith, K. A.; Lipp, R. J.; Sato, H. *Proceedings of the International Symposium on Fine Particles Processing*; Somasundaran, P., Ed.; American Institute of Mining, Metallurgical and Petroleum Engineers: New York, 1980; Vol. 2.
(2) Iwasaki, I.; Lipp, R. J. "Flocculation and Clarification of Mineral Suspensions"; EPA Water Pollution Control Series No. 14010 DRB; U.S. Government Printing Office; Washington, DC, 1971.
(3) Parks, G. A. *Chem. Rev.* **1965**, *65*, 177.
(4) Heerema, R. H.; Iwasaki, I. *Min. Eng. (Littleton, Colo.)* **1980**, *32*(10), 1510.
(5) James, R. O.; Healy, T. W. *J. Colloid Interface Sci.* **1972**, *40*, 53.
(6) Usui, S. *Prog. Surf. Membr. Sci.* **1972**, *5*, 223.
(7) Hast, N. *Ark. Kemi* **1956**, *9*, 343.
(8) Kasper, D. R. Ph.D. Thesis, California Institute of Technology, Pasadena, CA, 1971.
(9) Gregory, J. *J. Colloid Interface Sci.* **1973**, *42*, 448.
(10) Overbeek, J. Th. G. In *Colloid Science*; Kruyt, H. R., Ed.; Elsevier: Amsterdam, 1952; p 302.
(11) Krishnan, S. V.; Iwasaki, I. *Colloids Surf.* **1985**, *15*, 89.
(12) Smellie, R. H.; LaMer, V. K. *J. Colloid Sci.* **1958**, *13*, 589.

Received for review March 31, 1986. Accepted July 8, 1986. The financial support provided for this project by the National Science Foundation (under Grant ENG-7605835A02) and by the American Iron and Steel Institute (under Grant 20-409) is gratefully acknowledged.

Degradation of Tributyltin in San Diego Bay, California, Waters

Peter F. Seligman*

Code 522, Naval Ocean Systems Center, San Diego, California 92152-5000

Aldis O. Valkirs

Computer Sciences Corporation, San Diego, California 92110

Richard F. Lee

Skidaway Institute of Oceanography, Savannah, Georgia 31416

■ Several experiments were carried out to determine the degradation rate of tributyltin (TBT) in microcosms containing harbor water. Unlabeled or ^{14}C-labeled tributyltin was added to water samples collected from two stations in San Diego Bay, CA. Degradation rates were determined by calculating the rate of loss of the added parent TBT compound. Calculated half-lives in water collected from a yacht harbor (ambient concentration was 0.5 μg of TBT/L) were 6 and 7 days for light and dark treatments, respectively. Half-lives from a clean-water site (<0.03 μg of TBT/L) were 9 and 19 days for light and dark treatments, respectively. The principal degradation product in all experiments was dibutyltin with lesser amounts of monobutyltin. Complete mineralization, measured by the formation of $^{14}CO_2$, proceeded slowly with a half-life of 50–75 days. Tributyltin at high concentrations (744 μg/L) was not degraded in sunlight, indicating that photolysis was not taking place and that biological degradation was the primary degradative process for TBT at low ambient concentrations.

Introduction

Tributyltin (TBT) is increasingly used as an antifouling toxicant in boat paints and is also used as a wood preservative, molluscide, and insecticide (*1–3*). The tributyltin cation is highly toxic to certain aquatic organisms. At concentrations of 1 μg/L or less, TBT has been shown to be toxic to certain plankton species, including copepods and mussel larvae (*4, 5*). Long-term toxicity to adult mussels and fish has also been documented at 1 μg/L (*6, 7*).

The presence of TBT in marine and freshwater harbor areas has recently been reported, primarily associated with boating activity (*8–11*). Additionally, studies have documented the presence of monobutyltin (MBT) and dibutyltin (DBT) in environmental water samples where TBT was measured (*8, 11*). Monobutyltin and dibutyltin may enter aqueous systems to a minor degree by leaching from poly(vinyl chloride) and chlorinated poly(vinyl chloride) plastics (*12*). However, in the absence of such inputs, the presence of MBT and DBT is likely due to dealkylation of the TBT species, particularly in areas where antifouling paints containing TBT as a biocide are used routinely.

The degradation of alkyltins has been reported to proceed by successive dealkylation reactions to an inorganic tin salt as the final product (*13, 14*). Determination of TBT degradation rates is a key element in predicting steady-state concentrations of TBT from dynamic models. These predictions are important in risk assessments that address the use of TBT containing antifoulants and are useful in the development of water-quality standards and criteria.

Recent reports have documented photolysis and biodegradation in aquatic systems. Tributyltin added to a freshwater harbor sample degraded to DBT and MBT with a photolytic half-life calculated at >89 days (*15*). Tributyltin initially present in a freshwater harbor sample was found to degrade, in the dark, to MBT and DBT with an estimated half-life of 20 weeks (*16*). There is, however, a lack of information on TBT degradation rates under ambient environmental conditions; we are not aware of studies addressing TBT degradation in marine coastal waters.

0013-936X/86/0920-1229$01.50/0

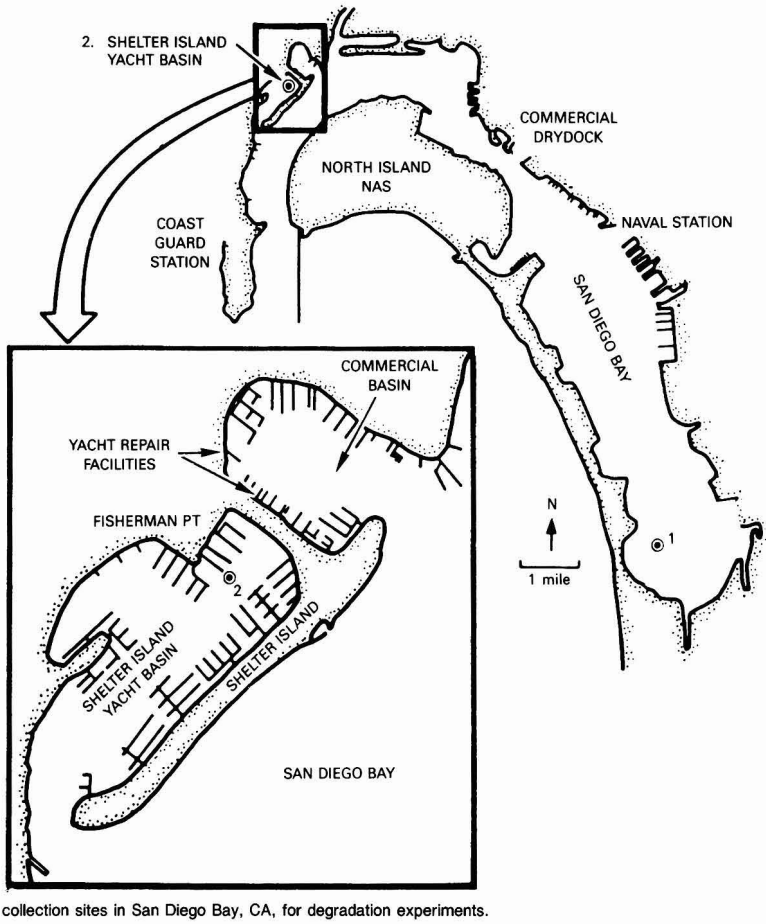

Figure 1. Water collection sites in San Diego Bay, CA, for degradation experiments.

Since TBT is found in areas associated with boating activity, a knowledge of the persistence of TBT in the marine environment is essential to predict potential environmental hazards associated with its widespread use. National attention has recently been focused on the use of TBT as a biocide in antifouling paints by initiation of a Special Review by the U.S. Environmental Protection Agency based on the potential risks to nontarget aquatic organisms [*Fed. Regist.* **1986**, *51*(5)]. The data presented in this study summarize experiments where radiolabeled or unlabeled TBT at concentrations near those found in some harbor areas was added to water from San Diego Bay. The degradation of TBT to DBT, MBT, and $^{14}CO_2$ was followed. Processes that were expected to affect the fate of TBT included indirect photolysis and biological degradation by bacteria and phytoplankton (*14*, *15*, *17*).

Experimental Section

Analysis of Butyltin Species in Seawater. Either a commercial tributyltin chloride standard (Pfaltz and Bauer, Inc.) or a tributyltin cation/distilled water solution was used as the primary TBT source added to ambient seawater. The TBT cation solution was prepared by the National Bureau of Standards (Gaithersburg, MD). Seawater was collected in 24-L polycarbonate plastic bottles from sites (station 1 or 2) within San Diego Bay (Figure 1). A 200-μm mesh Nytex screen was used to filter seawater, which permitted bacteria and phytoplankton to pass but excluded larger zooplankton species and particulate matter.

Initial TBT concentrations were adjusted to give test concentrations of 1 μg/L or less. Samples were analyzed by the hydride derivatization method with atomic absorption (HDAA) detection for determination of TBT, DBT, and MBT. The method has been successfully used to measure butyltin in seawater directly without preconcentration (*18*) and has been modified in our laboratory for direct determination of TBT as well as DBT and MBT in seawater (*11*, *19*). Analytical variability with replicated measurements of standards and natural seawater samples has routinely given standard deviations ranging from 5% to 10% of mean values at 0.01–0.05 μg of TBT/L.

Briefly, a sample is adjusted to a pH of 5.0–5.5 with 2 N acetic acid and reacted with a 4% sodium borohydride solution prepared in 1% sodium hydroxide in distilled water for 5 min. The volatile butyltin and inorganic tin hydrides formed are carried to a cryotrap placed in liquid nitrogen by helium carrier gas. The trap is packed with 0.01–0.015 g of 3% OV-1 on Chromosorb. After the hydrides have been formed and collected in the trap, they are carried into a quartz burner by removing the trap from the liquid nitrogen bath. The hydride compounds are separated by their differing volatility as they distill from the trap, which is allowed to come to room temperature.

Optimal evolution of tributyltin hydride requires heating the trap to 180 °C. Detection is accomplished in the quartz burner at 286.3 nm with a hydrogen–air flame. Detection limits for MBT, DBT, and TBT are 5 ng/L (approximately 2 ng of Sn at the detector).

Inorganic tin was not quantified as no significant increase was noted in its concentration in water over the course of the degradation studies. The mass balance of butyltin species present at any given time was the sum of MBT, DBT, and TBT reported as the chlorides.

Initial experiments indicated that analytical results from replicate treatment bottles could vary widely. Chemical measurements of butyltin species frequently exhibited standard deviations ranging from 5% to 30% or more of the mean value from three separate containers. Accordingly, experiments reported herein were performed with five replicate 1-L polycarbonate containers (microcosms) per treatment.

Radiolabeled Studies. For radiolabeled studies, [*butyl*-1-^{14}C]bis(tri-*n*-butyltin) oxide custom synthesized by New England Nuclear (3.67 mCi/mmol) was used. [^{14}C]TBT was added to 2 L of water collected from station 1 or 2. The final concentration of [^{14}C]TBT was 2 μg/L. At the end of various incubation periods, $^{14}CO_2$ was collected as previously described (*20*). Tributyltin and radiolabeled degradation products were extracted from the 2 L of water with 300 mL of chloroform. Spiked recovery of [^{14}C]TBT was between 97% and 99%.

The chloroform extract was taken to dryness on a rotary evaporator. The extract was redissolved in a small volume of methanol. An aliquot was counted with a liquid scintillation counter, and a second aliquot was applied to silicic acid thin-layer plates. The solvent system used to separate TBT and degradation products was isopropyl ether–acetic acid (98:2 v/v). Autoradiography, using X-ray film (X-Omat AR film, Eastman Kodak Co.), of the thin-layer plates was carried out to locate the position of TBT and degradation products. Authentic standards for thin-layer chromatography included bis(tributyltin) oxide, dibutyltin dichloride, and monobutyltin trichloride (Aldrich Chemical Co.). Unlabeled butyltin standards were visualized with a dithizone or pyrocatechol violet spray (*21*).

For adsorption studies, [^{14}C]TBTO was added to 2 L of seawater from station 1 or 2 to give a final concentration of 2 μg/L. After 24 h of incubation, three aliquots of water (300 mL) were passed through a glass fiber filter. The filter, after being washed with filtered seawater, was counted on a liquid scintillation counter. When [^{14}C]TBTO was added to filtered seawater (passed through a 0.2-μm filter), no radioactivity was found on the glass fiber filter. Since spiked recovery of whole unfiltered seawater was between 97% and 99%, a mass balance of 100% was assumed from particulate values and the filtered seawater fraction. Calculations of particulate radioactivity as percents were made from counts made on filters and the initial water concentration (2.0 μg/L).

Experimental Design. Experiment 1. Seawater, with an ambient TBT concentration of <0.03 μg/L, was collected from station 1 in South San Diego Bay (Figure 1) during late May 1985. Tributyltin cation is distilled water (NBS solution) was used to spike the seawater sample to give an initial TBT concentration of 0.55 μg/L. The initial DBT concentration was 0.008 μg/L. Replicate samples were incubated in 1-L clear polycarbonate bottles under ambient temperature (12.5–15.0 °C) and light conditions in a flow-through tank for a 9-day period. The bottles functioned as microcosms with ambient concentrations of bacteria and phytoplankton and were held approximately 10 cm under the surface of flowing seawater. The 5000-gal tank used to incubate samples was fitted with a neutral density screen, which reduced incident surface light by 41%. Polycarbonate was chosen because of its low adsorptivity to TBT (*22*).

The polycarbonate bottles were either exposed to light or wrapped completely in aluminum foil for "dark" conditions. Five replicate samples were removed for butyltin analysis from light, dark, and light/poisoned treatments. Sodium azide, at a concentration of 0.1 g/L, was added to light/poisoned samples to reduce microbial activity.

In addition to butyltin measurements, temperature, pH, oxygen, and chlorophyll measurements were made on replicate samples at each sampling interval. Oxygen measurements were made with a membrane probe attached to a calibrated meter. A standard extraction method, followed by fluorometric determination, was used to measure chlorophyll (*23*).

Experiment 2. Seawater was collected from station 1 (South San Diego Bay) and station 2 (Shelter Island Yacht Basin) during July 1985. Tributyltin cation in distilled water (NBS solution) was added to 80 L of water so that the initial TBT concentration was 0.99 μg/L. The concentration of DBT was 0.03 μg/L. Replicate samples were incubated under ambient sunlight light and water temperature (15.5–19.5 °C) conditions for an 8-day period in the same reservoir (fitted with a neutral density screen) described under Experiment 1.

Five replicate samples were removed for butyltin analysis from light, dark, light/poisoned, and dark/poisoned treatments. The sodium azide concentration in the dark/poisoned treatment was the same as that used in the light/poisoned treatment (0.01%). Temperature, pH, oxygen, and chlorophyll were also measured in replicate samples by methods previously described.

In order to test the extent of TBT degradation at higher initial concentrations, an additional TBT solution was prepared from near-shore seawater spiked with tributyltin chloride to a concentration of 744 μg/L. This solution was prepared in an 8-L polycarbonate bottle and held in reduced sunlight under flowing seawater conditions in the 5000-gal tank. Samples were withdrawn periodically from this solution to determine the extent of TBT degradation.

For the radiolabeled experiments, [^{14}C]TBTO was added to a number of 4-L Pyrex flasks containing 2 L of water from either station 1 or 2. The initial concentration of [^{14}C]TBTO was 2 μg/L. The water was extracted and analyzed for [^{14}C]TBT and degradation products as described above. Triplicate samples were analyzed for each time period (2, 4, and 6 days). Formalin (0.4% final concentration) was used as a poison.

Results and Discussion

The ambient TBT and DBT concentrations at station 1 located in South San Diego Bay were <0.03 μg/L. Thus, the added TBT and degradation products were easily detected. Rapid degradation of the TBT species was apparent at the low test concentrations used in this study (0.55, 0.99, and 2 μg/L), and the principal degradation product formed was DBT. Chromatographs shown in Figure 2 are representative of the TBT and DBT concentrations present initially and after a 5-day exposure period in experiment 2. The formation of DBT, and to a lesser extent MBT, is evident from an initial TBT concentration of 0.99 μg/L.

Adsorption experiments showed that between 8% and 11% of the [^{14}C]TBT after 24 h was taken up by suspended particles in the light or dark with water from stations 1 and 2. When azide was added to the water,

Table I. Tributyltin Half-Lives Calculated from Linear Regression of Disappearance of TBT Parent Compound

TBT, μg/L	water source	month	temp, °C	treatment	TBT half-life, days	mass balance, %[a]
			Tributyltin Spiked Water			
expt 1						
0.55	STA 1	May–June	12.5–15	light	13	104
0.55	STA 1	May–June	12.5–15	dark	19	94
0.55	STA 1	May–June	12.5–15	light + azide	28	111
expt 2						
0.99	STA 1	July	15.5–19.5	light	9	84
0.99	STA 1	July	15.5–19.5	dark	9	73
0.99	STA 1	July	15.5–19.5	dark + azide	18	85
0.99	STA 1	July	15.5–19.5	light + azide	14	84
			[^{14}C]Tributyltin Spiked Water			
expt 2						
2.0	STA 1	July	15.5–19.5	light	11	98
2.0	STA 1	July	15.5–19.5	dark	12	99
2.0	STA 1	July	15.5–19.5	dark + formalin	89	99
2.0	STA 2	July	15.5–19.5	light	6	97
2.0	STA 2	July	15.5–19.5	dark	7	98
2.0	STA 2	July	15.5–19.5	dark + formalin	94	99

[a] Mass balance refers to the sum of the monobutyltin, dibutyltin, and tributyltin species calculated at the end of the experiment compared to the initial values.

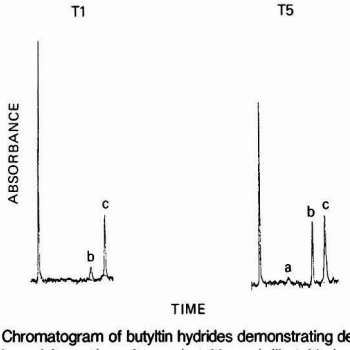

Figure 2. Chromatogram of butyltin hydrides demonstrating degradation of tributyltin and formation of monobutyltin and dibutyltin in seawater over a 5-day period: a = monobutyltin, b = dibutyltin, and c = tributyltin. T1 shows DBT and TBT peaks after 24 h (25-mL sample aliquot) and T5 after 5 days (50-mL sample aliquot).

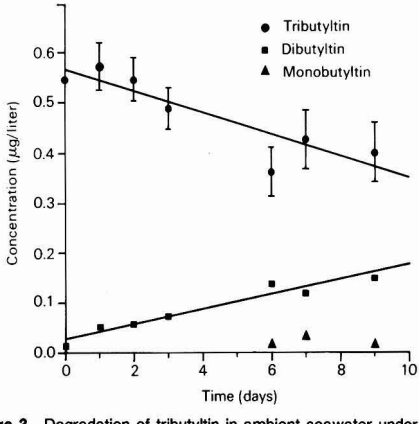

Figure 3. Degradation of tributyltin in ambient seawater under light conditions in experiment 1: (TBT) $y = -0.022x + 0.568$, $r^2 = -0.90$; (DBT) $y = 0.015x + 0.025$, $r^2 = 0.97$.

between 4% and 5% of the [^{14}C]TBT was associated with the particulate fraction. Thus, approximately 4%–6% of the [^{14}C]TBT was actively taken up by particles. Most of the TBT added to seawater samples remained in solution.

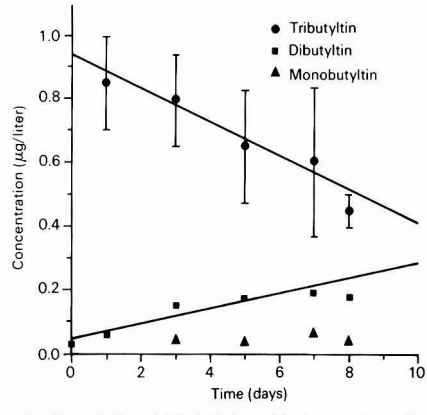

Figure 4. Degradation of tributyltin in ambient seawater under light conditions in experiment 2: (TBT) $y = -0.053x + 0.951$, $r^2 = -0.97$; (DBT) $y = 0.024x + 0.046$, $r^2 = 0.95$. Day 8 data were not used for regression analysis due to poor mass balance (65%).

Butyltin concentrations resulting from direct chemical speciation measurments were, therefore, associated primarily with TBT in solution. Mass balances of total butyltins (parent TBT compound and degradation products) at the end of our studies were 73% or more of initial values, indicating that most of the butyltin species were in solution or loosely associated with particulates and presumably available to borohydride reduction. Some butyltin adsorption to container walls no doubt occurred but did not appear to be a significant factor in these experiments.

The linear loss of parent (TBT) compound and an associated increase in DBT in water from station 1 are shown in Figures 3 and 4 and apparently follow zero-order kinetics. Table I provides TBT half-lives on the basis of regression analysis of TBT loss and the formation of primarily DBT. The half-lives calculated for unlabeled TBT by least-squares regressions of values determined by HDAA in light treatments in experiments 1 and 2 from South San Diego Bay were 13 and 9 days, respectively. In the dark, for Experiments 1 and 2, respectively, TBT half-lives were calculated to be 19 and 9 days. Tributyltin

labeled with ^{14}C and added to water from station 1 gave results similar (11–12-day half-life) to those obtained with unlabeled TBT. Dibutyltin was the principal ^{14}C degradation product formed. Only trace amounts of MBT and $^{14}CO_2$ were detected in the ^{14}C-labeled studies. By use of the formation of $^{14}CO_2$ as the measure of complete mineralization, the calculated half-life (time required for 50% of the initial [^{14}C]TBT to be degraded to $^{14}CO_2$) was 50 and 75 days for TBT added to water from station 1 in the light and dark treatments, respectively. In the formation of dibutyltin by living organisms, there is evidence for formation of β-(hydroxybutyl)dibutyltin, which in turn degrades to dibutyltin with the release of butene (*21*). In our system, [^{14}C]butene would probably be released to the air dead space above the water phase in the containers used and would not be collected in the $^{14}CO_2$ trap. The disappearance of parent TBT compound with concomitant formation of debutylated products is considered here to be an appropriate measure of degradation because of the substantial detoxification of TBT to aquatic organisms resulting from loss of a butyl group. Dibutyltin has been recently reported to be less toxic than TBT by at least 2 orders of magnitude in tests with algae and by 60-fold with mud crab larvae (*24–26*).

In treatments where sodium azide was added, TBT half-lives were longer, suggesting that microbial activity was the important degradative process in TBT decay at low concentrations. Although azide was added to suppress biological activity, the DBT degradation produced was also detected in the dark/azide treatment and increased over time. The azide may have been degraded during the course of the experiment or was too low a concentration (0.01%) to completely kill all microbes. In experiments conducted with [^{14}C]TBT, formalin was used to control microbial activity. Longer TBT half-lives (89–94 days) were calculated in dark treatments where formalin was used, further indicating a microbial association with TBT degradation (Table I).

Tributyltin concentrations of 2 μg/L or less were used in our studies to simulate environmentally realistic concentrations. Although these levels of TBT are not expected in open, well-flushed areas of bays or estuaries, we have measured TBT concentrations ranging from 0.49 to 0.93 μg/L at station 2 in the Shelter Island Yacht Basin during July–September 1985 (*11*). Additionally, recent evidence suggests that microbial degradation of organic compounds may proceed at low concentrations, while at higher concentrations degradation is reduced or not apparent (*27*). This process may be due either to inhibition of all microorganisms capable of metabolizing the compound or to the inhibition of the mineralizing, but not the cometabolizing populations (*27*). A study conducted concurrently with experiments 1 and 2 using TBT at a concentration of 744 μg/L under the same ambient light and temperature conditions indicated no degradation over a period of 144 days. Biodegradation was likely inhibited by direct toxicity of TBT at such a high concentration.

Ambient TBT and DBT concentrations at station 2 (Shelter Island Yacht Harbor) were 0.49 and 0.28 μg/L, respectively. These concentrations were much higher than those measured at station 1, presumably due to the high density of yachts (more than 2000) in the boat basin and the likelihood of TBT antifouling paint use. Higher TBT degradation rates were also noted at station 2 compared with station 1, with half-lives of 6 and 7 days calculated for light and dark treatments, respectively (Figure 5, Table I). The observed degradation was primarily due to microbial metabolism since the half-life was calculated at 94

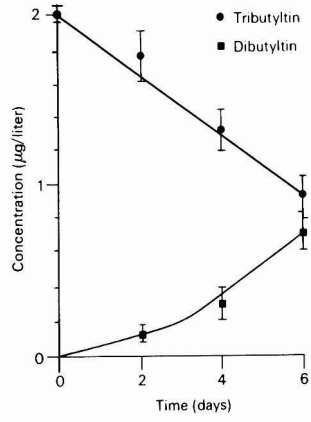

Figure 5. Degradation of ^{14}C-labeled tributyltin in seawater collected from Shelter Island Yacht Basin (experiment 2 under light conditions).

days when formalin was used as a biocide. Other studies have shown high linear degradation rates when radiolabeled pollutants were added to water that had previous exposure to the same pollutants (*20*). We speculate that microbes capable of degrading TBT are present in higher numbers at station 2 compared with station 1 and may represent an adapted population. Recent work with phytoplankton, however, did not demonstrate adaption to TBT after 12 weeks of exposure (*24*).

Tributyltin degradation rates reported as half-lives in this study were generally slightly longer under dark than under light conditions, suggesting that some algal metabolsim of TBT may have occurred in light treatments. In preliminary experiments we have found that a new degradation product is found in light treatments having the properties of a (hydroxybutyl)dibutyltin compound (*28*). Maguire et al. (*17*) have shown that approximately 50% of the TBT added to an axenic green algal culture was converted to DBT over a 4-week period. The authors recognized that the algal concentrations used in their study were about 2 orders of magnitude greater than those representative of actual lake or harbor levels. Degradation rates at environmental algal concentrations may, therefore, be lower. Under conditions where phytoplankton experience exponential growth forming "blooms", algae may play an important role in TBT degradation. In our studies, chlorophyll production increased rapidly during the first few days in light treatments in experiments 1 and 2, and then declined to initial levels, possibly due to nutrient depletion. Maximum chlorophyll levels did not exceed 4 μg/L, which was approximately twice the concentration measured initially in experiments 1 and 2. Algal growth was, therefore, limited to near environmental levels throughout our studies.

Direct photolysis of TBT was not expected to be important in our experiments since the polycarbonate bottles used absorbed most light below 360 nm. Butyltins essentially do not absorb light above 350 nm (*15*). Maguire et al. found that direct photolysis of TBT in distilled water and water from a freshwater harbor was slow with a half-life >89 days (*15*). When TBT was added to distilled water and to water containing fulvic acid, followed by exposure to a mercury lamp with a peak wavelength at 350 nm, the half-life decreased from 18 to 6 days, suggesting a photosensitized reaction had occurred (*15*). Tributyltin degradation was not evident in our studies at a high TBT concentration (744 μg/L) over a 144-day period, indicating

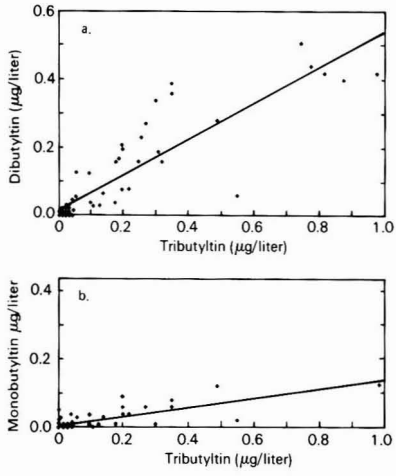

Figure 6. Least-squares regression of TBT vs. DBT and MBT measurements from San Diego Bay, CA, water samples. Samples were collected over a 3-year period from various sites: (a) [DBT] = 0.527[TBT] + 0.013, r^2 = 0.80, n = 78; (b) [MBT] = 0.130[TBT] + 0.006, r^2 = 0.59, n = 70.

that neither indirect photolysis nor chemical redistribution was a significant process under or experimental conditions.

Assuming the degradation measurements reported herein are representative of San Diego Bay waters, it follows that significant levels of degradation products (DBT and MBT) would be measured in ambient waters where flushing rates are slow. It is anticipated that these measurements would covary with the tributyltin cation concentration in a relatively constant ratio dependent on degradation and flushing rates. Butyltin concentrations from San Diego Bay samples (*11*) and subsequent measurements (unpublished data) indicate that DBT and MBT are nearly always present and tend to covary with TBT (Figure 6). Least-squares regression analysis from these San Diego Bay water samples tends to demonstrate this covariance. On average, about 30%–40% of the total butyltin species was DBT whereas, generally, only 10% or less was in the MBT form. These ratios of DBT and MBT are similar to those found after a week in our experimental systems and tend to support the stepwise dealkylation process observed in our microcosm degradation studies.

Conclusions

Tributyltin degrades rapidly in seawater during summer months at concentrations near 2 μg/L and less, which are close to levels recently reported in boat harbors with limited circulation. Dibutyltin is the principal degradation product formed with a lesser amount of monobutyltin also formed. Our experiments indicate microbial metabolism was the principal degradative process, using direct chemical measurements or radioactive-labeled compounds to follow the dealkylation of the parent TBT species to DBT and MBT. Algal metabolism may have played a lesser role while photolysis was not considered a significant process in these experiments.

Measurements of butyltin species in San Diego Harbor waters have demonstrated that degradation products (MBT and DBT) are present in nearly equal concentrations with TBT, providing further evidence for a relatively rapid degradation process. Efforts are continuing to examine seasonal degradative processes in various marine and estuarine systems for future use in aquatic models.

Acknowledgments

We gratefully acknowledge the analytical support provided by Giti Vafa.

Registry No. TBT, 688-73-3; DBT, 1002-53-5; monobutyltin, 2406-65-7.

Literature Cited

(1) Zuckerman, J. J.; Reisdorf, R. P.; Ellis, H. V., III; Wilkinson, R. R. In *Organometals and Organometalloids, Occurrence and Fate in the Environment*; Brinckman, F. E.; Bellama, J. M., Eds.; ACS Symposium Series 82; American Chemical Society: Washington, DC, 1981; pp 388–422.

(2) Thompson, J. A. J.; Sheffer, M. G.; Pierce, R. C.; Chau, Y. K.; Cooney, J. J.; Cullen, W. R.; Maguire, R. J. "Organotin Compounds in the Aquatic Environment: Scientific Criteria for Assessing Their Effects on Environmental Quality"; Publication No. 22494; National Research Council of Canada: Ottawa, Canada K1A 0R6, 1985; 284 pp.

(3) Hall, L. W.; Pinkney, A. E. *CRC Crit. Rev. Toxicol.* **1985**, *14*, 159.

(4) U'Ren, S. C. *Mar. Pollut. Bull.* **1983**, *14*, 303–306.

(5) Beaumont, A. R.; Budd, M. D. *Mar. Pollut. Bull.* **1984**, *15*, 402–405.

(6) Valkirs, A. O.; Davidson, B. M.; Seligman, P. "Sublethal Growth Effects and Mortality to Marine Bivalves and Fish from Long-Term Exposure to Tributyltin"; Technical Report No. 1042; Naval Ocean Systems Center: San Diego, CA, 1985.

(7) Ward, G. S.; Cramm, G. C.; Parrish, P. R.; Trachman, H.; Slesinger, A. "Bioaccumulation and Chronic Toxicity of Bis(tributyltin) Oxide (TBTO): Tests with a Saltwater Fish"; In *Aquatic Toxicology and Hazard Assessment: Fourth Conference*; Branson, D. R.; Dickson, K. L., Eds.; American Society for Testing and Materials: Chicago, IL, 1981; ASTM STP 737, pp 183–200.

(8) Maguire, R. J.; Chau, Y. K.; Bengert, G. A.; Hale, E. J.; Wong, P. T. S.; Kramar, O. *Environ. Sci. Technol.* **1982**, *16*, 698–702.

(9) Waldock, M. J.; Miller, D. *Coop. Res. Rep.—Int. Counc. Explor. Sea* **1983**, *CM/E:12* (mimeograph).

(10) Mueller, M. D. *Fresenius' Z. Anal. Chem.* **1984**, *317*, 32–36.

(11) Valkirs, A. O.; Seligman, P. F.; Stang, P. M.; Homer, V.; Lieberman, S. H.; Vafa, G.; Dooley, C. A. *Mar. Pollut. Bull.* **1986**, *17*, 319–324.

(12) Boettner, E. A.; Ball, G. L.; Hollingsworth, Z.; Aquino, R. *Organic and Organotin Compounds Leached from PVC and CPVC Pipe*; EPA Health and Effects Research Laboratory: Cincinnati, OH, 1982; EPA-600-SI-81-062.

(13) Brinckman, F. E. *J. Organomet. Chem. Libr.* **1981**, *12*, 343–376.

(14) Blunden, S. J.; Chapman, A. H. *Environ. Technol. Lett.* **1982**, *3*, 267–272.

(15) Maguire, R. J.; Carey, J. H.; Hale, E. J. *J. Agric. Food Chem.* **1983**, *31*, 1060–1065.

(16) Maguire, R. J.; Tkacz, R. J. *J. Agric. Food Chem.* **1985**, *33*, 947–953.

(17) Maguire, R. J.; Wong, P. T. S.; Rhamey, J. S. *Can. J. Fish. Aquat. Sci.* **1984**, *41*, 537–540.

(18) Hodge, V. F.; Seidel, S. L.; Goldberg, E. D. *Anal. Chem.* **1979**, *51*, 1256–1259.

(19) Valkirs, A. O.; Seligman, P. F.; Stang, P. M.; Lieberman, S. H.; Vafa, G. "Speciation of Butyltins and Methyltins in Marine Waters and Sediment by Hydride Derivatization"; Technical Report No. 1037; Naval Ocean Systems Center: San Diego, CA, 1985.

(20) Lee, R. F.; Ryan, C. *Can. J. Fish. Aquat. Sci.* **1983**, *40*(Suppl 2), 86–94.

(21) Kimmell, E. C.; Fish, R. H.; Casida, J. E. *J. Agric. Food Chem.* **1977**, *25*, 1–9.

(22) Dooley, C. A.; Homer, V. "Organotin Compounds in the Marine Environment: Uptake and Sorption Behavior";

Technical Report No. 917; Naval Ocean Systems Center: San Diego, CA, 1983.
(23) *Standard Methods for the Examination of Water and Wastewater*, 15th ed.; American Public Health Association: Washington, DC, 1980.
(24) Walsh, G. E.; McLaughlin, L. L.; Lores, E. M.; Louie, M. K.; Deans, C. H. *Chemosphere* **1985**, *14*, 383–392.
(25) Wong, P. T. S.; Chau, Y. K.; Kramar, O.; Bengert, G. A. *Can. J. Fish. Aquat. Sci.* **1982**, *39*, 483–488.
(26) Laughlin, R. B.; Johannesen, R. B.; French, W.; Guard, H.; Brinckman, F. E. *Environ. Toxicol. Chem.* **1985**, *4*, 343–351.
(27) Alexander, M. *Environ. Sci. Technol.* **1985**, *19*, 106–111.
(28) Lee, R. F., Skidaway Institute of Oceanography, Savannah, GA, 1985, unpublished data.

Received for review March 31, 1986. Accepted July 22, 1986. This work was sponsored by the Office of Chief of Naval Research, Energy Research and Development, under Program Element 63724N.

Contribution of Fine Particle Sulfates to Light Scattering in St. Louis Summer Aerosol

Teri L. Vossler and Edward S. Macias*

Department of Chemistry, Washington University, St. Louis, Missouri 63130

■ The contribution of fine particle $(NH_4)_2SO_4$ to total light scattering was calculated from measured sulfur size distributions and estimates of water that might be associated with this deliquescent species. The most common type of sulfur size distribution observed had a major sulfur mass peak between 0.5 and 1.0 μm in diameter and was associated with the highest levels of b_{scat}. A less common type with no peak above 0.5 μm was associated only with low values of b_{scat}. On average, $(NH_4)SO_4$ plus associated water contributed 68% of the total light scattering due to particles during the summer of 1984. The measured light scattering coefficient, b_{scat}, and $(NH_4)_2SO_4$ plus associated water were extremely well correlated (r = 0.97). b_{scat} and total fine particle mass were not as well correlated (r = 0.69), because the correlation between b_{scat} and non-sulfate fine mass was poor (r = 0.24). The average calculated light scattering efficiency of $(NH_4)_2SO_4$ plus water was 4.2 m^2/g. The higher values were associated with sulfur size distributions with a major peak above 0.5 μm.

Introduction

Numerous studies have implicated particulate sulfates as one of the major contributors to visibility reduction (*1–8*). Sulfates, mainly in the chemical form of $(NH_4)_2SO_4$, have been found to be the single largest contributor to ambient fine particle mass concentration in much of the urban U.S. Furthermore, the sulfate light scattering efficiency (light scattering coefficient per unit mass) has been found to be significantly higher than that of the other major fine particle constituents. The light scattering coefficient, b_{scat}, is defined as the scattering component of the light extinction coefficient, b_{ext}, of the Beer–Lambert Law:

$$I = I_0 \exp(-b_{ext}X) \quad (1)$$

I and I_0 are the transmitted and incident light intensities and X is the distance through which an object is observed. In urban atmospheres, light scattering constitutes a major portion of the total light extinction. Visibility has been inversely related to b_{ext} ($\approx b_{scat}$) by Koschmeider (*9*).

The majority (>85%) of particulate sulfate found in urban regions of the eastern and midwestern U.S. is carried by particles below 2.5 μm in diameter (*10*). These fine particles, especially those between 0.2 and 1.0 μm in diameter, scatter light more efficiently than particles in other size ranges (*11*). Sulfates have frequently been observed in precisely this size range (*12–14*). Furthermore, substantial water is often associated with this deliquescent salt. It is likely that the particle size and associated water explain the very efficient light scattering properties of sulfates.

Many researchers have made simultaneous measurements of total light scattering and chemical composition of ambient aerosols (*1*, *3–7*). Multiple regression analyses were then performed to determine the effective light scattering efficiencies of major aersols. In each case, sulfate scattering efficiences were significantly higher than those of other major components. These multiple regression analyses provide a statistical association between various pollutants and light scattering and are valuable for the insights they provide toward the light scattering efficiencies of the individual aerosol species. However, a calculation based on physical characteristics of the aerosol allows light scattering efficiencies to be determined on an individual sample basis and lends some insight into the physical basis of light scattering.

Hering and Friedlander (*14*) measured sulfur aerosol size distributions beteween 0.05 and >4 μm in the Los Angeles area. Ouimette (*15*) performed the same type of measurement in the California desert for multiple aerosol species. He used these size distributions and the Mie theory of light scattering to apportion light scattering to the various aerosol species. Sloane (*16*, *17*) calculated the light scattering coefficient by using the Mie theory of light scattering and individual species mass size distributions measured in Denver in the fall of 1978 (*12*). Calculations were performed for both external and internal aerosol mixtures, with provisions made to account for any water that might be associated with the measured fine aerosol. In an external aerosol mixture, each particle is composed of only one chemical species, while for an internal aerosol mixture each particle is composed of the same mixture of chemical species, the exact ratio of components being size dependant. Sloane obtained excellent agreement between the calculated and measured light scattering coefficients for both types of aerosol mixtures. On the basis of her results, neither type of aerosol mixture can be said not to represent the true situation that exists for the Denver aerosol.

In this work, the impact of fine aerosol sulfates on the deterioration of visibility in the St. Louis region is calculated directly from the measured sulfate size distributions and Mie theory. The analytical procedure employed in this study permits relatively short sampling times, on the order of 10 min to 2 h, allowing the observation of the variation of sulfur concentration and size distribution. On

0013-936X/86/0920-1235$01.50/0

the other hand, meteorological conditions, such as relative humidity, are not expected to change much during such short sampling periods. This was not the case with the Denver data base, where sampling times were 8 h for the impactor samples. Sloane (*16*) indicated that the relative humidity changed significantly over an 8-h period, lending even greater uncertainty to the estimation of water in association with the aerosol collected during that time. Reduction in sampling times should minimize this uncertainty.

Experimental Section

Sampling Site. Samples were collected on the roof of Louderman Hall, a Washington University chemistry building, located 6 miles west of downtown St. Louis. The nearest major expressway is located 1 mile to the south of the sampling site, though this is not expected to be of consequence in studying sulfates. The stack of the Washington University heating plant, although located less than 1 km from the sampling site, is not likely to impinge on the site. There were no major sulfur-emitting pollution sources in this primarily residential area. A total of 51 samples was collected during the summer of 1984 (June, July, and August). Sampling times were dependant on the light scattering coefficient measured during sampling.

Low-Pressure Impactor. A low-pressure impactor (LPI) (*18*, *19*) was used to collect and separate fine particles according to size down to less than 0.1 μm in diameter. The LPI consisted of eight collection stages, each of which was characterized by cutoff diameters corresponding to particles that are collected with 50% efficiency. These 50% efficiency cutoffs were 4.0, 2.0, 1.0, 0.5, 0.26, 0.12, 0.075, and 0.05-μm aerodynamic diameters and have been previously calibrated (*19*). The first four stages collected particles at atmospheric pressure. A critical orifice 0.038 cm in diameter preceded the final four stages and enabled the smaller particles to be separated on the basis of pressure reduction below each successive stage.

Stainless steel strips (0.56 cm × 2.54 cm × 0.0051 cm) were used as the collection substrate. Each was coated with 0.25 μL of 1% Vaseline (in toluene) in the impaction area to prevent particles from bouncing off the strips and becoming reentrained in the air stream. The amount of Vaseline was kept small, both to minimize the sulfate analysis blank and to avoid extinguishing the flame in the burner block of the sulfur analyzer. To eliminate much of the sulfur background, the strips were heated at 900 °C for 1 h before use in sampling. Much of the sulfur contained in the stainless steel was removed by this process.

TWOMASS. A TWOMASS sampler (*20*) was used to collect fine particles below 3 μm in diameter for mass concentration and total fine particle sulfur measurements. The TWOMASS had an upper impaction stage to collect coarse particles, with remaining fine particles collected on a filtration stage, which consisted of a thin glass fiber filter with a cellulose backing for strength. This additional sulfur measurement served as a check on the collection and measurement efficiency of the LPI.

For the sulfur analysis, 0.9 cm diameter pieces of filter containing sample spot and blank filter were cut out and each extracted ultrasonically in 0.5 mL of deionized water for 3–4 h. Six-microliter extracts of both samples and blank were evaporated onto stainless steel strips in a 115 °C oven. The strips were the same as those used in the LPI, but without the Vaseline. These were then analyzed in the same manner as the LPI samples, as described in a later section.

LPI Collection Efficiency. The sulfate particle collection efficiency of the LPI was monitored by simultaneous collection of total fine particles with the TWOMASS sampler, as described above. A plot of the sum of the sulfur concentrations measured for each LPI stage vs. the sulfur concentration measured for each TWOMASS sample is shown in Figure 1. Good agreement between the two quantities (r = 0.84, slope = 1.07) indicates that there was no significant loss of fine sulfate particles from the LPI. Although the individual LPI stage mass collection efficiencies could not be checked by this method, this is not expected to be a problem, as a light grease coating was used on each stage. Note that the LPI–TWOMASS comparison was made for only 22 samples, as the remainder of the TWOMASS samples were used for a destructive carbon analysis experiment rather than for sulfur analysis.

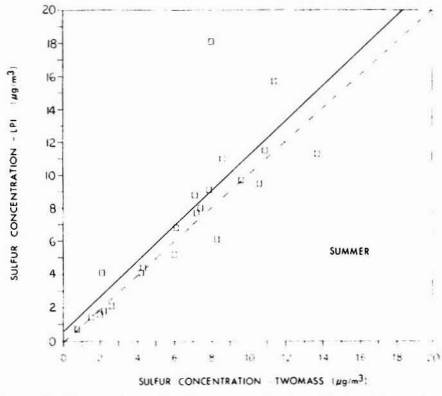

Figure 1. Comparison of sulfur concentration obtained from the sum of the LPI stages with sulfur concentration obtained from fine particle collection using the TWOMASS sampler. The solid line is the linear regression line with slope = 1.07 ± 0.16, intercept = 0.28 ± 1.15 μg/m^3, and r = 0.84. The dashed line has slope = 1 and intercept = 0.

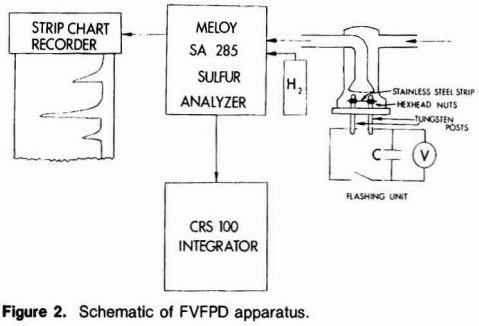

Figure 2. Schematic of FVFPD apparatus.

Sulfur Analysis. Samples were analyzed for sulfur by the method of flash volatilization and flame photometric detection (FVFPD) (*21*). The stainless steel strips on which samples were collected are secured to tungsten posts (part of the "flashing unit") as shown in Figure 2. The sample was then flash volatilized by discharging capacitor C with a capacitance of 380 F across the strip. The temperature attained by the strip during this process was about 1150 °C (see next section), which is more than adequate for decomposing the most common atmospheric sulfates (*22*). The flashing unit was connected to a Meloy SA 285 sulfur analyzer with a Teflon tube line. The output of this instrument was recorded on a CRS 100 integrator and a Heath Model SR-255B strip chart recorder.

Sulfur was measured between approximately 4 and 100 ng. Detection sensitivity was limited by the sulfur blank

Table I. Average Characteristics of St. Louis Summer Aerosol

sulfur size distribution type	no. obsd	measured b_{scat}, $m^{-1} \times 10^4$ [a]	b_{sp}, $m^{-1} \times 10^4$ [b]	b_{sp} calcd for $(NH_4)_2SO_4$ plus water, $m^{-1} \times 10^4$ [c]	$(NH_4)_2SO_4$ plus water concn, $\mu g/m^3$	dry $(NH_4)_2SO_4$ concn, $\mu g/m^3$	light scattering efficiency of $(NH_4)_2SO_4$ plus water, m^2/g [d]
summer, all	51	3.1	3.0	2.0	48	27	4.2
A	29	3.8	3.7	2.7	61	34	4.4
B	12	3.0	3.0	1.9	49	26	3.8
C	10	0.9	0.8	0.25	11	6.5	2.4

sulfur size distribution type	fine particle concn, $\mu g/m^3$	% fine particles as $(NH_4)_2SO_4$ plus water	% fine particles as $(NH_4)_2SO_4$	sulfur MMAD, μm [e]	σ_g, μm [f]	relative humidity, %
summer, all	68	71	40	0.50	1.80	46
A	80	76	43	0.50	1.72	46
B	71	69	36	0.52	1.86	53
C	22	48	30	0.36	1.94	41

[a] Light scattering by particles and gases as measured with a nephelometer. [b] Rayleigh scattering (calculated as recommended by ref 23) subtracted from b_{scat} to yield b_{sp}, the light scattering by particles only. [c] Light scattering calculated from sulfur size distributions and Mie theory. [d] b_{sp} calculated for $(NH_4)_2SO_4$ plus water divided by $(NH_4)_2SO_4$ plus water concentration. [e] Mass median aerodynamic diameter. [f] Geometric standard deviation of aerodynamic diameter.

of the stainless steel strips, which was typically 16 ± 4 ng. Analysis of multiple standards over the range of detection indicated an uncertainty of ±20% after subtraction of the blanks. Therefore, the uncertainty associated with sample analysis was ±20% or ±4 ng, whichever was greater.

Flashing Temperature for FVFPD. To determine the applied voltage required to attain the desired flashing temperature, a series of sulfate salts of known decomposition temperature were vaporized by the flashing process at a series of increasing applied voltages. A compound's thermal decomposition temperature was assumed to be attained or surpassed if all of the compound was vaporized on the first vaporization attempt. The following were the compounds and their thermal decomposition temperatures used in this test: $(NH_4)_2SO_4$ (<500 °C), $MgSO_4$ (895 °C), and Na_2SO_4 (1149 °C) (*22*).

To vaporize these test compounds that might possibly be found in the ambient air, while still maintaining the integrity of the stainless steel strips, the applied voltage was set at 16.5 V across the 380-F capacitor. At this voltage, the crucial portion of the strip where the sample was deposited reached at least 1149 °C, the thermal decomposition temperature of Na_2SO_4. Note that the most common ambient atmospheric sulfates in the fine particle mode decompose well below this temperature, so the chosen setting was more than adequate.

Standards and Calibrations for FVFPD. A series of $(NH_4)_2SO_4$–deionized water solutions were prepared so that aliquots of 4.1–6.0 μL would yield standards of approximately 5–100 ng of sulfur. The solution droplets were evaporated onto stainless steel strips (described previously) in a 115 °C oven. Blanks were prepared with 6.0 μL of deionized water in place of the $(NH_4)_2SO_4$ solutions. No significant differences were detected when 4.1–12 μL of deionized water was evaporated onto stainless steel strips and compared with blank strips. Therefore, the sulfur blank was attributed to the stainless steel strip.

Several different standards covering the range of sulfur found in the samples were measured periodically throughout each analysis session so that each standard would be measured several times. The average blank values were subtracted from the average value measured for each standard to get values from which a calibration could be calculated.

Sample Handling. After stainless steel strips were coated with Vaseline, each was mounted in the center of a 1-in. Plexiglass disk, secured in place with small paper clips, and each positioned below an LPI stage. Sample substrates were handled with disposable gloves and/or metal forceps. After samples were collected, strips were removed from the LPI and heat-sealed in clean polyethylene bags. Similar care was taken with the Vaseline blanks and the total fine particle filters from the TWOMASS sampler.

Nephelometer. The light scattering coefficient, b_{scat}, was measured with an MRI Model 1561 integrating nephelometer, which used a constantly lighted tungsten–halogen lamp as its light source. The instrument was calibrated as suggested by Ruby and Waggoner (*23*). The air entering the scattering chamber of the nephelometer was not preheated, and although the nephelometer was operated in an air-conditioned room, the temperatures measured at the inlet and outlet of the nephelometer were the same. Given these observations, it was concluded that the relative humidity inside the nephelometer was most likely the same as the ambient relative humidity for warm summer sampling days. The value of b_{scat} was obtained from the continuous output of a strip chart recorder.

Sulfur Size Distributions

Three different types of sulfur size distributions were observed for the LPI samples collected during the summer of 1984. The first and most common, designated type A, was identified as having only one major sulfur mass peak, which appeared between 0.5 and 1.0 μm in diameter. The second, designated type B, was identified as having two major peaks in the sulfur mass size distribution, one in the same size range as type A samples and the other below that size. The third, designated type C, had no peak above 0.5 μm and one or more sulfur mass peaks below 0.5 μm in diameter. The size distributions averaged for each type are shown in Figure 3. The average light scattering coefficients were calculated for each type of sulfur size distribution and are presented in Table I. The more abundant type A and B sulfur aerosols were associated with a significantly higher light scattering coefficient than type C, which had no major sulfur mass peak in the most efficient light scattering range.

Calculations

Mie Theory. The sulfate component of the light scattering coefficient was calculated from the sulfur size distributions, as measured with the LPI, and the Mie theory of light scattering (*24*). The important features of

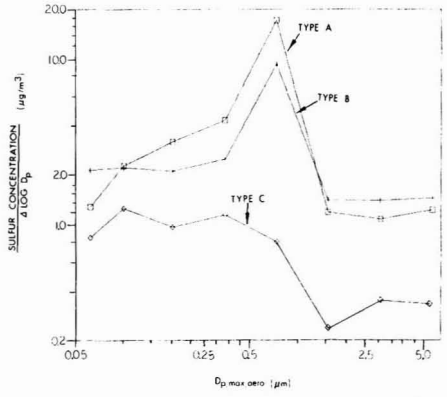

Figure 3. Average sulfur size distributions for each aerosol type. Concentrations weighted according to the size of the range of particle diameters that each LPI stage can collect. $D_{p,max,aero}$ refers to the particle aerodynamic diameter collected with maximum efficiency on any given LPI stage.

this theory, as they apply to this research, are presented here. The scattering of light per unit volume integrated over all wavelengths, λ, being scattered by the aerosol size interval D_p to $D_p + d(D_p)$ is given by

$$G(D_p) = \frac{3}{2D_p}\int_{\lambda_1}^{\lambda_2} K_{sp}(D_p,\hat{n},\lambda)f(\lambda)\,d\lambda \qquad (2)$$

K_{sp} is the particle scattering efficiency calculated from Mie theory and is a function of particle size (D_p), shape, index of fraction ($\hat{n}$), and wavelength of light being scattered (λ). It is defined as the energy being scattered by the particle divided by the energy intercepted, the latter being based on the particle's geometric cross-section. The factor $f(\lambda)$ $d\lambda$ is the fraction of incident radiation in the range λ to $\lambda + d\lambda$, where $f(\lambda)$ is normalized with respect to the total light intensity. The wavelength dependence of K_{sp} was removed by integrating over the range of wavelengths that corresponded to the nephelometer's spectral response (*25*). The data for the MRI Model 1561 nephelometer were used in order to compare calculated and measured light scattering coefficients.

Selection of Appropriate Quantities for Calculations. Selection of the appropriate quantities for D_p, ρ, and $\hat{n}$ is crucial to the calculation of light scattering. Two steps were taken to obtain an appropriate value for D_p. First, the particle aerodynamic diameter, which was collected with maximum efficiency, $D_{p,max}$, was calculated for each LPI stage, i, from the 50% collection efficiency diameters via

$$\log D_{p,max} = \frac{\log D_{p50,i} + \log D_{p50,i-1}}{2} \qquad (3)$$

Second, the geometric diameter, which was needed for the calculation of the optical properties, was obtained from the definition of aerodynamic diameters (*11*):

$$D_a = [\rho(C_s/C_a)]^{1/2}D_s \qquad (4)$$

The Stokes diameter, D_s, was taken as the geometric diameter for spherical particles. The slip correction factors, C_s and C_a, were disregarded. This approximation is expected to produce an error of <15%, which is well within the error associated with sampling and analysis procedures.

The particle density and index of refraction are functions of both chemical composition and the amount of water associated with the particle. Cobourn (*26*) concluded from his thermal analysis of sulfur species in St. Louis ambient aerosol that particulate sulfur tended to be in the more neutral form, most likely as $(NH_4)_2SO_4$, rather than in the acidic form, H_2SO_4. Any occurrence of H_2SO_4 tended to be brief and episodic in nature. Other experiments (*5*, *27*, *28*) indicate that it is acceptable to assume for the St. Louis region that fine particle sulfates exist primarily as $(NH_4)_2SO_4$. This is a deliquescent salt that absorbs water and grows when relative humidity is increased to 80% and above. However, hysteresis is observed whereby the droplets of $(NH_4)_2SO_4$ in solution remain supersaturated as relative humidities drop below that at which deliquescence occurs. It was assumed that droplets remain supersaturated down to about 30% relative humidity (*29*).

The light scattering properties of the particles are affected by the absorption of water and resultant particle growth. Tang's data (*29*) on the change in particle size with change in relative humidity for $(NH_4)_2SO_4$ were used to determine the amount of water associated with an $(NH_4)_2SO_4$ particle. The downslope of the $(NH_4)_2SO_4$ hysteresis curve is not very different from the relative humidity growth curve of hygroscopic H_2SO_4. Therefore, the assumption of pure $(NH_4)_2SO_4$ in this work will not introduce significant error in the determination of water associated with sulfate.

Particle density and index of refraction were calculated from the relative amounts of $(NH_4)_2SO_4$ and water in each sample. The other possible forms of sulfate—$(NH_4)_3H(SO_4)_2$, $(NH_4)HSO_4$, or H_2SO_4—are not very different from $(NH_4)_2SO_4$ in density or index of refraction. The wet particle density is given by

$$\rho = \frac{\rho_0}{(v/v_0)w} \qquad (5)$$

where ρ_0 is the dry particle density [1.77 g/cm³ for $(NH_4)_2SO_4$], w is the weight fraction of dry $(NH_4)_2SO_4$ in the wet particle, and v/v_0 is the wet volume to dry volume ratio obtained from ref 29. The wet particle refractive index was obtained from the volume-weighted average of the indices of refraction for $(NH_4)_2SO_4$ and water:

$$\hat{n} = \frac{V_{AMSF}\hat{n}_{AMSF} + V_{H_2O},\hat{n}_{H_2O}}{V_{TOTAL}} \qquad (6)$$

Results and Discussion

Representativeness of Data. Samples were collected in a nonperiodic fashion in order to observe a wide range of pollutant levels. For this reason, the data may not represent seasonal averages. Hourly b_{scat} readings taken about 2 miles from the Washington University sampling site obtained from St. Louis Country Air Pollution Control were used as a gauge to determine the representativeness of the Washington University data. The ratio of the average County Air Pollution b_{scat} value for all sampling intervals to the average of all hourly b_{scat} values for June, July, and August was 1.9. This bias toward higher b_{scat} episodes (lower visibility) will be reflected in the mass loadings measured, and possibly in the size distributions observed.

Ammonium Sulfate Light Scattering Efficiency from Mie Calculations. The $(NH_4)_2SO_4$ component of the light scattering coefficient was calculated for each sample from size distributions and Mie theory. The average values for all samples and for each size distribution type are presented in Table I, as are the average $(NH_4)_2SO_4$ plus water concentrations. The light scattering coefficient

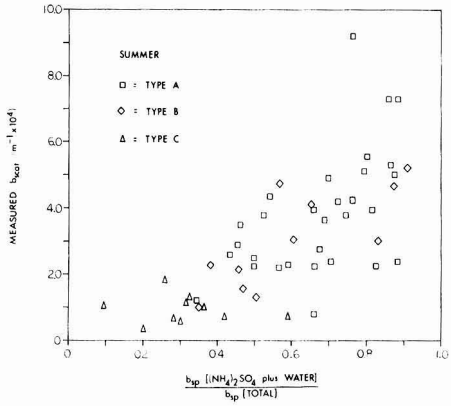

Figure 4. Relationship of total measured light scattering to sulfate fraction of light scattering by particles.

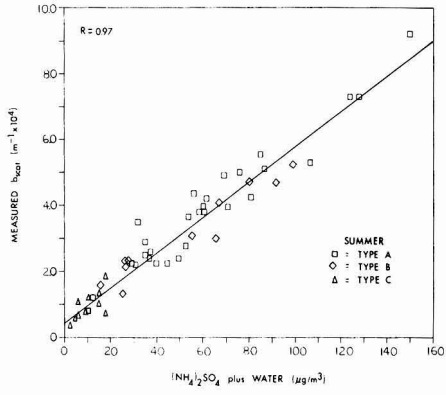

Figure 5. Relationship of total measured light scattering coefficient to concentration of fine aerosol ammonium sulfate plus associated water. The linear regression line with slope = 5.3 ± 0.2 m^2/g, intercept = (0.48 ± 0.11) × 10^{-4} m^{-1}, and r = 0.97 is shown.

for $(NH_4)_2SO_4$ plus water divided by the $(NH_4)_2SO_4$ plus water concentration, averaged 4.2 m^2/g for all samples and varied from <2 to >8 m^2/g. Differences in sulfur size distributions would be expected to give rise to differences in mass scattering efficiencies. These differences can be seen by calculating the average light scattering efficiences for the three types of sulfur size distributions observed in the St. Louis summer aerosol. The results of this calculation, shown in Table I, clearly indicate that type A and B samples yield higher mass scattering efficiencies (4.4 and 3.8 m^2/g) than type C samples (2.4 m^2/g).

Sloane had comparable success in modeling the Denver aerosol as both an external and an internal mixture (*17*). Although the aerosol was assumed to be an external mixture in this study, this may not necessarily represent the true form of the aerosol, on the basis of Sloane's results.

Relationship of Sulfates to Haze Episodes. The percent contribution of $(NH_4)_2SO_4$ (plus water) to total light scattering plotted as a function of measured light scattering coefficient, b_{scat} (Figure 4), reveals an interesting relationship. During episodes of higher b_{scat} (lower visibility) $(NH_4)_2SO_4$ contributes on the average a greater percentage of the total light scattering than on days of better visibility. Another striking feature of the data displayed in Figure 4 is the large variation in relative contribution of the scattering due to sulfates and associated species ranging from less than 10% to greater than 90% of the total scattering.

On the average, the $(NH_4)_2SO_4$ (plus water) contributes 65% of the total light scattering, b_{scat}, and 68% of the scattering by particles, b_{sp}, during the summer in St. Louis. This is similar to results obtained by studies carried out in other locations, as shown in Table II.

Ammonium Sulfate and Light Scattering. A multiple regression of b_{scat} with dry $(NH_4)_2SO_4$ and non-sulfate fine mass yielded estimates for light scattering efficiencies of 9.45 m^2/g for dry $(NH_4)_2SO_4$ [corresponding to 5.3 m^2/g for wet $(NH_4)_2SO_4$] but only 0.33 m^2/g for non-sulfate fine mass. This may indicate that most of the fine mass covaries with the $(NH_4)_2SO_4$ in this St. Louis summer data set. A strong correlation (r = 0.97) was observed between the total measured light scattering coefficient, b_{scat}, and total $(NH_4)_2SO_4$ plus associated water, as indicated in Figure 5. An estimate of the light scattering efficiency of 5.3 ± 0.2 m^2/g was calculated from the linear regression slope of these data. This result is similar to results obtained from other studies conducted in many different areas of the U.S. (*1–3*, 5, 8, 16), as indicated in Table II.

In this study we regressed total light scattering, including the relative humidity effect and Rayleigh scattering, with the wet $(NH_4)_2SO_4$ aerosol concentration. By contrast, most other researchers attributed the measured light scattering to several components by using a multiple regression model and used heated nephelometers to eliminate relative humidity effects.

When intercomparisons of multiple regression results are made, differences in experimental techniques and/or regression models should also be kept in mind. For instance, White and Roberts (*1*) measured aerosol species up to 20 μm in diameter (both coarse and fine particles). Subsequent studies separated fine and coarse particles and included only fine-mode aerosol masses in the multiple regression analyses. Further distinctions in regression models included separate mass concentration values for elemental and organic carbon. In some cases, the contribution of water to light scattering was estimated by operating heated and unheated nephelometers simultaneously. Researchers in Denver (*3*) and St. Louis (*5*) measured the extinction coefficient of light due to both particle absorption and scattering. Despite these differences, all conclude that sulfates have the highest effective scattering efficiency of the major aerosol species. From the above-mentioned studies, that scattering efficiency for dry $(NH_4)_2SO_4$ is about 6 m^2/g. Note that comparisons made even within the same data set can lead to inconsistent results if the quantities being compared were obtained by different methods.

As expected, the light scattering efficiency that we calculated from Mie theory and size distributions (4.2 m^2/g) differs from our result obtained by a linear regression calculation (5.3 m^2/g) performed on the same data set. The Mie calculation includes physical characteristics of only the $(NH_4)_2SO_4$ aerosol, whereas a regression calculation includes contributions from species that are covarient with $(NH_4)_2SO_4$.

Fine Particles and Light Scattering. The $(NH_4)_2SO_4$ plus water contributed an average of 71% to the total fine particle mass during our summer sampling. The contributions for each aerosol type are shown in Table I. On an individual sample basis, this ratio exceeded 100% in 23% of the cases. Assuming that the mass measurements of sulfur and total fine particles were not in error, the excess mass can be attributed either to an overestimation of the water associated with the fine aerosol sulfate or a loss of volatile components (or water) during the fine aerosol

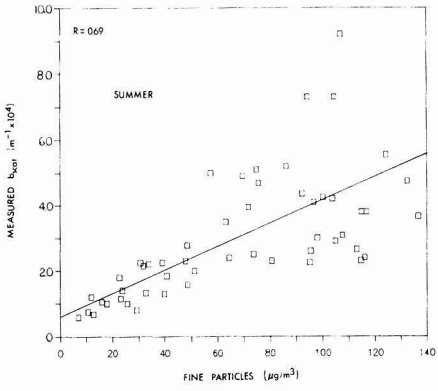

Figure 6. Relationship of total measured light scattering coefficient to fine particle concentration. The linear regression line with slope = 3.5 ± 0.5 m^2/g, intercept = (0.72 ± 0.42) × 10^{-4} m^{-1}, and r = 0.69 is shown.

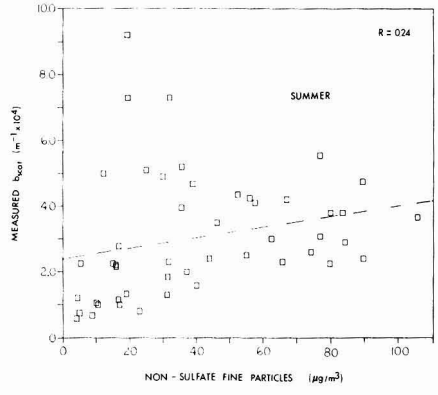

Figure 7. Relationship of total light scattering coefficient to non-sulfate component of fine particle concentration. The linear regression line with slope = 1.6 ± 1.0 m^2/g, intercept = (2.4 ± 0.5) × 10^{-4} m^{-1}, and r = 0.24 is shown.

collection with the TWOMASS sampler. Because either situation is possible, it is necessary to also consider the contribution of dry $(NH_4)_2SO_4$ to the total fine particle mass. This contribution was 40% on the average. The actual contribution of $(NH_4)_2SO_4$ plus associated water may be somewhere in between this lower limit of 40% and the 71% calculated for wet $(NH_4)_2SO_4$ particles.

A plot of measured b_{scat} as a function of the fine particle mass (Figure 6) indicates a fair correlation between the two quantities (r = 0.69). The light scattering efficiency of the St. Louis summer fine aerosol is 3.5 ± 0.5 m^2/g, on the basis of a least-squares linear regression calculation of the slope. This is similar to values obtained from other studies, as shown in Table II.

The fair correlation of light scattering and fine particle mass is in contrast to the excellent correlation (r = 0.97) observed between light scattering and $(NH_4)_2SO_4$, implying that the non-sulfate component of fine mass may not be an important contributor to light scattering during the summer in St. Louis. This is supported by Figure 7, which shows that light scattering and non-sulfate fine mass are poorly correlated (r = 0.24). The non-sulfate fine mass was obtained by subtracting dry $(NH_4)_2SO_4$ from the total fine particle mass to avoid a negative non-sulfate fine mass.

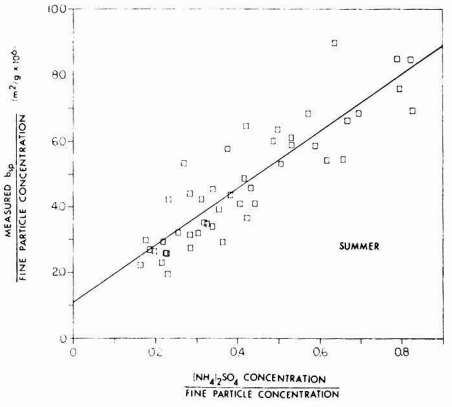

Figure 8. Relationship of fine particle light scattering efficiency to fraction of fine particles as dry ammonium sulfate. The linear regression line with slope = 8.7 ± 0.7 m^2/g, intercept = 1.1 ± 0.3 m^2/g, and r = 0.89 is shown.

The correlation does not improve by subtracting the additional mass contributed by water associated with the $(NH_4)_2SO_4$.

A further indication of the dominance of sulfate in the summer aerosol light scattering is implied by Figure 8, which presents individual sample fine particle scattering efficiencies as a function of the mass ratio of $(NH_4)_2SO_4$ to fine particles. As the $(NH_4)_2SO_4$ fraction increases, the fine particle scattering efficiency increases. One possible explanation for this is that $(NH_4)_2SO_4$ scatters light more efficiently than does the remainder of the aerosol. There is a good correlation (r = 0.89) between these two quantites. The slope plus intercept of 8.7 + 1.1 = 9.8 m^2/g corresponds to the light scattering efficiency of dry $(NH_4)_2SO_4$ if all light scattering is attributed to this species. Similarly, the intercept of 1.1 ± 0.3 m^2/g corresponds to the light scattering efficiency of the fine non-sulfate component, which does not covary with sulfate. Not only does $(NH_4)_2SO_4$ contribute the majority of the fine particle mass, but it also scatters light more efficiently than the remainder of the fine particle mass.

Mass Median Aerodynamic Diameters. The relationship of the cumulative fraction of fine sulfur aerosol mass larger than a given diameter vs. aerodynamic diameter indicated that the size distribution of fine sulfur aerosol is approximately log–normal for each sample. The mass median aerodynamic diameter (MMAD) and geometric standard deviation (σ_g) were calculated for each sample from the dry sulfur concentrations of each LPI stage. As shown in Table I, type A and B sulfur size distributions have nearly the same MMAD's, about 0.5 μm, which is in the size range that scatters light most efficiently. Type C samples, which have no sulfur peak above 0.5 μm, have a much lower MMAD.

The MMAD's for all summer samples are shown in Figure 9 as functions of relative humidity, b_{scat}, percent contribution of $(NH_4)_2SO_4$ plus water to b_{scat}, and calculated $(NH_4)_2SO_4$ light scattering efficiency. The latter figure indicates that the $(NH_4)_2SO_4$ aerosol contributes a greater percentage of the light scattering as its MMAD increases. It is reasonable to expect that the increasing size of the aerosol is due to an increasing relative humidity, resulting in particle growth by adsorption of water. However, Figure 9A shows that this relationship is not so simple, as the MMAD and relative humidity are poorly correlated (r = 0.32). Figure 9D indicates that increased

Table II. Results and Experimental Parameters (Where Available) of Various Visibility Studies in the U.S.

location	ref	season	light scattering efficiency for $(NH_4)_2SO_4$, m^2/g	method of calculation	% b_{scat} due to sulfates	% b_{ext} due to sulfates	% fine particle fraction as sulfates	% total sulfur in fine particle fraction	light scattering efficiency of fine particle mass, m^2/g	corr of light scattering and fine particle concn	MRI Model No. of nephelometer	nephelometer intake: heated vs. not heated
Los Angeles	1	summer	6.2	multiple regression		31			3.2 ± 0.9	0.96	1550	unheated
Denver	3	late fall	5.9[a]	multiple regression	40 (dry sulfate), 24 (water)				3.4	0.95	1550	heated
Shenandoah Valley	4	summer				78 (sulfate + water)	55		7.3	0.91	1550	heated
St. Louis	5	summer	5.5	multiple regression[c]	70	49[d]	35		3.0	0.69	1550	
St. Louis	5	winter	3.4	multiple regression	46	49[d]	47		3.8			
Detroit	6	summer	6.2	multiple regression		65 (sulfate + water)	50	94	4.8	0.83	1550	heated
Houston	7	summer			42		54	94	3.5	0.99		
New York	8	summer			50		24	85			1550	heated
St. Louis (RAPS)	30	summer					59	85				
Great Smoky Mountains	31	summer					61	85				
Denver	16	late fall	4.9	Mie calculation				95				
Denver	32	late fall	3.2, 3.4	Mie calculation								
Denver	32	late fall	5.8 ± 1.0	multiple regression								
St. Louis	this work	summer	5.3 ± 0.2	linear regression	82 (sulfate + water)[e]		40 (dry sulfate)		3.5 ± 0.5	0.69	1561	unheated
St. Louis	this work	summer	4.2 (sulfate + water)	Mie calculation	65 (sulfate + water)[f]		40 (dry sulfate)				1561	unheated
St. Louis	this work	summer	9.4 ± 0.3 (dry sulfate)	linear regression	83 (dry sulfate)		40 (dry sulfate)				1561	unheated

[a] As corrected by ref 29. [b] Percent of b_{sp} (light scattering by particles only) rather than percent of b_{scat}. [c] Several multiple regression models were employed. Model II results are presented here. [d] Average of winter and summer results. [e] Calculated from linear regression scattering efficiency. [f] Calculated from Mie theory scattering efficiency.

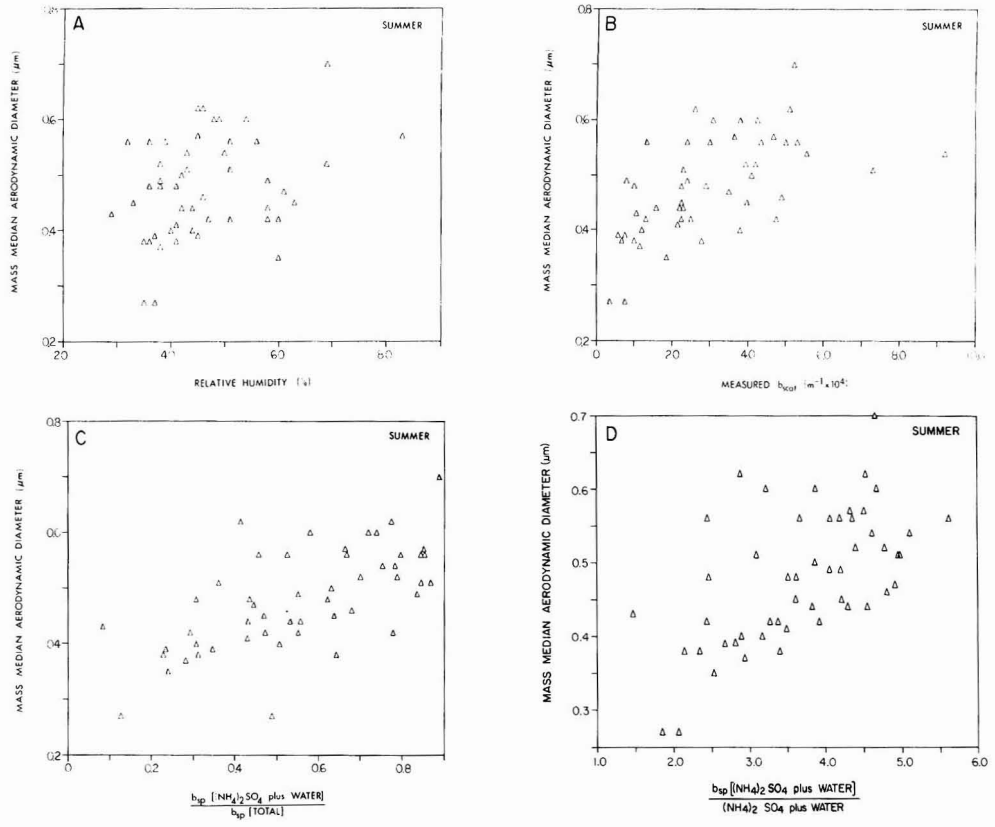

Figure 9. Relationship of sulfur mass median aerodynamic diameter (MMAD) to (A) relative humidity (r = 0.32), (B) measured light scattering coefficient (r = 0.57), (C) fractional contribution of ammonium sulfate plus water to particle light scattering (r = 0.65), and (D) calculated scattering efficiency of ammonium sulfate plus water (r = 0.58).

scattering revealed in Figure 9B is due to the size of the sulfate and is not simply a result of the increased amount of sulfate.

Summary and Conclusions

The St. Louis summertime fine sulfate aerosol was extremely well correlated (r = 0.97) with the light scattering coefficient, b_{scat}. This was in contrast to the very poor correlation (r = 0.24) between the non-sulfate fine mass and b_{scat}, implying that fine aerosol sulfates dominated light scattering during the summer and that the non-sulfate fine mass contribution was generally much less significant. This dominance of fine sulfate aerosol has been observed in several different areas of the U.S. and is generally attributed to the growth of sulfate aerosols into the most efficient light scattering size range.

Three different types of sulfur size distributions were observed in the St. Louis summer aerosol. Two of them, which dominated summer aerosol (types A and B), were similar in that they had a major sulfur mass peak between 0.5 and 1.0 μm in diameter, the size range that is responsible for the most efficient light scattering. In addition, these types of sulfur aerosols were characterized by high sulfate mass loadings and high b_{scat}. By contrast, the third type of sulfur size distribution (type C) had all sulfur mass peaks below 0.5 μm in diameter and were characterized by much lower sulfate mass loadings and b_{scat}.

These sulfur size distributions were used in Mie calculations of the contribution of $(NH_4)_2SO_4$ plus associated water to b_{scat}. Values for the wet $(NH_4)_2SO_4$ light scattering efficiency ranged from <2 to >8 m^2/g. The average wet $(NH_4)_2SO_4$ light scattering efficiency calculated by this method was 4.2 m^2/g. The average calculated scattering efficiencies for sulfur aerosol types A and B were similar to this value (4.4 and 3.8 m^2/g, respectively). However, the light scattering efficiency for sulfur aerosol type C was significantly lower (2.4 m^2/g), emphasizing the significance of particle size with respect to light scattering. The difference in light scattering efficiency cannot be explained by considering the type C aerosol to be dry $(NH_4)_2SO_4$.

The coincidence of small particle size (and hence reduced light scattering efficiency) with low sulfate loadings and low b_{scat} led to the relatively small contribution of type C sulfur aerosol (28%) to b_{scat}. At the other extreme, the coincidence of a sulfur mass peak in the 0.5–1.0 μm diameter size interval with high sulfate mass loadings and high b_{scat} led to the dominance of sulfate aerosol over the total light scattering (71% for type A and 62% for type B). The above conditions resulted in an overall increase in the percent contribution of $(NH_4)_2SO_4$ plus water to b_{scat} as b_{scat} increases.

In this work, a large number of time-resolved sulfate size distributions were used to calculate visibility parameters. It is clear from these results that the variable nature of the sulfur size distribution has a substantial impact on visibility that might be missed if one looks only at overall

averages of visibility parameters.

Registry No. $(NH_4)_2SO_4$, 7783-20-2.

Literature Cited

(1) White, W. H.; Roberts, P. T. *Atmos. Environ.* **1977**, *11*, 803.
(2) Cass, G. R. *Atmos. Environ.* **1979**, *13*, 1069.
(3) Groblicki, P. J.; Wolff, G. T.; Countess, R. J. *Atmos. Environ.* **1981**, *15*, 2473.
(4) Ferman, M. A.; Wolff, G. T.; Kelly, N. A. *J. Air Pollut. Control Assoc.* **1981**, *31*, 1074.
(5) Chu, L. C. Ph.D. Thesis, Washington University, St. Louis, MO, 1981.
(6) Wolff, G. T.; Ferman, M. A.; Kelly, N. A.; Stroup, D. P.; Ruthkosky, M. S. *J. Air Pollut. Control Assoc.* **1982**, *32*, 1216.
(7) Dzubay, T. G.; Stevens, R. K.; Lewis, C. W.; Hern, D. H.; Courtney, W. J.; Tesch, J. W.; Mason, M. A. *Environ. Sci. Technol.* **1982**, *16*, 514.
(8) Leaderer, B. P.; Bernstein, D. M.; Daisey, J. M.; Kleinman, M. T.; Kneip, T. J.; Knutson, E. O.; Lippman, M. L.; Lioy, P. J.; Rahn, K. A.; Sinclair, D.; Tanner, R. L.; Wolff, G. T. *J. Air Pollut. Control Assoc.* **1978**, *28*, 321.
(9) Horvath, H.; Noll, K. E. *Atmos. Environ.* **1969**, *3*, 543.
(10) Leaderer, B. P.; Holford, T. R.; Stolwijk, J. A. J. *J. Air Pollut. Control Assoc.* **1979**, *29*, 154.
(11) Friedlander, S. K. *Smoke, Dust, and Haze: Fundamentals of Aerosol Behavior*; Wiley: New York, 1977.
(12) Countess, R. J.; Cadle, S. H.; Groblicki, P. J.; Wolff, G. T. *J. Air Pollut. Control Assoc.* **1981**, *31*, 247.
(13) Tanner, R. L.; Marlow, W. H.; Newman, L. *Environ. Sci. Technol.* **1979**, *13*, 75.
(14) Hering, S. V.; Friedlander, S. K. *Atmos. Environ.* **1982**, *16*, 2647.
(15) Ouimette, J. R. Ph.D. Thesis, California Institute of Technology, Pasadena, CA, 1981.
(16) Sloane, C. S. *Atmos. Environ.* **1983**, *17*, 409.
(17) Sloane, C. S. *Atmos. Environ.* **1984**, *18*, 871.
(18) Hering, S. V.; Flagan, R. C.; Friedlander, S. K. *Environ. Sci. Technol.* **1978**, *12*, 667.
(19) Hering, S. V.; Freidlander, S. K.; Collins, J. J.; Richards, L. W. *Environ. Sci. Technol.* **1979**, *13*, 184.
(20) Macias, E. S.; Husar, R. B. In *Fine Particles: Aerosol Generation, Measurement, Sampling and Analysis*; Liu, B. Y. H., Ed.; Academic: New York, 1976; pp 536–564.
(21) Roberts, P. T.; Friedlander, S. K. *Atmos. Environ.* **1976**, *10*, 403.
(22) Ostroff, A. G.; Sanderson, R. T. *J. Inorg. Nucl. Chem.* **1959**, *9*, 45.
(23) Ruby, M. G.; Waggoner, A. P. *Environ. Sci. Technol.* **1981**, *15*, 109.
(24) van de Hulst, H. C. *Light Scattering by Small Particles*; Dover: New York, 1981.
(25) Sverdup, G. M. Ph.D. Thesis, University of Minnisota, Minneapolis, MN, 1977.
(26) Cobourn, W. G. Ph.D. Thesis, Washington University, St. Louis, MO, 1979.
(27) Charlson, R. J.; Vanderpol, A. H.; Covert, D. S.; Waggoner, A. P.; Ahlquist, N. C. *Atmos. Environ.* **1974**, *8*, 1257.
(28) Altshuller, A. P. *Atmos. Environ.* **1982**, *16*, 837.
(29) Tang, I. N. In *Generation of Aerosols and Facilities for Exposure*; Willeke, K., Ed.; Ann Arbor Science: Ann Arbor, MI, 1980; pp 153–167.
(30) Kneip, T. J.; Lioy, P. J., Eds. *Ann. N.Y. Acad. Sci.* **1980**, *338*, 126–144.
(31) Stevens, R. K.; Dzubay, T. G.; Shaw, R. W., Jr.; McClenny, W. A.; Lewis, C. W.; Wilson, W. E. *Environ. Sci. Technol.* **1980**, *14*, 1491.
(32) Hasan, H.; Dzubay, T. G. *Atmos. Environ.* **1983**, *17*, 1573.

Received for review February 24, 1986. Accepted July 25, 1986.

Molecular Beam Mass Spectroscopic Study of Trichloroethylene Flames

Wen-Donq Chang, Sankaram B. Karra, and Selim M. Senkan*

Department of Chemical Engineering, Illinois Institute of Technology, Chicago, Illinois 60616

■ The detailed chemical structure of atmospheric-pressure, premixed, laminar, one-dimensional flat flames of $C_2HCl_3/O_2/Ar$ was studied by molecular beam mass spectroscopy and under oxygen-rich conditions. The principal stable combustion intermediates were identified to be CO, $CHCl_3$, CCl_4, C_2Cl_4, C_2Cl_2, and $COCl_2$. In addition, a minor intermediate at m/e 282, corresponding to C_6Cl_6, was also detected.

Introduction

The chemistry of combustion of chlorinated hydrocarbons (CHC) in flames has been studied relatively little in the past. This is not surprising because their oxidation products, which include Cl_2 and HCl, are highly corrosive and toxic, rendering chlorinated hydrocarbons unsuitable as a fuel. However, there is a growing interest in the combustion of chlorinated hydrocarbons for the disposal of toxic and hazardous chemical wastes that frequently contain these classes of compounds. In addition, combustion of chlorinated hydrocarbons also offers the potential to manufacture important chlorinated and nonchlorinated hydrocarbons.

Previous work on atmospheric-pressure flames of individual chlorinated hydrocarbons has resulted in the establishment of the following two-step oxidation chemistry describing the combustion of these compounds (*1*): The first step is

$$C_xH_yCl_z + (x/2 + (y - z)/4)O_2 \rightarrow xCO + zHCl + ((y - z)/2)H_2O \quad (1)$$

for $z < y$. For $z > y$, the first stage reaction would be

$$C_xH_yCl_z + (x/2)O_2 \rightarrow xCO + yHCl + ((z - y)/2)Cl_2 \quad (1a)$$

where $C_xH_yCl_z$ denotes a general chlorinated hydrocarbon molecule. The second step then involves the HCl- and Cl_2-inhibited oxidation of CO by the following overall reaction:

$$CO + {}^1/_2O_2 \rightarrow CO_2 \quad (2)$$

Detailed modeling studies of the second stage, i.e., studies of the HCl- and Cl_2-inhibited oxidation of CO, also supported the global mechanism shown above (*2*, *3*).

For the oxygen-rich combustion of C_2HCl_3, the extent of HCl and Cl_2 inhibition becomes so great that its flames exhibit two reaction zones spatially separated by as much as 10 mm at 1 atm. The temperature increases by about 800–900 °C following the first reaction zone and remains relatively isothermal until the second reaction zone is reached.

0013-936X/86/0920-1243$01.50/0

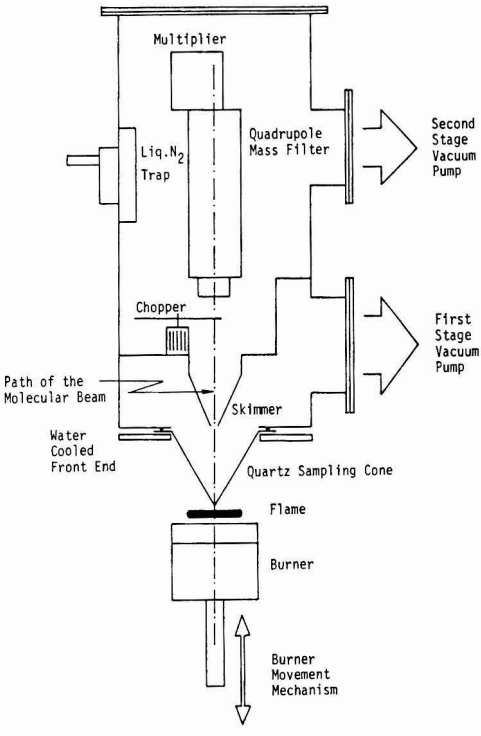

Figure 1. Schematic of molecular beam mass spectrometer system.

Earlier studies with oxygen-rich C_2HCl_3 flames using gas chromatography have also revealed the presence of a complex flame structure in the first zone in which the formation of a number of other chlorinated hydrocarbon intermediates was observed (*1*). However, the determination of the detailed flame chemistry as well as the precise mapping of the species profiles was not reported due to the limitations present in gas chromatographic analysis.

In this paper, the detailed chemical structure associated with the first flame zone of an oxygen-rich $C_2HCl_3/O_2/Ar$ premixed flame with respect to stable species is presented. The species compositions were determined by molecular beam sampling coupled with on-line mass spectroscopy. Research on the free radical chemistry of C_2HCl_3 flames currently is in progress, and the results of these investigations will be published at a later date. A detailed chemical kinetic model consistent with experimental measurements presented in this paper is being published elsewhere (*4*).

Experimental Section

The schematic of the overall experimental system is shown in Figure 1. This system was designed by incorporating the principal features of systems used in previous similar studies (*5–9*). Among the distinguishing features of the present system are its shorter sampling cone-to-ionizer distance and the improved precision of the burner movement mechanism.

Atmospheric-pressure premixed flat flames were stabilized over a 5 cm diameter circular, porous flat flame burner with a concentric shield gas distributor, details of which have been published earlier (*1*). Gases used in the experiments were acquired from the gas cylinders (Matheson Co.), and their flows were set and regulated by critical orifice flow meters. Liquid fuel transportation was accomplished by the combination of a liquid pump and a pressurized delivery system. The liquid fuel was injected into preheated Ar/O_2 mixtures at a heated tee. The rate of evaporation and the uniformity of the gas mixture were determined to be satisfactory from the sharpness and steadiness of the sooting limits. In separate experiments, species intensities at the flame front also were monitored for extended periods of time in order to better assess the extent of composition and flow oscillations that may be present in the system. These studies also revealed the absence of any significant oscillation in the system.

Final adjustment and control of the temperature of the precombustion gases were accomplished with the aid of a heating/cooling coil imbedded into the porous burner. Depending on the precombustion temperature desired, either thermostatted water or high-temperature oil may be circulated through the burner plug.

The burner assembly was mounted on vertical and horizontal slide translators, in which the vertical movement was effected by a stepper motor that in return was computer-controlled. The ultimate precision of the vertical movement was better than 0.02 mm, and this was achieved by sending a predetermined number of pulses to the stepper motor by the computer.

Sampling was accomplished by withdrawing gases from within the flame with a conical quartz cone that has a cone angle of about 80°. It was necessary to use such wide-angled sampling cones in order to rapidly quench flame reactions and to preserve the integrity of labile species. Although such wide-angled probes distort flame profiles under some conditions (*6*, *10*), no visible attachment of the flame to the quartz cone was observed in these studies. Flame–probe interactions will also be discussed later.

At the tip of the sampling cone was an orifice with a diameter of about 20 μm. At this diameter and at the temperatures associated with the first stage flame zone, which was of the order 1000 °C, the orifice Knudsen number (i.e., ratio of the mean free path to orifice diameter) corresponds to about 0.01 at 1 atm. This Knudsen number suggests the presence of a transitional flow regime between supersonic jet formation and slip flow (*11*).

Upon passage through the orifice, the gases accelerate and expand into the first vacuum stage of the analysis system, which was kept at about 10^{-4}–10^{-5} Torr by a 1000 L/s turbomolecular vacuum pump. From the core of the expanding jet, a molecular beam was obtained with the skimmer cone suitably placed above the quartz sampling cone. The vacuum within the skimmer chamber was kept in a range of 10^{-6}–10^{-8} Torr by use of a 360 L/s turbomolecular pump.

In order to maximize the beam intensity at the mass spectrometer, the distance between the sampling point and the ionizer must be kept as short as possible. However, this requirement adversely affects the extent of pumping that can be applied to the first chamber, suggesting that a compromise must be made. In the present system, the ionizer is located at about 20 cm from the tip of the quartz cone.

The molecular beam also was modulated at a fixed frequency in the range 150–300 Hz for the improved detection of the species at low concentrations. Modulation is particularly important for the measurement of radical species, which requires the utilization of low electron energies.

The mass spectrometer was a vertically mounted quadrupole system (Model C-50, Extranuclear Laboratories Inc., Pittsburgh, PA) and was operated under electron-impact ionization and analog detection modes.

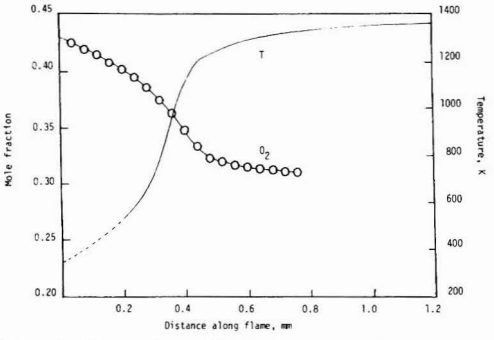

Figure 2. Mole fraction profiles for O_2 and temperature.

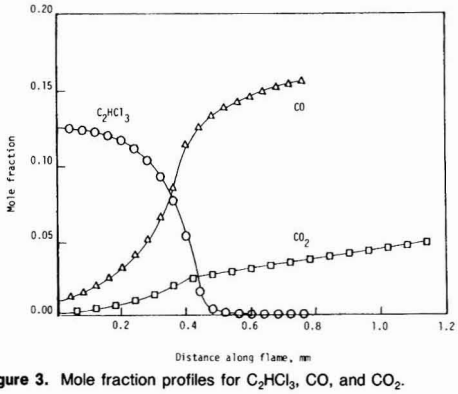

Figure 3. Mole fraction profiles for C_2HCl_3, CO, and CO_2.

Data acquisition was accomplished automatically with the aid of an IBM-PC microcomputer and a Data Translation 12-bit A/D board. The computer was programmed to read the demodulated mass intensity data directly from the lock-in amplifier and to control the movement of the burner relative to the quartz sampling cone. Species profiles were generated one at a time.

For many of the stable species, their intensity profiles acquired by the mass spectrometer subsequently were converted into mole fraction profiles by use of the results of microprobe sampling and gas chromatography in separate experiments, similar to those described previously (*1*). For cases in which such gas chromatographic calibration experiments were not possible, the method of relative ionization cross-sections was used (*10*, *12*).

Temperature profiles were measured, with a 0.1-mm Pt/Pt–13% Rh thermocouple coated by silica, in separate experiments. The temperature readings were corrected for radiation effects by conventional techniques (*1*). We estimate that an uncertainty of ±0.20 mm exists in the absolute position of the temperature profile.

Results and Discussion

The profiles presented in this work were measured along the first flame zone in an oxygen-rich trichloroethylene flame with the following precombustion gas mixture composition (by volume): C_2HCl_3, 12.5%; O_2, 42.7%; Ar, 44.8%. This composition corresponds to an equivalence ratio of 0.58 on the basis of the stoichiometry shown in eq 1a and 2. In all the experiments, the precombustion gas temperature was set at about 80 °C. Flames were stabilized under conditions in which they were lifted off by about 1 mm from the burner surface at a cold gas velocity of about 12.5 cm/s. This permitted the sampling and

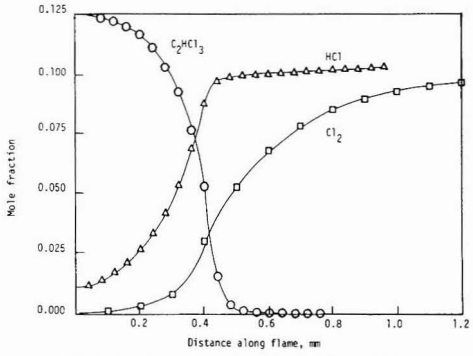

Figure 4. Mole fraction profiles for C_2HCl_3, HCl, and Cl_2.

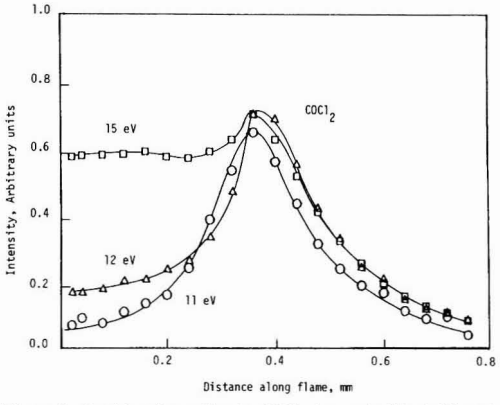

Figure 5. Ion intensity profiles for $COCl_2$, i.e., m/e 98, at different ionization energies.

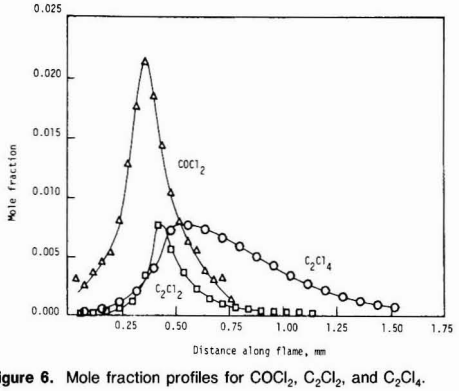

Figure 6. Mole fraction profiles for $COCl_2$, C_2Cl_2, and C_2Cl_4.

analysis of the precombustion gas mixture and was particularly helpful in establishing the correct orders of magnitudes for the mole fractions of the reactants.

The total burner travel distance was kept at about 2 mm, which was traversed by 0.02-mm intervals. This interval was determined to be of sufficient precision to give meaningful species profiles. The measured species profiles were highly reproducible within this range. We estimate an uncertainty of ±0.1 mm in the absolute positions of the species profiles. However, there is no such uncertainty in the relative position among different profiles.

In Figures 2–8 the mole fraction profiles for various species are presented relative to an identical reference

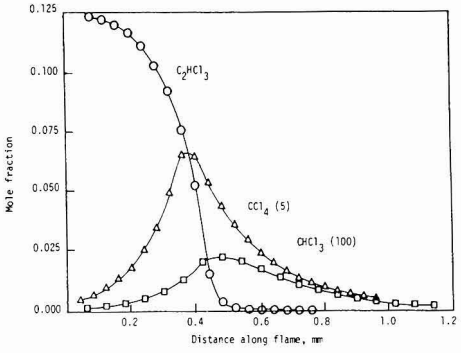

Figure 7. Mole fraction profiles for C_2HCl_3, CCl_4, and $CHCl_3$.

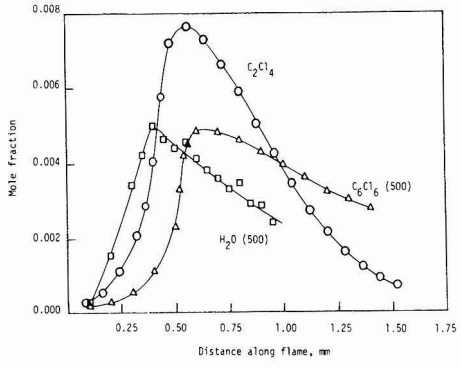

Figure 8. Mole fraction profiles for C_2Cl_4, H_2O, and C_6Cl_6.

plane from the burner surface. As a visual aid, actual data points (indicated by symbols) have been connected by lines. In addition, mole fractions have been normalized, whenever necessary, by multiplying them with appropriate scaling factors shown in parentheses. Figure 2 also shows the measured temperature profile along the flame. These profiles precisely map the behavior of each species along the flame zone and clearly illustrate the presence of a large variety of intermediates associated with the oxidation and/or decomposition of C_2HCl_3.

It must be recognized that the acquisition of accurate concentration profiles in flames by molecular beam mass spectroscopy is complicated because of a number of reasons. The most significant being the fact that the massive sampling probe tends to perturb the flame flow field in a complex manner, and this in return alters the flame structure (*13*, *14*). This perturbation can be significant under certain conditions, e.g., in low-pressure flames, and manifests itself most clearly by the attachment of the flame to the sampling probe. However, in high-pressure flames such an attachment appears to be less likely because of the relatively thin boundary layer thicknesses (*10*). No visible flame attachment was observed in our experiments.

The absence of significant probe perturbations in our experiments was also suggested by two additional observations. First, no discrepancy was noted between the species profiles obtained by moving the burner up or down. If flame attachment was present, some hysteresis would have been observed. Second, the overall length of the flame zone as determined by independent microprobe sampling experiments as well as by thermocouple traverses, both of which would minimally disturb the flame, was well within the 10% of the length determined by the molecular beam sampling cone. Consequently, we believe the profiles shown in Figures 2–8 represent the quantitative change in the chemistry of combustion of C_2HCl_3 with reasonable accuracy.

In Figure 3 the mole fractions for C_2HCl_3, CO, and CO_2 are presented at 27-eV electron energy. The general form of these profiles is in good agreement with the previous gas chromatographic work on C_2HCl_3 flames (*1*). In particular, the two-stage combustion feature of trichloroethylene, where CO forms as the primary intermediate in the first stage (within the first 0.50 mm), is apparent from the profiles presented in Figure 3. Some CO_2 also forms at the first stage.

It is particularly interesting to note the change in the rate of formation of CO_2 in Figure 3. In the early parts of the flame, the CO_2 mole fraction increases almost exponentially, but after about 0.4 mm the increase becomes linear. This suggests a change in CO oxidation mechanism coupled with HCl formation, which has been discussed elsewhere (*3*, *4*).

The profile shown in Figure 4 illustrate the relatively early formation of HCl and the presence of a considerable delay period for the appearance of Cl_2. The early formation of HCl has been attributed to the molecular elimination reaction

$$C_2HCl_3 + M \rightleftharpoons C_2Cl_2 + HCl + M \qquad (3)$$

after detailed chemical kinetic modeling of the combustion of C_2HCl_3 (*4*). Because of the relatively strong H–Cl bond, once formed, HCl does not participate in a reaction to any significant degree at the temperature present in the first flame zone (i.e., at temperatures less than 1000 °C). On the other hand, Cl_2 concentration does not reach an appreciable level early in the flame because of the rapid removal of Cl radicals by the abundant C_2HCl_3 via

$$Cl + C_2HCl_3 \rightleftharpoons C_2Cl_3 + HCl \qquad (4)$$

coupled with the following Cl_2 removal reactions:

$$CCl_3 + Cl_2 \rightleftharpoons CCl_4 + Cl \qquad (5)$$

$$CHCl_2 + Cl_2 \rightleftharpoons CHCl_3 + Cl \qquad (6)$$

$$C_2Cl_3 + Cl_2 \rightleftharpoons C_2Cl_4 + Cl \qquad (7)$$

$$COCl + Cl_2 \rightleftharpoons COCl_2 + Cl \qquad (8)$$

These reactions delay the appearance of Cl_2 until most of the fuel and intermediates are decomposed.

Other significant intermediates, besides CO, were determined to be $COCl_2$, C_2Cl_4, and C_2Cl_2. The observation of both C_2Cl_4 and $COCl_2$ concurs with the earlier GC experiments (*1*). However, the detection of C_2Cl_2 has been new, and this was made possible entirely by the capabilities of molecular beam sampling coupled with on-line mass spectroscopy.

Due to the high reactivity of chloroacetylenes with oxygen even at room temperatures (*15*), C_2Cl_2 would be expected to undergo reactions with O_2 in the sampling lines during its transit to the GC, thus rendering gas chromatography unsuitable for its detection. On the other hand, the rapid expansion associated with molecular beam sampling and the presence of low pressure in the mass spectrometer chamber preserve the integrity of many of the reactive species, including C_2Cl_2. This capability of molecular beam mass spectroscopy renders this technique particularly suitable for the preliminary studies of flames and other reactive mixtures.

The profiles for $COCl_2$ (m/e 98) were measured at as low electron energy as possible in order to minimize C_2HCl_3

fragmentation. C_2HCl_3 fragmentation would obscure the signal at m/e 98 because of the formation of C_2Cl_2 corresponding to the ^{37}Cl isotope. As shown in Figure 5, C_2HCl_3 fragmentation was significant even at electron energies as low as 12 eV. Only at about 11 eV does the mass signal at 98 exhibit the correct features of an intermediate, which we believe reasonably represents the behavior of $COCl_2$. The electron energy of about 11 eV still is above the reported ionization potential for C_2Cl_2 at 10.09 eV (*16*); however, free C_2Cl_2 (^{37}Cl) in the flame would be expected to contribute at most 10% to the mass signal intensity at 98 on the basis of the relative isotopic abundances of ^{35}Cl (75%) and ^{37}Cl (25%). The $COCl_2$ peak intensity occurs at about 0.36 mm from the burner surface, and its decomposition profile exhibits an exponential decay behavior in the near-isothermal post-first-flame zone.

Figure 5 also illustrates the precision of the burner movement and the data acquisition systems. These profiles reveal the repeatibility of the peak location within 0.02 mm. In addition, the absence of any apparent hysteresis suggests that flame–probe interactions were not significant.

The calculated mole fraction profile for C_2Cl_2 (m/e 94) presented in Figure 6 was based on intensity measurements at 12 eV, again to minimize contributions from the fragmentation of other species. Although the profiles for $COCl_2$ (m/e 98, 11 eV) and C_2Cl_2 (m/e 94, 12 eV) shown in Figure 6 appear similar, they also show some measurable differences. For example, C_2Cl_2 exhibits a longer induction period, and its profile exhibits a greater degree of assymetry than $COCl_2$. These differences, although subtle, support the validty of the $COCl_2$ profile in view of the possible obscuring effect that may be introduced by C_2Cl_2 (^{37}Cl) as discussed earlier.

The C_2Cl_4 profile (m/e 164) was measured at 27 eV, and it is also shown in Figure 6. As evident from this figure, the rate of decomposition of C_2Cl_4 was significantly slower than either $COCl_2$ or C_2Cl_2.

The formation and subsequent decomposition of chlorinated methanes also were noted during the combustion of C_2HCl_3, and the mole fraction profiles for CCl_4 and $CHCl_3$ are shown in Figure 7. The mole fractions for these species have been normalized with the scaling parameters indicated in parentheses.

The fragmentation of CCl_4 (m/e 152) was present at all the electron energy levels studied; thus, parent ion profiles were not determined. Consequently, the profiles for CCl_3 (m/e 117) were presumed to correspond to that for CCl_4. It was possible to monitor the parent ion profiles for $CHCl_3$ (m/e 118) even at electron energies of 27 eV.

The profiles for mass ions at m/e 18 (H_2O) and m/e 282 (C_6Cl_6) are shown in Figure 8. It appears that in highly chlorinated systems H_2O exhibits the characteristics of a combustion intermediate even under oxygen-rich conditions. This, however, can be explained in view of the following Deacon reaction:

$$H_2O + Cl_2 \rightleftharpoons 2HCl + {}^1/_2O_2 \qquad (9)$$

which favors the formation of HCl at elevated temperatures. That is, water initially formed during the decomposition of C_2HCl_3 subsequently would be converted into HCl by reactions involving chlorine. The detailed mechanism for this process is described elsewhere (*4*).

It was particularly interesting to note the rapid formation and the relatively slow decomposition of C_6Cl_6 (m/e 282), which we believe is hexachlorobenzene. The formation of C_6Cl_6 under oxygen-rich conditions is particularly significant because of its possible emission into the environment and because of its possible involvement in the production of chlorinated dibenzodioxins.

Data Analysis

In order to quantify the relative rates of destruction of chlorinated intermediates in C_2HCl_3 combustion and help identify surrogates for compliance monitoring in practical systems, the mole fraction profiles in the near-isothermal, post-first-flame zone were examined heuristically. This analysis complements the detailed chemical kinetic modeling of this flame published elsewhere (*4*).

As seen in Figure 4, the Cl_2 profile beyond 0.40 mm, i.e., in the near-isothermal post-first-flame region exhibits a bounded exponential growth behavior, for which the mole fraction profile can be represented by

$$[Cl_2] = [Cl_{2,f}](1 - \exp[-(z - 0.3)/a]) \qquad (10)$$

with a correlation coefficient better than 0.99. In eq 10, $[Cl_{2,f}]$ is the final chlorine mole fraction, z is the position along the flame in mm, and a is a characteristic growth parameter for Cl_2 that was determined to be 0.32 mm. Bounded exponential growth suggests that the underlying mechanism for Cl_2 formation is first order in the post-first-flame zone. This, therefore, rules out the Cl radical recombination being majorly responsible for Cl_2 build-up.

A heuristic mechanism that rationalizes the first-order growth of Cl_2 can be developed by assuming chlorine radical assisted decomposition of the chlorocarbon intermediates via the reversal of reactions 5–8. Such decomposition reactions may be represented by the following schematic reaction:

$$RCl + Cl \rightleftharpoons R + Cl_2 \qquad (11)$$

where RCl is an intermediate chlorocarbon species. The rate of formation of Cl_2 can then be related to the rate of disappearance of RCl as

$$-\frac{d[RCl]}{dt} = k[Cl][RCl] \qquad (12)$$

assuming that the reverse of reaction 11 is negligible. This, however, is not an unreasonable assumption beyond 0.4 mm, where the net decomposition of the chlorinated intermediates indeed takes place under near-isothermal conditions (see, for example, Figures 2 and 6). Equation 12 can be integrated readily for isothermal and stationary [Cl] conditions and yields

$$[RCl] = [RCl]_0 \exp(-k[Cl]t) \qquad (13)$$

where $k[Cl]$ may be interpreted as the decay parameter for RCl.

Since the conditions for RCl decay are met in the later stages of the flame, eq 13 must be shifted to account for this. The resulting expression is

$$[RCl] = [RCl]_{t_0} \exp[-k[Cl](t - t_0)] \qquad (14)$$

Using the stoichiometry given by eq 11, eq 14 can be manipulated to give the following relationship for $[Cl_2]$:

$$[Cl_2] = [Cl_{2,f}](1 - \exp[-k[Cl](t - t_0)]) \qquad (15)$$

which is identical in form with the experimentally measured mole fraction profile for $[Cl_2]$ presented in eq 10. This suggests that Cl radical attack is primarily responsible for the destruction of chlorocarbon intermediates, a conclusion supported in our detailed modeling work (*4*). From the comparison of expressions 10 and 15, the growth parameter for Cl_2 (i.e., a in eq 10) can be related to decay parameter for the RCl by

$$1/a = k[Cl]/u \qquad (16)$$

where u is the gas velocity. Using a typical flow velocity

Table I. Decay Parameters for Species according to First-Order Model

species	decay parameter, s^{-1}	species	decay parameter, s^{-1}
$COCl_2$	4760	C_2Cl_4	2860
C_2Cl_2	4280	C_6Cl_6	780
CCl_4	4780	CO	–
$CHCl_3$	4040		

of about 500 mm/s corresponding to the later stages of the flame, an average decay parameter for RCl can be calculated to be about 1560 s^{-1}.

It must be recognized, however, that eq 12 does not describe the fundamental chemical kinetic steps associated with the decay of RCl. The decay parameter k[Cl], although which may be related to elementary rate coefficients, is also expected to be a strong function of the diffusional transport phenomena (*4*).

The mole fraction profiles for the chlorohydrocarbon intermediates were then analyzed by forcing an exponential decay function to the experimental data, in a manner similar to the treatment of the Cl_2 profile. The first-order decay parameters were then calculated, and they are presented in Table I. These decay parameters illustrate the slow decomposition of C_2Cl_4 and C_6Cl_6 and suggest their potential use as performance indicators to monitor emissions from combustion systems burning C_2HCl_3, to complement CO monitoring.

Conclusions

The flames of C_2HCl_3 contain significant levels of CO, $COCl_2$, C_2Cl_4, C_2Cl_2, $CHCl_3$, CCl_4, and C_6Cl_6 as intermediates under oxygen-rich conditions. Although the formation of intermediates is a normal consequence of combustion, the highly inhibited nature of chlorinated hydrocarbon flames amplifies the levels of these intermediates. Therefore, combustion systems burning chlorinated hydrocarbons are more prone to pollutant emissions when compared to those burning conventional hydrocarbons.

The highly inhibited nature of chlorinated hydrocarbon flames, on the other hand, suggests the possibility that controlled oxidation/pyrolysis may be exploited as a manufacturing process to recover these intermediates.

A simple first-order model describing the mole fraction profiles of the intermediates suggests that Cl radical attack is primarily responsible for their destruction. The relative ranking of the decay parameters suggests the possible use of C_6Cl_6 and C_2Cl_4, in addition to CO, to monitor pollutant emissions from combustors burning trichloroethylene, and perhaps other chlorinated hydrocarbons.

Acknowledgments

We are grateful to Professor D. Gutman for many useful discussions.

Registry No. C_2HCl_3, 79-01-6; $CHCl_3$, 67-66-3; Cl_4, 56-23-5; C_2Cl_2, 25323-30-2; C_2Cl_4, 127-18-4; C_6Cl_6, 118-74-1; CO, 630-08-0; CO_2, 124-38-9; HCl, 7647-01-0; Cl_2, 7782-50-5; $COCl_2$, 75-44-5.

Literature Cited

(1) Bose, D.; Senkan, S. M. *Combust. Sci. Technol.* **1983**, *35*, 187.
(2) Senkan, S. M. *Combust. Sci. Technol.* **1984**, *38*, 197.
(3) Chang, W. D.; Senkan, S. M. *Combust. Sci. Technol.* **1985**, *43*, 49.
(4) Chang, W. D.; Karra, S. B.; Senkan, S. M. *Combust. Sci. Technol.* **1986**, *49*, 107.
(5) Greene, F. T.; Brewer, J.; Milne, T. A. *J. Chem. Phys.* **1964**, *40*, 1488.
(6) Biordi, J. C.; Lazzara, C. P.; Papp, J. F. "Fourteenth Symposium (International) on Combustion"; The Combustion Institute: Pittsburgh, PA, 1973; p 367.
(7) Gay, R. L.; Young, W. C.; Knuth, E. L. *Combust. Flame* **1975**, *24*, 391.
(8) Hastie, J. W. *Combust. Flame* **1973**, *21*, 187.
(9) Williams, G. J.; Wilkins, R. G. *Combust. Flame* **1973**, *21*, 325.
(10) Biordi, J. C. *Prog. Energy Combust. Sci.* **1977**, *3*, 151.
(11) Anderson, J. B.; Andres, R. P.; Fenn, J. B.; Maise, G. *Rarefied Gas Dynamics*; Academic: New York, 1968.
(12) Peeters, J.; Mahnen, G. "Fourteenth Symposium (International) on Combustion"; The Combustion Institute: Pittsburgh, PA, 1973; p 133.
(13) Yi, A. C.; Knuth, E. L. *Combust. Flame* **1986**, *63*, 369.
(14) Smith, O. I.; Chandler, D. W. *Combust. Flame* **1986**, *63*, 19.
(15) Smirnov, K. M.; Tomilov, A. D.; Shchekotikhin, A. I. *Russ. Chem. Rev. (Engl. Transl.)* **1967**, *36*, 326.
(16) Rosenstock, H. M.; Draxl, K.; Steiner, B. W.; Herron, J. T. *J. Phys. Chem. Ref. Data* **1977**, *6*, 235.

Received for review February 10, 1986. Revised manuscript received July 9, 1986. Accepted July 28, 1986. This work was supported by funds from the U.S. Environmental Protection Agency (Grants R810381-01 and R812544-01) and the Illinois Institute of Technology.

Environ. Sci. Technol. 1986, 20, 1249–1253

On the Nature of Atmospheric Oxidation Processes of SO_2 to Sulfate and of NO_2 to Nitrate on the Basis of Diurnal Variations of Sulfate, Nitrate, and Other Pollutants in an Urban Area

Satoshi Kadowaki

Aichi Environmental Research Center, 7-6 Nagare, Tsuji-machi, Kita-ku, Nagoya 462, Japan

■ Measurements of sulfate and nitrate (particulate plus gaseous) were made in Nagoya. Air samples were collected over a 2- or 3-h interval, and particulates were fractionated into the fine and coarse fractions. In addition, other pollutants and meteorological parameters were simultaneously monitored. Sulfur and nitrogen conversion ratios (F_s and F_n) defined in the text were calculated from the data. F_s and F_n in the summer increased by about 2 and 4 times those in the winter, respectively. F_n was always higher in the daytime than in the nighttime and correlated closely with oxidant concentration. On the other hand, there was hardly any difference in F_s of the daytime and the nighttime. Good correlation was found between F_s and relative humidity when the oxidant concentrations were more than 20 ppb. These results indicated that droplet-phase reactions are important for the SO_2 oxidation to sulfate, while gas-phase reactions are predominant for the NO_2 oxidation to nitrate.

Introduction

The conversion mechanisms and rates for sulfate and nitrate formations are of considerable interest because of concern over apparent widespread environmental effects associated with acid deposition, visibility reduction, and weather and climate changes.

These secondary aerosols result primarily from the oxidation of sulfur dioxide and nitrogen oxides. In order to clarify the oxidation processes and rates, numerous extensive studies have been conducted, including laboratory studies (e.g., *1–3*), theoretical and kinetic computer modeling studies (e.g., *4*, *5*), and field studies in ambient air (e.g., *6–8*) and in plumes (e.g., *9*, *10*).

It is generally recognized that the two most important oxidation processes are homogeneous gas-phase reactions involving free radicals such as OH and heterogeneous reactions in droplet phase and on aerosol particle surface. Davis et al. (*9*) showed that SO_2 and NO_2 oxidations in plume could largely be explained by the gas-phase reaction with the OH radical under midday summertime and low relative humidity (<50%) conditions. On the other hand, McMurry et al. (*11*, *12*) reported from the results of field observations and smog chamber experiments that droplet-phase reactions were important at high relative humidity (>75%), while gas-phase reactions were the predominant mechanism at low relative humidity (≃35%). More data on the effect of weather conditions, such as relative humidity and sunlight, on sulfate and nitrate formations are needed to reveal the oxidation processes in ambient air.

In almost all regions of Japan, there are two different summertime conditions, in which sulfate and nitrate formations are enhanced and photochemical smog episodes are often observed.

The first is low relative humidity and high sunlight before the rainy season called "Baiu" has set in. The second is high relative humidity and high sunlight after the rainy season is over. Therefore, it is useful for the clarification of the oxidation processes to compare sulfate and nitrate behavior under the two different summertime conditions.

In this study, field measurements were made of diurnal variations for sulfate, nitrate, selected gaseous pollutants, and meteorological conditions in Nagoya during the summer of 1983 and the winter of 1983 and 1984. From the results, sulfur and nitrogen conversion ratios were calcuated, as defined in the text, and the oxidation processes in urban air were discussed.

Experimental Section

Air samples were collected at the Aichi Environmental Research Center in a mixed residental/light industry area of Nagoya by use of a Model 21-000 Andersen sampler manufactured by 2000 INC. The sampler usually consists of eight stages followed by a backup filter. In this study to segregate atmospheric particulates into two size fractions of coarse and fine, ≥2.1 μm and <2.1 μm, the sampler was modified to consist of a 2.1-μm 50% e.c.d. stage followed by a Teflon filter plate and a Teflon backup filter (*13*).

Fluoropore Teflon filters of 80-mm diameter and 0.8-μm pore size (AF07P, Sumitomodenko Corp.) were used, because they are inert and produce negligible sulfate and nitrate artifacts. Gaseous nitric acid was collected with an 80-mm diameter 0.65-μm pore size nylon filter (Sartorius SM119) downstream of the Teflon backup filter.

Sampling was made in 2- or 3-h intervals at a flow rate of 1 cfm (28.3 L/min). The sampled Teflon and nylon filters were ultrasonically extracted for 20 min with 10 mL of deionized water and 10 mL of 0.1 N KOH, respectively. Extracts were analyzed for SO_4^{2-} and NO_3^- with a Dionex 2100 ion chromatograph using an HPIC AS-4 separator and anion fiber suppressor columns. Precision for SO_4^{2-} and NO_3^- was better than 8%. The detection limit of particulate sulfate and nitrate was about 0.1 $\mu g/m^3$ for a sample volume of 3.4 m^3 and based on the average filter blank plus 2 times the mean standard deviation of the filter blanks. For gaseous nitric acid, the detection limit was about 0.5 $\mu g/m^3$ under the same sample volume and blank correction for the particulate sulfate and nitrate.

Oxidant, NO_2, and SO_2 were monitored with a DKK Model GXH-71M-1(S) neutral-buffered KI solution spectroscopic analyzer, a DKK Model GPH-74 Saltzman spectroscopic analyzer, and a DKK Model GRH-73 conductometric analyzer, respectively. A UV absorption ozone analyzer (Model EG-2001, Ebara Jitsugyo Corp.) was also used to check oxidant concentrations measured by the oxidant analyzer.

Results and Discussion

Selected gaseous pollutant levels and meteorological conditions during the field measurements are summarized in Table I. High oxidant concentrations were observed in both of the sampling periods on June and August because of high sunlight in summertime. On the other hand, the difference in relative humidity was evidently recognized in the two summer sampling periods; the averages of relative humidity in June and August were 56% and 75%, respectively.

0013-936X/86/0920-1249$01.50/0

Table I. Summary of Gaseous Pollutant Levels and Meterological Conditions during Sulfate and Nitrate Measurements[a]

	sampling period[b]		
	June	Aug	Dec and Jan
SO_2, ppb	18 (6~32)	16 (8~30)	16 (8~35)
NO_2, ppb	27 (10~60)	17 (5~54)	35 (16~63)
oxidant, ppb	37 (2~89)	40 (1~113)	9 (0~18)
temp, °C	25 (17~31)	30 (25~35)	8 (1~14)
relative humidity, %	56 (25~96)	75 (53~97)	63 (41~86)
wind speed, m/s	1.7 (0.3~4.5)	1.5 (0.2~5.4)	2.0 (0.0~6.6)

[a] Arithmetic mean of 1-h averages (range of 1-h averages). [b] June 1983: 6/3, 6/4, 6/8, 6/9, and 6/10; Aug 1983: 8/5, 8/9, 8/11, and 8/12; Dec 1983 and Jan 1984: 12/7, 12/8, 12/14, and 1/10.

Tables II–IV give 2- or 3-h averaged concentrations of size-segregated sulfate and nitrate and gaseous nitrate for daytime and nighttime. As seen in Table II, the concentrations of coarse sulfate were very low in comparison with those of fine sulfate and almost constant in daytime and nighttime below about 0.5 $\mu g/m^3$.

The fine sulfate had generally higher concentrations in daytime than in nighttime. The difference, however, was not apparent except for the August data, in which the average concentration of fine sulfate in daytime (9.76 $\mu g/m^3$) was about 2 times higher than that in nighttime (5.20 $\mu g/m^3$). The highest fine sulfate concentration, 19.2 $\mu g/m^3$, was measured on August 5, 10:00–12:00 JST. These sulfate results indicate that the coarse sulfate, arising from primary particulate emissions, hardly contributes to the total sulfate concentration in the ambient air and that the fine sulfate formation from the oxidation of SO_2 is enhanced under the summertime condition of high relative humidity and high oxidant concentration.

In contrast to sulfate, the results of nitrate measurements were complicated as seen in Tables III and IV. Several investigators reported that the size distribution of particulate nitrate is bimodal and gives the seasonal and regional variations (*14–16*), and that the chemical compositions of the bimodal nitrate are mainly NH_4NO_3 and $NaNO_3$ (*14, 15, 17, 18*). On the other hand, Stelson et al. (*19, 20*) reported that fine particulate nitrate of NH_4NO_3 is easily dissociated into HNO_3 and NH_3 under high ambient temperature because of the high volatility of NH_4NO_3.

The results shown in Tables III and IV are consistent with the characteristic of nitrate described above. The average concentration ratio of gaseous nitrate to total nitrate was high in the summer and attained about 60%, but in the winter, particulate nitrate was predominant. The gaseous nitrate concentrations shown in Table IV possibly include the overestimate error owing to the volatilization of NH_4NO_3 from the filter to form HNO_3 during air sampling. There is, however, hardly any difference of the ratio in the summer between daytime and nighttime, so that the error seems to be small.

Both particulate and gaseous nitrate concentrations increased in the summer and daytime, especially in June. The maximum gaseous and particulate nitrate concentrations, 20.3 and 13.4 $\mu g/m^3$, were measured on June 3, 10:00–12:00 and 15:00–17:00 JST, respectively. These nitrate results indicate that particulate and gaseous nitrate formations are enhanced under the summertime condition of low relative humidity and high oxidant concentration

Table II. Average Concentrations ($\mu g/m^3$) of Size-Segregated Sulfate for Daytime and Nighttime at a Nagoya Urban Site

sampling period[a]	no. of samples (day/night)	coarse			fine			ratio of fine fraction to total SO_4^{2-}, %		
		day	night	mean	day	night	mean	day	night	mean
June	20/14	0.54	0.43	0.49	5.43	4.75	5.09	91	92	91
Aug	21/17	0.46	0.33	0.40	9.76	5.20	7.48	95	94	95
Dec and Jan	19/18	0.45	0.48	0.47	3.22	2.39	2.81	88	83	86

[a] Sampling periods are as shown in Table I.

Table III. Average Concentrations ($\mu g/m^3$) of Size-Segregated Particulate Nitrate for Daytime and Nighttime at a Nagoya Urban Site

sampling period[a]	no. of samples (day/night)	coarse			fine			ratio of fine fraction to particulate NO_3^-, %		
		day	night	mean	day	night	mean	day	night	mean
June	20/14	3.48	2.08	2.78	1.81	1.17	1.49	34	36	35
Aug	21/17	1.77	1.05	1.41	0.54	0.40	0.47	23	28	25
Dec and Jan	19/18	0.58	0.54	0.56	1.73	1.16	1.45	75	68	72

[a] Sampling periods are as shown in Table I.

Table IV. Average Concentrations ($\mu g/m^3$) of Gaseous and Particulate Nitrate for Daytime and Nighttime at a Nagoya Urban Site

sampling period[a]	no. of samples (day/night)	gaseous NO_3^-			particulate NO_3^-[b]			ratio of gaseous NO_3^- to total (gaseous and particulate) NO_3^-, %		
		day	night	mean	day	night	mean	day	night	mean
June	20/14	5.07	2.16	3.62	5.29	3.25	4.27	49	40	46
Aug	21/17	3.32	1.96	2.64	2.31	1.45	1.88	59	57	58
Dec and Jan	19/18	0.58	0.07	0.33	2.31	1.70	2.01	20	4	14

[a] Sampling periods are as shown in Table I. [b] Particulate NO_3^- = coarse NO_3^- + fine NO_3^- shown in Table III.

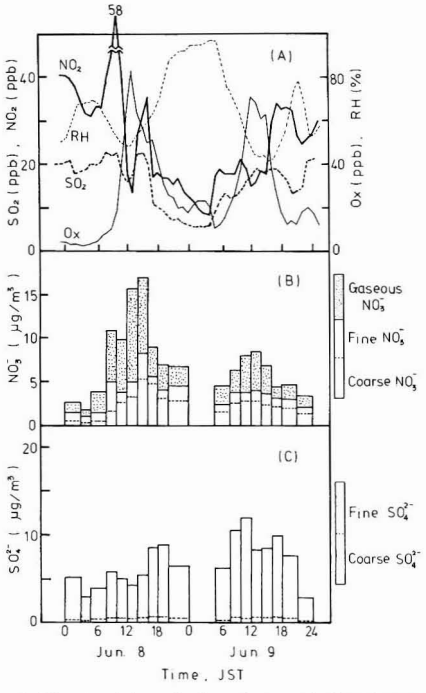

Figure 1. Diurnal variations of sulfate, nitrate, and selected parameters at a Nagoya urban site, June 8–9, 1983.

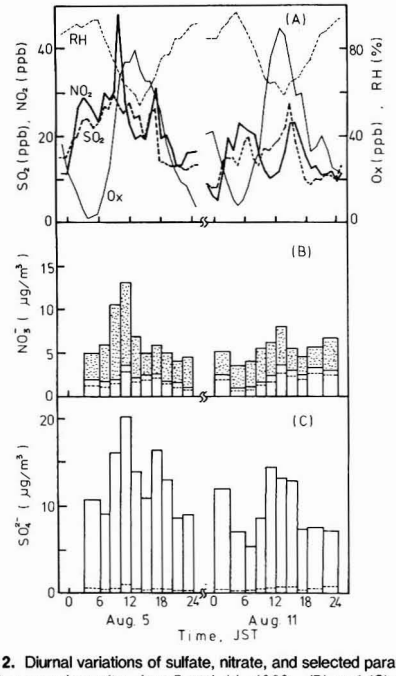

Figure 2. Diurnal variations of sulfate, nitrate, and selected parameters at a Nagoya urban site, Aug 5 and 11, 1983. (B) and (C) are as described in Figure 1.

and that the oxidation process of NO_2 to nitrate differs from that of SO_2 to sulfate.

Figures 1–3 show the representative diurnal variations of sulfate, nitrate, and selected parameters at a Nagoya

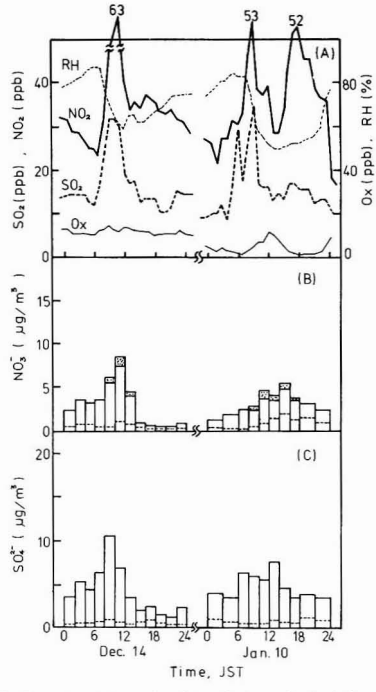

Figure 3. Diurnal variations of sulfate, nitrate, and selected parameters at a Nagoya urban site, Dec 14, 1983, and Jan 10, 1984. (B) and (C) are as described in Figure 1.

urban site. Comparing the diurnal patterns, it is shown that the diurnal patterns of nitrate in June and August and those of sulfate in August are qualitatively similar to oxidant concentrations. But in the other cases the relationships are obscure between the diurnal patterns of sulfate and nitrate and those of the selected parameters.

In order to clarify the difference between the SO_2 oxidation process to sulfate and the NO_2 oxidation process to nitrate, conversion ratios for sulfur (F_s) and nitrogen (F_n) were defined in the modified forms of the gas–particle distribution factors by Grosjean and Friedlander (*21*):

$$F_s = \frac{[\mathrm{f\ SO_4^{2-}}]}{[\mathrm{SO_2}] + [\mathrm{f\ SO_4^{2-}}]}$$

$$F_n = \frac{[\mathrm{p\ NO_3^-}] + [\mathrm{g\ NO_3^-}]}{[\mathrm{NO_2}] + [\mathrm{p\ NO_3^-}] + [\mathrm{g\ NO_3^-}]}$$

where $[\mathrm{f\ SO_4^{2-}}]$ = fine sulfate concentration (as SO_2, $\mu g/m^3$), $[SO_2]$ = gas-phase SO_2 concentration (converted from ppm to $\mu g/m^3$, averaged over the sampling period), $[\mathrm{p\ NO_3^-}]$ = total particulate nitrate concentration (as NO_2, $\mu g/m^3$), $[\mathrm{g\ NO_3^-}]$ = gaseous nitrate concentration (as NO_2, $\mu g/m^3$), and $[NO_2]$ = gas-phase NO_2 concentration (converted from ppm to $\mu g/m^3$, averaged over the sampling period).

Table V lists the average F_s and F_n calculated from the equations defined above. F_s and F_n in the summer were about 2 and 4 times higher than those in the winter, respectively.

F_n was always higher in the daytime than in the nighttime and did not change under the two different summertime conditions. On the other hand, there was hardly any difference in F_s for daytime and nighttime, and under the two different summertime conditions F_s was

Table V. Comparison of Sulfur Conversion Ratio (F_s) with Nitrogen Conversion Ratio (F_n) at a Nagoya Urban Site[a]

sampling period[b]	no. of samples (day/night)	av F_s, %			av F_n, %		
		day	night	mean	day	night	mean
June	20/14	6.7	7.8	7.3	12.1	7.7	9.9
Aug	21/17	10.4	9.1	9.8	12.0	8.2	10.1
Dec and Jan	19/18	4.0	3.9	4.0	2.9	1.9	2.4

[a] Conversion ratios of F_s and F_n are defined in the text. [b] Sampling periods are as shown in Table I.

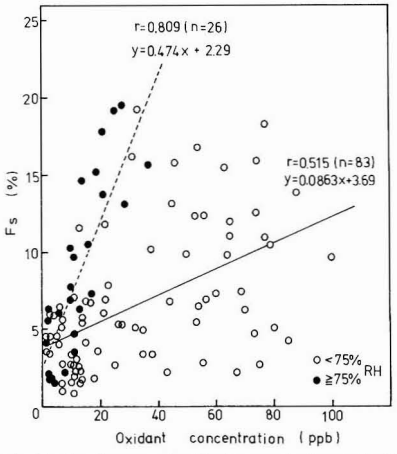

Figure 4. Scatter diagram of oxidant concentration and sulfur conversion ratio (F_s) observed at a Nagoya urban site. F_s is defined in the text.

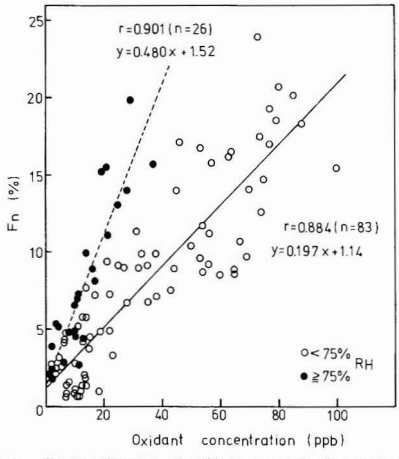

Figure 5. Scatter diagram of oxidant concentration and nitrogen conversion ratio (F_n) observed at a Nagoya urban site. F_n is defined in the text.

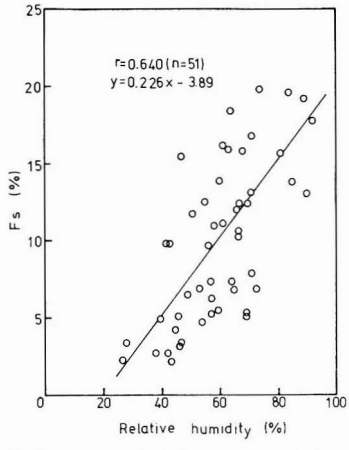

Figure 6. Scatter diagram of relative humidity and sulfur conversion ratio (F_s) observed at a Nagoya urban site. Data sets less than 20 ppb oxidant concentration are excluded from this scatter diagram.

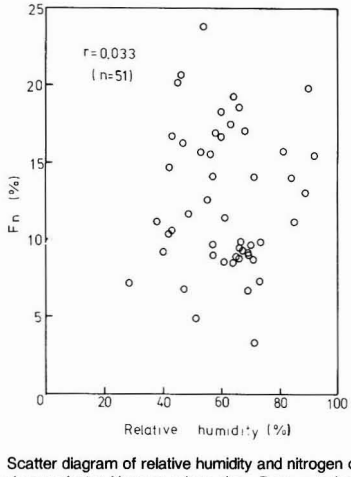

Figure 7. Scatter diagram of relative humidity and nitrogen conversion ratio (F_n) observed at a Nagoya urban site. Data sets less than 20 ppb oxidant concentration are excluded from this scatter diagram.

higher in August than in June. These results of F_s and F_n imply that photochemical oxidation plays an important role in the oxidation of SO_2 and NO_2; furthermore, the SO_2 oxidation may be enhanced at high relative humidities.

Figures 4 and 5 show the relationship between F_s, F_n, and oxidant concentration, respectively. In these figures the data sets observed at relative humidity above 75% were distinguished from the others as a black circle, because droplet- (liquid-) phase reactions might be predominant at high relative humidities. F_n increased with increasing oxidant concentration independently of relative humidity. However, F_s had an indistinct correlation to oxidant concentration at relative humidity less than 75%.

In Figures 6 and 7 are shown the relationship between F_s, F_n, and relative humidity, respectively, when oxidant concentration exceeded 20 ppb and photochemical oxidation took place in some degree. As shown in Figures 6 and 7, good correlation was obtained between F_s and relative humidity, but no correlation could be shown between F_n and relative humidity.

The results shown in Figures 4–7 suggest that for the conversion of SO_2 to sulfate relative humidity is an important factor as well as oxidant concentration (i.e., sunlight), while oxidant concentration is the only key ingre-

dient for the conversion of NO_2 to nitrate. It is, hence, concluded with respect to the mechanisms of gas-to-particle conversion in Nagoya urban air that the SO_2 oxidation processes to sulfate are mainly droplet-phase reactions, while gas-phase reactions are predominant for the NO_2 oxidation processes to nitrate.

Summary

The oxidation processes of SO_2 to sulfate and NO_2 to nitrate in urban air have been investigated on the basis of field measurements, which were made under two different summertime conditions and in winter. To characterize these oxidation processes, sulfur and nitrogen conversion ratios (F_s and F_n) defined in the text were calculated from the field data. Subsequently, effective factors on the conversion and the difference between the oxidation processes of SO_2 and those of NO_2 were discussed. Results of this analysis indicated that the enhancement of the conversion of SO_2 to sulfate requires high relative humidity as well as high oxidant concentration, while oxidant concentration is the only key ingredient for the conversion of NO_2 to nitrate. This difference was explained by the presumption that the SO_2 oxidation processes to sulfate are mainly droplet-phase reactions; on the other hand, for the NO_2 oxidation processes to nitrate gas-phase reactions are predominant. However, in this study NO and PAN are not taken into consideration in the equation of F_n, so that the values of F_n may be somewhat decreased compared to those including NO and PAN under the condition of daytime in summer when photochemical reactions take place actively and oxidant concentration is high. On the other hand, under the condition of winter or nighttime in summer when photochemical reactions hardly take place, the values of F_n may be somewhat increased compared to those including NO and PAN.

Acknowledgments

I take this opportunity to express my thanks to Professor A. Ono of Nagoya University for his continuing encouragement and many useful suggestions.

Registry No. SO_2, 7446-09-5; NO_2, 10102-44-0.

Literature Cited

(1) Spicer, C. W. *Environ. Sci. Technol.* **1983**, *17*, 112–120.
(2) Damschen, D. E.; Martin, L. R. *Atmos. Environ.* **1983**, *17*, 2005–2011.
(3) Meagher, J. F.; Olszyna, K. J. *Atmos. Environ.* **1984**, *18*, 2095–2104.
(4) Altshuller, A. P. *Atmos. Environ.* **1979**, *13*, 1653–1661.
(5) Calvert, J. G.; Stockwell, W. R. *Environ. Sci. Technol.* **1983**, *17*, 428A–443A.
(6) Weiss, R. E.; Larson, T. V.; Waggoner, A. P. *Environ. Sci. Technol.* **1982**, *16*, 525–532.
(7) Grosjean, D. *Environ. Sci. Technol.* **1983**, *17*, 13–19.
(8) Huntzicker, J. J.; Hoffman, R. S.; Cary, R. A. *Environ. Sci. Technol.* **1984**, *18*, 962–967.
(9) Davis, D. D.; Heaps, W.; Philen, D.; McGee, T. *Atmos. Environ.* **1979**, *13*, 1197–1203.
(10) Forrest, J.; Garber, R. W.; Newman, L. *Atmos. Environ.* **1981**, *15*, 2273–2282.
(11) McMurry, P. H.; Reder, D. J. *Atmos. Environ.* **1981**, *15*, 2315–2327.
(12) McMurry, P. H.; Wilson, J. C. *Atmos. Environ.* **1982**, *16*, 121–134.
(13) Kadowaki, S. *Bull. Aichi Environ. Res. Cent.* **1983**, *11*, 40–46.
(14) Kadowaki, S. *Atmos. Environ.* **1977**, *11*, 671–675.
(15) Cronn, D. R.; Charlson, R. J.; Knights, R. L.; Crittenden, A. L.; Apell, B. R. *Atmos. Environ.* **1977**, *11*, 929–937.
(16) Cadle, S. H. *Atmos. Environ.* **1985**, *19*, 181–188.
(17) Isawa, Y.; Ono, A. *J. Meteorol. Soc. Jpn.* **1979**, *57*, 599–606.
(18) Mamane, Y.; Puescel, R. F. *Atmos. Environ.* **1980**, *14*, 629–639.
(19) Stelson, A. W.; Friedlander, S. K.; Seinfeld, J. H. *Atmos. Environ.* **1979**, *13*, 369–371.
(20) Stelson, A. W.; Seinfeld, J. H. *Atmos. Environ.* **1982**, *16*, 983–992.
(21) Grosjean, D.; Friedlander, S. K. *J. Air Pollut. Control Assoc.* **1975**, *25*, 1038–1044.

Received for review February 28, 1986. Accepted June 19, 1986.

Environ. Sci. Technol. 1986, 20, 1254–1257

Determination of Organofluorine in Air†

Erik Kissa

Jackson Laboratory, Chemicals and Pigments Department, E. I. du Pont de Nemours and Company, Wilmington, Delaware 19898

■ Organofluorine air contaminants at sub parts per million or higher levels are collected on a solid adsorbent (activated charcoal or graphitized carbon) or in water and then combusted in an oxyhydrogen torch. Combustion converts organic fluorine to hydrogen fluoride, and the fluoride ion is determined with a fluoride ion-selective electrode. The method avoids sample desorption problems and the separation of complex mixtures by commonly used gas chromatographic methods. The maximum concentration each fluoro compound can have in the air sample is calculated from the organofluorine concentration. A specific method may not be needed if the calculated maximum concentration is below an acceptable limit. In conjunction with a specific method, the organofluorine method can detect unidentified fluoro compounds in air not accounted for by the specific method.

Introduction

The presence of organofluorine in air has been of concern in two areas of the environment. The concentrations of chlorofluorocarbons in the atmosphere have been determined (*1–9*) and their long-term effects investigated. Fluoro chemicals in industrial air have been monitored (*10*) to protect the health of the workers. Analytical techniques have been developed to determine fluoro chemicals in the stratosphere at the parts per trillion level and in industrial air at parts per billion or parts per million levels, depending on the allowable concentration of the air contaminant. This paper deals with monitoring organofluorine in air at occupational sites where organic fluoro compounds are produced or used.

The determination of fluoro compounds in air involves two steps: collection of an air sample and determination of the fluoro compound in the sample, usually by gas chromatography. Sampling techniques used for collecting fluoro compounds in air have included grab sampling (*1–3, 6–8, 11, 12*), concentration by cryogenic techniques (*7, 8, 11*), trapping in a solvent (*13*), or, most commonly, adsorption on a solid adsorbent (*5, 9–12, 14–16*). The latter method is convenient and, when followed by thermal desorption, delivers the fluoro compound without dilution. However, adsorption on solid adsorbents poses a problem and a dilemma. The common adsorbents, activated charcoal and graphitized carbon, hold fluoro chemicals firmly, and thermal desorption is usually not quantitative (*13*). On the other hand, Tenax GC, a 2,6-diphenyl-*p*-phenylene oxide polymer, releases fluoro compounds more readily, but is a less efficient sorbent (*12, 13*). Aside from the problem of incomplete desorption, chemical reactions may occur at temperatures needed for thermal desorption and convert the fluoro compound into species not accounted for by the analytical method (*13*).

The collected fluoro compounds in air samples have been determined by gas chromatography (GC) using flame-ionization (FI) (*5, 13, 16*) or electron-capture (EC) detectors (*1–3, 6, 9, 13–15*), and by gas chromatography/mass spectrometry (GC/MS) (*5, 7–9*). Separation and identification of fluoro compounds in mixtures with other halocarbons and air contaminants can be difficult. Some fluoro chemicals, for example hexafluoroacetone, form hydrates that have a retention time different from that of the parent compound. To overcome this problem, several detectors have been used simultaneously (*11, 12*) or the fluoro compounds have been determined by specific ion MS. GC is especially complex when each fluorine-containing air contaminant is in turn a mixture of telomers (homologues differing in the number of tetrafluoroethylene units in their fluorocarbon chain). Quantitation of an air contaminant consisting of homologous telomers requires calibration of each peak area of interest with the corresponding pure telomer. Inevitable errors made in determining individual telomers add up when calculating the sum of their concentrations.

The multitude of problems and complications associated with the specific determination of a fluorine-containing organic air contaminant led us to the concept of determining the total organofluorine concentration in air. When only one air contaminant contains fluorine, the concentration of fluorine in the sample represents the concentration of that fluoro compound in air. If several air contaminants contain fluorine, the fluorine concentration can be used to calculate the maximum concentration each fluoro contaminant can possibly have in the air sample. The maximum concentration of a particular air contaminant is calculated with the assumption that all of the fluorine is related to that particular component. If the maximum concentration of the suspected contaminant is below the acceptable limit, the specific method may not be needed.

If a fluoro compound in air is monitored also by a specific method, the total organofluorine concentration can be determined simultaneously to detect any unidentified fluoro compounds present in air. Sometimes only the total organofluorine concentration needs to be determined, for example, when any organic fluoro contaminant in air is objectionable, as for quality control in a laboratory where trace fluorine analysis are performed.

The concept of total organofluorine in air has proved quite useful, and the analytical techniques for its determination are reported here.

Experimental Section

Materials. Adsorption tubes (6 × 70 mm), specified by NIOSH (*10*), containing two sections (100 and 50 mg) of coconut-based activated charcoal, 20/40 mesh, were purchased from SKC (catalog no. 226-01) or Supelco (catalog no. 2-0267). Alternatively, larger adsorption tubes (8 × 110 mm) containing 600 mg of activated charcoal were used (SKC, catalog no. 226-09), or tubes were packed in our laboratory with 150 mg of activated charcoal, graphitized carbon (Ambersorb XE-347), or Tenax GC (a 2,6-diphenyl-*p*-phenylene oxide polymer).

The fluoro compounds 2*H*-hexafluoro-2-propanol (HFIP), hexafluoroacetone (HFA), telomer alcohols [$CF_3(CF_2CF_2)_nCH_2CH_2OH$], and 1,2,2-trifluoro-1,1,1-tri-

†This is Research and Development Division Publication No. 618. Presented at the 190th American Chemical Society Meeting, Chicago, IL, Sept 8–13, 1985, as CS 18.

0013-936X/86/0920-1254$01.50/0

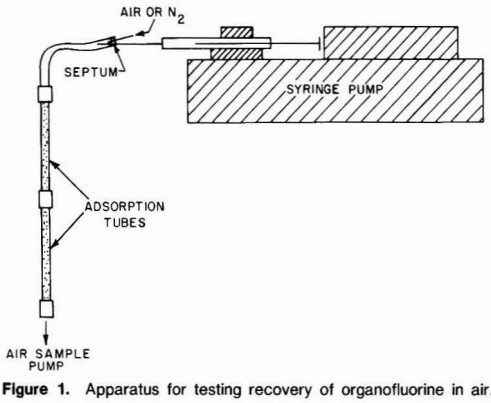

Figure 1. Apparatus for testing recovery of organofluorine in air.

chloroethane used were produced by Du Pont.

Recovery Test. The apparatus used for recovery tests is shown in Figure 1. The Sage syringe pump, Model 341A (Fisher Scientific Co., catalog no. 14-831-40, was equipped with a gas-tight 100-μL syringe (Hamilton, catalog no. 1710N) introduced into the glass evaporation cell through a septum. Nitrogen, pure air from a cylinder, or ambient air was introduced into the evaporation cell through a second hypodermic needle inserted into the septum. The evaporation cell was connected to a pump (SKC, Model 222-3) via two adsorption tubes or a train of impingers, described by us previously (*17*), containing 20 mL of water each and cooled in ice. The flow rate was 120–140 mL/min.

The fluoro compounds were diluted with methanol to facilitate sampling of minute amounts determined by weighing the syringe before and after the delivery. The amount of organic fluorine delivered was varied from 6 to 2440 μg. Nitrogen or air was drawn for 1 h after the delivery of the fluoro compound into the evaporation cell was completed. The recovery of the fluoro compound was determined by combusting the sorbent (activated charcoal removed from the adsorption tube or an aliquot volume of water withdrawn from the impinger) in the oxyhydrogen torch. The cell was washed with methanol and the amount of residual fluorine found in the cell deducted from the amount of organofluorine delivered by the syringe. The results were corrected for a "blank" fluorine value obtained by injecting the solvent (methanol) instead of the sample solution into the evaporation cell.

Combustion Method. The oxyhydrogen torch, originally designed by Wickbold (*18*, *19*), scaled down and modified by Sweetser (*20*), was made of quartz and equipped with a bypass system to allow uninterrupted operation of the torch during sample changeover and withdrawal of the combusted analyte. The combustion procedure and a detailed description of the apparatus will be published elsewhere.

In preparation for combustion, the adsorption tube is scored with a file and broken open. The silylated glass wool plug in the tube is discarded because the plug was found to contain fluorine. Both sections of the adsorbent and the urethane foam sections in the tube are placed into a porcelain combustion boat (Coors 60035; Fisher Scientific Co., catalog no. 07-660C) and transferred into the oxyhydrogen torch made of quartz. If water is used for trapping organic fluorine, 10 mL of the combined contents of the impingers is introduced into the combustion boat by a syringe in several portions. Hydrogen fluoride, formed by combustion of organofluorine in the analyte, is trapped in a scrubber containing water. The contents of the scrubber were washed into a 200-mL volumetric flask, made of polypropylene, and fluoride was determined with a fluoride ion-selective electrode. The procedure for the determination of fluoride in the combusted analyte has been recently described by us (*21*).

The result is corrected for a blank fluorine value of the adsorbent from an unused tube. The fluorine value found is corrected for inorganic fluoride, if present in air. Inorganic fluoride in air, such as hydrofluoric acid, is trapped in water and determined by the ion-selective electrode without combustion. Alternatively, hydrofluoric acid also can be adsorbed on activated charcoal and desorbed in water for its determination.

Table I. Determination of Fluoride with the Ion-Selective Electrode

fluoride, μg		SD	
calcd[a]	found[b]	μg	% rel
0.10	0.14	0.008	6.7
6.0	5.9	0.04	0.67
60	60.2	0.34	0.57

[a] The amount of fluoride (μg) in 200 mL of a standard NaF solution containing an acetic acid/sodium acetate buffer (*21*). [b] Average of six determinations.

Table II. Recovery of HFIP Absorbed in Water

air vol, L	HFIP as organofluorine, μg of F: taken	found	recovery, %	HFIP, ppm: by combustion	by GC (*13*)
32.6	7.4	7.9	106	0.052	nd[a]
42.1	60.8	54.5	90	0.28	0.30
35.0	657	652	99	3.98	3.84
25.3	9770	9270	95	78.3	76.8

[a] nd, not detected.

Results and Discussion

Detection Limits and Precision. The detection limits of fluoro compounds collected in water or on solid adsorbents and combusted in the oxyhydrogen torch depend on the background fluorine in the sorbent used and the precision of the combustion procedure. A key element of the combustion procedure is the ion-selective electrode method (*21*) that we developed for determining fluoride in the combusted analyte. The method can determine even small amounts of fluoride (down to 100 ng) with adequate precision (Table I). Hence, the detection limits and the overall precision of the method for determining organofluorine in air depend mainly on the fluorine content of the sorbent and its consistency.

The fluorine content of activated charcoal (blank value of an adsorption tube containing 150 mg of charcoal) is sufficiently low and reproducible to allow the detection of small amounts of organic fluorine in air (the standard deviation of 23 determinations performed during 10 days was found to be ± 0.21 μg of F, mean value of the blank 0.36 μg of F).

Sorption in Water. The use of water for trapping airborne fluoro chemicals has the advantage that the same sample can be analyzed by several methods, for example, for a specific fluoro chemical or for inorganic fluoride. The prerequisite for using water as the collection medium is solubility of the fluoro chemical in water.

The collection efficiency of a water-soluble fluoro chemical in water is illustrated with 2*H*-hexafluoro-2-

Table III. Organofluorine in Industrial Air

sampling			fluorine found, mg/m³			
date	time, h	air vol, L	inorganic	organic by combustion	organic by GC[a]	fluoro compd determined by GC
7/15	6.0	34.9	0	0.031	0.053	13 ppb HFA[b]
8/2	0.5	3.7	0.24	184	207	44.2 ppm HFIP[c,d]
8/4	16	120.1	0.006	1.02	0.14	0.03 ppm HFIP[c]
8/5	1.3	10.1	0	1.56	1.28	0.27 ppm HFIP[c]

[a] Calculated for the identified and determined fluoro compound. [b] Hexafluoroacetone; adsorbed on Ambersorb XE-347 and desorbed thermally into a 6 ft long column, $^1/_4$ in. o.d., packed with 80/100 mesh Carbosieve B; isothermal gas chromatography at 300 °C using a Hall detector. [c] Gas chromatography conditions described in ref 13. [d] Air in the packing booth; protective clothing and respiratory equipment required.

Table IV. Recovery of Organofluorine in Air by Adsorption on Charcoal and Combustion

fluoro compd	amount, μg of F evaporated	amount, μg of F found	recovery, %	F in the second tube[b]
$CF_3(CF_2)_nCH_2CH_2OH$	10.3	10.2	99	5
	97.3	88.3	91	1
$CF_3(CF_2)_5CH_2CH_2OH$	6.5	7.0	108	3
	369	350	95	0
$(CF_3)_2CHOH$	6.7	6.5	98[a]	3
	34.2	31.6	95[a]	2
	174	161	93[a]	0
	175	181	104	1
	2439	2303	94	0
$CF_2ClCFCl_2$	44.5	36.7	82	43[c]
	87.1	70.2	79	47[c]
	8.6	7.9	93[a]	1
	86.5	84.6	98[a]	1

[a] Collected in nitrogen. [b] Percent of total F adsorbed. [c] Collected in humid air.

propanol (HFIP) (Table II). The sorption of HFIP is essentially complete in two impingers. When four impingers were connected in series, as an average 81% of HFIP was absorbed in the first impinger, 15% in the second, 3% in the third, and 0.6% in the fourth (*13*).

The recovery of HFIP in air is very satisfactory even at sub parts per million levels. The agreement with recovery values obtained by gas chromatography of HFIP is excellent. The concentration of organofluorine in plant air was found to be in reasonable agreement with the fluorine content calculated from the HFIP concentration determined by the specific GC method, except for one day when the sampling time was long and HFIP concentration in air low (Table III). Only 14% of organofluorine was HFIP-related, indicating that in addition to HFIP other fluoro compounds were present in air during that particular day. The detection of fluorine-containing air contaminants by GC would have required constant monitoring of air contaminants by GC/MS, an elaborate procedure dependent on the representation of every fluoro compound in the air sample by a peak in the gas chromatogram. This shows the power of the total organofluorine method coupled with a specific method for determining a fluoro chemical air contaminant.

The amounts of inorganic fluorine in the air samples determined by the fluoride ion-selective electrode in the contents of the impingers without combustion were very low (Table III).

Collection of Fluoro Compounds on Solid Adsorbents. We have collected fluoro chemicals on various solid adsorbents including activated charcoal, graphitized carbon, silica, Tenax, etc. The choice of the adsorbent is determined mainly by its adsorption efficiency; the ease of desorption, an important factor in conventional methods for determining air pollutants, is of no consequence here. Activated carbon and graphitized carbon were found to be the most efficient adsorbents.

The recovery of fluoro compounds adsorbed on activated charcoal is shown in Table IV. Adsorption on 150 mg of activated charcoal in a small (7 cm long) adsorption tube is essentially complete except for volatile halogenocarbons such as 1,2,2-trifluoro-1,1,2-trichloroethane in humid air. In dry air or nitrogen, adsorption is nearly quantitative, but for the adsorption of volatile fluoro compounds in humid air, two small adsorption tubes (150 mg of activated charcoal in each tube) or a large adsorption tube (600 mg of activated charcoal) has to be used. The detrimental effect of water on adsorption of fluorocarbons (*10*) and chlorocarbons (*22*) on charcoal has been observed by others.

The subject method also is applicable to particulate air contaminants. Particulate organofluorine-containing matter in air is collected on filters made of mixed cellulose esters and combusted together with the filter.

The organofluorine method described in this paper also is useful for the study of adsorption and desorption, especially thermal desorption, of fluoro compounds on solid adsorbents. This will be the subject of a forthcoming paper.

Acknowledgments

I thank C. J. Hensler and Shane S. Que Hee for their helpful comments on the manuscript.

Literature Cited

(1) Lovelock, J. E. *Atmos. Environ.* **1972**, *6*, 917–925.
(2) Lovelock, J. E.; Maggs, R. J.; Wade, R. J. *Nature (London)* **1973**, *241*, 194–196.
(3) Su, C. W.; Goldberg, E. D. *Nature (London)* **1973**, *245*, 27.
(4) Wilkniss, P. E.; Lamontagne, R. A.; Larson, R. E.; Swinnerton, J. W.; Dickson, C. R.; Thompson, T. *Nature (London), Phys. Sci.* **1973**, *245*, 45–47.
(5) Bertsch, W.; Zlatkis, A.; Liebich, H. M.; Schneider, H. J. *J. Chromatogr.* **1974**, *99*, 673–683.
(6) Hester, N. E.; Stephens, E. R.; Taylor, O. C. *J. Air Pollut. Control Assoc.* **1974**, *24*, 591–595.
(7) Grimsrud, E. P.; Rasmussen, R. A. *Atmos. Environ.* **1975**, *9*, 1010–1013.
(8) Grimsrud, E. P.; Rasmussen, R. A. *Atmos. Environ.* **1975**, *9*, 1014–1017.
(9) Russell, J. W.; Shadoff, L. A. *J. Chromatogr.* **1977**, *134*, 375–384.
(10) *NIOSH Manual of Analytical Methods*, 2nd ed.; U.S. Department of Health, Education, and Welfare: Cincinnati, OH, 1977; Part II, Methods S102, S107, S108, S109, S111, S125, S129, S131, and S132.
(11) Cox, R. D.; Earp, R. F. *Anal. Chem.* **1982**, *54*, 2265–2270.
(12) Reineke, F. J.; Bächmann, K. *J. Chromatogr.* **1985**, *323*, 323–329.
(13) Kissa, E. *J. Chromatogr.* **1985**, *319*, 407–411.

(14) Bruner, F.; Bertoni, G.; Crescentini, G. *J. Chromatogr.* **1978**, *167*, 399–407.
(15) Vidal-Madjar, C.; Gonnord, M. F.; Benchah, F.; Guiochon, G. *J. Chromatogr. Sci.* **1978**, *16*, 190–196.
(16) Hubbard, S.; Russwurm, G. M.; Walburn, S. G. *Atmos. Environ.* **1981**, *15*, 905–908.
(17) Kissa, E. *Anal. Chem.* **1983**, *55*, 1222–1225.
(18) Wickbold, R. *Angew. Chem.* **1952**, *64*, 133–135.
(19) Wickbold, R. *Angew. Chem.* **1954**, *66*, 173.
(20) Sweetser, P. B. *Anal. Chem.* **1956**, *28*, 1766–1768.
(21) Kissa, E. *Anal. Chem.* **1983**, *55*, 1445–1448.
(22) Gregory, E. D.; Elia, V. J. *Am. Ind. Hyg. Assoc. J.* **1983**, *44*, 88–96.

Received for review April 21, 1986. Accepted August 14, 1986.

NOTES

Radioactivity Size Distributions of Ambient Aerosols in Helsinki, Finland, during May 1986 after the Chernobyl Accident: Preliminary Report

Esko I. Kauppinen*

Laboratory of Heating and Ventilating, Technical Research Centre of Finland, SF-02150 Espoo, Finland

Risto E. Hillamo

Air Quality Department, Finnish Meteorological Institute, SF-00810 Helsinki, Finland

S. Hannele Aaltonen and Kari T. S. Sinkko

Surveillance Department, Finnish Centre for Radiation and Nuclear Safety, SF-00101 Helsinki, Finland

■ Ambient aerosol size distributions of ^{131}I, ^{103}Ru, ^{132}Te, and ^{137}Cs radionuclides were measured in Helsinki, Finland, during May 7–14, 1986. Radioactivity size distributions were unimodal. The geometric mean diameter of ^{131}I was in the size range 0.33–0.57 μm a.e.d. Other isotopes had geometric mean diameters in the size range 0.65–0.93 μm a.e.d.

Introduction

Following the accident at Chernobyl nuclear power station on April 26, 1986, great amounts of radioactive aerosols were emitted into the troposphere. Particle size distributions of radioactive isotopes should be known, in order to understand and to be able to predict the behavior, transport, and deposition of radioactive material. In this report, preliminary results of ambient radioactive aerosol size distribution measurements during May 7–14 in Helsinki, Finland, are given.

Experimental Methods

Sampling. Aerosol samples were collected with 11-stage multijet compressible flow low-pressure impactors (modified HAUKE 25/0.015 LPI) covering 0.03–16-μm aerodynamic diameter size range (*1–3*).

A Liu-type aerosol inlet was connected to the LPI inlet to minimize the effect of wind on the aspiration efficiency (*4*). Polycarbonate films of 10-μm thickness were used as impaction substrates. To prevent coarse-particle bounce, the films on the stages collecting particles greater than 1 μm a.e.d. were greased thinly with a uniform layer of Apiezon L-grease. The amount of grease on the film was 30–300 μg.

Samples were collected during May 7–14, 1986. Sampling periods are given in Table I. Weather conditions and air trajectories are given elsewhere (*5*). The sampling site was the roof of the Finnish Meteorological Institute building (about 25 m above ground level) in downtown Helsinki.

Table I. Impactor Sampling Periods (Local Time)

sample	start	end
2	May 7, 4.22 p.m.	May 9, 3.28 p.m.
3	May 9, 3.22 p.m.	May 12, 9.47 a.m.
4	May 12, 10.00 a.m.	May 14, 11.10 a.m.

Analysis. The mass of collected particles was determined by weighing substrate films carefully before and after sampling with a microbalance (Mettler M3). Before gravimetric analysis, the films were exposed to an ion stream generated by a polonium α-active source, in order to reduce the effects of electrical charge on the weighing results.

Before radioactivity analysis, the films (donut shaped, in the middle of which are the particle deposition spots) were cut into four equal pieces and laid above each other, in order to achieve better γ-counting geometry. As a result, the samples could be approximated with disket geometry.

The amount of radioactive isotopes in the sample was determined by measuring its γ-spectrum with a cylindrical Ge(Li) detector. The crystal of the detector is drifted coaxially with one end open, and the active volume is about 130 cm^3, corresponding to 30% relative efficiency at 1332 keV. The sample was placed on the end cap of the detector. Measurements were performed in a background shield of 12 cm of lead gradually lined with cadmium (1 mm) and copper (0.5 mm) (*6*). During the measurement, the crystal was ventilated with aged pressurized air to reduce the iodine background.

Measuring times were 45 min for the substrate film of each impactor stage of samples 2 and 3 and 100 min for the films of sample 4, respectively. The measured spectra

0013-936X/86/0920-1257$01.50/0

Table II. Aerodynamic Cut Diameters of the Impactor with the Measured Mass and Activity Concentrations on Each of the Impactor Stages

sample	stage	$D_{50,ae}$, μm[a]	Δm, $\mu g/m^3$	ΔA, mBq/m^3 ^{103}Ru	^{131}I	^{132}Te	^{137}Cs
2	1	0.028	0.3	ND[b]	2.4	ND	ND
	2	0.052	0.5	ND	3.0	ND	ND
	3	0.077	1.9	ND	9.6	ND	ND
	4	0.14	4.6	ND	25.9	ND	ND
	5	0.29	6.8	2.5	27.9	ND	ND
	6	0.48	7.0	5.5	17.6	7.1	4.6
	7	1.0	2.9	5.0	4.4	5.0	ND
	8	2.0	7.3	ND	ND	ND	ND
	9	4.0	11.6	ND	3.5	ND	ND
	10	8.0	14.1	ND	ND	ND	ND
	11	16	10.6	ND	ND	ND	ND
3	1	0.028	0.2	ND	ND	ND	ND
	2	0.052	0.2	ND	ND	ND	ND
	3	0.077	1.3	ND	4.0	ND	ND
	4	0.14	3.4	3.2	9.5	ND	ND
	5	0.29	4.6	11.5	8.3	ND	3.2
	6	0.48	5.6	15.5	8.9	ND	3.2
	7	1.0	2.4	7.0	3.1	ND	1.7
	8	2.0	3.0	1.5	1.9	ND	ND
	9	4.0	3.3	ND	ND	ND	ND
	10	8.0	1.4	ND	ND	ND	ND
	11	16	7.6	7.2	3.0	ND	ND
4	1	0.028	0.2	ND	ND	ND	ND
	2	0.052	0.4	ND	ND	ND	ND
	3	0.077	1.4	ND	ND	ND	ND
	4	0.14	3.7	ND	ND	ND	ND
	5	0.29	6.1	2.7	4.4	ND	ND
	6	0.48	9.0	6.0	5.2	ND	ND
	7	1.0	5.1	2.5	2.7	ND	ND
	8	2.0	4.3	ND	ND	ND	ND
	9	4.0	4.0	ND	ND	ND	ND
	10	8.0	3.5	ND	ND	ND	ND
	11	16	3.2	ND	ND	ND	ND

[a] The aerodynamic diameter at the upstream stagnation pressure of the impactor stage. [b] Not detected.

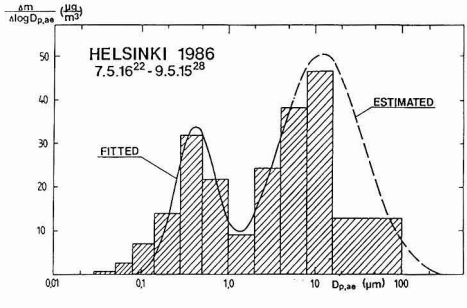

Figure 1. Measured (histogram) and fitted (curve) mass size distributions of sample 2. A maximum particle size of 100 μm is assumed when plotting the histogram.

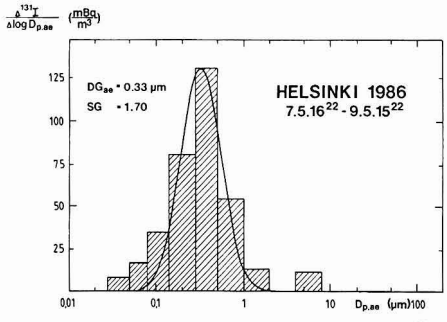

Figure 2. Example of measured (histogram) and fitted (curve) ^{131}I size distributions.

were analyzed with the computer program GAMMA-83, which calculates the concentrations of the nuclides in the sample (*7*). The efficiency calibration of the disket geometry with sample height of 0 mm above the crystal was used in calculating the activities. The results of ^{131}I were calculated from the peak at 364.5 keV.

The measured mass and activity concentrations on each of the impactor stages are shown in Table II.

Data Reduction. Aerosol size distributions were determined from analysis results by assuming the collection efficiency of each impactor stage to be a step function at the cut-point particle size; i.e., no cross-sensitivity corrections were made. The cut points of incompressible flow stages were calculated by Marple's theory (*8*). The cut points of high-velocity compressible flow stages were determined by assuming a constant Stk_{50} value, calculating the jet core velocity from the pressure drop across the stage, and evaluating the Cunningham slip correction factor at the upstream stagnation pressure of the impactor stage (*3, 9, 10*). The calculated cut points $D_{50,ae}$ are shown in Table II. To determine the structure of the size distributions, a log normal distribution was fitted to each measured size distribution with the DISFITE fitting program (*11*).

Results

Examples of measured mass and ^{131}I differential size distributions (histograms) and their log normal fits (curves) are shown in Figures 1 and 2. Distribution functions above 4 μm a.e.d. are estimates, due to decreasing aspi-

Table III. Geometric Mean Diameters (Aerodynamic) DG_{ae}, Geometric Standard Deviations SG, and Modal Concentrations C for Radioactivity Size Distributions and for Mass and Surface Area Size Distributions of the Accumulation Mode

	sample 2			sample 3			sample 4		
	DG_{ae}, μm	SG	C, mBq/m³	DG_{ae}, μm	SG	C, mBq/m³	DG_{ae}, μm	SG	C, mBq/m³
mass	0.42	1.7	20[a]	0.44	1.8	15[a]	0.57	1.9	25[a]
surface area	0.32	1.7	321[b]	0.31	1.8	251[b]	0.38	1.9	318[b]
^{103}Ru	0.83	1.8	14	0.63	1.9	46	0.65	1.7	12
^{131}I	0.33	1.7	98	0.36	2.3	39	0.57	2.0	17
^{132}Te	0.93	~1.5	13						
^{137}Cs				0.63	1.8	9			

[a] Accumulation mode mass concentration, μg/m³. [b] Accumulation mode surface area concentration, μm²/cm³.

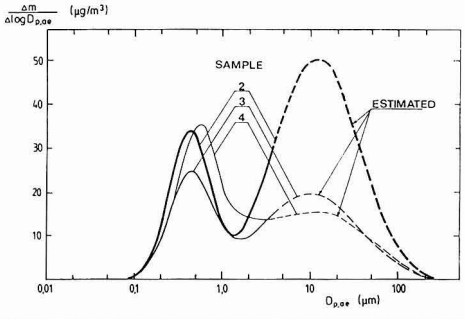

Figure 3. Mass size distribution curves. Sampling periods are given in Table I.

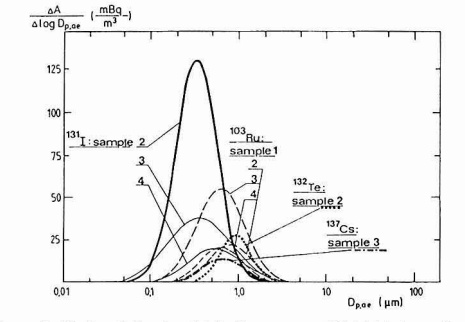

Figure 4. Radioactivity size distribution curves of Helsinki atmospheric aerosols.

ration efficiency of the inlet and increasing impactor wall losses in this size range. Mass size distribution curves of samples 2–4 are shown in Figure 3. They are clearly bimodal, exhibiting accumulation and coarse-particle modes and a gap between these at a size range of 1–2 μm a.e.d.

Radioactivity size distribution curves of those isotopes, which could be determined with relatively short γ-counting times, are shown in Figure 4. All distributions are unimodal. The modal parameters [geometric mean diameter (aerodynamic), geometric standard deviation, and modal concentration] for the accumulation-mode mass and surface area (calculated from mass distribution assuming unit density spherical particles) size distributions and for radioactivity size distributions are given in Table III.

^{131}I size distributions differ clearly from size distributions of other radioactive isotopes. The geometric mean size of ^{131}I is smaller than that of other isotopes. In samples 2 and 3, it is almost equal to the surface area geometric mean diameter of the accumulation mode, and in sample 4 it is equal to the mass geometric mean diameter of the accumulation mode. The geometric mean size of ^{131}I seems to grow whereas the geometric mean size of ^{103}Ru decreases, as the aerosol ages.

In sample 3, ^{131}I and ^{103}Ru are also found in particles of $D_{ae} > 16$ μm (not shown in Figure 4). This is probably due to rainy weather which occurred during the sampling period, i.e., radioactivity carried by the raindrops.

Registry No. ^{103}Ru, 13968-53-1; ^{132}Te, 14234-28-7; ^{137}Cs, 10045-97-3; ^{131}I, 10043-66-0.

Literature Cited

(1) Berner, A.; Lurzer, C. J. *Phys. Chem.* **1980**, *84*, 2079–2083.
(2) Berner, A. In *Aerosols. Science, Technology, and Industrial Applications of Airborne Particles*; Liu, B. Y. H.; Pui, D. Y. H.; Fissan, H. J., Eds.; Elsevier: New York, 1984; pp 139–142.
(3) Kauppinen, E.; Hillamo, R.; Ruuskanen, J.; Hakkarainen, T.; Rouhiainen, P. *J. Aerosol Sci.* **1986**, *17*, 506–510.
(4) Lui, B. Y. H.; Pui, D. Y. H. *Atmos. Environ.* **1981**, *15*, 589–600.
(5) Savolainen, A.-L.; Hopeakoski, T.; Kilpinen, J.; Kukkonen, P.; Kulmala, A.; Valkama, I. "Dispersion of Radioactive Releases Following the Chernobyl Nuclear Power Plant Accident. Interim Report"; Finnish Meteorological Institute Report No. 1986:2, 1986; Finnish Meteorological Institute, Helsinki.
(6) Sinkko, K.; Aaltonen, H. "Calculation of the True Coincidence Summing Correction for Different Sample Geometries in Gamma-Ray Spectroscopy"; Report STUK-B-VALO 40, 1985; Finnish Centre for Radiation and Nuclear Safety, Helsinki.
(7) Sinkko, K. "Computer Analysis of Gamma-Ray Spectra in Sample Measurements" (in Finnish); Licentiate Thesis, Department of Physics, University of Helsinki, Helsinki, 1981.
(8) Rader, D. J.; Marple, V. A. *Aerosol Sci. Technol.* **1985**, *4*, 141–15.
(9) Flagan, R. C. *J. Colloid Interface Sci.* **1982**, *87*, 291–299.
(10) Biswas, P.; Flagan, R. C. *Environ. Sci. Technol.* **1984**, *18*, 611–616.
(11) Whitby, K. T.; Whitby, E. R. "DISFITE-Size Distribution and Fitting Program"; PTL Publication No. 441, 1982; Particle Technology Laboratory, University of Minnesota, Minneapolis, MN.

Received for review June 27, 1986. Accepted August 25, 1986.

Environ. Sci. Technol. 1986, 20, 1260–1262

Field Audit Results with Organic Gas Standards on Volatile Organic Ambient Air Samplers Equipped with Tenax GC

Howard L. Crist* and William J. Mitchell

Quality Assurance Division, Environmental Monitoring Systems Laboratory, U.S. Environmental Protection Agency, Research Triangle Park, North Carolina 27711

■ The results from two field audits of Tenax GC equipped sampling systems measuring the volatile organic compound (VOC) concentrations in ambient air are reported. Each audit standard contained at least four of the following compounds at the low parts per billion (ppb) level: C_6H_6, $C_6H_5CH_3$, C_6H_5Br, C_6H_5Cl, $CHCl_3$, CCl_4, and C_2Cl_4. The results of the audits were consistent and highlight some of the errors associated with sampling for VOC's with Tenax. For example, a large negative bias was evident for CCl_4 even when the sampled volume was less than 10% of the published breakthrough volume. However, regardless of the volume sampled, a 23–36% positive bias was evident for all but one C_2Cl_4 sample. A positive bias was also evident for both C_6H_6 and $C_6H_5CH_3$. The agreement between successive audits showed that the system is a viable means to audit the performance of VOC sampling systems at field sites.

Introduction

Tenax GC adsorbent is widely used for collection of volatile organic compounds (VOC's) in ambient air (*1*, *2*). Because of the uncertainties associated with using only a single adsorbent cartridge to collect organics in air (*3*), EPA/EMSL uses four cartridges to sample simultaneously the same air parcel. However, each cartridge samples at a different flow rate in order to collect air volumes that differ widely (10–80 L). In the past, the performance audits on this latter VOC monitoring system were limited to the analysis of tubes containing Tenax that had been spiked in the laboratory with selected VOC's. This practice was not an entirely adequate quality-assurance procedure because sampling, an integral part of the monitoring system, was not evaluated with this technique.

This situation changed with the recent development of gas cylinders containing stable mixtures of toxic volatile organic compounds at the low parts per billion (ppb) level. These National Bureau of Standards (NBS) materials made on-site field audits of the entire air monitoring system possible (*4*). This article describes two field audits of ambient air sampling systems using Tenax that were conducted with these NBS VOC reference standards. Since the cylinders contained several aromatic and aliphatic hydrocarbons/halocarbons at 1–12 ppb, they were used without sample dilution. These audits provided an assessment of the accuracy and precision of an EPA-operated ambient air sampler that used Tenax to collect VOC's from air. However, they also provided information on the capabilities of Tenax under field sampling conditions that will be useful for those considering the use of Tenax for VOC's.

Experimental Section

The audit materials, contained in 150-ft^3, aluminum cylinders with a balance gas of N_2, were gravimetrically prepared by the NBS and then analyzed by at least two different analytical methods. The single standard used in the first field audit (1983) contained the following mixture of aliphatic and aromatic compounds: $CHCl_3$ (3.8 ppb), C_2Cl_4 (12.4 ppb), CCl_4 (7.7 ppb), C_6H_6 (8.7 ppb), and $C_6H_5CH_3$ (6.4 ppb). The two standards used in the second field audit (1985) contained either four aromatics or four aliphatics. The cylinder with the aromatics contained C_6H_6 (0.93 ppb), $C_6H_5CH_3$ (0.88 ppb), C_6H_5Cl (1.42 ppb), and C_6H_5Br (1.22 ppb). The cylinder with the aliphatics contained $CHCl_3$ (1.08 ppb), C_2Cl_4 (1.85 ppb), CCl_4 (1.15 ppb), and C_2H_3Cl (0.90 ppb). The preparation and analysis of low ppb VOC standards by NBS has been reported previously (*5*). The audit standards were analyzed by NBS before and after the performance evaluation to verify stability of the components during the audit. The reanalysis showed that the concentrations were unchanged. The estimated uncertainty in the certified concentrations is less than 0.08 ppb for all compounds. The gravimetrically determined concentrations (ppb) of VOC's in the cylinder were converted into nanograms per liter units with the ideal gas equation ($PV = nRT$). The amounts (ng) of VOC's delivered to the Tenax cartridges were then calculated from the volume of gas sampled.

At both field sites the mass flow controllers used in the VOC samplers were audited with laminar flow elements certified by the NBS. At both sites the gas flow from the cylinder was controlled with a 350 CGA reducing adapter and needle valve. The gas passed from the cylinder to the sampler through 39 cm of 3 mm o.d., 316 SS tubing that was connected to the sampler with a Sovirel fitting equipped with Teflon gaskets. Before the field audits began, the gas delivery system was checked for losses by passing SO_2 at the low ppb level through it and measuring the outlet concentration. No losses were found.

Three audit runs were done in the 1983 audit with run times of 30, 30, and 60 min. In each run, two samplers were audited with one sampler operating at 50 cm^3/min and the other at 95 cm^3/min. Four, 3-h audit runs were done in the 1985 audit, two from the aromatic cylinder and two from the aliphatic cylinder. In each run four samplers were audited simultaneously with the samplers operating at one of the following flows: 55, 110, 220, and 440 cm^3/min. Each sampler contained 1.2 g of Tenax in a glass (1983 audit) or 316 SS (1985 audit) tube approximately 15 mm (o.d.) × 100 mm long.

At the completion of the audit, the samples were returned to the laboratory by common carrier where they were analyzed by GC/MS/COMP in the same manner as the actual air samples. The GC/MS calibration standards were prepared in a glass flask equipped with a resealable valve for withdrawal of aliquots by syringe. Small amounts of pure VOC's were introduced into the flask where they were volatilized with heat and agitation to provide a stable, uniform gas standard (*6*). The GC/MS was calibrated by direct injections of this gaseous VOC standard into the "splitless" injection port with a gas-tight microsyringe. The Tenax cartridges were analyzed by thermal desorption at 270 °C for 8 min into the GC/MS using a NuTech Model 320 thermal desorption unit (*7*).

The Tenax used in the audit was cleaned up by Soxhlet extraction with methanol and pentane (8 h each) and, after removal of the solvent, was also thermally desorbed at 270 °C for 4 h.

Table I. 1983 Aliphatic/Aromatic Audit Results[a]

run	vol, L	compd[b]	amount, ng delivered	amount, ng reported	bias, %
1	1.5	C_6H_6	43.4	49.4	13.8
		$C_6H_5CH_3$	37.6	48.1	27.9
		$CHCl_3$	28.9	31.5	9.0
		C_2Cl_4	131	136	3.8
		CCl_4	75.6	54.2	-28.3
	2.85	C_6H_6	82.4	96.1	16.6
		$C_6H_5CH_3$	71.4	92.5	29.6
		$CHCl_3$	54.9	58.0	5.6
		C_2Cl_4	249	271	8.8
		CCl_4	144	102	-29.2
2	1.5	C_6H_6	43.4	55.8	28.6
		$C_6H_5CH_3$	37.6	58.9	56.6
		$CHCl_3$	28.9	35.4	22.5
		C_2Cl_4	131	151	15.3
		CCl_4	75.6	57.1	-24.5
	2.85	C_6H_6	82.4	98.7	19.8
		$C_6H_5CH_3$	71.4	98.6	38.1
		$CHCl_3$	54.9	60.4	10.0
		C_2Cl_4	249	291	16.9
		CCl_4	144	103	-28.5
3	3.0	C_6H_6	87.5	110	25.7
		$C_6H_5CH_3$	75.9	124	63.4
		$CHCl_3$	56.9	63.4	11.4
		C_2Cl_4	265	308	16.2
		CCl_4	152	114	-25.0
	5.7	C_6H_6	166	185	11.4
		$C_6H_5CH_3$	144	185	28.5
		$CHCl_3$	108	108	0.0
		C_2Cl_4	503	577	14.7
		CCl_4	290	194	-33.1

[a] C_6H_6 and $C_6H_5CH_3$ results corrected for field blanks of 9 and 11 ng/cartridge, respectively. [b] Breakthrough volumes (L) are C_6H_6 (50), $C_6H_5CH_3$ (240), $CHCl_3$ (20), C_2Cl_4 (200), and CCl_4 (20).

Results and Discussion

All sample flows were within 2% of the flow audit standards. Table I presents the organic audit results from the 1983 audit; Tables II and III present the results for the 1985 aromatic and aliphatic audits, respectively. (C_2H_3Cl is not reported because its breakthrough volume was exceeded in all samples.) Breakthrough volumes cited are from Krost (*8*). In these tables, the percent bias was calculated as

$$\% \text{ bias} = \frac{\text{ng reported} - \text{ng delivered}}{\text{ng delivered}} \times 100$$

In reviewing these results, bear in mind that they are for a Tenax-equipped sampler sampling a clean, dry N_2 stream containing only a few organics—an ideal sampling situation. Therefore, they cannot be applied directly to such a system sampling ambient air.

Although major differences existed between the two audits, the results are surprisingly similar. Some of the major differences between the audits were as follows: (1) the VOC concentrations in the 1983 audit were 3–12 times higher than those in the 1985 audit; (2) an aromatic/aliphatic mixture was used in the 1983 audit whereas separate aliphatic and aromatic mixtures were used in the 1985 audit; (3) the sampled volumes in the 1983 audit (1.5–5.7 L) were smaller than those in the 1985 audit (9.6–78.9 L). Despite these differences, the following similarities are apparent:

(1) C_6H_6 and $C_6H_5CH_3$. A positive bias is evident for all $C_6H_5CH_3$ results and for C_6H_6 for all but the two highest sampled volumes. (These latter volumes are 27–29 L above the published breakthrough volume of 50 L for benzene.) These results suggest that these compounds were either released directly from the Tenax or formed chemically during or after sampling. When one considers the extent of the apparent contamination, the overall agreement between runs is good.

Table II. 1985 Aromatic Audit Results[a]

run	vol, L	compd[b]	amount, ng delivered	amount, ng reported	bias, %
1	10.1	C_6H_6	30	62	107
		$C_6H_5CH_3$	34	49	44
		C_6H_5Cl	67	NR[c]	
		C_6H_5Br	80	91	13.8
	20.3	C_6H_6	61	65	6.6
		$C_6H_5CH_3$	68	81	19.1
		C_6H_5Cl	135	NR	
		C_6H_5Br	162	11	-93.2
	39.4	C_6H_6	119	122	2.5
		$C_6H_5CH_3$	133	148	11.3
		C_6H_5Cl	262	NR	
		C_6H_5Br	314	369	17.5
	78.9	C_6H_6	238	224	-5.9
		$C_6H_5CH_3$	266	304	14.3
		C_6H_5Cl	524	513	-2.1
		C_6H_5Br	628	634	1.0
2	9.6	C_6H_6	29	46	58.6
		$C_6H_5CH_3$	33	48	45.5
		C_6H_5Cl	64	NR	
		C_6H_5Br	77	91	18.2
	19.3	C_6H_6	59	73	23.7
		$C_6H_5CH_3$	66	92	39.4
		C_6H_5Cl	131	NR	
		C_6H_5Br	157	184	17.2
	38.1	C_6H_6	117	138	17.9
		$C_6H_5CH_3$	131	164	25.2
		C_6H_5Cl	258	281	8.9
		C_6H_5Br	309	348	12.6
	76.8	C_6H_6	236	233	-1.3
		$C_6H_5CH_3$	264	321	21.6
		C_6H_5Cl	519	538	3.7
		C_6H_5Br	622	680	9.3

[a] C_6H_6 and $C_6H_5CH_3$ results corrected for field blanks of 33 and 10 ng/cartridge, respectively. [b] Breakthrough volumes (L) are C_6H_6 (50), $C_6H_5CH_3$ (240), C_6H_5Cl (470), and C_6H_5Br (1100). [c] Not reported.

Table III. 1985 Aliphatic Audit Results

run	vol, L	compd[a]	amount, ng delivered	amount, ng reported	bias, %
1	10.0	$CHCl_3$	53	68	28.3
		CCl_4	74	57	-23.0
		C_2Cl_4	125	171	36.8
	19.8	$CHCl_3$	105	119	13.3
		CCl_4	147	96	-34.7
		C_2Cl_4	249	324	30.1
	38.5	$CHCl_3$	204	149	-27.0
		CCl_4	286	143	-50.0
		C_2Cl_4	484	606	25.2
	76.4	$CHCl_3$	404	177	-56.2
		CCl_4	568	175	-69.2
		C_2Cl_4	961	1184	23.2
2	10.1	$CHCl_3$	53	72	35.8
		CCl_4	75	54	-28.0
		C_2Cl_4	127	167	31.5
	20.0	$CHCl_3$	106	123	16.0
		CCl_4	149	85	-43.0
		C_2Cl_4	252	331	31.3
	38.9	$CHCl_3$	206	141	-31.6
		CCl_4	289	81	-72.0
		C_2Cl_4	489	607	24.1
	77.3	$CHCl_3$	409	153	-62.6
		CCl_4	575	134	-76.7
		C_2Cl_4	972	NR[b]	

[a] Breakthrough volumes (L) are $CHCl_3$ (20), CCl_4 (20), and C_2Cl_4 (200). [b] Not reported.

The standard deviations of the percent bias for benzene and toluene were 10.9 and 15.4, respectively. On the basis of our laboratory's experience, the estimated precision of the analysis of Tenax field samples for many compounds is only ±30%.

The two highest percent bias values for benzene were rejected at the 5% significance level with the Dixon ratio test for outliers and were not included in the calculation of standard deviation.

(2) C_6H_5Cl. This compound was detected only after the Tenax had been exposed to a large quantity of C_6H_5Cl. Although the amount of data is limited, the results achieved for percent bias are in close agreement (-2.1%, 8.9%, and 3.7%).

(3) C_6H_5Br. A positive bias is evident in the results, but overall precision and accuracy were above expectations with a mean and standard deviation of 12.8 and 6.1, respectively. The lowest percent bias value was rejected with the Dixon ratio test for outliers.

(4) $CHCl_3$. At low volumes a positive bias was evident, but as the breakthrough volume (20 L) was approached, the collection efficiency apparently decreased sharply. (It would not be surprising if breakthrough occurs at even lower volumes when complex air matrices are sampled.)

(5) CCl_4. A negative bias was found even when the sampled volume was less than 10% of the breakthrough volume (20 L). This would indicate that Tenax is not suitable for quantitatively sampling for CCl_4. This negative bias was also found by the NBS as a result of experiments to determine the recovery efficiencies of certain VOC's loaded on Tenax (*9*).

(6) C_2Cl_4. A positive bias was found in all cases where C_2Cl_4 was detected.

Conclusions

Field audit results on Tenax-equipped samplers identified some problems with these type of samplers. The results obtained in the audits showed that successful onsite field evaluations of air monitoring systems using Tenax can be conducted with gas cylinders containing VOC's. By use of cylinders certified or analyzed by the NBS, traceability to a common reference can be established. Ambient air monitoring systems using other collection techniques should also be amenable to this audit approach.

Because actual atmospheric sampling conditions, pollutants, and pollutant concentrations cannot be exactly duplicated, this audit approach does not assess the performance of a VOC sampling system under conditions encountered during actual sampling. It does provide information, however, that can indicate if the sampling/analytical measurement system is operating properly and within expectations.

Registry No. C_6H_6, 71-43-2; $C_6H_5CH_3$, 108-88-3; C_6H_5Br, 108-86-1; C_6H_5Cl, 108-90-7; $CHCl_3$, 67-66-3; CCl_4, 56-23-5; C_2Cl_4, 127-18-4; Tenax GC, 24938-68-9.

Literature Cited

(1) Clark, A. I.; McIntyre, A. E.; Perry, R. *J. Chromatogr.* **1982**, *252*, 147–157.
(2) Pellizzari, E. D. *Environ. Sci. Technol.* **1982**, *16*, 781–785.
(3) Walling, J. F. *Atmos. Environ.* **1984**, *18*, 855–859.
(4) Crist, H. L.; Rook, H. L. "Proceedings of Air Pollution Control Association/American Society for Quality Control Conference on Quality Assurance in Air Pollution Measurements", Boulder, CO, Oct 1984; Air Pollution Control Association: Pittsburgh, PA, 1984.
(5) Zielinski, W. L.; Rhoderick, G. C.; Cuthrell, W. F. "Pittsburgh Conference on Analytical Chemistry and Applied Spectroscopy", New Orleans, LA, Feb 1985; Pittsburgh Conference on Analytical Chemistry and Applied Spectroscopy, Inc.: Pittsburgh, PA, 1985; Abstr. 989.
(6) Morris, C.; Berkley, R.; Bumgarner, J. *Anal. Lett.* **1983**, *16*(A20), 1585–1593.
(7) Berkley, R. E.; Bumgarner, J. L.; Driscoll, D. J.; Morris, C. M.; Wright, L. H. "Standard Operating Procedure for the GC/MS Determination of Volatile Organic Compounds Collected on Tenax"; U.S. EPA, Research Triangle Park, NC, unpublished procedure, 1984; EMSL/RTP-SOP-EMD021.
(8) Krost, K. J.; Pellizzari, E. D.; Wallburn, S. G.; Hubbard, S. A. *Anal. Chem.* **1982**, *54*, 810–817.
(9) Gunther, F.; Chesler, S.; May, W. "Development of Predictable Loadings on Solid Sorbents"; National Bureau of Standards, Gaithersburg, MD; U.S. EPA/NBS Interagency Agreement, unpublished report, 1985.

Received for review March 17, 1986. Revised manuscript received July 15, 1986. Accepted August 5, 1986. The information contained in this paper does not necessarily reflect Environmental Protection Agency policy.

Environ. Sci. Technol. 1986, 20, 1263–1269

Influence of the Nature of Soil Organics on the Sorption of Toluene and Trichloroethylene

Doug R. Garbarini[†] and Leonard W. Lion*

Department of Environmental Engineering, Cornell University, Ithaca, New York 14853

■ Predictive relationships that are presently employed for estimating the soil–water partitioning of nonionic organic pollutants do not account for the variable nature of soil organic matter. The capacity of selected components of soil organic matter to sorb trichloroethylene (TCE) and toluene, two nonionic volatile organic pollutants commonly encountered in contaminated groundwaters, is examined here. Sorption coefficients were determined and correlated with selected physico-chemical characteristics of the sorbents. Results indicate that the components of soil organic matter had widely varying affinities for toluene and TCE that cannot be solely explained by their organic carbon content. Multivariate regression results show that use of a sorbent's oxygen content as well as its carbon content yields a more accurate prediction of the sorptive partitioning coefficient than relationships that rely solely on the sorbent's carbon content.

Introduction

In the U.S. there are numerous reports of contamination of aqueous environmental systems, such as groundwaters, by nonionic organic pollutants (*1*). The concern over such reports has resulted in extensive research designed to predict the reactions and fate of organic solutes in soils, sediments, and aquifer matrices.

The interaction of nonionic organic compounds with solid phases is often found to be quite important in predicting their ultimate fate. Many researchers, investigating this aspect of the problem, have shown that sorptive binding is highly correlated to the organic content of the sorbent (*2–9*). Such reports are, in part, an extension of earlier studies related to pesticide mobility and effectiveness in soil systems (*10–15*), including those of Lambert (*16*, *17*) and Lambert et al. (*18*), who studied the sorption of nonionic organic pesticides. Lambert et al. (*18*) suggested sorption could be attributed to an active fraction of the soil organic matter and considered soil to be analagous to a chromatographic column with a stationary phase of organic matter into which a nonionic organic compound could partition. More recently, Chiou (*2*) has also suggested that the uptake of neutral organics by soils results from their partitioning into soil organic matter and related this partitioning to the solute's aqueous solubility and to its liquid–liquid (e.g., octanol–water) partition coefficient. This theorized role of soil organic matter is consistent with the use of a constant partitioning model to determine distribution coefficients (K_d's):

$$X/M = K_d C_{eq} \tag{1}$$

where X = mass of compound sorbed, M = mass of sorbent, and C_{eq} = equilibrium concentration of sorbate in the aqueous phase. Contaminant sorption can also be expressed on an organic carbon (K_{oc}) or organic matter (K_{om}) basis:

$$K_{oc} = K_d/f_{oc} \text{ or } K_{om} = K_d/f_{om} \tag{2}$$

where f_{oc} and f_{om} = fraction of sorbent as organic carbon or organic matter, respectively.

The same linear partitioning relationship is also consistent with the application of the Freundlich adsorption isotherm

$$X/M = KC_{eq}^{1/n} \tag{3}$$

when $n = 1$ or the Langmuir adsorption isotherm

$$X/M = \frac{(X/M)_{max} C_{eq} K}{1 + C_{eq} K} \tag{4}$$

at low solute concentrations (i.e., when $1 \gg C_{eq}K$).

The actual physico-chemical mechanism (i.e., adsorption vs. partitioning) of the reaction between dissolved organic pollutants and soils is still under discussion (*19*), and the term sorption is used loosely here to refer to either process.

The value of K_{oc} in eq 2 has been found to be nearly the same for a variety of soils and a given nonionic organic compound. Several investigators have developed empirical equations that predict distribution coefficients for a range of contaminants on soils (*2*, *3*, *5*, *7*). The equations are based upon the contaminant's octanol–water partition coefficient (K_{ow}) or its water solubility (S_w) and the fraction organic carbon of the sorbent. For example

$$\log K_{oc} = 0.686 \log (S_w) + 4.723 \tag{5}$$

[as determined by Means et al. (*5*) with $r^2 = 0.98$ for 14 different sorbents and 4 polyaromatic hydrocarbons]

$$\log K_d = 0.72 \log (K_{ow}) + \log (f_{oc}) + 0.49 \tag{6}$$

[as determined by Schwarzenbach et al. (*7*) with $r^2 = 0.95$ for 13 non polar organic solutes and 6 different sorbents with $f_{oc} > 0.001$ (note, the number of sorbents used for the regression was not explicitly stated by Schwarzenbach et al.; however, on the basis of their discussion it is assumed that six were used)].

The use of such empirical equations, and K_{oc} values in general, assumes that all organic carbon or organic matter will interact in an identical fashion with a given neutral organic contaminant. These predictive relationships provide good order of magnitude estimates of soil or sediment sorption. However, it is unlikely that organic matter will behave identically from soil to soil or sediment to sediment when one considers the qualitative variability that exists. For example, the fats–waxes–resins fraction in soil [implicated by Hartley (*20*) as being responsible for soil uptake of organic contaminants] may compose from 2 to over 20% of the organic matter (*21*).

Lambert et al. (*18*) were among the first to theorize that organic matter was the sole determinant in sorption of neutral organic compounds; however, these authors noted that not all organic matter was active in the sorption process and suggested that various soils be indexed according to their active fraction. Mingelgrin et al. (*19*) in a literature search of K_{om} values for various nonionic compounds and various sorbents found cases where the range of K_{om}'s was larger than an order of magnitude, likely exceeding differences that might be attributed to technique.

MacIntyre et al. (*22*), in examining K_d's for mixtures of neutral organic compounds on sorbents before and after

[†]Present address: Emergency and Remedial Response Division, U.S. Environmental Protection Agency, New York, NY 10278.

0013-936X/86/0920-1263$01.50/0

oxidation of labile organic matter, actually observed increased K_d values on the oxidized sorbents in some instances. Similar deviations from constancy for K_{oc} values can be observed in the works of others (*23–27*). This evidence suggests that the inorganic matrix is involved in the sorption process, either directly by sorbing contaminant or indirectly by influencing the role of organic matter, and/or that all organic matter does not behave identically.

The research described here was designed to investigate the role of selected physico-chemical characteristics of organic sorbents, which exist in soils and sediments, in relation to their sorption of organic pollutants. As noted above, information is presently available on the interrelation of soil organic properties to the binding of pesticides, herbicides, or high molecular weight pollutants such as polychlorinated biphenyls (PCB's). However, such data are generally lacking for the nonionic components of fuels and solvents, which are responsible for many present-day groundwater pollution incidents (*1*, *28*, *29*). In the investigation described below, toluene and trichloroethylene (TCE) have been employed as representative constituent components of fuels and degreasers.

Materials and Methods

Materials. To ensure a broad spectrum of physical and chemical parameters to which partitioning constants might be correlated, soil extracts, extracted soil fractions, and several commercial materials (chosen to model soil organic compounds or their precursors) were used as sorbents. The commercially obtained materials were humic acid salt (Aldrich Chemical Co.), Sigmacell type 20 cellulose and the corn protein zein (Sigma Chemical Co.), Indulin AT pine lignin (Westvaco Chemical Division), and tannic acid (Fischer Scientific). These materials were used without further modification in sorption experiments. The soil chosen for fractionation was taken from a swampy lowland area of Cornell University's Sapsucker Woods. The sample was collected in March 1984 from under a cover of snow, ice, water, and approximately an inch of plant litter. The soil was homogenized, and portions of the soil were immediately frozen for later use, or stored at 4 °C and used within a week for humic and fulvic acid extraction. The soil, soil extracts, and soil-extracted materials (except fats–waxes–resins) were ground and passed through a No. 20 sieve prior to use.

The Sapsucker Woods soil was extracted twice, under nitrogen at 4 °C, to yield the humic and fulvic acid fractions as follows. Three kilograms (wet) of soil was placed in a 20-L Nalgene basin containing 15 L of 0.5 N NaOH and stirred continuously for 20 h. After settling, the supernatant was separated from the residue, i.e., humin, by siphoning through glass wool. The humic acids in the supernatant were then precipitated by acidification to pH 1 with concentrated HCl. The acid-soluble organics (fulvic acid fraction) were siphoned through glass wool and stored at 4 °C. The precipitated humic acids were then redissolved in 0.5 N NaOH, and the above procedure was repeated. The solid humic acids were washed by repeating a procedure of centrifuging at 10000*g* for 15 min, decanting the supernatant, and resuspending the humic acids in distilled water, until the supernatant tested negatively for chloride. The extracted humics were then frozen and freeze-dried.

The fulvic acid solution was filtered (Whatman GF/C) and concentrated on a column of Amberlite XAD-2 resin (Rohm and Haas Co.). The resin had been purified and activated by refluxing for 2 days with methanol in a Soxhlet apparatus, followed by rinsing with distilled water, NaOH, and HCl. Column removal efficiency was monitored by measuring effluent absorbance at 254 nm. When removal efficiencies declined, a 0.5 N NH_4OH solution was used to elute the adsorbed fulvic acids. The column was then rinsed with methanol followed by HCl prior to resuming the concentration of fulvic acid. Eluted fulvic acids were frozen and freeze-dried.

The fraction of original soil remaining after two base extractions was rinsed numerous times with distilled water and freeze-dried to yield the humin fraction. A portion of this fraction was treated further to reduce its organic carbon content, by oxidation with hydrogen peroxide (30%) at 85 °C with the procedure of Tessier et al. (*30*). This "oxidized humin" fraction was then oven-dried at 105 °C. The whole soil and these extracted soil residues were also employed as sorbents in this investigation.

Two other sorbents were used in this study: the ethyl ether extracted soil and the resultant organic extract (fats–waxes–resins). These were obtained through a 24-h ethyl ether Soxhlet extraction of the whole soil as described by Stevenson (*31*). The extracted soil was dried at 105 °C to volatilize the ethyl ether while the extract was dried to a constant weight at the same temperature.

Characterization of Sorbents. All the sorbents used in this study were characterized for percent carbon, hydrogen, nitrogen, oxygen plus sulfur, ash, and moisture. Total acidity, dissolved organic carbon (mean fraction of dissolved organic carbon over the range of total organic carbon concentrations employed in sorption experiments), and particle size analyses were also determined for the commercial organic materials (model compounds) and the soil-extracted fulvic and humic acids. The carbon, hydrogen, and nitrogen (CHN) analyses were performed by the Cornell Agronomy Department Service Laboratories, using a Perkin-Elmer 240C elemental analyzer. Total organic carbon (Beckman 915A total carbon analyzer) and nitrogen (Kjeldahl) analyses of the Aldrich humic acids were consistent with results of the CHN elemental analysis. Oxygen plus sulfur contents were calculated as the difference between 100% and the sum of the percent carbon, hydrogen, nitrogen, and ash contents of the dry material. Percent ash determinations were by weight difference upon combustion at 750 °C for 4 h (*32*), while moisture contents were determined by weight difference after oven-drying at 105 °C for 24 h. Sulfur contents are generally quite low in the types of organic materials examined (*21*); therefore, percent oxygen plus sulfur contents are anticipated to be principally a measure of percent oxygen for the organic materials.

Particle size analyses of organic suspensions were performed on a HIAC particle counter, with a HIAC Model CMH-300 particle sensor (applicable to the 5–300-μm particle size range). For each particle size distribution, the following parameters were used to characterize the suspension:

$$d_{av} = \text{arithmetic mean diameter} = \sum nd/\sum n \quad (7)$$

$$d_v = \text{volume mean diameter} = (\sum nd^3/\sum n)^{1/3} \quad (8)$$

$$d_s = \text{surface mean diameter} = (\sum nd^2/\sum n)^{1/2} \quad (9)$$

where d = midsize of the particle size interval and n = number of particles within a given particle size interval. A particle concentration was also determined for each suspension as

$$\text{particles/mg} = \text{number of particles/mg of sorbent}$$

Dissolved organic carbon analyses were conducted with a Beckman Model 915A total carbon analyzer, after centrifugation of the samples at 12000*g* for 15 min. Analyses

were made on at least five different solids concentrations of each sorbent (only three for the fulvic acids), spanning the range of solids concentrations used in the sorption experiments. The Baryta adsorption ($BaOH_2$) method (*33*) was employed for total acidity analysis.

Sorption Studies. We have recently described a head-space procedure for conducting sorption experiments and for determining the resultant partition constants (*34*). This method was also employed in this research. Briefly, sorption experiments were conducted in glass hypovials (nominal capacity of 50 mL) sealed with Teflon-lined rubber septa and aluminum crimp caps (Pierce Chemical Co.). Twenty-five milliliters of 0.2 N sodium phosphate buffer and a 100-μL aliquot of TCE or toluene stock solution (approximate concentrations of 1290 and 210 mg/L, respectively) were added to vials containing variable amounts of sorbents and to vials without sorbent. The bottles were rapidly capped, rotated at 20 °C, and then equilibrated in a 25 °C water bath prior to gas-phase analysis by gas chromatography (GC). Typically, four or more replicates of seven sorbent masses ranging from 40 mg to 1 g (up to 8 g for tannic acid and 4 g for fulvic acids) for the organic sorbents and from 40 mg to 4 g (up to 17 g for the humin fraction) for extracted soil components were analyzed. Kinetics experiments demonstrated that sorption was complete and that losses were negligible, within the precision of the GC technique, for the experimental equilibration periods employed (8 h for toluene and 24 h for TCE).

Phosphate buffer was employed to swamp out contributions by the sorbent to ionic strength and also to limit changes in solution pH, since preliminary experiments revealed the extent of TCE sorption by both lignin and Aldrich humic acids to be affected by pH (i.e., increased sorption with decreased pH). Carter has reported similar pH effects in his research on binding of DDT to dissolved humic acids (*35*). Experimental pHs remained well within ±1 pH unit of the buffer (6.8) except those with high masses of tannic acid. The observations on the effect of pH on sorbents such as Aldrich humic acid, lignin, zein, and cellulose indicate that observed values of K_d are insensitive to pH changes of the magnitude that occurred. Large quantities of sorbent (up to 8 g) were required to determine K_d's for tannic acid, since the extent of TCE and toluene sorption was small. Therefore, pH effects may have occurred at the highest solids concentration with this sorbent. However, since the solution was buffered, pH effects would not be present at the lower solids concentrations and data points for this sorbent at both low and high solids concentrations fall on the same line.

When the activity coefficient (γ) and Henry's law constant (H_c) for a volatile organic compound (VOC) are known, the equilibrium gas concentration (C_g) of a VOC in a closed system serves as a direct measure of its liquid concentration (C_l) since $C_l = C_g/(H_c\gamma)$. Therefore, the ratio of the gas concentration of a bottle without sorbent to the gas concentration of a bottle with sorbent will be the same as the ratio of the liquid concentrations of those bottles. If gas chromatographic peak heights or peak areas are normalized to a uniform bottle size and head-space volume (to account for differences in individual bottle volumes and volume displaced by various masses of sorbent) and if a constant partitioning model (such as eq 1) is obeyed, then as previously shown the following relationship can be used to determine the distribution constant for sorption (*34*):

$$C_T/C_{eq} = K_d[M/(V_l + H_c\gamma V_g)] + 1 \qquad (10)$$

where C_T and C_{eq} are the volatile test compound gas concentrations in equilibrium with aqueous phases of sealed vials containing the phosphate buffer solution (control) and buffer plus sorbent, respectively; V_l and V_g are the liquid- and gas-phase volumes contained in the experimental vials, and K_d, H_c, and γ are as previously defined.

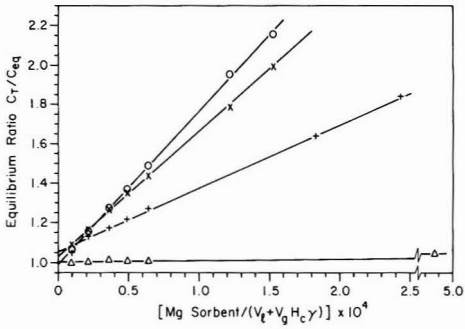

Figure 1. Sorption of TCE by lignin (O), cellulose (Δ), Aldrich humic acid (+), and zein (×).

The experimental procedure employed avoids problems inherent in other methods, such as "particle effects" caused by inadequate separation of colloidal-sized particles or the presence of dissolved organic matter and losses through volatilization (*34*). Since concentrations of the gas phase are analyzed and related to aqueous phase concentrations through Henry's law, no solid–liquid phase separation is performed, and incomplete separation of colloidal-sized or dissolved macromolecular sorbent cannot interfere with the analysis. Previous results with this procedure (*34*) have shown that sorption reactions carried out at solid/solution ratios ranging from 0 to 1:1 may be described by a single linear partition coefficient (all $r^2 > 0.95$). These results and those obtained with the organic sorbents employed in this study indicate particle effects that may result from solid–solid interactions are negligible for the range of solids concentrations employed. The head-space procedure is also advantageous in that knowledge of the mass of solute employed is not required for determination of K_d's, eliminating the necessity for use of carrier solvents, plating techniques, or extractions that are sometimes used in investigations of volatile, low-solubility, nonionic organic solutes (*34*).

Results and Discussion

Correlation of the Physico-Chemical Parameters with Distribution Coefficients. The physico-chemical characteristics and K_d's and K_{oc}'s determined for the organic compounds employed in this study are given in Table I. K_d values are the slopes of linearly regressed data fit to eq 10. Typical results are illustrated in Figure 1. It should be noted that linear correlation coefficients for all such plots were high (r^2 values > 0.98) except those for oxidized humin and cellulose. The masses of oxidized humin (up to 4 g) and of cellulose (up to 2 g) employed displayed a very limited capacity to sorb TCE and toluene (maximum sorption of both TCE and toluene was less than 6 and 4% by oxidized humin and cellulose, respectively). Therefore, C_T/C_{eq} data for these sorbents were not significantly different from 1.0 (i.e., C_T/C_T) or each other, within the precision of the technique, resulting in poor interrelationships between C_T/C_{eq} ratios and mass of sorbent employed. The fact that eq 10 provides an excellent fit to the data for the other sorbents suggests that a linear sorption isotherm is obeyed over the range of solids concentrations employed.

Table I. Physico-Chemical Characteristics, K_d's, and K_{oc}'s for Organic Sorbents[a]

	% ash	% C	% H	% N	% O + S	total acidity, milli-equiv/g	mean fraction, D.O.C./ T.O.C.	d_{av}, μm	d_{surf}, μm	d_{vol}, μm	total particles, per mg	K_d[b] toluene	K_d[b] TCE	K_{oc} toluene	K_{oc} TCE
Sapsucker Woods humic acid	70.6	12.38	2.03	1.09	13.9	1.93	0.44	11.75	14.34	18.37	235 000	10.1 ± 0.14	7.07 ± 0.12	81.2	57.1
Sapsucker Woods fulvic acid	39.7	19.23	3.56	7.03	30.5	2.51	1.00	12.26	13.76	15.70	1 900	2.59[c]	0.79[c]	13.5	4.13
tannic acid	0.0	50.53	3.75	0.05	45.7	9.30	0.82	11.90	14.06	17.25	900	7.76 ± 0.09	8.72 ± 0.28	15.4	17.3
lignin	4.0	64.57	5.71	0.83	24.9	2.89	0.09	12.49	15.68	20.36	335 000	97.2 ± 1.8	77.2 ± 0.87	151	120
zein	1.3	57.21	7.21	14.42	19.9	1.21	0.02	22.06	30.61	40.76	38 800	70.3 ± 1.5	63.4 ± 0.86	123	111
cellulose	0.0	45.26	6.12	0.11	48.5	0.48	0.00	14.11	16.00	18.11	540 000	0.02 ± 0.25	0.92 ± 0.20	0.05	2.0
Aldrich humic acid	31.7	47.86	2.87	0.64	16.9	2.24	0.76	9.27	10.12	11.47	152 000	42.4 ± 1.4	32.1 ± 0.55	88.1	67.1

[a] Calculated on a dry weight basis. [b] Reported intervals are ± 1 SD. [c] Because of the limited sorption capacity of fulvic acid for toluene and TCE, sorption experiments were performed with large masses of this sorbent (4000 mg for sorption of TCE and 600 and 2000 mg for sorption of toluene). The limited quantity of fulvic acid sorbent precluded use of a range of sorbent masses; K_d values are determined as the slope of a line passing through the point (0, 1) and one data point or through two data points, for TCE and toluene, respectively.

Table II. Coefficients of Determination for Toluene and TCE K_d's and Physico-Chemical Parameters of Organic Compounds

parameter	TCE K_d, $r^2 \times 100$	toluene K_d, $r^2 \times 100$
total acidity	3.1	2.6
mean fraction D.O.C.	24.4	27.4
total no. of particles	7.7	8.5
vol. mean diameter	22.1	29.7
surf. mean diameter	17.3	24.3
arithmetic mean diameter	11.2	17.2
% carbon	49.3	52.7
% hydrogen	24.3	30.0
% nitrogen	8.2	12.0
% oxygen + sulfur	22.0	19.6
% ash	12.5	15.9

Examination of Table I shows that the sorbents employed possessed a broad range of values for the physico-chemical parameters examined. In addition, it may be seen that the observed K_d values do not converge to a similar K_{oc} value when normalized by the fraction of organic carbon, indicating that components of organic matter found in soils may have affinities for nonionic organic compounds which cannot simply be explained by their organic carbon content.

It has been suggested that good correlations of organic carbon with sorption may be an artifact of some other physico-chemical parameter to which organic carbon itself is highly correlated (*36*). Accordingly, the deviation from the predictive capability of organic carbon was evaluated in relationship to the other chemical and physical characteristics of sorbents characterized in this study.

In several studies in which sorption of hydrophobic compounds onto sediments and soils has been examined (*3*, *9*, *37*, *38*), particle size has been shown to be important in determining extent of sorption. Horzempa et al. (*38*) have shown the specific surface area of sorbents to be correlated with the magnitude of measured K_d values. Volume and surface mean diameters obtained from HIAC particle size analysis were employed here as representative physical characteristics of the suspension, which might provide some insight into whether the mechanism of the sorption reaction is one of partitioning or surface binding. Another physical parameter, the mean fraction dissolved organic carbon (DOC), was chosen to examine whether the physical form of the sorbent (dissolved vs. particulate) was related to the observed magnitude of K_d.

Simple coefficients of determination among the physico-chemical characteristics of the organic compounds and K_d's for toluene and TCE are given in Table II. K_d's for toluene and TCE are most strongly correlated with percent organic carbon and to a lesser extent with percent oxygen plus sulfur, percent hydrogen, mean fraction DOC, and mean volume and surface diameters. None of the physical parameters examined (such as particle concentration, volume and surface mean diameters, or mean fraction DOC) were strongly correlated with K_d. This evidence suggests, in part, that the binding of TCE and toluene to organic sorbents in the particulate form is not significantly different from that of dissolved sorbents. This observation is consistent with results of Carter et al. (*35*), who found binding of DDT to dissolved humic acids to be similar (on an organic carbon basis) to reported values for DDT binding to particulate organic carbon. Also, Diachenko (*39*) reported sorption of hexachloro-1,3-butadiene to be insensitive to the physical form of humic acids. Lack of significant correlation of K_d with parameters resulting from HIAC characterizations of the suspensions (i.e., d_{av},

Table III. Elemental Analyses, K_d's, and K_{oc}'s for Soil Fractions[a]

	% ash	% C	% H	% N	% O + S	K_d toluene	K_d TCE	K_{oc} toluene	K_{oc} TCE
Sapsucker Woods (S.W.) soil	81.6	7.51	1.29	0.57	9.0	11.3	7.95	151	106
S.W. ethyl ether extracted soil	81.2	7.05	1.23	0.57	10.0	11.5	8.61	164	122
humin	97.6	0.88	0.15	0.04	1.3	2.36	1.28	268	145
oxidized humin	98.5	0.14	0.11	0.10	1.2	0.49	0.40	348	287
fats–waxes–resins	0.0	83.3	12.3	0.71	3.7	ND[b]	383	ND[b]	460

[a] Calculated on a dry weight basis. [b] ND = not determined.

d_v, and d_s) prohibits the formation of conclusions with respect to the mechanism of TCE and toluene sorption reactions with organic matter.

Since regression of K_d's for toluene and TCE against organic carbon content of the organic compounds could only account for 52.7 and 49.2% of the variance in K_d's, respectively, and since none of the other physical or chemical parameters examined were highly correlated with K_d in and of themselves, a stepwise regression procedure was used to see if a multivariable model might better explain the data. For both toluene and TCE, the best "fit" model as predicted by the stepwise procedure and partial F statistics can be expressed in terms of a sorbent's percent organic carbon content and percent oxygen plus sulfur content:

$$K_{TCE} = 1.38(\%\ \text{O.C.}) - 1.40(\%\ \text{oxygen + sulfur}) + 8.74 \quad (11)$$

$$r^2 = 0.89$$

$$K_{tol} = 1.63(\%\ \text{O.C.}) - 1.76(\%\ \text{oxygen + sulfur}) + 13.95 \quad (12)$$

$$r^2 = 0.88$$

Since the above relationships are developed from experiments with materials of high organic content in the absence of a mineral matrix, their application to whole soils (particularly those of low organic content) should be approached with caution. Nevertheless, when the above equations are used to calculate K_d's for the whole Sapsucker Woods soil, the predicted values of 6.5 and 10.4, for TCE and toluene, respectively, are reasonably close to the observed K_d's (7.95 and 11.3). These equations do not satisfactorily predict observed K_d's for residues of the Sapsucker Woods soil after extraction of organics.

The multivariate regression results suggest that a sorbent's carbon to oxygen plus sulfur ratio may be of importance. As described under Materials and Methods, percent oxygen plus sulfur is assumed to be a measure of percent oxygen. Single-variable regression of K_d's vs. C/O ratios for the organic sorbents yielded r^2 values of 0.76 for toluene and 0.77 for TCE. This single-variable correlation is substantially improved over that obtained with the percent organic carbon content of the sorbent.

These results for toluene and TCE are consistent with the observations of Hance (*13*), who suggested that an organic material's ability to sorb organic pesticides was related to its relative hydrophilic/hydrophobic balance as indicated, in part, by its number of oxygen-containing functional groups. Similarly, Pierce et al. (*26*) attributed DDT binding to humic acids to hydrophobic bonding with nonpolar portions of the humic molecule and to lippoidal molecules entrapped within the humic polymer. The results presented above reveal an increase in sorption as the carbon-to-oxygen ratio increases. This is most strongly indicated by K_d values for cellulose and fulvic acids vs. those for lignin and zein and may be indicative of a decrease in sorption as the relative hydrophobicities of these sorbents decrease.

The data obtained indicate it may be important to consider the specific nature of the organic materials that may be present in a soil. For example, examination of Table I shows that cellulose displayed negligible sorption of toluene and TCE. Cellulose, the most abundant carbohydrate component of higher plants, is readily decomposed by microorganisms, and therefore would probably not account for a large percentage of the organic matter in a well-humified soil or sediment (*40*). However, the percentage of organic matter as cellulose may be quite significant in undecomposed organic layers of forest soils, in some peat soils, and in marsh ecosystems. By way of illustration, in a study of sorption of the hydrophobic pesticide linuron to sorbents containing approximately 1% organic matter and 99% quartz, Doherty and Warren (*36*) found extent of sorption of these sorbents to be related to their relative degree of decomposition. The conversion of their observed K_d values to K_{om} values shows that the sorbent with a largely decomposed muck soil organic matter sorbed more than 8.5 times as much linuron as a sorbent with a largely undecomposed sphagnum moss soil organic matter and 2.6 times more than a sorbent containing an intermediately decomposed fibrous peat soil organic matter.

Tannic acid, a major component of the dissolved organic matter in southeastern streams and rivers, also showed a low extent of sorption in this study, especially on a K_{oc} basis. This was not the case for the corn protein zein. Zein yielded K_d's of 70.3 and 63.4 for toluene and TCE, respectively. K_d's and K_{oc}'s for lignin were the highest of all organic compounds examined. Since lignin is abundant in the biosphere and is relatively resistant to degradation, it is likely to be present in significant quantities in some soil systems. Because of its polymeric macromolecular nature and resistance to short-term decomposition, lignin has been suggested as a precursor to humic substances (*21*, *31*). Lignin, as compared to humic and fulvic acids, has a notable lack of carboxylic groups (*21*, *31*), making it less hydrophilic and possibly accounting for its higher K_d's and K_{oc}'s.

It is of particular interest to note the behavior of humic and fulvic acid sorbents in this study since the importance of humic-type substances in influencing the fate of organic pollutants is well documented. Humic and fulvic acids behaved quite differently on an organic carbon basis, with K_{oc}'s differing by more than a factor of 6. When the residual humin [i.e., the whole Sapsucker Woods soil, less humic and fulvic acids (relevant characteristics of this sorbent are given in Table III)] is included in this comparison, the observed variation in K_{oc} is greater than an order of magnitude. However, the Aldrich humic acid and the soil-extracted humic acid behaved fairly similarly on an organic carbon basis.

The disparity amongst the binding of extracted fulvic and humic acids has also been noted in studies of DDT

sorption (*41*, *42*). The fact that fulvic acids generally are more polar and have larger numbers of carboxylic groups and smaller C/O ratios than humic acids might lead one to expect such observations.

The observed disparity between the sorptive properties of humic and fulvic acids may have important implications in soil systems. For instance, forest soils contain high percentages of fulvic acids while in grassland soils the opposite is generally true, and humic to fulvic acid ratios ranging from 0.3 to 2.5 have been observed in different soils (*21*). On the basis of solubility considerations, one would expect soil fulvic acids to be relatively more mobile than soil humic acids, and transport of organic pollutants such as TCE and toluene could be enhanced when bound to dissolved fulvic acids. However, as indicated by the K_d values in Table I, the humic acids employed in this study had a much greater partition coefficient than the fulvic acids.

Comparison of Sorption of TCE and Toluene to Extracted Soils and Whole Soil. The elemental analysis and K_d's and K_{oc}'s for the soil fractions are given in Table III.

As expected, the K_d's for the other humic fractions, i.e., humin and oxidized humin, both low in percent organic carbon, were lower than those for the whole soil. This was not true for the humin K_{oc} value, where a significant increase over the whole soil was observed. This observation is particularly interesting, especially as related to aquifer materials, which are often low in organic carbon content, since organic matter has been cited as controlling sorption at organic carbon contents as low as 0.1% (*3*). Similar evidence of relatively large K_{oc} values for sorbents of low organic content vs. sorbents of higher organic contents have been reported for sorption of DDT (*27*) and acetophenone (*25*). Postulated explanations include the possibility that the intimate association of soil organic matter with the soil inorganic matrix strongly modifies the particle surfaces and/or the nature and properties of soil organic matter. In addition, in studies examining sorption capacity of a material before and after oxidation of a portion of the sorbent's organic matter, K_{oc} values have been found to increase (*22*, *24*, *25*, *27*, *43*).

Shin et al. (*27*) have speculated that observed increases in K_{oc}, such as those noted above, may be attributed to increases in the surface to carbon content (greater surface area of carbon available for reaction). This was attributed to a greater extent of interiorized carbon in skeletal humic acid structures of organic soils vs. organomineral colloids in mineral soils where a central clay micelle is assumed. Turchenek et al. (*44*), in their study of organomineral complexes, found heavier fractions of soils, especially finer clays, contained humic and fulvic materials of a more aliphatic nature than other fractions examined. Khan et al. (*25*) and Banwart et al. (*24*) noted the importance of 2:1 expanadable clays in sorption of organic solutes by soils low in organic carbon. The point to be made is that if the inorganic matrix is not directly implicated in observed increases in K_{oc}'s of sorbents with low organic matter contents, then it may indirectly effect the type and/or character of the organic material present. In such a case, the organic matter of matrices with low organic carbon contents may be different from organic matter in sorbents of high organic matter content and more effective in binding organic solutes.

An extremely high K_d for TCE was obtained on the fats–waxes–resins extract from the Sapsucker Woods soil, which accounted for 6% of the soil organic carbon (insufficient material was available for measurement of K_d for toluene with this sorbent). Such behavior might be expected, since TCE and this sorbent are both highly hydrophobic. The fats–waxes–resins soil fraction has been described by Hartley as being a "solvent" for organic pesticides (*20*). The soil less fats–waxes–resins yielded slightly higher K_{oc}'s than the whole soil. Increases in K_{oc}'s after wax extraction have been reported elsewhere (*27*, *43*). McGlamery [as cited by Dunnigan (*45*)] attributed such increases to an "unmasking" of active adsorption sites.

Conclusions

The data presented here indicate that different constituents and fractions of organic matter behave dissimilarly in regard to their sorption of TCE and toluene. Regression analysis of the data show that relationship using both organic carbon and oxygen or the C/O ratio were more highly correlated with observed K_d values than organic carbon alone. The observed relationships suggest that, for the sorbents evaluated in this study, the relative hydrophobicity of a sorbent is important.

The above results (and results of other investigators described above) also suggest that it is reasonable to expect organic matrices in natural systems that have varying origins, degrees of humification, and degrees of association with inorganic matrices to exhibit dissimilarities in their ability to sorb nonionic organic contaminants. Empirical equations that employ a single soil characteristic (such as f_{oc}) to predict sorption of organic contaminants are necessarily limited in their ability to reflect the detailed differences in soil organic matter. In cases where a more detailed estimate of K_{oc} is desired, use of a two-parameter model employing soil organic carbon and oxygen content may prove to be more satisfactory.

Acknowledgments

We thank two anonymous ES&T reviewers for their helpful comments on the manuscript.

Registry No. C, 7440-44-0; O_2, 7782-44-7; cellulose, 9004-34-6; lignin, 9005-53-2.

Literature Cited

(1) Pye, V. I.; Patrick, R. *Science (Washington, D.C.)* **1983**, *221*, 713–718.
(2) Chiou, C. T.; Peters, L. J.; Freed, V. H. *Science (Washington, D.C)* **1979**, 206, 831–832.
(3) Karickhoff, S. W.; Brown, D. S.; Scott, T. A. *Water Res.* **1979**, *13*, 241–248.
(4) Kenaga, E. E.; Goring, C. A. I. In *Aquatic Toxicology*; Easton, J. C.; Paris, P. R.; Henricks, A. C., Eds.; American Society for Testing and Materials: Philadelphia, PA, 1980; pp 78–115.
(5) Means, J. C.; Wood, S. G.; Hassett, J. J.; Banwart, W. L. *Environ. Sci. Technol.* **1980**, *12*, 1524–1528.
(6) Means, J. C.; Hassett, J. J.; Wood, S. G.; Banwart, W. L. In *Polynuclear Aromatic Hydrocarbons*; Jones, P. W.; Leber, P., Eds.; Ann Arbor Science: Ann Arbor, MI, 1979; pp 327–340.
(7) Schwarzenbach, R. D.; Westall, J. *Environ. Sci. Technol.* **1981**, *15*, 327–340.
(8) Weber, W. J., Jr.; Voice, T. C.; Pirbazari, M.; Hunt, G. E.; Ulanoff, D. M. *Water Res.* **1983**, *17*, 1443–1453.
(9) Choi, W. W.; Chen. K. Y. *Environ. Sci. Technol.* **1976**, *10*, 782–786.
(10) Grover, R. *Weed Sci.* **1971**, *19*, 417–418.
(11) Briggs, G. G. In *Proceedings of Seventh British Insecticide and Fungicide Conference*; Association of British Manufacturers of Agricultural Chemicals: London, 1973; pp 83–86.
(12) Harris, C. R. *Nature (London)* **1964**, *202*, 724.
(13) Hance, R. J. *Weed Res.* **1965**, *5*, 108–114.
(14) Hance, R. J. *Weed Res.* **1965**, *5*, 98–107.

(15) Day, B. B.; Jordan, L. S.; Jolliffe, V. A. *Weeds* **1968**, *16*, 209–213.
(16) Lambert, S. M. *J. Agric. Food Chem.* **1967**, *15*, 572–576.
(17) Lambert, S. M. *J. Agric. Food Chem.* **1968**, *16*, 340–343.
(18) Lambert, S. M.; Porter, P. E.; Schieferstein, R. H. *Weeds* **1965**, *13*, 185–190.
(19) Mingelgrin, U.; Gerstl, Z. *J. Environ. Qual.* **1983**, *12*, 1–11.
(20) Hartley, G. S. In *Herbicides and the Soil*; Woodford, E. K.; Sager, G. R., Eds.; Blackwell Scientific: Oxford, 1960; pp 63–78.
(21) Stevenson, F. J. *Humus Chemistry: Genesis, Composition, Reactions*; Wiley: New York, 1982.
(22) Mac Intyre, W. G.; Smith, C. L.; deFur, P. O.; Su, C. W. Final Report ESL-TR-82-06, 1982; Air Force Engineering and Services Center, Engineering Services Laboratory, National Technical Information Service: Springfield, VA, 1982.
(23) Rao, P. S. C.; Davidson, J. M.; In *Environmental Impact of Nonpoint Source Pollution*; Overcash, M. R.; Davidson, J. M.; Eds.; Ann Arbor Science: Ann Arbor, MI, 1980; p 23.
(24) Banwart, W. L.; Khan, A.; Hassett, J. J. *J. Environ. Sci. Health, Part B* **1980**, *B15*, 165–179.
(25) Khan, A.; Hassett, J. J.; Banwart, W. L.; Means, J. C. Wood, S. G. *Soil Sci.* **1979**, *128*, 297–302.
(26) Pierce, R. H., Jr.; Olney, C. E.; Felbeck, G. T., Jr. *Geochim. Cosmochim. Acta* **1974**; *38*, 1061–1073.
(27) Shin, Y.; Chodan, J. J.; Walcott, A. R. *J. Agric. Food Chem.* **1970**, *18*, 1129–1133.
(28) *Contamination of Groundwater by Toxic Organic Chemicals*; Council on Environmental Quality: Washington, DC 1981.
(29) *Draft Upstate New York Groundwater Management Program*; New York State Department of Environmental Conservation: 1985; WMP-94.
(30) Tessier, A.; Campbell, P. G. C.; Bison, M. *Anal. Chem.* **1979**; *51*, 844–851.
(31) Stevenson, F. J. In *Methods of Soil Analysis: Part 2. Chemical and Microbiological Properties*; American Society of Agronomy: Madison, WI, 1965; pp 1409–1421.
(32) Schnitzer, M. In *Soil Organic Matter Studies*; International Atomic Energy Agency: Vienna, 1977; Vol. 2, pp 117–132.
(33) Schnitzer, M.; Khan, S. U. *Humic Substances in the Environment*; Marcel Dekker: New York, 1972.
(34) Garbarini, D. R.; Lion, L. W. *Environ. Sci. Technol.* **1985**, *19*, 1122–1128.
(35) Carter, C. W.; Suffet, I. H. *Environ. Sci. Technol.* **1982**, *16*, 735–740.
(36) Doherty, P. J.; Warren, G. F. *Weed Res.* **1969**, *9*, 20–26.
(37) Steen, W. C.; Paris, D. F.; Baughman, G. L. *Water Res.* **1978**, *12*, 655–657.
(38) Horzempa, L. M.; Di Toro, D. M. *Water Res.* **1983**, *17*, 851–859.
(39) Diachenko, G. W. Ph.D. Thesis, University of Maryland, 1981.
(40) De Haan, S. In *Soil Organic Matter Studies*; International Atomic Energy Agency: Vienna, 1977; Vol. 1, pp 21–30.
(41) Carter, C. W.; Suffet, I. H. In *Fate of Chemicals in the Environment*; Swan, R. L.; Eschenroeder, A., Eds.; American Chemical Society: Washington, DC, 1983; pp 215–229.
(42) Ballard, T. M. *Soil Sci. Soc. Am. Proc.* **1971**, *35*, 145–147.
(43) Issacson, P. J.; Frink, C. R. *Environ. Sci. Technol.* **1984**, *18*, 43–48.
(44) Turchenek, L. W.; Oades, J. M. *Geoderma* **1979**, *21*, 311–343.
(45) Dunnigan, E. P. McIntosh, T. H. *Weed Sci.* **1971**, *19*, 279–282.

Received for review October 3, 1985. Revised manuscript received July 10, 1986. Accepted August 12, 1986. This research was supported by the U.S. Air Force Office of Scientific Research under Contract F-49620-82-C-0035 and through Subcontract SCEEE 83 RIP/02.

Calibration of Peroxyacetyl Nitrate Measurements with an NO_x Analyzer

L. Fortunat Joos* and Werner F. Landolt

Swiss Federal Institute of Forestry Research, CH-8903 Birmensdorf, Switzerland

Heinz Leuenberger

Swiss Federal Laboratories for Testing Materials and Research, CH-8600 Dübendorf, Switzerland

■ A method for the calibration of peroxyacetyl nitrate (PAN) measurements that uses an NO_x analyzer and can be applied in the field is described. The calibration range lies between 0.5 and 100 ppb, corresponding to the range of concentrations occurring in ambient air. The calibration procedure involves the entire apparatus, including sample intake lines and chromatographic equipment. Possible distortion due to byproducts originating during the synthesis of PAN is precluded by an integrated prepurification step. The method offers a useful alternative to existing procedures. It is verified through an independent procedure (ion chromatography). A system for automatic PAN measurement in the field is also described.

Introduction

Peroxyacetyl nitrate (PAN) occurs in the atmosphere as a trace gas. It is an excellent indicator of anthropogenic photosmog, as it occurs only in very low concentrations in unpolluted air (*1*).

So far, PAN has rarely been included in routine measurements, since its great instability gives rise to a number of difficulties in analysis. The calibration of measuring equipment is particularly problematic.

The purpose of this paper is to present a new calibration method that is also applicable in the field. The calibration mixture is analyzed on the spot with an NO_x analyzer. Problems that might otherwise arise with the transportation of the synthesized PAN to the station are eliminated. The entire measuring apparatus is included in the calibration procedure. Possible errors due to decomposition, absorption, or dilution are kept to the minimum.

The results were verified in the laboratory with a different method (ion chromatography following PAN hydrolysis in KOH solution).

Experimental Section

Measuring Apparatus. Samples of ambient air are separated in a separation column (Teflon; length 60 cm; exterior diameter $^1/_4$) in.; packed with 4.8% QF1 + 0.13% diethylene glycol on 80/100-mesh Chromosorb G AW-DMCS; oven temperature in the field 35 °C and in the laboratory 25 °C). The carrier gas (argone/methane, 95/5)

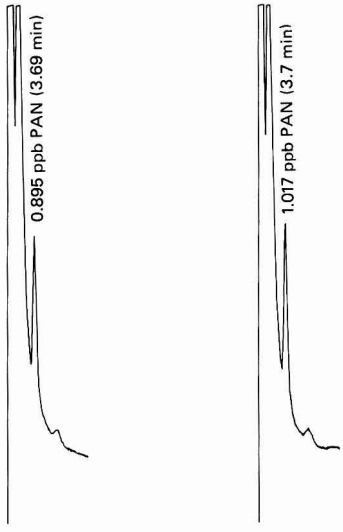

Figure 1. Chromatograms of ambient air obtained in the course of routine measurements (Dübendorf CH, 11/8/1985).

with a flow of 40 mL/min is moistened with $CuSO_4 \cdot 5H_2O$. PAN is detected with an Ni 63 electron capture detector (Hewlett-Packard or Carlo Erba Model 40). The air to be analyzed is sucked continuously at 260 mL/min through a sample loop (stainless steel, 3 or 5 mL). The intake line is of Teflon and is 150 cm long and has an interior diameter of 4 mm. Both sample injection (Valco, hexaport valve) and evaluation of the ECD signals are conducted with commercial integrators (Spectra-Physics Model 4100 or Hewlett-Packard Model 3392 A). Chromatograms from a routine measurement are shown in Figure 1.

Calibration of the measuring system is carried out with an NO_x analyzer (Monitor Labs 8840; range 0–200 ppb or 0–500 ppb) and an ion chromatograph (Dionex 2110 I; column, HPLC AS 4 P/N 35311). The NO_x analyzer is calibrated with a commercial calibrator (Monitor Labs calibrator 8500), using permeation tubes for NO_2 and standard gas mixtures for NO. For preparative work, separation columns packed with ethylene glycol are utilized (glass or Teflon; length 100 cm, interior diameter 3 mm, packed with 5% PEG 1025 on Chromosorb W AW 80/100 mesh or length 50 cm, packed with 5 % PEG 400 on Diatomite CQ 100/120 mesh; carrier gas argon/methane, dry).

The PAN for the calibration is synthesized by photolysis of ethyl nitrite and oxygen (*2*) or in solution (*3*). The PAN peak was identified by various methods, like thermal instability, absorption in basic solutions, and formation of nitrite ion during decay. The chemicals used are normal commercial products (Fluka, Switzerland).

Calibration with NO_x Analyzer. The calibration is based on the detection of PAN with a commercial NO_x analyzer in the NO_x mode. As studies by a number of authors (*1*, *4–7*) as well as the high rate of thermal decomposition of PAN (*8*) indicate, PAN entering the molybdenum converter of the analyzer, which is heated to 310 °C, is entirely converted to NO and thus fully detected as an NO_x compound. Byproducts formed during synthesis and decay products such as methyl and ethyl nitrate and ethyl nitrite (*5*) and, of course, $NO^{\bullet}$ and $NO_2^{\bullet}$ are also detected quantitatively. Figure 2 shows the arrangement of the instruments for calibration.

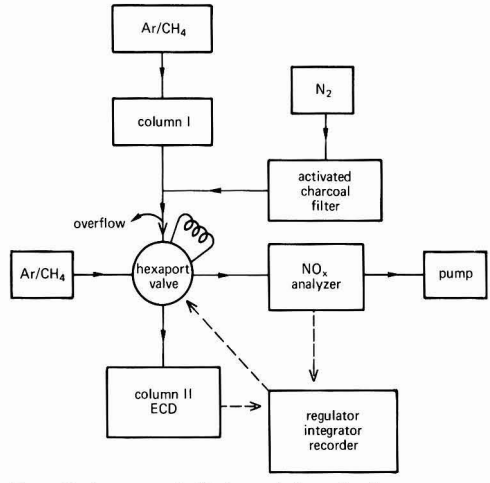

Figure 2. Arrangement of instruments for calibration.

A sample of the synthesized PAN is introduced into separation column I (5% PEG 1025), where PAN is isolated from the byproducts, and thus possible problems of interference of PAN with other compounds are precluded. This process is monitored on the recorder of the NO_x analyzer.

Immediately at the column outlet, the carrier gas flow (20 mL/min, argon/methane, 95/5) is diluted with nitrogen filtered through activated charcoal to roughly 300 mL/min. The major part (260 mL/min) is passed directly through the sample intake line and sample injector valve to the NO_x path of the analyzer. The gas not needed by the analyzer escapes into the atmosphere through an overflow.

The analyzer detects the components containing NO_x, which have been separated in the column (Figure 3). At the moment that the PAN concentration reaches its maximum, the sample loop of the gas regulation valve is switched to the carrier gas flow of the column for measuring ambient air.

The purified PAN–dilution gas mixture is separated and then passes to the ECD, where it is measured. The concentration of the gas passed through the measuring system (GC—ECD) under calibration equals the maximum concentration registered by the analyzer on introduction of the sample. In each case, this is added to the area of the PAN peak detected by the ECD and integrated by the integrator. The points thus obtained are joined to produce a calibration graph. The calibration factor (area counts/ppb of PAN) is given by the reciprocal of the gradient of the regression lines through the points.

In order to ensure that the concentration registered by the analyzer really is the same as that entering the measuring system, certain conditions must be fulfilled.

The NO_x analyzer must respond rapidly to changes in concentration in order to capture the PAN peak. The analyzer we used had an experimentally determined time constant of $T = 3 \pm 1$ s $[\exp(-t/T)]$.

The PAN peak is eluted as a Gauss curve:

$$\text{concn}(t) = A \exp(-0.5t^2/\tau^2)$$

A = maximum concentration. τ = half the peak width at concn = $A \exp(-0.5)$ should be greater than 30 s. This means a retention time of 20 min for PAN in the separation column. In our system the residence time of PAN

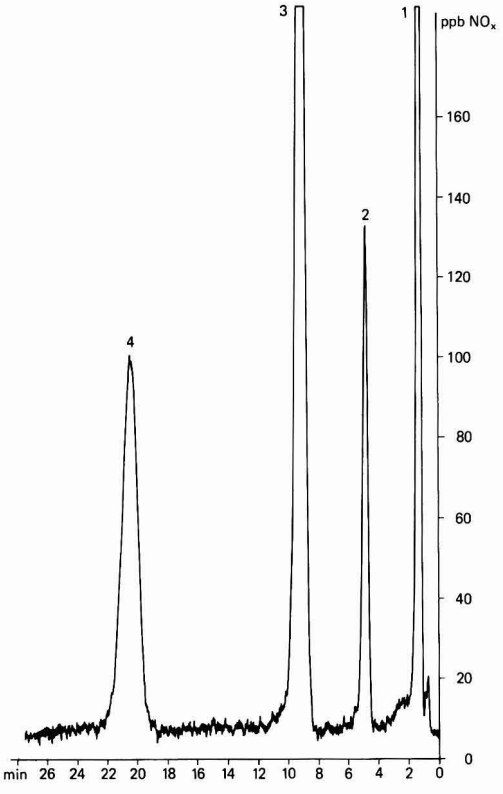

Figure 3. Chromatogram of a sample taken during photolysis of ethyl nitrite and oxygen as detected by the NO_x analyzer (range 0–200 ppb): (1) ethyl nitrite; (2) methyl nitrate; (3) ethyl nitrate; (4) PAN.

between the sample injector valve and the photocell is less than 5 s.

Figure 4 shows the analyzer response for a standard Gauss curve with the above parameters determined from a simple numerical model. The error resulting from the response lag is less than 4%. The sample should reach the GC–ECD at or shortly before registration of the peak maximum, but this presents no problems.

With this method, calibration points for concentrations from about 10 to 20 ppb/vol can be determined without additional precautions. At our measuring stations in rural areas of Switzerland, however, we found very low concentrations of PAN in the ambient air; 90% of the measurements at Birmensdorf made in Summer 1984 were below 1 ppb/vol (*9*). To determine whether the calibration gradients obtained at relatively high PAN concentrations (20–100 ppb/v) are also applicable at low levels, the original loop, with a volume of 3.08 mL, was replaced with a smaller one of 121 μL. That gave a dilution factor of 25.45 and allowed registration of calibration points at levels below 1 ppb/vol.

The two loops were of stainless steel and had a similar flow resistance. During calibration, both were at the same temperature (25 °C). Even so, two completely different calibration factors, differing by factor of 2, were obtained. The calibration curves registered with the large and small sample loops were recorded on the same day in each trial. No drift or scatter in the calibration values was observed. We assume that this effect is due to differing rates of PAN decomposition in the two loops.

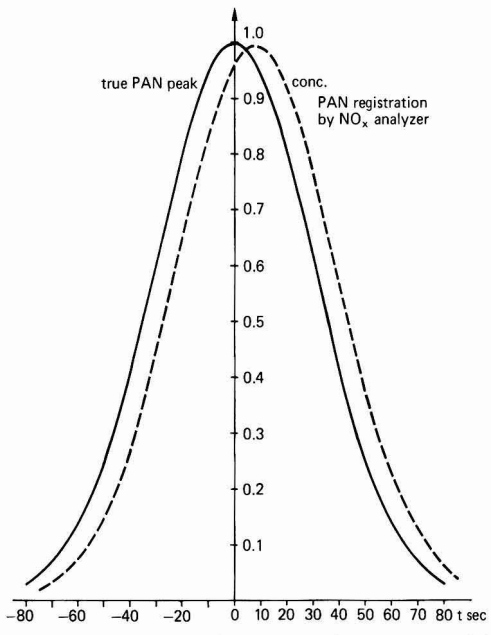

Figure 4. Responses of the NO_x analyzer for a Gauss curve (numerical model). True concentration: $c(t) = \exp(-0.5t^2/\tau^2)$. Response of analyzer: $\exp(-t/T)$. Concentration registered by analyzer: $f(t + TL)$. $\tau = 30$ s; $T = 3$ s; lag time TL = 5 s.

Consequently, for verification of the calibration factors, both loops were connected into the calibration gas flow, one as usual at the hexaport valve and the other directly upstream. This ensured that total PAN decomposition remained constant whichever loop was in use.

The calibration factors obtained with this arrangement were identical (Figure 5) and show that the ECD also responds linearly in the lower measuring range. This means further that the calibration factors derived in the upper ppb range are also valid for low PAN concentrations.

Calibration with Ion Chromatography. The PAN solution was purified by means of preparative gas chromatography (column 5% PEG on Diatomit CQ 100/120 mesh). The purified PAN was then collected in an appropriate Tedlar plastic film bag (*10*) and diluted with pure nitrogen.

The concentration of PAN in the Tedlar bag was determined by hydrolysis of the mixture in 1% KOH solution (*1*, *2*) and subsequent measurement of the nitrite ion with ion chromatography (*3*). Before hydrolysis, the calibration mixture was passed through the same lines and valves as the ambient air, while at the same time samples were introduced into the analytical column through a 0.1-mL sample loop, as for the calibration with the NO_x analyzer in series with the original sample loop (5 mL). In one case the samples were introduced with a 10-μL syringe. The PAN concentration registered was compared with the area of the peak determined with the ECD.

The curves obtained through ion chromatography agree very closely with those derived with the new method (Figure 6).

Discussion

Not surprisingly, the main difficulties in the calibration and measurement of PAN arise from its great instability. If reliable results are to be obtained, all parts of the ap-

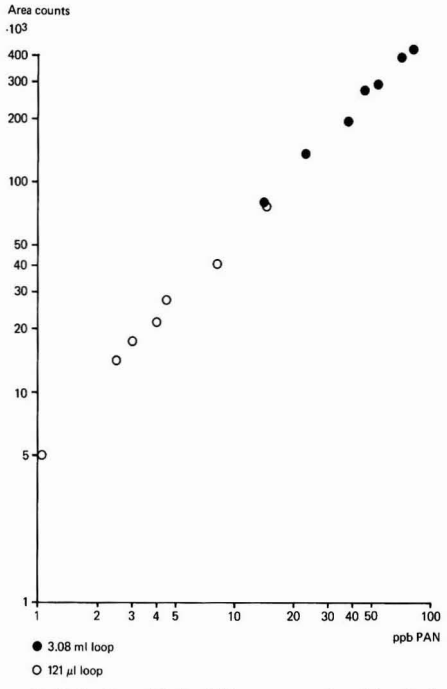

Figure 5. Calibration points for PAN measurement as determined with an NO_x analyzer (integrator: SP 4100). (O) Calibration points obtained with the small sample loop (121 µL). ppb of PAN = −0.1274 + (1.9336 × 10^{-4}) (area counts); r = 0.9966. Calibration factor 5172 area counts/ppb of PAN. (●) Calibration points obtained with the large sample loop (3.08 mL). ppb of PAN = 2.295 + (1.909 × 10^{-4}) (area counts); r = 0.9939. Calibration factor 5238 area counts/ppb of PAN.

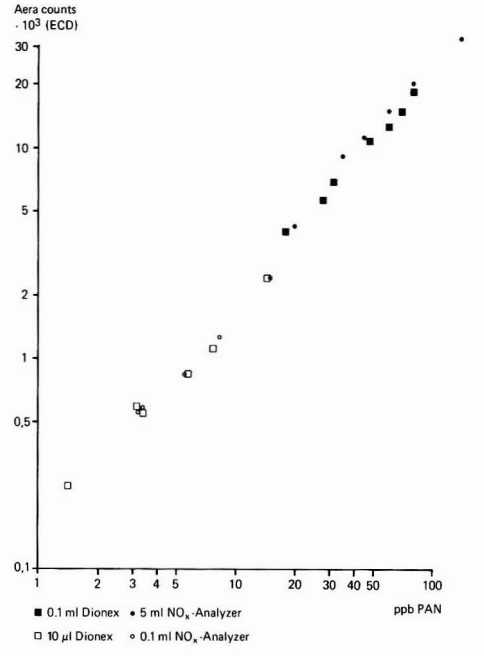

Figure 6. Calibration points for PAN measurement as determined with an NO_x analyzer and through ion chromatography (integrator HP 3392 A). (□) Calibration points from ion chromatography: One area value is the mean of five samples introduced into the GC–ECD with a 10-µL syringe; maximum deviation of the area values 20%. ppb of PAN = 0.0381 + (0.00603)(area counts); r = 0.9987. Calibration factor 165.8 area counts/ppb of PAN. (O) Calibration points from NO_x analyzer with 0.1-mL sample loop: ppb of PAN = 0.352 + (0.00648)(area counts); r = 0.9979. Calibration factor 154.3 area counts/ppb of PAN. Difference between the two calibration factors 7%. (■) Calibration points from ion chromatography: One area value is the mean of five samples introduced into the GC–ECD through the 0.1-mL sample loop; maximum deviation of the area values 5%. ppb of PAN = 0.271 + (0.0045)(area counts); r = 0.9978. Calibration factor 222.2 area counts/ppb of PAN. (●) Calibration points from NO_x analyzer with 5-mL sample loop: ppb of PAN = 0.421 + (0.00395)(area counts); r = 0.9988. Calibration factor 253.2 area counts/ppb of PAN Difference between the two calibration factors 12%.

paratus coming into contact with PAN should be included in the calibration procedure. In the method described here, utilizing an NO_x analyzer, PAN is measured as rapidly and in as pure a state (directly after elution from column I) as possible, and the entire apparatus is calibrated at once. The introduction of PAN into other containers is unnecessary (*2*, *3*, 10–12). The step between purification and measurement is carried out dynamically and rapidly. Possible distortion of the calibration by decomposition in syringes (*10*, *12*) or containers is thus precluded.

Another advantage is the absence of a dilution phase during routine measurements. Furthermore, the use of appropriate sample loops permits calibration points within the actual measuring range to be obtained with little additional effort.

This calibration method with an NO_x analyzer can be employed in the field. It has proved very successful in the calibration of our measuring system in a forest station.

The isolation of PAN in a first separation column precludes possible interference problems due to other components containing nitrogen oxides (*4*, *5*, *8*, *11*, *13*). Consequently, the PAN needed for the calibration may be produced in whichever way is most convenient.

The time consumption for this method of calibration of measuring instruments is roughly half a day, considerably less than that for other methods.

Apart from an NO_x analyzer such as is in general use, no additional equipment is needed. The NO_x analyzer can be subsequently used for analysis.

The NO_x and PAN data obtained from air analysis show a very high relative accuracy; this is particularly valuable for studies on levels of nitrogen oxides.

The method of calibration using an NO_x analyzer is simple in application and gives easily reproducible results.

Acknowledgments

We are grateful to H. Mächler, C. Fäsi, and R. Baumann for their valuable technical assistance and their support.

Registry No. PAN, 2278-22-0.

Literature Cited

(1) Singh, H. B.; Salas, L. J. *Atmos. Environ.* **1983**, *17*, 1507.
(2) Sandalls, F. J.; Penkett, S. A.; Jones, B. M. R. AERE Report R 7807; HMSO, London, 1974.
(3) Nielson, T.; Hansen, A. M.; Thomsen, E. A. *Atmos. Environ.* **1982**, *16*, 2447.
(4) Cox, R. A.; Derwent, R. G.; Holt, P. M.; Kerr, J. A. *J. Chem. Soc., Faraday Trans. 1* **1976**, *9*, 2061.
(5) Winer, A. M.; Peters, J. W.; Smith, J. P.; Pitts, J. N. *Environ. Sci. Technol.* **1974**, *8*, 1118.
(6) Grosjean, D. *Environ. Sci. Technol.* **1983**, *17*, 13.
(7) Grosjean, D.; Harrison, J. *Environ. Sci. Technol.* **1985**, *19*, 862.

(8) Cox, R. A.; Roffey, M. J. *Environ. Sci. Technol.* **1977**, *11*, 900.
(9) Landolt, W.; Joos, F. *Schweiz. Z. Forstwes.* **1985**, *136*(5), 421.
(10) Holdren, M. W.; Spicer, C. W. *Environ. Sci. Technol.* **1984**, *18*, 113.
(11) Stephens, E. R. In *Advances in Environmental Science and Technology*; Pitts, J. N.; Metcalf, R. I., Eds.; Wiley-Interscience: New York, 1969; Vol. 1, pp 119–46.
(12) Kravetz, T. M.; Steven, W. M.; Mendenhall, G. D. *Environ. Sci. Technol.* **1980**, *14*, 1262.
(13) Grosjean, D.; Fung, K.; Collins, J.; Harrison, J.; Breitung, E. *Anal. Chem.* **1984**, *56*, 569.

Received for review December 26, 1985. Revised manuscript received June 29, 1986. Accepted August 5, 1986. This study was partially supported by the Swiss National Science Foundation (NFP).

A Passive Sampler for Formaldehyde in Air Using 2,4-Dinitrophenylhydrazine-Coated Glass Fiber Filters

Jan-Olof Levin,* Roger Lindahl, and Kurt Andersson

National Board of Occupational Safety and Health, Research Department in Umeå, S-900 06 Umeå, Sweden

■ A method utilizing diffusive sampling of formaldehyde in air has been developed. A glass fiber filter, impregnated with 2,4-dinitrophenylhydrazine (DNPH) and phosphoric acid and mounted into a modified aerosol-sampling cassette, is used for sampling by controlled diffusion. The formaldehyde hydrazone formed is desorbed and determined by high-performance liquid chromatography with UV detection. The sampling rate of the sampler was determined to 61 mL/min, with a standard deviation of 5%. The sampling rate is independent of formaldehyde concentrations between 0.1 and 5 mg/m^3 and sampling times between 15 min and 8 h. The sensitivity of the diffusive method is approximately 0.005 mg/m^3 (5 ppb) in an 8-h sample, and the reproducibility is better than 3%.

Introduction

Formaldehyde is an important industrial chemical, a well-known irritant, and a suspected carcinogen (*1*). Occupational exposure occurs in the range 0.1–5 mg/m^3 formaldehyde in air (*2*), and levels of 0.01–0.1 mg/m^3 are often found in offices and homes (*3*). Consequently, sensitive and reliable methods for determining formaldehyde in air are required.

A number of analytical methods for the determination of airborne formaldehyde have been published, including spectrophotometric (*4–6*) and chromatographic methods. One of the most rapid and sensitive methods is high-performance liquid chromatography on the 2,4-dinitrophenylhydrazone of formaldehyde, a method used by several investigators (*7–9*). For sampling of ambient air, absorber solutions have been most frequently used; these are not suited for field work, however, especially not in personal monitoring. We have previously reported the use of XAD-2 coated with 2,4-dinitrophenylhydrazine (DNPH) for the sampling of several aldehydes, including formaldehyde, acrolein, and glutaraldehyde (*8, 10, 11*). Other workers have subsequently used other DNPH-coated solid sorbents (*9, 12–15*). We recently reported an improved method, utilizing DNPH-coated glass fiber filters. In this sampling system, air can be sampled at a rate of up to 1 L/min, affording a sensitivity of about 0.001 mg/m^3 (1 ppb), on the basis of 50-L air sample (*16*). Coated filters of the same type were tested for diffusive sampling (*16*). We now report an extensive evaluation of this passive sampler. We have determined the sampling rate and the effect of formaldehyde concentration, sampling time, air velocity, and air humidity on the sampling rate. The sampler has also been evaluated in the field.

Experimental Section

Chemicals. Solvents used were methanol (Merck, p.a.) and acetonitrile (Rathburn, HPLC grade S). Formaldehyde 2,4-dinitrophenylhydrazone was prepared from formaldehyde (Merck, 37%, p.a.), 2,4-dinitrophenylhydrazine (DNPH) (Fluka, p.a.), and concentrated HCl and recrystallized twice from ethanol, mp 166 °C.

Coated Filters for Active Sampling. The coated filters were prepared according to a previously described procedure (*16*). This procedure was modified to include glycerin in the coating solution. The filters were coated in the following manner: To 300 mg of DNPH·HCl, recrystallized twice from 4 M HCl and dried for only a few minutes, was added 0.5 mL of 85% phosphoric acid (Merck, p.a.), 1.5 mL of 20% glycerin (May & Baker, p.a.) in ethanol, and 9.0 mL of acetonitrile. The 13 mm diameter glass fiber filters, organic- and binder-free (type AE, 0.3-μm pore size, SKC, Inc.), were immersed in the solution for a few seconds. The filters were then allowed to dry for 2 h at room temperature, after which they were stored in a desiccator over saturated sodium chloride solution to assure constant relative humidity. It is possible to store the filters in this way for several months. Filters coated in this manner contain approximately 2 mg of DNPH. The filters were used in two-section polypropylene filter holders (No. 225-32, SKC, Inc.), and the collection efficiency of the filters was determined as previously described (*16*).

Coated Filters for Diffusive Sampling. To 300 mg of DNPH·HCl was added 6 mL of 8.5% phosphoric acid and 25 mL of acetonitrile. A 0.5-mL portion of the solution (5 mg of DNPH) was added with a 0.5-mL Voll pipet to each 37 mm diameter glass fiber filter, organic- and binder-free (type AE, 0.3-μm pore size, SKC, Inc.). The filters were dried for 30 min at room temperature and conditioned in the same way as the filters for active sampling.

Dosimeter for Diffusive Sampling. The coated filters for diffusive sampling were used in a modified 37-mm filter holder, shown in Figure 1. One section of the standard two-section cassette (No. M0037AO, Millipore Corp., MA) was cut into two parts, and one part was used as the front section of the sampler to create a controlled diffusion barrier consisting of an uncoated glass fiber filter between two stainless steel grids (No. 7908/B30, Casella London Ltd., G.B.), according to Figure 1. The other part of the section was pasted on a piece of polyacrylic ester plastic

0013-936X/86/0920-1273$01.50/0

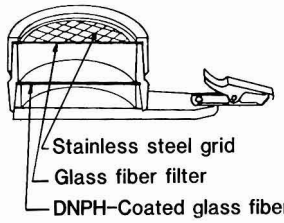

Figure 1. Filter cassette for 37-mm filters modified for diffusive sampling.

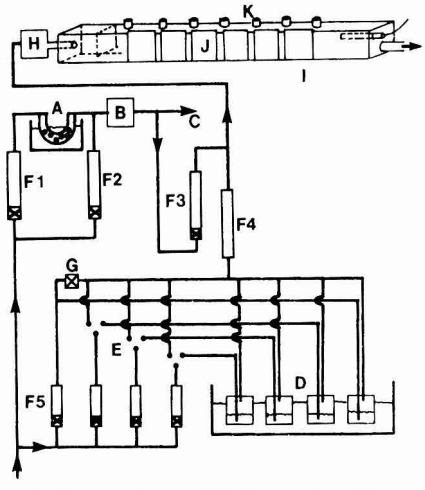

Figure 2. Apparatus for formaldehyde generation: (A) paraformaldehyde; (B) mixing chamber; (C) IR detector; (D) gas dispersion bottles with water; (E) valves; (F) flow regulators; (G) needle valve; (H) mixing chamber; (I) testing chamber; (J) door; (K) port.

equipped with a clip. The front cross-sectional area of the sampler was 7.1 cm^2, and the length of the controlled diffusion path was 10 mm.

Generation of Standard Atmospheres of Formaldehyde. Formaldehyde was generated in a dynamic system by decomposition of paraformaldehyde at 25–30 °C. The generation system is described in Figure 2. Pressurized clean air, regulated by flow regulator F1 (20–160 mL/min), was passed through a U-tube containing paraformaldehyde (A) and thermostated at 25–30 °C, depending on the formaldehyde concentration required. The formaldehyde generated was further diluted by clean air regulated by F2 (2–25 L/min). After the mixing chamber B, part of the formaldehyde containing air was split off (C) to a Miran 1A portable air analyzer (Foxboro Co.) for determination of the formaldehyde concentration prior to the second dilution step. The dilution in the second step was controlled by flow regulators F3 (0.4–4 L/min) and F4 (15–160 L/min). The use of humidified air for dilution enabled different relative humidities to be attained. Air with a certain relative humidity was generated by passing clean air through one to four gas-dispersion bottles (D) containing water, according to Figure 2. By varying the flow through the regulators F5 (4–40 L/min) and by selecting the number of bottles by means of the three valves E, the relative humidity of the air passing through F4 could be varied between 2 and 95%. Minor adjustments were made with needle valve G. The humidified air and the formaldehyde gas were mixed in a mixing chamber (H), and the gas stream was led into the testing chamber (I). The chamber (70 × 48 × 900 mm) was made of PTFE and equipped with six removable doors (J) and seven ports for active sampling (K). The relative humidity in the chamber was monitored with a Humicap relative humidity meter (Vaisala OY, Helsinki, Finland). Air velocity was measured with a thermoanemometer (type 641N, Wilh. Lambrecht KG, Göttingen, West Germany) 2 mm above the diffusion barrier (face velocity).

Table I. Recovery of Formaldehyde 2,4-Dinitrophenylhydrazone from 2,4-Dinitrophenylhydrazine-Coated Filters Containing 3% Glycerin, after Drying the Filters in an Air Flow of 0.2 L/min and 2% Relative Humidity before Exposure to Formaldehyde Vapor

drying time, min	recovery, %	RSD, %[a]	N[b]
30	95	3	4
120	96	4	4
300	90	2	6

[a] RSD = relative standard deviation. [b] N = number of experiments.

Personal Sampling. Personal sample pumps (Model 223-3, SKC, Inc.) with a flow of 200 mL/min were used for active sampling in a dissection room of a hospital. Parallel samples were taken with the diffusive samplers.

Liquid Chromatography. The formaldehyde 2,4-dinitrophenylhydrazone was eluted from both 13- and 37-mm filters by shaking for 1 min with 3 mL of acetonitrile in a 4-mL glass vial. The solution was filtered through a Millex-SR filter, and 10 μL was injected into the liquid chromatograph. Details of the liquid chromatographic determination were described previously (*16*). The hydrazone was detected at 365 nm with a detection limit of approximately 0.5 ng (signal to noise ratio 4:1), corresponding to 0.07 ng of formaldehyde.

Results and Discussion

Active Sampling. As previously reported, the recovery of gas-phase-generated formaldehyde as 2,4-dinitrophenylhydrazone from 13-mm DNPH-impregnated filters ranges between 81 and 103% (*16*). The lowest recovery was observed when formaldehyde was generated at 20% relative humidity (*16*). The reaction between formaldehyde and DNPH on coated filters is incomplete in extremely dry atmospheres, i.e., below 10% relative humidity. This problem was solved by adding glycerin to the coating solution, resulting in better retention of water. Table I shows the recovery of formaldehyde hydrazone from coated filters exposed to a flow of dry air at 200 mL/min for various periods before exposure to formaldehyde vapor. As the table shows, recovery is still 90% after 5 h of a flow of 200 mL/min at 2% relative humidity.

The active sampling method was used as reference method in all experiments with the diffusive sampler. The DNPH-coated 13-mm glass fiber filters used in the active mode permitted determination of formaldehyde down to approximately 1 $\mu g/m^3$ in a 50-L air sample. The formaldehyde blank of 0.05 μg/filter corresponds to 1 $\mu g/m^3$ in a 50-L air sample.

Passive Sampling. Passive sampling has several advantages. No pumps are needed, which facilitates handling in the field. Sampling can be performed by junior personnel, and it is often possible to obtain integrated concentration values over long periods. Most methods for passive sampling employ the principle of controlled diffusion (*17*). Controlled diffusion is achieved by placing the adsorbent in one end of a tube (Palmes' tube) (*18*) or by using a diffusion barrier. Since the adsorption process

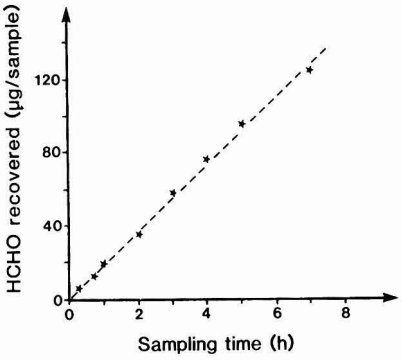

Figure 3. Effect of sampling time on sampling rate of diffusive sampler: formaldehyde concentration 5 mg/m^3, relative humidity 50%, and face velocity 0.3 m/s. The dotted line represents a sampling rate of 61 mL/min. Each point represents at least three determinations.

Table II. Effect of Formaldehyde Concentration on Sampling Rate of Diffusive Sampler[a]

HCHO concn, mg/m^3	sampling time, min	sampling rate, mL/min	RSD, %	N[c]
0.1	240	60	5	6
0.2	15	59	4	6
1.0	15	60	4	3
5.0	15	60	3	6
5.0	240	62	2	3

[a] Relative humidity 20% and face velocity 0.3 m/s. [b] RSD = relative standard deviation. [c] N = number of experiments.

is reversible, substantial back-diffusion of volatile substances may occur if the concentration on the adsorbent becomes too large. To minimize such back-diffusion, most passive samplers have sampling rates below 10 mL/min. In the case of a reagent-coated adsorbent yielding a nonvolatile derivative, there is no back-diffusion, and hence, the size of the sampler is the sole limiting factor for the sampling rate.

The diffusive sampler developed by us was made from a commercially available standard 37-mm filter holder, modified according to Figure 1. The sampler was studied with the test chamber shown in Figure 2.

Sampling Rate of Diffusive Sampler. If the diffusion coefficient for formaldehyde is set to 0.16 cm^2/s, the sampling rate of the passive sampler is calculated to 68 mL/min, according to Fick's law of controlled diffusion (*19*).

The sampling rate was experimentally determined by exposing six samplers at a time in the test chamber while six active samples were taken simultaneously with a sampling rate of 100 mL/min. A number of experiments were performed with different sampling times, different formaldehyde concentrations, and different values of relative humidity and face velocity. A total of 79 experiments with the passive sampler gave a mean sampling rate of 60.9 mL/min, with a standard deviation of 3.7 mL/min.

Effect of Sampling Time on Sampling Rate. Figure 3 shows the effect of sampling time on the sampling rate. It can be seen from the graph that the sampling rate is constant when sampling times between 15 and 420 min at a level of 5 mg/m^3 formaldehyde and a relative humidity of 50% are used. The dotted line represents a sampling rate of 61 mL/min.

Effect of Formaldehyde Concentration on Sampling Rate. The diffusive sampler was exposed to formaldehyde levels from 0.1 to 5.0 mg/m^3. Table II shows the

Table III. Effect of Relative Humidity on Sampling Rate of Diffusive Sampler[a]

RH, %[b]	sampling time, min	sampling rate, mL/min	RSD, %[c]	N[d]
8	15	61	11	6
20	15	60	3	6
20	240	62	2	3
50	15	62	8	3
50	240	63	3	3
85	15	60	6	12
85	240	62	4	6

[a] Formaldehyde concentration 5 mg/m^3 and face velocity 0.3 m/s. [b] RH = relative humidity. [c] RSD = relative standard deviation. [d] N = number of experiments.

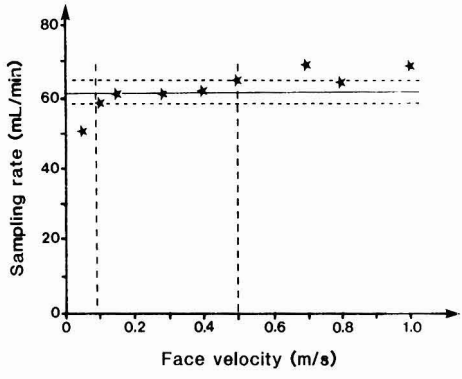

Figure 4. Effect of face velocity on sampling rate of diffusive sampler: formaldehyde concentration 1 mg/m^3, relative humidity 50%, and sampling time 20 min. The area within the dotted lines represents a sampling rate of 61 mL/min with a standard deviation of 5%. Each point represents at least three determinations.

sampling rate of the sampler at different formaldehyde concentrations with sampling times of 15 and 240 min and with a relative humidity of 20%. As the table shows, the sampling rate is not influenced by the formaldehyde concentration within the range studied. Since the sampling rate is contant, there are no saturation or adsorption effects of the diffusion barrier or sampler walls.

Effect of Relative Humidity on Sampling Rate. The sampler was evaluated at relative humidities of 8, 20, 50, and 85%. Sampling times of 15 and 240 min were used. The results are shown in Table III. It can be seen that the sampling rate is not affected by the relative humidity of the sampled air.

Effect of DNPH Load on Sampling Rate. The DNPH load of the filters used for diffusive sampling is approximately 5 mg. The loading is not critical for the sampling rate since varying the DNPH load between 5 and 8.5 mg had no effect on the sampling rate.

Effect of Face Velocity on Sampling Rate. The effect of air velocity on the sampling rate was studied by varying the face velocity between 0.05 and 1.0 m/s. The results of these studies are shown in Figure 4. As shown in the figure, the sampling rate decreases at 0.05 m/s and increases at 0.7 m/s. However between 0.1 and 0.5 m/s the sampling rate is 61 mL/min with a standard deviation of 5%. Most diffusive samplers require an air velocity of approximately 0.1 m/s (*18*), which is maintained under most personal sampling conditions.

Reproducibility and Sensitivity of Diffusive Sampler. The reproducibility of the diffusive sampling method was found to be better than 3%. Since the diffusive

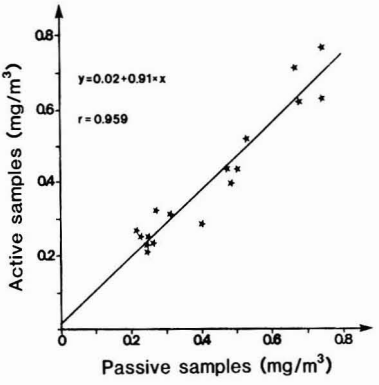

Figure 5. Correlation between passive and active personal samples from the field investigation in a hospital dissection room.

sampler has a sampling rate as high as 61 mL/min, the sampler can be used for short-time sampling. With a formaldehyde blank of 0.15 μg/filter, the sensitivity of a 15-min sample is approximately 0.2 mg/m³. In an 8-h sample the sensitivity will become 0.005 mg/m³ (5 ppb).

Formaldehyde Blank and Storage Stability of Diffusive Sampler. It is important to use formaldehyde-free acetonitrile in the preparation of filters. If the filters are prepared according to the procedure described, the formaldehyde blank should be less than 0.05 μg/filter for active sampling, and 0.15 μg/filter for passive sampling, and with a reproducibility of approximately 20%. Since formaldehyde is a ubiquitous contaminant in man-made environments, care must be taken to protect coated filters and loaded samplers from formaldehyde contamination. The unexposed samplers were stored individually in sealed bags made of laminated aluminum. The formaldehyde blank of the samplers did not increase after 2 months of storage in these bags. The sampling rate of the diffusive sampler was not affected by 2 months storing of the unexposed sampler. Once formed, the hydrazone is stable on the filter since no decrease in recovery of formaldehyde hydrazone could be noted after storage of the exposed samplers for 1 month. In all storing experiments the samplers were kept in the aluminum bags at room temperature.

Field Evaluation of Diffusive Sampler. The sampler was evaluated in a field investigation—a dissection room of a hospital—where medical students were dissecting human organs that had been embalmed with formalin. The formaldehyde level was 0.1–0.5 mg/m³, and the sampling time was 15–150 min. Personal sampling with diffusive samplers was used in parallel with active sampling at 0.2 L/min. Good agreement was found between the results obtained from passive and active sampling. Figure 5 shows the correlation between the active and passive samples. The coefficient of correlation is 0.959, and the slope of the line is 0.91.

Summary

A diffusive sampler using 2,4-dinitrophenylhydrazine-coated glass fiber filters has been evaluated. It was found to have a sampling rate of 61 mL/min with a relative standard deviation of 4 mL/min. In the range 0.1–5 ppm, the sampling rate was not influenced by formaldehyde concentration. Relative humidity between 8 and 85% did not affect the sampling rate, and sampling times between 15 min and 8 h could be used without any change in sampling rate. The sampling rate was found to be constant in the air velocity range 0.1–0.5 m/s. Reproducibility of the method was better than 3%. A sensitivity of 5 ppb was achieved in an 8-h sample and of 0.2 ppm in a 15-min sample. The sampler has proven very useful for monitoring formaldehyde exposure in working environments as well as homes.

Registry No. DNPH, 119-26-6; HCHO, 50-00-0; phosphoric acid, 7664-38-2.

Literature Cited

(1) Hart, R. W.; Terturro, A.; Neimeth, L., Eds. *Environ. Health Perspect.* **1984**, *58*, 334.
(2) Hart, R. W.; Terturro, A.; Neimeth, L., Eds. *Environ. Health Perspect.* **1984**, *58*, 325.
(3) Stock, T. H.; Mendez, S. R. *Am. Ind. Hyg. Assoc. J.* **1985**, *46*, 313.
(4) *NIOSH Manual of Analytical Methods*, 2nd ed.; National Institute for Occupational Safety and Health: Cincinnati, OH, 1978; Vol. 1, P&CAM 125.
(5) Levaggi, D. A.; Feldstein, M. *J. Air Pollut. Control Assoc.* **1970**, *20*, 312.
(6) Miksch, R. R.; Anthon, D. W.; Fanning, L. Z.; Hollowell, G. D.; Revzan, K.; Glanville, J. *Anal. Chem.* **1981**, *53*, 2118.
(7) Kuwata, K.; Uebori, M.; Yamasaki, H. *J. Chromatogr. Sci.* **1979**, *17*, 264.
(8) Andersson, K.; Andersson, G.; Nilsson, C.-A.; Levin, J.-O. *Chemosphere* **1979**, *8*, 823.
(9) Fung, K.; Grosjean, D. *Anal. Chem.* **1981**, *53*, 168.
(10) Andersson, K.; Hallgren, C.; Levin, J.-O.; Nilsson, C.-A. *Scand. J. Work, Environ. Health* **1981**, *7*, 282.
(11) Andersson, K.; Hallgren, C.; Levin, J.-O.; Nilsson, C.-A. *Chemosphere* **1981**, *10*, 275.
(12) Beasley, R. K.; Hoffman, C. E.; Rueppel, M. L.; Worley, J. W. *Anal. Chem.* **1980**, *52*, 1110.
(13) Grosjean, D.; Fung, K. *Anal. Chem.* **1982**, *54*, 1221.
(14) Kuwata, K.; Uebori, M.; Yamasaki, H.; Kuge, Y. *Anal. Chem.* **1983**, *55*, 2013.
(15) Lipari, F.; Swarin, S. J. *Environ. Sci. Technol.* **1985**, *19*, 70.
(16) Levin, J.-O.; Andersson, K.; Lindahl, R.; Nilsson, C.-A. *Anal. Chem.* **1985**, *57*, 1032.
(17) Rose, V. E.; Perkins, J. L. *Am. Ind. Hyg. Assoc. J.* **1982**, *43*, 605.
(18) Palmes, E. D.; Gunnison, A. F. *Am. Ind. Hyg. Assoc. J.* **1973**, *37*, 78.
(19) Kring, E. V.; Thornley, G. D., Dessenberger, C.; Lautenberger, W. J.; Ansul, G. R. *Am. Ind. Hyg. Assoc. J.* **1982**, *43*, 786.

Received for review February 10, 1986. Revised manuscript received May 29, 1986. Accepted August 5, 1986.

AUTHOR INDEX TO VOLUME 20, 1986

Aaltonen, S. H. See Kauppinen, E. I.
Abdelnasser, M.
——; Hyland, M.; Jespersen, N. D.
Synthesis of mutagenic compounds in crankcase oils. 145
Abraham, M. H. See Kamlet, M. J.
Abrahamsson, K. See Xie, T. M.
Adams, F. C. See Van Cleuvenbergen, R. J. A.
Adams, R. E.
——; James, R. H.; Farr, L. B.; Thomason, M. M.; Miller, H. C.; Johnson, L. D.
Analytical methods for determination of selected principal organic hazardous constituents in combustion products. 711
Addison, R. F.
——; Zinck, M. E.; Smith, T. G.
PCBs have declined more than the DDT group residues in Arctic ringed seals (Phoca hispida) between 1972 and 1981. 253
Adewuyi, Y. G.
——; Carmichael, G. R.
Kinetics of oxidation of dimethyl sulfide by hydrogen peroxide in acidic and alkaline medium. 1017
Aggett, J.
——; Roberts, L. S.
Insight into the mechanism of accumulation of arsenate and phosphate in hydro lake sediments by measuring the rate of dissolution with ethylenediaminetetraacetic acid. 183
Ahlborg, U. G. See Victorin, K.
Aieta, E. M.
——; Roberts, P. V.
Application of mass-transfer theory to the kinetics of a fast gas-liquid reaction: chlorine hydrolysis. 44
Kinetics of the reaction between molecular chlorine and chlorite in aqueous solution 50
Ainsworth, C. C. See Zachara, J. M.
Akimoto, H. See Takagi, H.
——; Takagi, H.
Formation of methyl nitrite in the surface reaction of nitrogen dioxide and methanol. 2. Photoenhancement. 393
Alegret, S. See Ephraim, J.
Alexander, L. R.
——; Patterson, D. G.; Myers, G. L.; Holler, J. S.
Safe handling of chemical toxicants and control of interferences in human tissue analysis for dioxins and furans. 725
Alexander, M. D. See Darnall, D. W.; Greene, B.
Alford-Stevens, A. L.
Analyzing PCBs. 1194
Almich, B. P.
——; Budde, W. L.; Shobe, W. R.
Waste monitoring. 16
Amdur, M. O.
——; Sarofim, A. F.; Neville, M.; Quann, R. J.; McCarthy, J. F.; Elliott, J. F.; Lam, H. F.; Rogers, A. E.; Conner, M. W.
Coal combustion aerosols and sulfur dioxide: an interdisciplinary analysis. 138
Amy, G. L. See Collins, M. R.
Anderson, L. J.
——; Johnson, J. D.; Christman, R. F.
Extent of ozone's reaction with isolated aquatic fulvic acid. 739
Andersson, K. See Levin, J. O.
Andren, A. W. See Burkhard, L. P.; Dickhut, R. M.
Aoki, T.
——; Uemura, S.; Munemori, M.
Continuous flow method for simultaneous determination of nitrate and ammonia in water. 515
Arbuckle, W. B.
Comment on "Henry's law constants for the polychlorinated biphenyls". 527
Using UNIFAC to calculate aqueous solubilities. 1060
Arey, J. See Tuazon, E. C.
Armstrong, D. E. See Burkhard, L. P.; Dickhut, R. M.; Swackhamer, D. L.
Aschmann, S. M. See Tuazon, E. C.
Atkinson, R. See Tuazon, E. C.

Baggerman, T. See De Leer, Ed. W. B.
Baker, J. E.
——; Capel, P. D.; Eisenreich, S. J.
Influence of colloids on sediment-water partition coefficients of polychlorobiphenyl congeners in natural waters. 1136
Baldwin, R. A. See Kauffman, J. W.
Barcelona, M. J.
——; Helfrich, J. A.
Well construction and purging effects on ground-water samples. 1179
Barrio-Lage, G.
——; Parsons, F. Z.; Nassar, R. S.; Lorenzo, P. A.
Sequential dehalogenation of chlorinated ethenes. 96
Batchelor, B.
——; McEwen, J. B.; Perry, R.
Kinetics of aluminum hydrolysis: measurement and characterization of reaction products. 891
Baumgardner, R. E. See Lewis, C. W.
Bellama, J. M. See Matthias, C. L.
Bernard, P. C.
——; Van Grieken, R. E.; Eisma, D.
Classification of estuarine particles using automated electron microprobe analysis and multivariate techniques. 467
Berridge, B. See Marple, L.
Berry, D. K.
Air toxics. 647
Bicking, M. See Ephraim, J.
Bidleman, T. F.
——; Billings, W. N.; Foreman, W. T.
Vapor-particle partitioning of semivolatile organic compounds: estimates from field collections. 1038
Billings, W. N. See Bidleman, T. F.
Bloyd, C. N. See Rubin, E. S.
Bormann, F. H. See Wang, D.
Boyd, S. A.
——; Mortland, M. M.
Radical formation and polymerization of chlorophenols and chloroanisole on copper(II)-smectite. 1056
Bozzelli, J. W. See Chuang, S. C.
Brinckman, F. E. See Matthias, C. L.
Brinton, T. I. See Chiou, C. T.
Brncich, D. M. See Haas, C. N.
Brooks, M. G. See Friedman, L. C.
Brown, D. W. See Krone, C. A.
Brown, N. J. See Lionel, T.
Brunck, R. See Marple, L.
Budde, W. L. See Almich, B. P.
Burkhard, L. P.
——; Andren, A. W.; Loux, N. T.; Armstrong, D. E.
Henry's law constants for the polychlorinated biphenyls. Reply to comments. 527
Burris, D. R.
——; MacIntyre, W. G.
Solution of hydrocarbons in a hydrocarbon-water system with changing phase composition due to evaporation. 296
Burrows, D. G. See Krone, C. A.
Buser, H. R. See Mueller, M. D.
Polybrominated dibenzofurans and dibenzo-p-dioxins: thermal reaction products of polybrominated diphenyl ether flame retardants. 404
——; Mueller, M. D.
Methylthio metabolites of polychlorobiphenyls identified in sediment samples from two lakes in Switzerland. 730

Campbell, P. G. C. See Rapin, F.
Canuel, E. A. See Wakeham, S. G.
Capel, P. D. See Baker, J. E.
Carignan, R. See Rapin, F.
Carmichael, G. R. See Adewuyi, Y. G.
Carter, W. P. L. See Tuazon, E. C.
Cass, G. R. See Gray, H. A.; Nazaroff, W. W.; Russell, A. G.
Chakraborti, D. See Van Cleuvenbergen, R. J. A.
Chang, H. C. See Nishioka, M.
Chang, W. D.
——; Karra, S. B.; Senkan, S. M.
Molecular beam mass spectroscopic study of trichloroethylene flames. 1243
Chen, J. J. See Thompson, H. C. Jr.
Cheney, J. L. See Eatough, D. J.
Chiou, C. T.
——; Malcolm, R. L.; Brinton, T. I.; Kile, D. E.
Water solubility enhancement of some organic pollutants and pesticides by dissolved humic and fulvic acids. 502
Chiou, K. Y.
——; Manuel, O. K.
Tellurium and selenium in aerosols. 987
Christman, R. F. See Anderson, L. J.
Chuang, S. C.
——; Bozzelli, J. W.
Conversion of chloroform to hydrochloric acid by reaction with hydrogen and water vapor. 568
Claxton, L. D. See Kleindienst, T. E.; Shepson, P. B.
Cliath, M. M. See Elabd, H.
Clifford, D. See Sengupta, A. K.
——; Subramonian, S.; Sorg, T. J.
Water treatment processes. III. Removing dissolved inorganic contaminants from water. 1072
Cline, D. M. See Shackelford, W. M.
Cohen, M. L.
——; Steinmetz, W. D.
Foliar washoff of pesticides by rainfall. 521
Cohen, Y.
Organic pollutant transport. 538
Coleman, W. M. III. See Laughlin, R. B. Jr.
Collins, M. R.
——; Amy, G. L.; Steelink, C.
Molecular weight distribution, carboxylic acidity, and humic substances content of aquatic organic matter: implications for removal during water treatment. 1028
Coniglio, W. A. See Cothern, C. R.
Conner, M. W. See Amdur, M. O.
Cooper, D. W. See Rudnick, S. N.
Cornwell, J. C.
Diagenetic trace-metal profiles in Arctic lake sediments. 299
Cothern, C. R.
——; Coniglio, W. A.; Marcus, W. L.
Estimating risk to human health. Trichloroethylene in drinking water is used as the example. 111
Craft, D.
A BASIC program to plot Stiff diagrams. 204
Crist, H. L.
——; Mitchell, W. J.
Field audit results with organic gas standards on volatile organic ambient air samplers equipped with Tenax GC. 1260
Cronan, C. S. See Plankey, B. J.
Cupitt, L. T. See Kleindienst, T. E.; Shepson, P. B.
Cushey, M. A. See Rubin, E. S.
Czuczwa, J. M.
——; Hites, R. A.
Airborne dioxins and dibenzofurans: sources and fates. 195

Daisey, J. M. See Lioy, P. J.
Darnall, D. W. See Greene, B.
——; Greene, B.; Henzl, M. T.; Hosea, J. M.; McPherson, R. A.; Sneddon, J.; Alexander, M. D.

Selective recovery of gold and other metal ions from an algal biomass. 206
Dasgupta, P. K. See Dong, S.
——; Gupta, V. K.
Membrane-based flow injection system for determination of sulfur(IV) in atmospheric water. 524
Davani, B. See Eiceman, G. A.
Davidson, C. I.
——; Lin, S. F.; Osborn, J. F.; Pandey, M. R.; Katmandu, N.; Rasmussen, R. A.; Khalil, M. A. K.
Indoor and outdoor air pollution in the Himalayas. 561
De Galan, L. See De Leer, Ed. W. B.
DeKalb, E. L. See Norton, G. A.
De Leer, Ed. W. B.
——; Baggerman, T.; Van Schaik, P.; Zuydeweg, C. W. S.; De Galan, L.
Chlorination of ω-cyanoalkanoic acids in aqueous medium. 1218
Dellinger, B. See Graham, J. L.
De Pinto, J. V.
——; Young, T. C.; McIlroy, L. M.
Great lakes water quality improvement. 752
DeRosa, P. M. See Dietrich, A. M.
Dickhut, R. M.
——; Andren, A. W.; Armstrong, D. E.
Aqueous solubilities of six polychlorinated biphenyl congeners at four temperatures 807
Dietrich, A. M.
——; Gallagher, D. L.; DeRosa, P. M.; Millington, D. S.; DiGiano, F. A.
Enhancement of N-nitrosamine formation on granular-activated carbon from N-methylaniline and nitrite. 1050
Dietz, R. N. See D'Ottavio, T. W.
DiGiano, F. A. See Dietrich, A. M.
Di Toro, D. M.
——; Mahony, J. D.; Kirchgraber, P. R.; O'Byrne, A. L.; Pasquale, L. R.; Piccirilli, D. C.
Effects of nonreversibility, particle concentration, and ionic strength on heavy-metal sorption. 55
Doering, P. H. See Wakeham, S. G.
Doherty, R. M. See Kamlet, M. J.
Dong, S.
——; Dasgupta, P. K.
Solubility of gaseous formaldehyde in liquid water and generation of trace standard gaseous formaldehyde. 637
D'Ottavio, T. W.
——; Goodrich, R. W.; Dietz, R. N.
Perfluorocarbon measurement using an automated dual-trap analyzer. 100
Drossman, H. See Dulin, D.
Duffy, C. P. See Quackenboss, J. J.
Dulin, D.
——; Drossman, H.; Mill, T.
Products and quantum yields for photolysis of chloroaromatics in water. 72
Durham, J. L. See Knapp, K. T.
Dzombak, D. A. See Fish, W.
——; Fish, W.; Morel, F. M. M.
Metal-humate interactions. 1. Discrete ligand and continuous distribution models. 669

Eatough, D. J. See Hansen, L. D.
——; White, V. F.; Hansen, L. D.; Eatough, N. L.; Cheney, J. L.
Identification of gas-phase dimethyl sulfate and monoethyl sulfate in the Los Angeles atmosphere. 867
Eatough, N. L. See Eatough, D. J.
Eckert, C. A.
——; Van Alsten, J. G.; Stoicos, T.
Supercritical fluid processing. 319
Edgerton, S. A.
——; Khalil, M. A. K.; Rasmussen, R. A.
Source emission characterization of residential wood-burning stoves and fireplaces: fine particle methyl chloride ratios for use in chemical mass balance modeling. 803
Edney, E. O. See Kleindienst, T. E.; Shepson, P. B.
Eiceman, G. A.
——; Davani, B.; Ingram, J.
Depth profiles for hydrocarbons and polycyclic aromatic hydrocarbons in soil beneath waste disposal pits from natural gas production. 508
Eisenreich, S. J. See Baker, J. E.
——; Metzer, N. A.; Urban, N. R.; Robbins, J. A.
Response of atmospheric lead to decreased use of lead in gasoline. 171
Eisma, D. See Bernard, P. C.
Eitzer, B. D.
——; Hites, R. A.
Airborne dioxins and dibenzofurans: sources and fates. Reply. 1186
Elabd, H.
——; Jury, W. A.; Cliath, M. M.
Spatial variability of pesticide adsorption parameters. 256
Ellestad, T. G. See Knapp, K. T.
Elliott, J. F. See Amdur, M. O.
Elzerman, A. W. See Talbot, R. W.
Emi, H. See Otani, Y.
Ephraim, J. See Marinsky, J. A.
——; Alegret, S.; Mathuthu, A.; Bicking, M.; Malcolm, R. L.; Marinsky, J. A.
A unified physicochemical description of the protonation and metal ion complexation equilibria of natural organic acids (humic and fulvic acids). 2. Influence of polyelectrolyte properties and functional group heterogeneity on the protonation equilibria of fulvic acid. 354
——; Marinsky, J. A.
A unified physicochemical description of the protonation and metal ion complexation equilibria of natural organic acids (humic and fulvic acids). 3. Influence of polyelectrolyte properties and functional heterogeneity on the copper ion binding equilibria in an Armadale Horizons Bh fulvic acid sample. 367

Farley, K. J.
——; Morel, F. M. M.
Role of coagulation in the kinetics of sedimentation. 187
Farr, L. B. See Adams, R. E.
Farrington, J. W.
——; Wakeham, S. G.; Livramento, J. B.; Tripp, B. W.; Teal, J. M.
Aromatic hydrocarbons in New York Bight polychaetes: ultraviolet fluorescence analyses and gas chromatography/gas chromatography-mass spectrometry analyses. 69
Faust, B. C.
——; Hoffmann, M. R.
Photoinduced reductive dissolution of α-iron oxide (α-Fe_2O_3) by bisulfite. 943
Feerer, J. L.
——; Miller, A. G.; Ramirez, W. F.
X-ray photoelectric spectroscopy determination of a conceptual leaching model of retorted oil shale. 695
Felice, L. J. See Zachara, J. M.
Fiessinger, F. See Maloney, S. W.
Fish, W. See Dzombak, D. A.
——; Dzombak, D. A.; Morel, F. M. M.
Metal-humate interactions. 2. Application and comparison of models. 676
Fogelqvist, E. See Xie, T. M.
Folsom, B. R.
——; Popescu, N. A.; Wood, J. M.
Comparative study of aluminum and copper transport and toxicity in an acid-tolerant freshwater green alga. 616
Foreman, W. T. See Bidleman, T. F.
Forsyth, D. S.
——; Marshall, W. D.
Ionic alkylleads in herring gulls from the Great Lakes region. 1033
Fox, M. F.
——; Kester, D. R.; Hunt, C. D.
Vertical transport processes of an acid-iron waste in a MERL stratified mesocosm. 62
Fox, S. H. See Saltzman, B. E.
French, W. See Laughlin, R. B. Jr.
Friedman, A. J. See Krone, C. A.
Friedman, L. C.
——; Schroder, L. J.; Brooks, M. G.
Recovery of several volatile organic compounds from simulated water samples: effect of transport and storage. 826

Gallagher, D. L. See Dietrich, A. M.
Garbarini, D. R.
——; Lion, L. W.
Influence of the nature of soil organics on the sorption of toluene and trichloroethylene. 1263
Garrison, A. A. See Yokley, R. A.
Gauthier, T. D.
——; Shane, E. C.; Guerin, W. F.; Seitz, W. R.; Grant, C. L.
Fluorescence quenching method for determining equilibrium constants for polycyclic aromatic hydrocarbons binding to dissolved humic materials. 1162
Giger, W. See McEvoy, J.
Glass, G. E.
——; Loucks, O. L.
Implications of a gradient in acid and ion deposition across the northern Great Lakes states. 35
Gohre, K.
——; Scholl, R.; Miller, G. C.
Singlet oxygen reactions on irradiated soil surfaces. 934
Goodrich, R. W. See D'Ottavio, T. W.
Goto, M.
——; Hayashi, N.; Goto, S.
Adsorption and desorption of phenol on anion-exchange resin and activated carbon. 463
Goto, S. See Goto, M.
Graedel, T. E.
——; McGill, R.
Degradation of materials in the atmosphere. 1093
Graham, J. L.
——; Hall, D. L.; Dellinger, B.
Laboratory investigation of the thermal degradation of a mixture of hazardous organic compounds. 1. 703
Grant, C. L. See Gauthier, T. D.
Gray, H. A.
——; Cass, G. R.; Huntzicker, J. J.; Heyerdahl, E. K.; Rau, J. A.
Characteristics of atmospheric organic and elemental carbon particle concentrations in Los Angeles. 580
Greene, B. See Darnall, D. W.
——; Hosea, M.; McPherson, R.; Henzl, M.; Alexander, M. D.; Darnall, D. W.
Interaction of gold(I) and gold(III) complexes with algal biomass. 627
Griest, W. H.
——; Tomkins, B. A.
Influence of carbonaceous particles on the interaction of coal combustion stack ash with organic matter. 291
Gschwend, P. M. See Wu, S. C.
Guard, H. E. See Laughlin, R. B. Jr.
Guerin, W. F. See Gauthier, T. D.
Gupta, V. K. See Dasgupta, P. K.

Haag, W. R.
——; Hoigne, J.
Singlet oxygen in surface waters. 3. Photochemical formation and steady-state concentrations in various types of waters. 341
Haas, C. N.
——; Keralius, M. G.; Brncich, D. M.; Zapkin, M. A.
Alteration of chemical and disinfectant properties of hypochlorite by sodium, potassium, and lithium. 822
Halfon, E.
——; Reggiani, M. G.
On ranking chemicals for environmental hazard. 1173
Hall, D. L. See Graham, J. L.
Hansen, L. D. See Eatough, D. J.
——; White, V. F.; Eatough, D. J.
Determination of gas-phase dimethyl sulfate and monomethyl sulfate. 872
Harrison, R. M. See Hewitt, C. N.
Hassett, J. P. See Yin, C.
Hatakeyama, S. See Takagi, H.
Hayamizu, T. See Nishimura, H.
Hayashi, N. See Goto, M.
Helfrich, J. A. See Barcelona, M. J.
Henzl, M. See Greene, B.
Henzl, M. T. See Darnall, D. W.
Herlitz, H. G.
Plasma technology. Use of high-temperature plasma shows promise for metal recovery and hazardous destruction. 1102
Hewitt, C. N.
——; Harrison, R. M.
Formation and decomposition of trialkyllead compounds in the atmosphere. 797
Heyerdahl, E. K. See Gray, H. A.
Higgo, J. J. W.
——; Rees, L. V. C.
Adsorption of actinides by marine sediments: effect of the sediment/seawater ratio on the measured distribution ratio. 483
Hillamo, R. E. See Kauppinen, E. I.
Hites, R. A. See Czuczwa, J. M.; Eitzer, B. D.; Jaffe, R.
Ho, P. C.
Photooxidation of 2,4-dinitrotoluene in aqueous solution in the presence of hydrogen peroxide. 260
Hodge, V. F.
——; Stallard, M. O.

Platinum and palladium in roadside dust. 1058
Hodson, R. E. See Hwang, H. M.
Hoffmann, M. R. See Faust, B. C.
Hoigne, J. See Haag, W. R.
Holland, D. M.
——; McElroy, F. F.
Analytical method comparisons by estimates of precision and lower detection limit. 1157
Holler, J. S. See Alexander, L. R.
Honkasalo, S. See Victorin, K.
Horner, R. R. See Mar, B. W.
Horowitz, A. J.
Comparison of methods for the concentration of suspended sediment in river water for subsequent chemical analysis. 155
Hosea, J. M. See Darnall, D. W.
Hosea, M. See Greene, B.
Hunt, C. D. See Fox, M. F.
Huntzicker, J. J. See Gray, H. A.
Hushon, J. M.
Response to chemical emergencies. 118
Hwang, H. M.
——; Hodson, R. E.; Lee, R. F.
Degradation of phenol and chlorophenols by sunlight and microbes in estuarine water. 1002
Hyland, M. See Abdelnasser, M.

Ingram, J. See Eiceman, G. A.
Itkonen, A. See Jantunen, M. J.; Victorin, K.
Itkonen, A. O.
——; Jantunen, M. J.
Emissions and particle-size distribution of some metallic elements of two peat/oil-fired boilers. 335
Iwasaki, I. See Krishnan, S. V.

Jaber, H. M. See Podoll, R. T.
Jaffe, R.
——; Hites, R. A.
Fate of hazardous waste derived organic compounds in Lake Ontario. 267
James, R. H. See Adams, R. E.
Jantunen, M. J. See Itkonen, A. O.; Victorin, K.
——; Liimatainen, A.; Ramdahl, T.; Itkonen, A.
Rapid changes in peat fly ash mutagenicity after release into the atmosphere: a controlled dilution bag study. 684
Jespersen, N. D. See Abdelnasser, M.
Johnson, J. D. See Anderson, L. J.
Johnson, L. D. See Adams, R. E.
Detecting waste combustion emissions. 223
Jones, R. A. See Lee, G. F.
Joos, L. F.
——; Landolt, W. F.; Leuenberger, H.
Calibration of peroxyacetyl nitrate measurements with an NO_x [nitrogen oxides] analyzer. 1269
Josefsson, B. See Xie, T. M.
Jury, W. A. See Elabd, H.

Kadowaki, S.
On the nature of atmospheric oxidation processes of sulfur dioxide to sulfate and of nitrogen dioxide to nitrate on the basis of diurnal variations of sulfate, nitrate, and other pollutants in an urban area. 1249
Kamlet, M. J.
——; Doherty, R. M.; Veith, G. D.; Taft, R. W.; Abraham, M. H.
Solubility properties in polymers and biological media. 7. An analysis of toxicant properties that influence inhibition of bioluminescence in Photobacterium phosphoreum (the Microtox test). 690
Kanaoka, C. See Otani, Y.
Kanarek, M. S. See Quackenboss, J. J.
Karamchandani, P. See Venkatram, A.
Karnosky, D. F. See Wang, D.
Karra, S. B. See Chang, W. D.
Kashdan, E. R.
——; Ranade, M. B.; Purdue, L. J.; Rehme, K. A.
Interlaboratory evaluation of two inlets for sampling particles less than 10μm. 911
Katmandu, N. See Davidson, C. I.
Katzenstein, A. W.
Acidification of southern Appalachian lakes. Comments. 302
Kauffman, J. W.
——; Laughlin, W. C.; Baldwin, R. A.
Microbiological treatment of uranium mine waters. 243
Kauppinen, E. I.
——; Hillamo, R. E.; Aaltonen, S. H.; Sinkko, K. T. S.
Radioactivity size distributions of ambient aerosols in Helsinki, Finland, during May 1986 after Chernobyl accident: preliminary report. 1257
Kenaga, E. E.
Assessing chemical hazards. 660
Kendall, D. C. See Thompson, H. C. Jr.
Kennedy, V. C. See Laird, L. B.
Keralius, M. G. See Haas, C. N.
Kester, D. R. See Fox, M. F.
Khalil, M. A. K. See Davidson, C. I.; Edgerton, S. A.
Kile, D. E. See Chiou, C. T.
Kim, Y. H. See Woodrow, J. E.
Kinniburgh, D. G.
General purpose adsorption isotherms. 895
Kirchgraber, P. R. See Di Toro, D. M.
Kissa, E.
Determination of organofluorine in air. 1254
Kleindienst, T. E. See Shepson, P. B.
——; Shepson, P. B.; Edney, E. O.; Claxton, L. D.; Cupitt, L. T.
Wood smoke: measurement of the mutagenic activities of its gas- and particulate-phase photooxidation products. 493
Knapp, K. T.
——; Durham, J. L.; Ellestad, T. G.
Pollutant sampler for measurements of atmospheric acidic dry deposition. 633
Koda, S. See Takagi, H.
Koehler, J. L. M. See Rudnick, S. N.
Kominsky, J. R. See Thompson, H. C. Jr.
Korfmacher, W. A. See Thompson, H. C. Jr.
Kraemer, T. F.
Radon in unconventional natural gas from Gulf coast geopressured-geothermal reservoirs. 939
Kramer, J. R. See Stroes-Gascoyne, S.
Krishnan, S. V.
——; Iwasaki, I.
Heterocoagulation vs. surface precipitation in quartz-magnesium hydroxide system. 1224
Krone, C. A.
——; Burrows, D. G.; Brown, D. W.; Robisch, P. A.; Friedman, A. J.; Malins, D. C.
Nitrogen-containing aromatic compounds in sediments from a polluted harbor in Puget Sound. 1144

Laird, L. B.
——; Taylor, H. E.; Kennedy, V. C.
Snow chemistry of the Cascade-Sierra Nevada Mountains. 275
Lam, H. F. See Amdur, M. O.
Landolt, W. F. See Joos, L. F.
Laughlin, R. B. Jr.
——; French, W.; Guard, H. E.
Accumulation of bis(tributyltin) oxide by the marine mussel Mytilus edulis. 884
——; Guard, H. E.; Coleman, W. M. III.
Tributyltin in seawater: speciation and octanol-water partition coefficient. 201
Laughlin, W. C. See Kauffman, J. W.
Lawler, D. F.
Removing particles in water and wastewater. 856
Lee, G. F.
——; Jones, R. A.
Detergent phosphate bans and eutrophication. 330
Lee, M. L. See Nishioka, M.
Lee, R. F. See Hwang, H. M.; Seligman, P. F.
Leith, D. See Rudnick, S. N.
Lettenmaier, D. P. See Mar, B. W.
Letz, R. See Quackenboss, J. J.
Leuenberger, H. See Joos, L. F.
Levin, J. O.
——; Lindahl, R.; Andersson, K.
A passive sampler for formaldehyde in air using 2,4-dinitrophenylhydrazine-coated glass fiber filters. 1273
Lewis, C. W.
——; Baumgardner, R. E.; Stevens, R. K.; Russwurm, G. M.
Receptor modeling study of Denver winter haze. 1126
Liimatainen, A. See Jantunen, M. J.
Lin, S. F. See Davidson, C. I.
Lindahl, R. See Levin, J. O.
Lindstroem, K.
——; Oesterberg, F.
Chlorinated carboxylic acids in softwood kraft pulp spent bleach liquors. 133
Lion, L. W. See Garbarini, D. R.
Lionel, T.
——; Martin, R. J.; Brown, N. J.
A comparative study of combustion in kerosene heaters. 78
Lioy, P. J.
——; Daisey, J. M.
Airborne toxic elements and organic substances. 8
Livramento, J. B. See Farrington, J. W.
Lonneman, W. A.
——; Seila, R. L.; Meeks, S. A.
Non-methane organic composition in the Lincoln Tunnel. 790
Lorenzo, P. A. See Barrio-Lage, G.
Loucks, O. L. See Glass, G. E.
Loux, N. T. See Burkhard, L. P.
Luria, M.
——; Van Valin, C. C.; Wellman, D. L.; Pueschel, R. F.
Contribution of Gulf area natural sulfur to the North American sulfur budget. 91

McCarthy, J. F. See Amdur, M. O.
MacCarthy, P. See Malcolm, R. L.
McCarty, P. L.
——; Smith, D. P.
Anaerobic wastewater treatment. 1200
McElroy, F. F. See Holland, D. M.
McEvoy, J.
——; Giger, W.
Determination of linear alkylbenzenesulfonates in sewage sludge by high-resolution gas chromatography/mass spectrometry. 376
McEwen, J. B. See Batchelor, B.
McGill, R. See Graedel, T. E.
Macias, E. S. See Vossler, T. L.
McIlroy, L. M. See De Pinto, J. V.
MacIntyre, W. G. See Burris, D. R.
Mackay, D.
——; Paterson, S.; Schroeder, W. H.
Model describing the rates of transfer processes of organic chemicals between atmosphere and water. 810
MacLeod, H. See Tuazon, E. C.
McPherson, R. See Greene, B.
McPherson, R. A. See Darnall, D. W.
McQuaker, N. R.
——; Rajala, G. E.; Pengilly, D.
Measurement of total reduced sulfur compounds in ambient air. 517
Mahony, J. D. See Di Toro, D. M.
Malaby, K. L. See Norton, G. A.
Malcolm, R. L. See Chiou, C. T.; Ephraim, J.
——; MacCarthy, P.
Limitations in the use of commercial humic acids in water and soil research. 904
Malins, D. C. See Krone, C. A.
Mallevialle, J. See Maloney, S. W.
Maloney, S. W.
——; Manem, J.; Mallevialle, J.; Fiessinger, F.
Transformation of trace organic compounds in drinking water by enzymic oxidative coupling. 249
Mamantov, G. See Yokley, R. A.
Manem, J. See Maloney, S. W.
Manuel, O. K. See Chiou, K. Y.
Mar, B. W.
——; Horner, R. R.; Richey, J. S.; Palmer, R. N.; Lettenmaier, D. P.
Data acquisition. Cost-effective methods for obtaining data on water quality. 545
Marcus, W. L. See Cothern, C. R.
Marinsky, J. A. See Ephraim, J.
——; Ephraim, J.
A unified physicochemical description of the protonation and metal ion complexation equilibria of natural organic acids (humic and fulvic acids). 1. Analysis of the influence of polyelectrolyte properties on protonation equilibria in ionic media: fundamental concepts. 349
Markuszewski, R. See Norton, G. A.
Marnicio, R. J. See Rubin, E. S.
Marple, L.
——; Berridge, B.; Throop, L.
Measurement of the water-octanol partition coefficient of 2,3,7,8-tetrachlorodibenzo-p-dioxin. 397
——; Brunck, R.; Throop, L.
Water solubility of 2,3,7,8-tetrachlorodibenzo-p-dioxin. 180

Marshall, W. D. See Forsyth, D. S.
Martin, K. P. See Rudnick, S. N.
Martin, R. J. See Lionel, T.
Mathuthu, A. See Ephraim, J.
Matsui, S. See Otani, Y.
Matthias, C. L.
—; Bellama, J. M.; Olson, G. J.; Brinckman, F. E.
Comprehensive method for determination of aquatic butyltin and butylmethyltin species at ultratrace levels using simultaneous hydridization extraction with gas chromatography–flame photometric detection. 609
Mattigod, S. V. See Sullivan, P. J.
Mauney, T. See Soltys, P. A.
Meeks, S. A. See Lonneman, W. A.
Metzer, N. A. See Eisenreich, S. J.
Milanovich, F. P.
Detecting chloroorganics in groundwater. 441
Miles, C. J. See Trehy, M. L.
Mill, T. See Dulin, D.; Podoll, R. T.
Miller, A. G. See Feerer, J. L.
Miller, G. C. See Gohre, K.
Miller, H. C. See Adams, R. E.
Millington, D. S. See Dietrich, A. M.
Mitchell, W. J. See Crist, H. L.
Morel, F. M. M. See Dzombak, D. A.; Farley, K. J.; Fish, W.
Mortland, M. M. See Boyd, S. A.
Mueller, M. D. See Buser, H. R.
—; Buser, H. R.
Halogenated aromatic compounds in automotive emissions from leaded gasoline additives. 1151
Munemori, M. See Aoki, T.
Munro, N. B.
—; Travis, C. C.
Drinking-water standards. 768
Munz, C.
—; Roberts, P. V.
Effects of solute concentration and cosolvents on the aqueous activity coefficient of halogenated hydrocarbons. 830
Myers, G. L. See Alexander, L. R.

Nassar, R. S. See Barrio-Lage, G.
Natusch, D. F. S. See Soltys, P. A.
Nazaroff, W. W.
—; Cass, G. R.
Mathematical modeling of chemically reactive pollutants in indoor air. 924
Nero, C. M. See Shepson, P. B.
Neville, M. See Amdur, M. O.
Newell, A. D.
—; Sanders, J. G.
Relative copper binding capacities of dissolved organic compounds in a coastal-plain estuary. 817
Nishimura, H.
—; Hayamizu, T.; Yanagisawa, Y.
Reduction of nitrogen oxide (NO_2) to nitrogen oxide (NO) by rush and other plants. 413
Nishioka, M.
—; Chang, H. C.; Lee, M. L.
Structural characteristics of polycyclic aromatic hydrocarbon isomers in coal tars and combustion products. 1023
Noguchi, G. E. See Rice, C. P.
Norton, G. A.
—; DeKalb, E. L.; Malaby, K. L.
Elemental composition of suspended particulate matter from the combustion of coal and coal/refuse mixtures. 604
—; Markuszewski, R.; Shanks, H. R.
Morphological and chemical characterization of iron-rich fly ash fractions. 409

O'Byrne, A. L. See Di Toro, D. M.
Oesterberg, F. See Lindstroem, K.
Olson, G. J. See Matthias, C. L.
Oppelt, E. T.
Hazardous waste destruction. 312
Osborn, J. F. See Davidson, C. I.
Otani, Y.
—; Kanaoka, C.; Usui, C.; Matsui, S.; Emi, H.
Adsorption of mercury vapor on particles. 735

Palmer, R. N. See Mar, B. W.
Pandey, M. R. See Davidson, C. I.
Parsons, F. Z. See Barrio-Lage, G.
Pasquale, L. R. See Di Toro, D. M.
Paterson, S. See Mackay, D.
Patterson, D. G. See Alexander, L. R.
Patterson, H. H. See Plankey, B. J.
Pellenbarg, R. E.
—; Tevault, D. E.
Evidence for a sedimentary siloxane horizon. 743
Pengilly, D. See McQuaker, N. R.
Perry, R. See Batchelor, B.
Piccirilli, D. C. See Di Toro, D. M.
Pitts, J. N. Jr. See Tuazon, E. C.
Plankey, B. J.
—; Patterson, H. H.; Cronan, C. S.
Kinetics of aluminum fluoride complexation in acidic waters. 160
Podoll, R. T.
—; Jaber, H. M.; Mill, T.
Tetrachlorodibenzodioxin: rates of volatilization and photolysis in the environment. 490
Popescu, N. A. See Folsom, B. R.
Pueschel, R. F. See Luria, M.
Purdue, L. J. See Kashdan, E. R.

Quackenboss, J. J.
—; Spengler, J. D.; Kanarek, M. S.; Letz, R.; Duffy, C. P.
Personal exposure to nitrogen dioxide: relationship to indoor/outdoor air quality and activity patterns. 775
Quann, R. J. See Amdur, M. O.

Rajala, G. E. See McQuaker, N. R.
Ramdahl, T. See Jantunen, M. J.
Ramirez, W. F. See Feerer, J. L.
Ranade, M. B. See Kashdan, E. R.
Rapin, F.
—; Tessier, A.; Campbell, P. G. C.; Carignan, R.
Potential artifacts in the determination of metal partitioning in sediments by a sequential extraction procedure. 836
Rasmussen, R. A. See Davidson, C. I.; Edgerton, S. A.
Rathbun, R. E.
—; Tai, D. Y.
Gas-film coefficients for the volatilization of ethylene dibromide from water. 949
Rau, J. A. See Gray, H. A.
Rees, J. F. See Wilson, B. H.
Rees, L. V. C. See Higgo, J. J. W.
Reggiani, M. G. See Halfon, E.
Rehme, K. A. See Kashdan, E. R.
Reinhard, M. See Vogel, T. M.
Resch, C. T. See Zachara, J. M.
Rice, C. P.
—; Samson, P. J.; Noguchi, G. E.
Atmospheric transport of toxaphene to Lake Michigan. 1109
Richey, J. S. See Mar, B. W.
Robbins, J. A. See Eisenreich, S. J.
Roberts, L. S. See Aggett, J.
Roberts, P. V. See Aieta, E. M.; Munz, C.
Robisch, P. A. See Krone, C. A.
Rogers, A. E. See Amdur, M. O.
Rowland, K. L. See Thompson, H. C. Jr.
Rubin, E. S.
—; Cushey, M. A.; Marnicio, R. J.; Bloyd, C. N.; Skea, J. F.
Controlling acid deposition: the role of FGD. 960
Rudnick, S. N.
—; Koehler, J. L. M.; Martin, K. P.; Leith, D.; Cooper, D. W.
Particle collection efficiency in a venturi scrubber: comparison of experiments with theory. 237
Rushing, L. G. See Thompson, H. C. Jr.
Russell, A. G.
—; Cass, G. R.; Seinfeld, J. H.
On some aspects of nighttime atmospheric chemistry. 1167
Russwurm, G. M. See Lewis, C. W.

Saltzman, B. E.
—; Fox, S. H.
Biological significance of fluctuating concentrations of carbon monoxide. 916
Samson, P. J. See Rice, C. P.
Sanders, J. G. See Newell, A. D.
Sarofim, A. F. See Amdur, M. O.
Schell, W. R.
Deposited atmospheric chemicals. 847
Scholl, R. See Gohre, K.
Schroder, L. J. See Friedman, L. C.
Schroeder, W. H. See Mackay, D.
Schure, M. R. See Soltys, P. A.
Seiber, J. N. See Woodrow, J. E.
Seila, R. L. See Lonneman, W. A.
Seinfeld, J. H. See Russell, A. G.
Seitz, W. R. See Gauthier, T. D.
Seligman, P. F.
—; Valkirs, A. O.; Lee, R. F.
Degradation of tributyltin in San Diego Bay, California, waters. 1229
Sengupta, A. K.
—; Clifford, D.
Important process variables in chromate ion exchange. 149
Senkan, S. M. See Chang, W. D.
Shackelford, W. M.
—; Cline, D. M.
Organic compounds in water. 652
Shane, E. C. See Gauthier, T. D.
Shanks, H. R. See Norton, G. A.
Shepson, P. B. See Kleindienst, T. E.
—; Kleindienst, T. E.; Edney, E. O.; Nero, C. M.; Cupitt, L. T.; Claxton, L. D.
Acetaldehyde: the mutagenic activity of its photooxidation products. 1008
Shobe, W. R. See Almich, B. P.
Sinkko, K. T. S. See Kauppinen, E. I.
Skea, J. F. See Rubin, E. S.
Smith, D. P. See McCarty, P. L.
Smith, E. H. See Weber, W. J. Jr.
Smith, G. B. See Wilson, B. H.
Smith, L. M. See Thompson, H. C. Jr.
Smith, T. G. See Addison, R. F.
Sneddon, J. See Darnall, D. W.
Snodgrass, W. J. See Stroes-Gascoyne, S.
Sobek, A. A. See Sullivan, P. J.
Soltys, P. A.
—; Mauney, T.; Natusch, D. F. S.; Schure, M. R.
Time-resolved solvent extraction of coal fly ash: retention of benzo[a]pyrene by carbonaceous components and solvent effects. 175
Sorg, T. J. See Clifford, D.
Spengler, J. D. See Quackenboss, J. J.
Staahlberg, M. See Victorin, K.
Stallard, M. O. See Hodge, V. F.
Stalling, D. L. See Thompson, H. C. Jr.
Stauffer, R. E.
Cycling of manganese and iron in Lake Mendota, Wisconsin. 449
Steelink, C. See Collins, M. R.
Steinmetz, W. D. See Cohen, M. L.
Stevens, R. K. See Lewis, C. W.
Stoicos, T. See Eckert, C. A.
Stroes-Gascoyne, S.
—; Kramer, J. R.; Snodgrass, W. J.
A new model describing the adsorption of copper on manganese dioxide. 1047
Subramonian, S. See Clifford, D.
Sullivan, P. J.
—; Mattigod, S. V.; Sobek, A. A.
Dissolution of iron sulfates from pyritic coal waste. 1013
Swackhamer, D. L.
—; Armstrong, D. E.
Estimation of the atmospheric and nonatmospheric contributions and losses of polychlorinated biphenyls for Lake Michigan on the basis of sediment records of remote lakes. 879

Taft, R. W. See Kamlet, M. J.
Tai, D. Y. See Rathbun, R. E.
Takagi, H. See Akimoto, H.
—; Hatakeyama, S.; Akimoto, H.; Koda, S.
Formation of methyl nitrite in the surface reaction of nitrogen dioxide and methanol. 1. Dark reaction. 387
Talbot, R. W.
—; Elzerman, A. W.
Acidification of southern Appalachian lakes. Reply to comments. 302
Taylor, H. E. See Laird, L. B.
Teal, J. M. See Farrington, J. W.
Tessier, A. See Rapin, F.
Tevault, D. E. See Pellenbarg, R. E.
Thomason, M. M. See Adams, R. E.
Thompson, H. C. Jr.
—; Kendall, D. C.; Korfmacher, W. A.; Rowland, K. L.; Rushing, L. G.; Chen, J. J.; Kominsky, J. R.; Smith, L. M.; Stalling, D. L.
Assessment of the contamination of a multibuilding facility by polychlorinated biphenyls, polychlorinated dibenzo-p-dioxins, and polychlorinated dibenzofurans. 597
Throop, L. See Marple, L.
Tomkins, B. A. See Griest, W. H.
Travis, C. C. See Munro, N. B.
Trehy, M. L.
—; Yost, R. A.; Miles, C. J.
Chlorination byproducts of amino acids in natural waters. 1117
Tripp, B. W. See Farrington, J. W.
True, M. B. See Zafiriou, O. C.
Tuazon, E. C.
—; Atkinson, R.; Aschmann, S. M.; Arey,

J.; Winer, A. M.; Pitts, J. N. Jr.
Atmospheric loss processes of 1,2-dibromo-3-chloropropane and trimethyl phosphate. 1043
——; MacLeod, H.; Atkinson, R.; Carter, W. P. L.
α-Dicarbonyl yields from the NO_x-air photooxidations of a series of aromatic hydrocarbons in air. 383

Uemura, S. See Aoki, T.
Uno, I. See Wadden, R. A.
Urban, N. R. See Eisenreich, S. J.
Usui, C. See Otani, Y.

Valentine, R. L.
Bromochloramine oxidation of N,N-diethyl-p-phenylenediamine in the presence of monochloramine. 166
Valkirs, A. O. See Seligman, P. F.
Van Alsten, J. G. See Eckert, C. A.
Van Cleuvenbergen, R. J. A.
——; Chakraborti, D.; Adams, F. C.
Occurrence of tri- and dialkyllead species in environmental water. 589
Van Grieken, R. E. See Bernard, P. C.
Van Schaik, P. See De Leer, Ed. W. B.
Van Valin, C. C. See Luria, M.
Veith, G. D. See Kamlet, M. J.
Venkatram, A.
——; Karamchandani, P.
Source-receptor relationships. A look at acid deposition modeling. 1084
Victorin, K.
——; Jantunen, M. J.; Itkonen, A.; Ahlborg, U. G.; Staahlberg, M.; Honkasalo, S.
Mutagenic effluents from a coal-fired power plant: short-term variations and relation to power load and other load-dependent emissions. 400
Vogel, T. M.
——; Reinhard, M.
Reaction products and rates of disappearance of simple bromoalkanes, 1,2-dibromopropane, and 1,2-dibromoethane in water. 992
Vossler, T. L.
——; Macias, E. S.
Contribution of fine particle sulfates to light scattering in St. Louis summer aerosol. 1235

Wadden, R. A.
——; Uno, I.; Wakamatsu, S.
Source discrimination of short-term hydrocarbon samples measured aloft. 473
Wakamatsu, S. See Wadden, R. A.
Wakeham, S. G. See Farrington, J. W.
——; Canuel, E. A.; Doering, P. H.
Behavior of aliphatic hydrocarbons in coastal seawater: mesocosm experiments with [^{14}C]octadecane and [^{14}C]idecane. 574
Wang, D.
——; Bormann, F. H.; Karnosky, D. F.
Regional tree growth reductions due to ambient ozone: evidence from field experiments. 1122
Weber, W. J. Jr.
——; Smith, E. H.
Removing dissolved organic contaminants from water. 970
Wehry, E. L. See Yokley, R. A.
Wellman, D. L. See Luria, M.
White, V. F. See Eatough, D. J.; Hansen, L. D.
Wilson, B. H.
——; Smith, G. B.; Rees, J. F.
Biotransformations of selected alkylbenzenes and halogenated aliphatic hydrocarbons in methanogenic aquifer material: a microcosm study. 997
Wilson, J. D.
"Airborne dioxins and dibenzofurans: sources and fates". Comments. 1185
Winer, A. M. See Tuazon, E. C.
Wood, J. M. See Folsom, B. R.
Woodrow, J. E.
——; Seiber, J. N.; Kim, Y. H.
Measured and calculated evaporation losses of two petroleum hydrocarbon herbicide mixtures under laboratory and field conditions. 783
Wu, S. C.
——; Gschwend, P. M.
Sorption kinetics of hydrophobic organic compounds to natural sediments and soils. 717

Xie, T. M.
——; Abrahamsson, K.; Fogelqvist, E.; Josefsson, B.
Distribution of chlorophenolics in a marine environment. 457

Yanagisawa, Y. See Nishimura, H.
Yin, C.
——; Hassett, J. P.
Gas-partitioning approach for laboratory and field studies of mirex fugacity in water. 1213
Yokley, R. A.
——; Garrison, A. A.; Wehry, E. L.; Mamantov, G.
Photochemical transformation of pyrene and benzo[a]pyrene vapor-deposited on eight coal stack ashes. 86
Yost, R. A. See Trehy, M. L.
Young, T. C. See De Pinto, J. V.

Zachara, J. M.
——; Ainsworth, C. C.; Felice, L. J.; Resch, C. T.
Quinoline sorption to subsurface materials: role of pH and retention of the organic cation. 620
Zafiriou, O. C.
——; True, M. B.
Interferences in environmental analysis of nitric oxide by nitric oxide plus ozone detectors: a rapid screening technique. 594
Zapkin, M. A. See Haas, C. N.
Zinck, M. E. See Addison, R. F.
Zuydeweg, C. W. S. See De Leer, Ed. W. B.

Front Section Subject Index

Critical Reviews

Viruses in drinking water, 216

Features

Air toxics, 647
Airborne toxic elements and organic substances, 8
Analyzing PCBs, 1194
Controlling acid deposition: the role of FGD, 960
Data acquisition, for water quality, 545
Degradation of materials in the atmosphere, 1093
Deposited atmospheric chemicals, 847
Destruction of hazardous wastes, 312
Detecting waste combustion emissions, 223
Education for environmental engineering, 432
Estimating risk to human health, 111
Great Lakes water quality improvement, 752
Organic compounds in water, 652
Organic pollutant transport, 538
Response to chemical emergencies, 118
Source-receptor relationships, 1084
Supercritical fluid processing, 319
Victim compensation, 425
Visibility: an evolving issue, 760
Waste monitoring, 16

Regulatory Focus

Analysis of the new safe drinking water law, 1101
Banning land disposal of hazardous wastes, 327
EPA drinking water proposals, 22
FIFRA amendments, 438
Fiscal year 1987 budget, 552
Groundwater guidelines, 862
Hazardous air pollution control, 122
Legislative agenda for 1986, 228
New guidelines for risk assessment, 981
Superfund finally, 1207
The greenhouse effect, 767
Update on air quality issues, 659

Views

Assessing chemical hazards, 660
Biological monitoring, 124
Detecting chloroorganics in groundwater, 441
Detergent phosphate bans and eutrophication, 330
Drinking-water standards, 768
Environmental awards, 231
Environmental protection, the business of, 553
Implementing Superfund, 23
Plasma technology, 1102
Reducing climatic change, 1208

Editorials

Critique for new safe drinking water law, 1067
Drinking water and risk, 747
Environmental health, 107
Global experiment, 419
Tomorrow's goals based on yesterday's woes, 843
Toxic chemicals in surface waters, 3
Toxicology of acid rain, 211
Update on feature articles, 531
Waste reduction technology, 1189
What price a clean environment?, 955
Where's the technology, 643
Writing wrongs, 307

Series

Opportunities in Chemistry (The Pimentel Report Series)
- Chemistry and national well-being, 128
- Cleaner water and safe disposal of wastes, 663
- Guarding against climate change, 555
- Ozone in the stratosphere, 328
- Reducing acid rain, 439
- Turning detection into protection, 229

Water Treatment Processes Series
- Anaerobic treatment processes, 1200
- Removing dissolved inorganic contaminants, 1072
- Removing dissolved organic contaminants, 970
- Removing particles from water and wastewater, 855

Letters

Acid deposition, 534
Chemical emergencies, 420
Drinking water standards, 1068
Risk assessments, 420

KEYWORD INDEX TO VOLUME 20, 1986

Absorption air pollution pptn model 810
Absorption kinetics chlorine hydrolysis 44
Accident reactor fallout Chernobyl 1257
Acetaldehyde photooxidn product mutagen= icity pollution 1008
Acetylene air pollution tunnel exhaust 790
Acid chlorinated spent pulping liquor 133
Acid deposition aluminum complexation water 160
Acid deposition modeling review 1084
Acid dry deposition air sampler 633
Acid rain flue gas desulfurization 960
Acidic iron waste settling seawater 62
Acidity sulfate lake Appalachian polemic 302
Actinide adsorption seawater sediment ratio 483
Activated carbon nitrosation catalyst methy= laniline 1050
Activated carbon phenol adsorption waste= water 463
Activity aq soly calcn UNIFAC 1060
Activity chlorinated hydrocarbon aq 830
Adipose tissue chlorodibenzodioxin chlorodi= benzofuran polemic 1186
Adsorption actinide seawater sediment ratio 483
Adsorption copper manganese dioxide 1047
Adsorption isotherm soln solid soil 895
Adsorption mercury vapor incineration soot 735
Adsorption phenol wastewater activated carbon 463
Adsorption variability napropamide soil analysis 256
Aerosol ammonium sulfate light scattering 1235
Aerosol atm org elemental carbon 580
Aerosol atm tellurium selenium 987
Aerosol coal combustion sulfur dioxide 138
Aerosol Gulf Mexico atm sulfur 91
Aerosol particle detn sampling inlet 911
Aerosol pollution wood combustion source 803
Aerosol radioactive Chernobyl 1257
Air ammonium sulfate light scattering 1235
Air analysis nitrogen dioxide chemilumines= cence 1157
Air analysis sulfur reduced compd 517
Air arom hydrocarbon photooxidn hydroxyl 383
Air dimethyl monomethyl sulfate detn 872
Air formaldehyde passive sampler 1273
Air org sampling Tenax evaluation 1260
Air organofluorine detn fluoride formation 1254
Air perfluorocarbon detn gas chromatog 100
Air peroxyacetyl nitrate detn calibration 1269
Air pollutant dry deposition sampler 633
Air pollutant partitioning vapor particle 1038
Air pollutant source receptor review 1084
Air pollution absorption pptn model 810
Air pollution building contamination 597
Air pollution hydrocarbon source Tokyo 473
Air pollution indoor outdoor Himalayas 561
Air pollution lead gasoline compn 171
Air pollution material degrdn review 1093
Air pollution refuse derived fuel 604
Air pollution toxic chem review 647
Air water chem transfer model 810
Alga gold adsorption 627
Algae aluminum copper metab toxicity 616
Aliph hydrocarbon estuary pollutant fate 574
Alkali cation hypochlorite disinfection water 822
Alkylbenzene halogenated aliph hydrocarbon biodegrdn 997
Alkylbenzenesulfonate linear detn sewage sludge 376
Alkylead herring gull Great Lakes 1033
Alkyllead pollution rain snow water 589
Aluminum fluoride complexation water kinetics 160
Aluminum hydrolysis product detn water 891
Aluminum metab toxicity Chlorella 616
Americium adsorption seawater sediment ratio 483
Amino acid chlorination byproduct water 1117
Ammonia dioxide dry deposition air sampler 633
Ammonia nitrate simultaneous detn water 515
Ammonium ion atm pptn US 35
Ammonium sulfate aerosol light scattering 1235
Anaerobic biodegrdn landfill leachate 997
Anaerobic wastewater treatment 1200
Anion exchange phenol removal wastewater 463
Anthracene assocn humic acid fluorescence 1162
Aq particle interaction metal sorption 55
Aquatic org matter copper binding 817
Aquifer biodegrdn alkylbenzene halogenated hydrocarbon 997
Arom chloro photolysis water pollution 72
Arom fluorination pollution Lake Ontario 267
Arom haloorg leaded gasoline exhaust 1151
Arom hydrocarbon coal liq tar 1023
Arom hydrocarbon photooxidn air hydroxyl 383
Arom polycyclic assocn humus water 1162
Arom polycyclic hdyrocarbon soil pollution 508
Arom polycyclic hydrocarbon photodegrdn ash 86
Arom polycyclic hydrocrbon detn polychaete 69
Arom removal water enzymic oxidn 249
Arsenate sediment incorporation iron compd 183
Arsenoorg detn flue gas incinerator 711
Atm deposition snow northwest USA 275
Atm input PCB lake sediment 879
Atm material degrdn review 1093
Atm org elemental carbon aerosol 580
Atm oxidn nitrogen sulfur dioxide 1249
Atm pptn lead gasoline compn 171
Atm pptn pH gradient US 35
Atm sulfur aerosol Gulf Mexico 91
Atm transport toxaphene modeling USA 1109
Atm water tetravalent sulfur detn 524
Benzopyrene extn fly ash solvent 175
Benzopyrene sorption fly ash 291
Biacetyl formation arom hydrocarbon photo= oxidn 383
Bias groundwater analysis well casing 1179
Binding metal humate model 676
Binding metal humate theory 669
Biodegrdn alkylbenzene halogenated aliph hydrocarbon 997
Biodegrdn hydrocarbon coastal seawater 574
Biol treatment uranium mine wastewater 243
Bioluminescence Photobacterium toxicant 690
Biphenyl polychlorinated analysis 1194
Biphenyl polychlorinated aq soly 807
Biphenyl polychlorinated building contami= nation 597
Biphenyl polychlorinated Henry const po= lemic 527
Biphenyl polychlorinated Henry law const polemic 527
Bisulfite photodissoln iron oxide 943
Bleaching pulp liquor chlorinated acid 133
Blood carboxyHb carbon monoxide 916
Bog atm deposition record Pennsylvania 847
Brominated phenyl ether thermolysis 404
Bromoalkane reaction rate disappearance water 992
Bromochloramine reaction aq diethylphenyl= enediamine 166
Bromoethane reaction rate product water 992
Building contamination biphenyl polychlori= nated 597
Building material corrosion atm review 1093
Butyltin degrdn seawater pollution 1229
Butyltin oxide accumulation Mytilus 884
Butyltin species detn natural water 609
Cadmium iron waste transport seawater 62
Cancer risk drinking water pollutant 768
Carbon activated catalyst nitrosation methy= laniline 1050
Carbon dioxide pollution Himalayas Nepal 561
Carbon monoxide carboxyHb blood 916
Carbon monoxide kerosine heater 78
Carbon monoxide pollution Himalayas Nepal 561
Carbon org elemental atm aerosol 580
Carbon particle mercury vapor adsorption 735
Carbonaceous aerosol pollution Los Angeles 580
Carbonaceous particle fly ash property 291
CarboxyHb blood carbon monoxide 916
Carboxylic acid pulp bleaching liquor 133
Catalyst exhaust platinum palladium pollu= tion 1058
Catalyst nitrosation methylaniline activated carbon 1050
Centrifugation river sediment preconcn analysis 155
Chem emergency expert system review 118
Chem reactive air pollutant model 924
Chem toxic air pollution review 647
Chem toxic hazard assessment review 660
Chemiluminescence detector interference nitrogen oxide detn 594
Chemiluminescence nitrogen dioxide detn precision 1157
Chernobyl radioactive fallout Finland 1257
Chloral amino acid chlorination water 1117
Chlorella aluminum copper metab toxicity 616
Chlorella binding recovery metal 206
Chlorella gold adsorption 627
Chlorinated acid spent pulping liquor 133
Chlorinated cyano compd water chlorination 1218
Chlorinated hydrocarbon activity aq 830
Chlorination byproduct amino acid water 1117
Chlorination water chlorinated cyano compd 1218
Chlorination water disinfection lithium 822
Chlorine chlorite aq redox kinetics 50
Chlorine hydrolysis absorption kinetics 44
Chlorite chlorine aq redox kinetics 50
Chloro arom photolysis water pollution 72
Chloroacetonitrile amino acid chlorination water 1117
Chloroanisole chlorophenol reaction copper smectite 1056
Chlorobenzodioxin partition water octanol 397
Chlorobiphenyl methylthio lake sediment pollution 730
Chlorocarbon incineration reaction product 568
Chlorocarbon thermolysis 703
Chlorodibenzodioxin environment source fate polemic 1185 1186
Chlorodibenzodioxin volatilization photolysis environment 490
Chlorodibenzofuran environment source fate polemic 1185 1186
Chloroethene dehalogenation microbial groundwater pollution 96
Chloroform reaction hydrogen water 568
Chloromethane air pollution Himalayas Nepal 561
Chloromethane pollution tracer woodsmoke aerosol 803
Chloroorg amino acid chlorination water 1117

Chloroorg detn groundwater fiber fluorome= try 441
Chlorophenol chloroanisole reaction copper smectite 1056
Chlorophenol photolysis microbial degrdn water 1002
Chlorophenolic transport fate marine pollu= tion 457
Chromatog water anion exchange 149
Cloud water tetravalent sulfur detn 524
Coagulation effect sedimentation kinetics 187
Coagulation water purifn aluminum detn 891
Coal combustion aerosol sulfur dioxide 138
Coal fly ash compn morphol 409
Coal fly ash mutagenicity 400
Coal fly ash photodegrdn polyarom 86
Coal liq tar arom hydrocarbon 1023
Coal refuse combustion particulate compn 604
Coal waste iron sulfate leaching 1013
Coastal seawater hydrocarbon pollutant fate 574
Cobalt sorption aq particle interaction 55
Colloid PCB pollution partitioning lake 1136
Colorimetric detn aluminum hydrolysis product 891
Com humic acid soil study 904
Combustion chlorocarbon 703
Combustion coal aerosol sulfur dioxide 138
Combustion coal refuse particulate compn 604
Combustion gas indoor pollution Himalayas 561
Combustion kerosine heater emission 78
Combustion trichloroethylene flame 1243
Combustion wood aerosol pollution source 803
Complexation copper fulvic acid model 367
Computer program water quality data 204
Computer system chem spill review 118
Convection kerosine heater combustion 78
Cooling water chromate recovery 149
Copper adsorption manganese dioxide 1047
Copper binding aquatic org matter 817
Copper complexation fulvic acid model 367
Copper iron waste transport seawater 62
Copper metab toxicity Chlorella 616
Copper smectite chlorophenol chloroanisole reaction 1056
Corrosion material atm review 1093
Cotton leaf model insecticide washoff 521
Crank case mutagen lubricating oil 145
Creosote pollution sediment Puget Sound 1144
Cyano chlorinated compd water chlorination 1218
Cyanoalkanoic acid chlorination water 1218
Dark reaction nitrogen dioxide methanol 387
Data acquisition program water quality 545
Data processing environmental waste moni= toring 16
DDT Phoca 253
Degrdn hazardous org compd 703
Degrdn material atm review 1093
Degrdn microbial photolysis chlorophenol water 1002
Dehalogenation microbial chloroethene groundwater pollution 96
Dehydrobromination halogenated aliph water 992
Desorption phenol activated carbon 463
Destruction thermal hazardous waste review 312
Desulfurization flue gas economics technol 960
Detection limit principal component analysis 1157
Detector interference nitrogen oxide detn 594
Detergent phosphate ban eutrophication water 330
Dibenzodioxin lab contamination 725
Dibenzodioxin polybrominated thermolysis diphenyl ether 404
Dibenzodioxin polychlorinated building contamination 597
Dibenzodioxin polychlorinated source fate 195
Dibenzofuran polybrominated thermolysis diphenyl ether 404
Dibenzofuran polychlorinated building con= tamination 597
Dibenzofuran polychlorinated source fate 195
Dibromochloropropane reaction hydroxyl ozone kinetics 1043
Dibutyltin detn water 609
Dichloroethene dehalogention microbial groundwater pollution 96
Diethylphenylenediamine reaction aq bromo= chloramine 166
Dimethyl sulfate air pollution California 867
Dimethyl sulfate detn air gas 872
Dimethyl sulfide oxidn hydrogen peroxide 1017
Dinitrophenylhydrazine sampler formalde= hyde air 1273
Dinitrotoluene photooxidn UV hydrogen peroxide 260
Disappearance bromoalkane reaction rate water 992
Disinfection hypochlorite water alkali cation 822
Disinfection water ozonization fulvic acid 739
Dissoln hydrocarbon water evapn compn 296
Dissoln reductive iron oxide photoinduced 943
Drinking water pollutant cancer risk 768
Drinking water volatile org hazard 111
Dust roadside platinum palladium exhaust 1058
Economics flue gas desulfurization technol 960
Elec stove nitrogen dioxide pollution 775
Emission combustion kerosine heater 78
Emission power plant ash mutagenicity 400
Environment org pollutant transport review 538
Environment pollution waste incineration polemic 1185
Environmental analysis nitrogen oxide 594
Environmental hazard assessment org chem 1173
Environmental monitoring water data acqui= sition 545
Environmental pollution alkyllead Great Lakes 1033
Environmental waste monitoring data pro= cessing 16
Enzymic oxidn arom removal water 249
Estuarine org matter copper binding 817
Estuary aliph hydrocarbon pollutant fate 574
Estuary particle x ray analysis 467
Ethylene dibromide water volatilization 949
Eutrophication water detergent phosphate ban 330
Evapn petroleum hydrocarbon herbicide 783
Exchange chromatog water anion 149
Exhaust dust roadside platinum palladium 1058
Exhaust gas air pollution Tokyo 473
Exhaust gas alkyllead air pollution 589
Exhaust gas org pollution tunnel 790
Exhaust leaded gasoline haloorg arom 1151
Extn benzopyrene fly ash solvent 175
Extn sequential geol sediment analysis 836
Fallout radioactive Finland Chernobyl 1257
Fast gas liq kinetics 44
Fiber optics chloroorg detn groundwater 441
Filtration river sediment preconcn analysis 155
Fish fluorinated arom Lake Ontario 267
Fish toxicant toxicity prescreen Photobacter= ium 690
Flame retardant polybrominated ether ther= molysis 404
Flame trichloroethylene chem mass spectros= copy 1243
Flow injection sulfur atm water 524
Flue dsut metal recovery plasma review 1102
Flue gas desulfurization economics technol 960
Flue gas hazardous org detn 711
Flue gas incineration org sampling 223
Flue gas kerosine heater 78
Flue gas particulate metal concn 335
Flue gas refuse derived fuel 604
Fluorescence quenching pollutant assocn humus 1162
Fluorination arom pollution Lake Ontario 267
Fluorometry ammonia nitrate detn water 515
Fluorometry fiber chloroorg detn groundwa= ter 441
Fluoroorg detn air fluoride formation 1254
Fly ash benzopyrene extn solvent 175
Fly ash coal compn morphol 409
Fly ash coal mutagenicity 400
Fly ash coal photodegrdn polyarom 86
Fly ash compn coal refuse 604
Fly ash interaction org matter 291
Fly ash mercury vapor adsorption 735
Fly ash metal peat combustion 335
Fly ash peat mutagenicity increase 684
Formaldehyde air passive sampler 1273
Formaldehyde soly water 637
Fuel refuse derived fly ash 604
Fulvic acid aquatic ozonization 739
Fulvic acid copper complexation model 367
Fulvic acid protonation 354
Fulvic acid protonation polyelectrolyte prop= erty 349
Fulvic acid soly enhancement pollutant 502
Fume coal combustion sulfur dioxide 138
Functional group fulvic acid protonation 354
Gas chromatog alkylbenzenesulfonate sewage sludge 376
Gas chromatog butyltin species water 609
Gas chromatog perfluorocarbon detn air 100
Gas chromatog polyarom detn polychaete 69
Gas film coeff ethylene dibromide 949
Gas partitioning mirex fugacity water 1213
Gas stove nitrogen dioxide pollution 775
Gasoline compn lead air pollution 171
Gasoline leaded exhaust haloorg arom 1151
Gasoline vapor air pollution Tokyo 473
Geol sediment analysis sequential extn 836
Geopressured radon natural gas 939
Geothermal radon natural gas 939
Ginkgo redn nitrogen dioxide 413
Glyoxal formation arom hydrocarbon photo= oxidn 383
Gold adsorption Chlorella 627
Gold binding recovery Chlorella 206
Grass redn nitrogen dioxide 413
Groundwater analysis well casing purging 1179
Groundwater chloroorg detn fiber fluorome= try 441
Groundwater pollution microbial dehalogena= tion chloroethene 96
Groundwater pollution polycyclic arom hy= drocarbon 508
Halogenated aliph hydrocarbon alkylbenzene biodegrdn 997
Halomethane org matter removal water 1028
Haloorg arom leaded gasoline exhaust 1151
Haloorg radical formation copper smectite 1056
Hazard assessment toxic chem review 660
Hazard environmental assessment org chem 1173
Hazardous org compd degrdn 703
Hazardous org detn incineration offgas 711
Hazardous waste disposal plasma review 1102
Hazardous waste incineration offgas sampling 223
Hazardous waste thermal destruction review 312
Hdyrocarbon arom polycyclic soil pollution 508
Health physics radioactive aerosol Chernobyl 1257
Health pollution New Jersey review 8
Heater kerosine combustion emission 78
Hematite coal fly ash 409
Henry const polychlorinated biphenyl polem= ic 527
Henry law const polychlorinated biphenyl polemic 527
Herbicide petroleum hydrocarbon evapn 783
Herring gull alkylead Great Lakes 1033
Heterocoagulation magnesium hydroxide quartz suspension 1224
Horseradish peroxidase arom removal water 249
Humate metal binding model 676
Humate metal binding theory 669
Humic acid anthracene assocn fluorescence 1162
Humic acid com soil study 904
Humic acid protonation polyelectrolyte property 349
Humic acid soly enhancement pollutant 502
Humic substance water trihalomethane formation 1028
Hydrocarbon air pollution Himalayas Nepal 561
Hydrocarbon air pollution source Tokyo 473
Hydrocarbon arom coal liq tar 1023
Hydrocarbon arom photooxidn air hydroxyl 383
Hydrocarbon arom polycyclic photodegrdn ash 86
Hydrocarbon chlorinated activity aq 830
Hydrocarbon dissoln water evapn compn 296

Hydrocarbon halogenated aliph alkylbenzene biodegrdn 997
Hydrocarbon petroleum herbicide evapn 783
Hydrocarbon pollutant fate coastal seawater 574
Hydrocrbon polycyclic arom detn polychaete 69
Hydrogen chloroform hydrogen chloride formation 568
Hydrogen ion atm pptn US 35
Hydrogen peroxide enzyme water purifn 249
Hydrogen peroxide oxidn dimethyl sulfide 1017
Hydrogen peroxide UV dinitrotoluene photooxidn 260
Hydrolysis bromoalkane 992
Hydrolysis chlorine absorption kinetics 44
Hydrolysis product aluminum detn water 891
Hydrophobic pollutant geochem Lake Superior 1136
Hydroxyl arom hydrocarbon photooxidn air 383
Hydroxyl reaction dibromochloropropane kinetics 1043
Hydroxyl reaction kinetics alkyllead atm 797
Hydroxyl reaction trimethyl phosphate kinetics 1043
Hypochlorite disinfection water alkali cation 822
Incineration chlorocarbon 703
Incineration chlorocarbon reaction product 568
Incineration hazardous waste offgas sampling 223
Incineration hazardous waste review 312
Incineration offgas hazardous org detn 711
Incineration soot mercury vapor adsorption 735
Incineration waste chlorodibenzodioxin chlorodibenzofuran pollution 195
Incinerator building air pollution 597
Indoor air pollution nitrogen dioxide 775
Indoor air reactive pollutant model 924
Indoor outdoor air pollution Himalayas 561
Inorg removal water wastewater review 1072
Interference nitrogen oxide detn environment 594
Ion chromatog methyl sulfate detn 872
Ion exchange quinoline subsoil pH 620
Iron acidic waste settling seawater 62
Iron cycling Lake Mendota Wisconsin 449
Iron oxide reductive dissoln photoinduced 943
Iron sulfate leaching coal waste 1013
Juncus redn nitrogen dioxide 413
Kerosine heater combustion emission 78
Kinetics absorption chlorine hydrolysis 44
Kinetics aluminum hydrolysis colorimetric analysis 891
Kinetics org sorption sediment soil 717
Kinetics oxidn dimethyl sulfide peroxide 1017
Kinetics reaction hydroxyl alkyllead atm 797
Kinetics redox chlorine chlorite aq 50
Kinetics sedimentation coagulation effect 187
Lab contamination dibenzodioxin 725
Lake manganese iron cycling Wisconsin 449
Lake pollution fluorination arom Ontario 267
Lake pollution toxaphene atm transport 1109
Lake sediment arsenate phosphate accumulation 183
Lake sediment chlorodibenzodioxin chlorodibenzofuran source 195
Lake sediment diagenetic metal Alaska 299
Lake sediment PCB loading volatilization 879
Lake sediment pollution methylthio chlorobiphenyl 730
Lake sulfate acidity Appalachian polemic 302
Lake water sediment pollution PCB 1136
Landfill leachate anaerobic biodegrdn 997
Leachate landfill anaerobic biodegrdn 997
Leaching iron sulfate coal waste 1013
Leaching model retorted oil shale 695
Lead air pollution gasoline compn 171
Lead alkyl reaction hydroxyl atm 797
Lead iron waste transport seawater 62
Leaded gasoline exhaust haloorg arom 1151
Leaf insecticide washoff model cotton 521
Light scattering ammonium sulfate aerosol 1235
Linear alkylbenzenesulfonate detn sewage sludge 376
Lithium chlorination water disinfection 822
Lubricating oil crank case mutagen 145
Lung damage coal combustion aerosol 138
Magnesium hydroxide heterocoagulation quartz suspension 1224
Magnetite coal fly ash 409
Manganese cycling Lake Mendota Wisconsin 449
Manganese dioxide adsorption copper 1047
Marine environmental analysis nitrogen oxide 594
Marine pollution chlorophenolic transport fate 457
Marine sediment siloxane Washington State 743
Mass spectrometry alkylbenzenesulfonate sewage sludge 376
Mass spectrometry polyarom detn polychaete 69
Mass transfer gas liq kinetics 44
Material degrdn atm review 1093
Mechanism photooxidn aq dinitrotoluene 260
Mercury vapor adsorption incineration soot 735
Metal binding recovery Chlorella 206
Metal concn flue gas particulate 335
Metal corrosion atm review 1093
Metal diagenetic lake sediment Alaska 299
Metal humate binding model 676
Metal humate binding theory 669
Metal partitioning detn geol sediment 836
Metal recovery steelmaking plasma review 1102
Metal sorption aq particle interaction 55
Methane air pollution Himalayas Nepal 561
Methanol nitrogen dioxide reaction photoenhancement 393
Methanol nitrogen dioxide surface reaction 387
Methanol water sample org detn 826
Methyl nitrite formation UV irradn 393
Methyl sulfate air pollution California 867
Methyl sulfate detn air gas 872
Methylaniline nitrosation activated carbon catalyst 1050
Methylglyoxal formation arom hydrocarbon photooxidn 383
Methylthio chlorobiphenyl lake sediment pollution 730
Microbial degrdn photolysis chlorophenol water 1002
Microbial dehalogenation chloroethene groundwater pollution 96
Mirex fugacity water gas partitioning 1213
Model chem reactive air pollutant 924
Model chem transfer air water 810
Model copper complexation fulvic acid 367
Model insecticide washoff leaf cotton 521
Model leaching retorted oil shale 695
Model org sorption sediment soil 717
Model sedimentation kinetics coagulation effect 187
Model venturi scrubber particle collection 237
Modeling acid deposition review 1084
Modeling air pollution Denver Colorado 1126
Modeling atm chem night 1167
Modeling org pollutant transport review 538
Modeling toxaphene atm transport USA 1109
Molybdenum removal uranium mine wastewater 243
Montmorillonite sorption metal particle interaction 55
Morphol coal fly ash 409
Multistage heater kerosine combustion 78
Mutagen crank case lubricating oil 145
Mutagenicity acetaldehyde photooxidn product pollution 1008
Mutagenicity coal fly ash 400
Mutagenicity increase peat fly ash 684
Mutagenicity wood smoke photooxidn product 493
Mytilus butyltin oxide accumulation 884
Napropamide adsorption variability soil analysis 256
Natural gas geopressured radon 939
Natural gas polycyclic arom hydrocarbon 508
Natural water butyltin species detn 609
Neptunium adsorption seawater sediment ratio 483
Nickel sorption aq particle interaction 55
Nitrate ammonia simultaneous detn water 515
Nitrate formation atm oxidn 1249
Nitrate ion atm pptn US 35
Nitrate reaction org gas night 1167
Nitric acid dry deposition sampler 633
Nitric acid formation night atm 1167
Nitric oxide formation plant 413
Nitric oxide pulse ozone detector interference 594
Nitroarom sediment pollution Puget Sound 1144
Nitrogen dioxide air pollution exposure 775
Nitrogen dioxide detn chemiluminescence precision 1157
Nitrogen dioxide dry deposition sampler 633
Nitrogen dioxide methanol reaction photoenhancement 393
Nitrogen dioxide methanol surface reaction 387
Nitrogen dioxide mutagen crank case 145
Nitrogen dioxide pollutant oxidn atm 1249
Nitrogen dioxide redn plant polysaccharide 413
Nitrogen oxide arom photooxidn hydroxyl 383
Nitrogen oxide detn environment interference 594
Nitrogen oxide ion atm pptn US 35
Nitrogen oxide kerosine heater 78
Nitrogen pentoxide hydrolysis night atm 1167
Nitrosation methylaniline activated carbon catalyst 1050
Octanol water coeff tributyltin salinity 201
Octanol water partition chlorobenzodioxin 397
Oil shale retorted leaching model 695
Oil spill dissoln evapn 296
Org air New Jersey review 8
Org air sampling Tenax evaluation 1260
Org chem environmental hazard assessment 1173
Org chem transfer air water 810
Org compd water pollution review 652
Org elemental carbon atm aerosol 580
Org hazardous detn incineration offgas 711
Org matter characterization water purifn 1028
Org matter fly ash interaction 291
Org pollutant transport modeling review 538
Org pollution tunnel exhaust gas 790
Org removal water wastewater review 970
Org sampling flue gas incineration 223
Org soil sorption toluene trichloroethylene 1263
Org sorption kinetics sediment soil 717
Org volatile detn water storage 826
Org volatile drinking water hazard 111
Org volatile partitioning vapor particle 1038
Organofluorine detn air fluoride formation 1254
Oxidant detn water bromochloramine reactivity 166
Oxidn chlorocarbon 703
Oxidn enzymic arom removal water 249
Oxidn kinetics dimethyl sulfide peroxide 1017
Oxidn nitrogen sulfur dioxide atm 1249
Oxygen singlet formation concn water 341
Oxygen singlet irradiated soil surface 934
Ozone pollution poplar growth inhibition 1122
Ozone pulse detector nitric oxide interference 594
Ozone reaction aquatic fulvic acid 739
Ozone reaction dibromochloropropane kinetics 1043
Ozonization aquatic fulvic acid 739
Paint solvent air pollution Tokyo 473
Particle collection efficiency venturi scrubber 237
Particle estuary x ray analysis 467
Particle interaction aq sorption metal 55
Particle iron waste settling seawater 62
Particle removal water wastewater review 856
Particle size fly ash compn 604
Particle vapor org volatile partitioning 1038
Particulate carbon air Los Angeles 580
Particulate compn coal refuse combustion 604
Particulate flue gas metal concn 335
Particulate pollution methyl sulfate California 867
Partition chlorobenzodioxin water octanol 397
Partitioning org volatile vapor particle 1038
Partitioning water sediment PCB pollution 1136
PCB analysis 1194
PCB aq soly temp effect 807

PCB loading volatilization lake sediment 879
PCB Phoca 253
PCB water sediment pollution lake 1136
Peat bog atm deposition record 847
Peat combustion fly ash metal 335
Peat fly ash mutagenicity increase 684
Pentachlorophenol manuf chlorodibenzodiox= in chlorodibenzofuran pollution 195
Perfluorocarbon detn air gas chromatog 100
Peroxidase horseradish arom removal water 249
Peroxyacetyl nitrate detn air calibration 1269
Pesticide pollutant water soly enhancement 502
Pesticide soil adsorption variability analysis 256
Petroleum hydrocarbon herbicide evapn 783
Petroleum refinery air pollution Tokyo 473
pH gradient atm pptn US 35
Phenanthrene assocn humic acid fluorescence 1162
Phenol adsorption wastewater activated carbon 463
Phenyl brominated ether thermolysis 404
Phoca DDT PCB 253
Phosphate detergent ban eutrophication water 330
Phosphate sediment incorporation iron compd 183
Photobacterium prescreen toxicant toxicity fish 690
Photochem air pollution acetaldehyde oxidn 1008
Photodegrdn polyarom coal fly ash 86
Photoenhancement methanol nitrogen diox= ide reaction 393
Photoinduced reductive dissoln iron oxide 943
Photolysis chloro arom water pollution 72
Photolysis iron oxide bisulfite 943
Photolysis microbial degrdn chlorophenol water 1002
Photolysis soil singlet oxygen 934
Photolysis volatilization chlorodibenzodioxin environment 490
Photooxidn arom hydrocarbon air hydroxyl 383
Photooxidn dinitrotoluene UV hydrogen peroxide 260
Photooxidn product acetaldehyde mutagenic= ity pollution 1008
Photooxidn product wood smoke mutagenici= ty 493
Photosensitization singlet oxygen soil 934
Plant polysaccharide redn nitrogen dioxide 413
Plasma technol review 1102
Plutonium adsorption seawater sediment ratio 483
Poa redn nitrogen dioxide 413
Pollutant air partitioning vapor particle 1038
Pollutant air source Denver Colorado 1126
Pollutant air source receptor review 1084
Pollutant assocn humus fluorescence quench= ing 1162
Pollutant deposition atm peat bog 847
Pollutant dry deposition air sampler 633
Pollutant hydrocarbon fate coastal seawater 574
Pollutant org transport modeling review 538
Pollutant pesticide water soly enhancement 502
Pollutant settling kinetic water coagulation 187
Pollutant transfer model air water 810
Pollutant water fate singlet oxygen 341
Pollution aerosol wood combustion source 803
Pollution alkyllead rain snow water 589
Pollution environmental alkyllead Great Lakes 1033
Pollution groundwater microbial dehalogena= tion chloroethene 96
Pollution groundwater quinoline sorption subsoil 620
Pollution lake sediment methylthio chlorobi= phenyl 730
Pollution marine chlorophenolic transport fate 457
Pollution org drinking water hazard 111
Pollution seawater iron waste transport 62
Pollution sediment nitroarom Puget Sound 1144
Pollution sediment siloxane Washington State 743
Pollution sediment waste incineration polem= ic 1185
Pollution water chloro arom photolysis 72
Pollution water chlorophenol photolysis biodegrdn 1002
Pollution water coal waste leaching 1013
Pollution water Great review 752
Pollution water org compd review 652
Pollution water org sorption kinetics 717
Polyacrylic acid soly enhancement pollutant 502
Polyarom photodegrdn coal fly ash 86
Polychaete polycyclic arom hydrocrbon detn 69
Polychlorinated biphenyl analysis 1194
Polychlorinated biphenyl building contami= nation 597
Polychlorinated biphenyl Henry const po= lemic 527
Polychlorinated biphenyl Henry law const polemic 527
Polychlorinated dibenzodioxin dibenzofuran source fate 195
Polycyclic arom assocn humus water 1162
Polycyclic arom hdyrocarbon soil pollution 508
Polycyclic arom hydrocarbon photodegrdn ash 86
Polycyclic arom hydrocrbon detn polychaete 69
Polyelectrolyte property fulvic acid protona= tion 349 354
Polymn chlorophenol chloroanisole copper smectite 1056
Polysaccharide plant redn nitrogen dioxide 413
Poplar growth inhibition ozone pollution 1122
Potassium air pollution Himalayas Nepal 561
Potassium chlorination water disinfection 822
Power plant emission ash mutagenicity 400
Pptn absorption air pollution model 810
Pptn atm pH gradient US 35
Precision principal component analysis 1157
Principal component analysis precision 1157
Processing supercrit fluid review 319
Protonation fulvic acid 354
Protonation fulvic acid polyelectrolyte prop= erty 349
PTFE well casing groundwater analysis 1179
Pulp mill pollution seawater sediment 457
Pulping liquor spent chlorinated acid 133
Pulse ozone detector nitric oxide interference 594
Purging well casing groundwater analysis 1179
Purifn water coagulation aluminum detn 891
PVC well casing groundwater analysis 1179
Pyrene assocn humic acid fluorescence 1162
Pyritic coal waste leaching sulfate 1013
Quality water Great Lake review 752
Quartz sorption metal particle interaction 55
Quartz suspension magnesium hydroxide heterocoagulation 1224
Quinoline sorption subsoil pH ionization 620
Quinolinium ion exchange subsoil 620
Radiant heater kerosine combustion 78
Radical formation haloorg copper smectite 1056
Radioactive fallout Finland Chernobyl 1257
Radon geopressured natural gas 939
Rain acid flue gas desulfurization 960
Rain snow water alkyllead pollution 589
Reaction rate disappearance bromoalkane water 992
Reactive chem air pollutant model 924
Reactivity com humic acid 904
Reactor accident fallout Chernobyl 1257
Redn nitrogen dioxide plant polysaccharide 413
Redox kinetics chlorine chlorite aq 50
Reductive dissoln iron oxide photoinduced 943
Refuse coal combustion particulate compn 604
Regeneration anion exchange phenol 463
Retorted oil shale leaching model 695
Review air pollutant source receptor 1084
Review air pollution New Jersey 8
Review chem emergency expert system 118
Review inorg removal water wastewater 1072
Review material degrdn atm 1093
Review org compd water pollution 652
Review org pollutant transport modeling 538
Review org removal water wastewater 970
Review particle removal water wastewater 856
Review plasma technol 1102
Review pollution water Great Lakes 752
Review supercrit fluid processing 319
Review thermal destruction hazardous waste 312
Review toxic chem air pollution 647
Review toxic chem hazard assessment 660
Ringed seal DDT PCB 253
River nitrate ammonia simultaneous detn 515
River sediment preconcn analysis 155
Roadside dust platinum palladium exhaust 1058
Rush redn nitrogen dioxide 413
Safety chem emergency response review 118
Safety dibenzodioxin lab 725
Safety radioactive aerosol Chernobyl 1257
Safety radon natural gas 939
Safety toxic air pollution review 647
Sampler passive formaldehyde air 1273
Sampler pollutant dry deposition air 633
Sampling hazardous waste incineration off= gas 223
Sampling inlet aerosol particle detn 911
Sampling org air Tenax evaluation 1260
Scrubber venturi particle collection efficiency 237
Seal DDT PCB 253
Seawater acidic iron waste settling 62
Seawater coastal hydrocarbon pollutant fate 574
Seawater pollution butyltin degrdn 1229
Seawater pollution chlorophenolic pulp mill 457
Seawater sediment ratio actinide adsorption 483
Seawater tributyltin speciation 201
Sediment fluorinated arom Lake Ontario 267
Sediment geol analysis sequential extn 836
Sediment lake arsenate phosphate accumula= tion 183
Sediment lake chlorodibenzodioxin chlorodi= benzofuran source 195
Sediment lake diagenetic metal Alaska 299
Sediment Lake lead environment methylated 1033
Sediment lake PCB loading volatilization 879
Sediment marine chlorophenolic pulp mill 457
Sediment marine siloxane Washington State 743
Sediment pollution nitroarom Puget Sound 1144
Sediment pollution waste incineration po= lemic 1185
Sediment river preconcn analysis 155
Sediment seawater ratio actinide adsorption 483
Sediment suspended estuary analysis classifi= cation 467
Sediment water pollution PCB lake 1136
Sedimentation kinetics coagulation effect model 187
Selenium removal uranium mine wastewater 243
Selenium tellurium atm aerosol 987
Selenourea detn flue gas incinerator 711
Sequential extn geol sediment analysis 836
Sewage sludge linear alkylbenzenesulfonate detn 376
Shale oil retorted leaching model 695
Siloxane marine sediment Washington State 743
Singlet oxygen formation concn 341
Singlet oxygen irradiated soil surface 934
Sludge sewage linear alkylbenzenesulfonate detn 376
Smectite copper chlorophenol chloroanisole reaction 1056
Smog dimethyl monomethyl sulfate Califor= nia 867
Smog modeling Denver Colorado 1126
Smoke wood photooxidn product mutagenic= ity 493
Smoke wood pollution tracer chloromethane 803
Snow compn chem northwest USA 275
Snow water rain alkyllead pollution 589
Sodium chlorination water disinfection 822
Soil adsorption isotherm soln solid 895
Soil analysis adsorption variability napro= pamide 256
Soil filtration uranium mine wastewater 243
Soil org sorption toluene trichloroethylene 1263

Soil pollution polycyclic arom hdyrocarbon 508
Soil water study humic acid 904
Solvent benzopyrene extn fly ash 175
Soly aq activity calcn UNIFAC 1060
Soly PCB aq temp effect 807
Soly tetrachlorodibenzodioxin water detn 180
Soly water pollutant pesticide enhancement 502
Soot incineration mercury vapor adsorption 735
Sorbent methyl sulfate sampling air 872
Sorption kinetics org sediment soil 717
Sorption metal aq particle interaction 55
Sorption quinoline subsoil pH ionization 620
Sorption toluene trichloroethylene soil org 1263
Source hydrocarbon air pollution Tokyo 473
Stainless steel casing groundwater analysis 1179
Steelmaking metal recovery plasma review 1102
Stiff diagram water quality data 204
Storage volatile org detn water 826
Stove elec nitrogen dioxide pollution 775
Subsoil sorption quinoline pH ionization 620
Sulfate acidity lake Appalachian polemic 302
Sulfate aerosol Gulf Mexico 91
Sulfate ammonium aerosol light scattering 1235
Sulfate ion atm pptn US 35
Sulfate iron leaching coal waste 1013
Sulfate removal uranium mine wastewater 243
Sulfur atm Gulf Mexico aerosol 91
Sulfur dioxide coal combustion aerosol 138
Sulfur dioxide dry deposition sampler 633
Sulfur dioxide pollutant oxidn atm 1249
Sulfur dioxide removal flue gas 960
Sulfur formation atm oxidn 1249
Sulfur oxide ion atm pptn US 35
Sulfur reduced compd detn air 517
Sulfur tetravalent detn atm water 524
Supercrit fluid processing review 319
Surface irradiated soil singlet oxygen 934
Surface pptn magnesium hydroxide quartz 1224
Surface reaction methanol nitrogen dioxide 387
Surface reaction nitrogen oxide methanol 393
Tar liq arom hydrocarbon 1023
TCDD vapor pressure environmental pollution 490
Tellurium selenium atm aerosol 987
Tenax GC adsorbent org evaluation 1260
Tetrabutyltin detn water 609
Tetrachlorodibenzodioxin detn flue gas incinerator 711
Tetrachlorodibenzodioxin soly water detn 180
Tetrachloroethene dehalogenation microbial groundwater pollution 96
Tetraethyllead reaction kinetics hydroxyl atm 797
Tetramethyllead reaction kinetics hydroxyl atm 797
Thermal destruction hazardous waste review 312
Thermolysis brominated phenyl ether 404
Thermolysis chlorocarbon 703
Toluene sorption soil org 1263
Toxaphene atm transport modeling USA 1109
Toxic chem air pollution review 647
Toxic chem hazard assessment review 660
Toxic pollution New Jersey review 8
Toxicant toxicity fish prescreen Photobacterium 690
Trace metal lake sediment Alaska 299
Transfer chem air water model 810
Transport org pollutant modeling review 538
Transport storage sample water analysis 826
Transport toxaphene atm modeling USA 1109
Tributyltin detn water 609
Tributyltin speciation seawater 201
Trichloroethene dehalogenation microbial groundwater pollution 96
Trichloroethylene drinking water health hazard 111
Trichloroethylene flame chem mass spectroscopy 1243
Trichloroethylene sorption soil org 1263
Triethyllead formation reaction hydroxyl atm 797
Trimethyl phosphate reaction hydroxyl ozone 1043
Trimethyllead formation reaction hydroxyl atm 797
Triterpenoid polychaete New York Bight 69
Tunnel org pollution exhaust gas 790
UNIFAC soly aq activity calcn 1060
UNIFAC soly polychlorinated biphenyl polemic 527
Uranium mine wastewater soil filtration 243
UV fluoresccence polyarom detn polychaete 69
UV hydrogen peroxide dinitrotoluene photooxidn 260
UV irradn methyl nitrite formation 393
Vanadium iron waste transport seawater 62
Vapor particle org volatile partitioning 1038
Vapor pressure TCDD environmental pollution 490
Venturi scrubber particle collection efficiency 237
Volatile org air sampling Tenax 1260
Volatile org detn water storage 826
Volatile org drinking water hazard 111
Volatile org partitioning vapor particle 1038
Volatilization ethylene dibromide water 949
Volatilization hydrocarbon coastal seawater 574
Volatilization loading PCB lake sediment 879
Volatilization photolysis chlorodibenzodioxin environment 490
Volatilization water pollutant transfer model 810
Waste acidic iron settling seawater 62
Waste hazardous disposal plasma review 1102
Waste hazardous incineration offgas sampling 223
Waste incineration chlorodibenzodioxin chlorodibenzofuran pollution 195
Waste monitoring environmental data processing 16
Wastewater anaerobic treatment 1200
Wastewater inorg dissolved removal review 1072
Wastewater org dissolved removal review 970
Wastewater particle removal theory review 856
Water analysis oxidant bromochloramine reactivity 166
Water chloroform hydrogen chloride formation 568
Water hydrocarbon dissoln evapn compn 296
Water inorg dissolved removal review 1072
Water mirex fugacity gas partitioning 1213
Water natural butyltin species detn 609
Water nitrate ammonia simultaneous detn 515
Water oxygen singlet formation concn 341
Water pollution coal waste leaching 1013
Well casing purging groundwater analysis 1179
Winter haze modeling Denver Colorado 1126
Wood combustion aerosol pollution source 803
Wood smoke photooxidn product mutagenicity 493
Woodsmoke aerosol chloromethane pollution tracer 803
X ray analysis estuary particle 467
Zinc oxide reaction sulfur dioxide 138

CHEMICAL RESEARCH FACULTIES:

AN INTERNATIONAL DIRECTORY

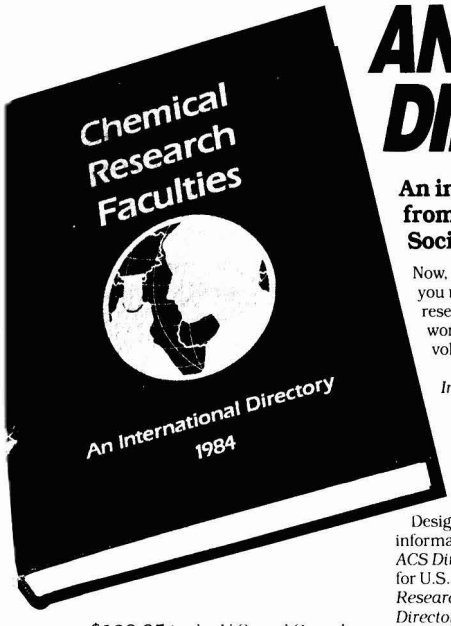

$129.95 in the U.S. and Canada
$155.95 in all other countries

An invaluable new resource from the American Chemical Society.

Now, for the first time, *all* the information you need about chemical research and researchers at universities around the world has been gathered into one volume.

Chemical Research Faculties: An International Directory contains a wealth of facts on more than 8,900 faculty members and 737 departments in 62 countries. And it's a book no academic institution or chemically oriented business can afford to be without.

Designed to provide the same type of information on an international scale that the *ACS Directory of Graduate Research* gives for U.S. and Canadian schools, *Chemical Research Faculties: An International Directory* includes listings for chemistry, chemical engineering, biochemistry, and pharmaceutical/medicinal chemistry.

It offers informative statistical tables on graduate programs worldwide. Organizes data on 63 chemical societies in 51 nations. And is cross-referenced three ways—by faculty, institution, and research subject—for easy use.

Indispensable for industry and academia alike.

If you're involved in chemical research, *Chemical Research Faculties: An International Directory* can keep you abreast of the latest developments in your area of specialization.

If you advise graduate students, it can help you steer them toward the programs they're seeking.

And if you're in a business even remotely related to chemical research, just one of the thousands of leads this book contains could pay for the purchase price many times over.

Why not fill out the order form right now? Or call 800/424-6747 and charge your VISA, MasterCard, or American Express.

And let *Chemical Research Faculties: An International Directory* open up a whole new world of professional possibilities.

ORDER FORM

☐ **YES! Please rush me my copy of the new international directory!**

	QTY.	U.S./ CANADA	EXPORT	TOTAL
Chemical Research Faculties: An International Directory	_____	**$129.95**	**$155.95**	_____
California residents, add 6% tax				_____
AMOUNT ENCLOSED				_____

☐ I have enclosed a check for $_____ payable to the American Chemical Society.
☐ Purchase Order #_____ enclosed.
Charge my ☐ VISA ☐ MasterCard ☐ American Express ☐ Barclaycard ☐ Access.

Name of cardholder _____

Account # _____

Expires _____ Interbank # _____
(MasterCard and Access)

Signature _____

Note: Please allow four to six weeks for delivery. Foreign payment must be made in U.S. currency by international money order, UNESCO coupons, or U.S. bank draft. Order through your local bookseller or directly from the American Chemical Society. Orders from individuals must be prepaid.

PLEASE SHIP BOOKS TO:

Name _____

Address _____

_____

_____

33

MAIL THIS ORDER FORM TO: American Chemical Society
Distribution Office, Department 33
1155 16th Street, N.W.
Washington, D.C. 20036

☐ **Please send me more information about the *ACS Directory of Graduate Research 1983*, which gives similar data for U.S. schools.**

Departmental Information
includes address and phone number, name of department head, advanced degrees offered, and principal areas of research.

Faculty Information
includes name, year of birth, title, degrees (with years and institutions), areas of specialization, current research, and recent publications.

Chemical Society Information
lists address, principal officer, publications, purpose, organizational structure, and number of members.

Guide to Chemical Research Institutions
lists all countries, universities, and departments in order of appearance, providing an overview of each section.

Four Organizational Sections
break down listings into chemistry, chemical engineering, biochemistry, and pharmaceutical/ medicinal chemistry.

Faculty Index
helps you keep up with colleagues' moves and learn more about others in your area of specialization.

Statistical Tables
provide for each country the number of master's and doctoral degrees conferred in 1981 and 1982—as well as the number of full-time faculty, post-doctoral appointments, and students enrolled in advanced degree programs.

Institutional Index
provides a merged alphabetical listing that lets you find institutions known by name but not location.

Index of Research Subjects
helps you locate universities, departments, and individuals doing research related to your own.

800-424-6747

Learn how to protect yourself and minimize your risk from chemicals and hazards in the laboratory

Laboratory Safety and Health

An Audio Course Produced by the American Chemical Society

An important concern for every industrial and academic laboratory is an effective safety and occupational health program. This new audio course helps you meet this vital need.

With this course, you'll become familiar with the basic guidelines for safe laboratory practices and master prudent safety methods. You'll also discover the *secrets* of laboratory safety and

- be able to minimize your risk of exposure
- know about the law and how it protects you
- effectively use safety equipment and protective facilities

You'll also cover a variety of safety- and health-related topics, including safety philosophy, federal regulations, occupational illness, known carcinogens, and more. You'll gain an understanding of the necessary guidelines for dealing with accidents in the lab and for making health and safety an integral part of effective lab practices.

Intended for bench chemists, science teachers, upperclass undergraduates, graduate students, and others involved with the use of chemicals, this course will enable management and supervisory personnel to develop an effective safety program.

Brief Course Outline

- Introduction: Overview of Course; Safety Philosophy
- Scope of the Problem: Life's Hazards; Hazard vs Risk; Deaths, Accidents, and Illness
- The Question of Liability: Negligence and the Prudent Person; Case Studies
- Hazards in the Laboratory: Chemical; Mechanical; Electrical; Radiation; Pressure and Vacuum Operations; Biological; Noise; Physical
- Working with Chemicals: Ordering; Manipulations; Inventory; Storage; Waste Disposal
- Safety Rules and Recommended Practices
- Protective Equipment: Glasses, Goggles, and Face Shields; Lab Coats; Shoes; Hearing Protection; Gloves; Respirators
- Protective and Emergency Facilities: Eyewash Fountains; Safety Showers; Fire Blankets; Fume Hoods; Fire Fighting Equipment
- Responding to Emergencies: Evacuation; Obtaining Assistance; Temporary Care; Fires; Chemical Spills
- Reporting Incidents and Accidents
- Introduction to Industrial Hygiene and Toxicology
- Federal Regulations: OSHA/NIOSH; EPA; NRC
- The Reference Library: Publications; Federal Agencies, Associations, and Professional Societies
- Summary: The Effective Safety Program

About the Instructor

Dr. James Kaufman is Professor of Chemistry at Curry College in Milton, Massachusetts, and a laboratory safety consultant. He authored *Laboratory Safety Guidelines* when he worked at Dow Chemical Company and which has been widely distributed to industry and academe. He is a member of the ACS Council Committee on Chemical Safety and is active in the ACS Division of Chemical Health and Safety.

Unit (Catalog No. C-87)
Four cassettes (4.0 hours playing time) and 168-page manual: $295.00, U.S. & Canada; $354.00, export. Additional manuals: $20.00 each, U.S. & Canada; $24.00 each, export.

To place your order, use the coupon below or CALL TOLL FREE 800-424-6747 and use your credit card or purchase order number. Please use the Priority Code and Catalog Number when ordering.

No-Risk Guarantee
All ACS Audio Courses come to you with a money-back guarantee. If you are not completely satisfied, return the course within ten days for a full refund or cancellation of invoice.

American Chemical Society, Distribution Office, Priority Code 40, 1155 Sixteenth Street, N.W., Washington, DC 20036

Yes! Please send me the following:

Qty. Total

_____ Complete course(s), *Laboratory Safety and Health* at $295.00 each (U.S. & Canada) or $354.00 each (export). Catalog No. C-87 $ _____

_____ Additional manuals at $20.00 each (U.S. & Canada) or $24.00 each (export). $ _____

TOTAL $ _____

☐ Payment enclosed (make checks payable to the American Chemical Society.
☐ Purchase order enclosed. P.O. # _____
Charge my ☐ MasterCard ☐ VISA ☐ American Express ☐ ACCESS ☐ Barclaycard ☐ Diners Club/Carte Blanche

Account # _____
Expires _____ Interbank # _____ (MC and ACCESS only)
Name of cardholder _____
Signature _____
Ship to: _____
Name _____
Title _____
Organization _____
Address _____
City, State, ZIP _____